frontiers | Research Topics

Biotic changes in terrestrial environments around the Eocene–Oligocene transition

Edited by
Lucja A. Fostowicz-Frelik, Qian Li and Grégoire Métais

Published in
Frontiers in Earth Science
Frontiers in Ecology and Evolution

ISSN 1664-8714
ISBN 978-2-8325-3864-7
DOI 10.3389/978-2-8325-3864-7

About Frontiers

Frontiers is more than just an open access publisher of scholarly articles: it is a pioneering approach to the world of academia, radically improving the way scholarly research is managed. The grand vision of Frontiers is a world where all people have an equal opportunity to seek, share and generate knowledge. Frontiers provides immediate and permanent online open access to all its publications, but this alone is not enough to realize our grand goals.

Frontiers journal series

The Frontiers journal series is a multi-tier and interdisciplinary set of open-access, online journals, promising a paradigm shift from the current review, selection and dissemination processes in academic publishing. All Frontiers journals are driven by researchers for researchers; therefore, they constitute a service to the scholarly community. At the same time, the *Frontiers journal series* operates on a revolutionary invention, the tiered publishing system, initially addressing specific communities of scholars, and gradually climbing up to broader public understanding, thus serving the interests of the lay society, too.

Dedication to quality

Each Frontiers article is a landmark of the highest quality, thanks to genuinely collaborative interactions between authors and review editors, who include some of the world's best academicians. Research must be certified by peers before entering a stream of knowledge that may eventually reach the public - and shape society; therefore, Frontiers only applies the most rigorous and unbiased reviews. Frontiers revolutionizes research publishing by freely delivering the most outstanding research, evaluated with no bias from both the academic and social point of view. By applying the most advanced information technologies, Frontiers is catapulting scholarly publishing into a new generation.

What are Frontiers Research Topics?

Frontiers Research Topics are very popular trademarks of the *Frontiers journals series*: they are collections of at least ten articles, all centered on a particular subject. With their unique mix of varied contributions from Original Research to Review Articles, Frontiers Research Topics unify the most influential researchers, the latest key findings and historical advances in a hot research area.

Find out more on how to host your own Frontiers Research Topic or contribute to one as an author by contacting the Frontiers editorial office: frontiersin.org/about/contact

Biotic changes in terrestrial environments around the Eocene–Oligocene transition

Topic editors

Lucja A. Fostowicz-Frelik — Institute of Paleobiology, Polish Academy of Sciences, Poland

Qian Li — Institute of Vertebrate Paleontology and Paleoanthropology, Chinese Academy of Sciences (CAS), China

Grégoire Métais — Centre National de la Recherche Scientifique (CNRS), France

Citation

Fostowicz-Frelik, L. A., Li, Q., Métais, G., eds. (2023). *Biotic changes in terrestrial environments around the Eocene–Oligocene transition*. Lausanne: Frontiers Media SA. doi: 10.3389/978-2-8325-3864-7

Table of contents

frontiers | Frontiers in Earth Science

TYPE Editorial
PUBLISHED 20 October 2023
DOI 10.3389/feart.2023.1305471

OPEN ACCESS

EDITED AND REVIEWED BY
Timothy Ian Eglinton,
ETH Zürich, Switzerland

*CORRESPONDENCE
Łucja Fostowicz-Frelik,
lfost@twarda.pan.pl

RECEIVED 01 October 2023
ACCEPTED 11 October 2023
PUBLISHED 20 October 2023

CITATION
Fostowicz-Frelik Ł, Li Q and Métais G (2023), Editorial: Biotic changes in terrestrial environments around the Eocene–Oligocene transition. *Front. Earth Sci.* 11:1305471. doi: 10.3389/feart.2023.1305471

Editorial: Biotic changes in terrestrial environments around the Eocene–Oligocene transition

Łucja Fostowicz-Frelik[1]*, Qian Li[2] and Grégoire Métais[3]

[1]Institute of Paleobiology, Polish Academy of Sciences, Warsaw, Poland, [2]Key Laboratory of Vertebrate Evolution and Human Origins of Chinese Academy of Sciences, Institute of Vertebrate Paleontology and Paleoanthropology, Beijing, China, [3]Centre de Recherche en Paléontologie—Paris, UMR 7207 (CNRS, MNHN, Sorbonne Université), Muséum National d'Histoire Naturelle, Paris, France

KEYWORDS

mammals, Eocene-Oligocene transition, paleoenvironments, stratigraphy, Asia

Editorial on the Research Topic
Biotic changes in terrestrial environments around the Eocene–Oligocene transition

The biotic event associated with the Eocene-Oligocene transition (EOT) is arguably one of the most significant in the Cenozoic history of life. At the planetary scale, the EOT is marked by a climatic shift from "greenhouse" to "icehouse" world (e.g., Zachos et al., 2001) caused by multiple factors including the final isolation of the Antarctic initiating development of permanent ice sheets on this continent and setting of the circum-Antarctic current, which had global consequences in the Earth-wide cooling and climate drying. These changes in temperature and air circulation facilitated the appearance of the first large-scale open habitats and substantially changed biotas across the globe. In Asia, the enhanced aridification across the EOT, coupled with the India–Asia collision and remarkable global sea-level drop profoundly changed the geography of Central Asia, creating land bridges that allowed biogeographic re-organization of terrestrial biotas.

In Western Europe, the EOT is concomitant with a major turnover in terrestrial vertebrate fauna, the so-called *Grande Coupure*, first identified by Stehlin (1909) in the Paris Basin, which marked the demise of endemic Eocene assemblages (Hooker et al., 2009), and the influx of multiple clades of Asian mammals. Likewise, the "Mongolian remodeling" (Meng and McKenna, 1998) shows a significant biotic reorganization reflecting an aridification of the Mongolian Plateau. These pulses in faunal migration, generally radiating from Asia to other continents, are thought to be the result from a complex interplay between the orogenic evolution of Asia (mostly India–Asia collision) and the global cooling and aridification of Asia induced by the combined partial pressure of CO_2 (pCO_2) drawdown and the westward retreat of the Paratethys Sea initiated at ~40 Ma (Bosboom et al., 2014). This profound biotic reorganization eventually led to shaping of modern aspect ecosystems with the faunal content we know today.

The base of the Oligocene (Global Boundary Stratotype Section for the base of the Ruppelian stage) was formally established on the open marine sediment series of the Massignano section (Italy; see Premoli Silva and Jenkins, 1993), close to the top of chron C13r, which gives a numerical age ~34.0 Ma (Speijer et al., 2020). In order to reconstruct the changes in the terrestrial environments we need to refer to other Eocene-Oligocene sediment series documenting EOT. Some of the exceptionally preserved strata displaying the

Eocene–Oligocene boundary can be found in Asian (e.g., Wasiljeff et al., 2020) or North American deposits (see e.g., Fostowicz-Frelik, 2013 and references therein).

In recent years, the interest in the EOT and pre-EOT faunal research has been centered on continental China (e.g., Wang et al., 2010; Wang et al., 2012; Li et al., 2016a; Li et al., 2016b), southeastern Europe and Western Asia (Balkanatolia; Licht et al., 2022; Métais et al. in press), and tropical-equatorial area of South America (Antoine et al., 2021). According to the currently available biostratigraphic data, the Eocene-Oligocene boundary in China is probably located in the upper part of the Xianaogangdai Formation at the Erden Obo Section, Siziwang Qi, Nei Mongol, which is a set of reddish muddy siltstone or silty mudstone. The rodent assemblage, consisting of the most abundant and diverse small mammal taxa, displays a significant change across the boundary (Li et al., 2016a; Li et al., 2017). The preliminary paleomagnetic results also support the placement of the Eocene–Oligocene boundary in the upper part of the Xianaogangdai Formation. Another area with a documented Eocene–Oligocene boundary is Ulantatal, Alax Zuoqi and Balagong, in Hangjin Qi, Nei Mongol (Zhang et al., 2016; Wang et al. this volume). Based on the paleomagnetic reversal stratigraphy and faunal correlation in Ulantatal, the deposition time of this sediment series was established at between 35 and 27 Ma, thus exposing a long sedimentary succession ranging from the latest Eocene to the late Oligocene (Wasiljeff et al., 2020). Moreover, the assemblage of small mammals from the Kekeamu Section of this area, including the Eocene-Oligocene boundary (Wasiljeff and Zhang, 2022), displays an array of primitive and derived morphologies that resemble faunal elements known from the late Eocene and early Oligocene of China and Mongolia (Xu et al., 2023), and pointing to gradual faunal changes that started before the EOT.

In South China, the lower part of the Chaijiachong Formation was established as late Eocene on the basis of mammal fauna, although some recent discoveries show the possibility of lower Oligocene taxa admixture in strata bearing the Chaijiachong fauna in Qujing, Yunnan (Maridet and Ni, 2013). Further paleontological survey in the Youganwo Formation in Maoming, Guangdong, or in the Shinao Formation (Southwestern Guizhou and Eastern Yunnan, China) would improve our knowledge of the late Eocene faunas of Southeast Asia, so far only documented by the Krabi fauna of southern Thailand (Ducrocq et al., 1995).

The aim of the current volume was to bring our readers up to speed on recent discoveries in the field of mammal biostratigraphy, faunal diversity, and biotic changes in Asian terrestrial environments during the EOT and pre-EOT. This volume focuses on the continental Asian fossil record of the mammalian fauna and mammal paleocommunities, showing gradual changes in fauna as it transforms from the mid-Eocene climatic optimum (MECO) all the way through the Eocene–Oligocene biotic crisis. This Frontiers Research Topic presents studies depicting these events in different regions of China from Tibetan Plateau (see Ni et al.), Xinjiang (Li et al.) and Inner Mongolia (Bai et al.; Wang et al.; Zhang et al.) to south Chinese Guangdong Province (Averianov et al.), showing the response to changing environment in different mammalian groups. We do not focus on any particular group of mammals, although studies on rodents, the world's most numerous and diverse group dominate in taxonomical (see Ni et al.; Li et al.) and stratigraphic and paleogeographic aspects (Li et al.; Wang et al.). Further contributions feature also new taxa of artiodactyls (Bai et al.), and carnivores (Averianov et al.; Zhang et al.), complementing the picture of the paleo-trophic chains active during the late Eocene and early Oligocene in Asia.

Author contributions

ŁF-F: Writing–original draft, Writing–review and editing. QL: Writing–original draft, Writing–review and editing. GM: Writing–original draft, Writing–review and editing.

Conflict of interest

The authors declare that the research was conducted in the absence of any commercial or financial relationships that could be construed as a potential conflict of interest.

Publisher's note

References

Antoine, P.-O., Yans, J., Castillo, A. A., Stutz, N., Abello, M. A., Adnet, S., et al. (2021). Biotic community and landscape changes around the Eocene–Oligocene transition at Shapaja, Peruvian Amazonia: regional or global drivers? *Glob. Planet. Change* 202, 103512. doi:10.1016/j.gloplacha.2021.103512

Bosboom, R., Dupont-Nivet, G., Grothe, A., Brinkhuis, H., Villa, G., Mandic, O., et al. (2014). Timing, cause and impact of the late Eocene stepwise sea retreat from the Tarim Basin (west China). *Palaeogeogr. Palaeoclimatol. Palaeoecol.* 403, 101–118. doi:10.1016/j.palaeo.2014.03.035

Ducrocq, S., Chaimanee, Y., Suteethorn, V., and Jaeger, J. J. (1995). Mammalian faunas and the ages of the continental Tertiary fossiliferous localities from Thailand. *J. Southeast Asian Earth Sci.* 12, 65–78. doi:10.1016/0743-9547(95)00021-6

Fostowicz-Frelik, Ł. (2013). Reassessment of *Chadrolagus* and *Litolagus* (Mammalia: Lagomorpha) and a new genus of North American Eocene lagomorph from Wyoming. *Am. Mus. Novit.* 3773, 1–76. doi:10.1206/3773.2

Hooker, J. J., Grimes, S. T., Mattey, D. P., Collinson, M. E., and Sheldon, N. D. (2009). "Refined correlation of the late Eocene-early Oligocene Solent Group and timing of its climate history,". *Late Eocene Earth: Hothouse, Icehouse, and Impacts*. Editors C. Koeberl, and A. Montanari (Geological Society of America Special Paper), 452, 179–195.

Li, Q., Meng, J., and Wang, Y.-Q. (2016a). New cricetid rodents from strata near the Eocene-Oligocene boundary in Erden Obo section (Nei Mongol, China). *PLoS ONE* 11, e0156233. doi:10.1371/journal.pone.0156233

Li, Q., Wang, Y.-Q., and Fostowicz-Frelik, Ł. (2016b). Small mammal fauna from Wulanhuxiu (Nei Mongol, China) implies the Irdinmanhan–Sharamurunian (Eocene) faunal turnover. *Acta Palaeontol. Pol.* 61, 759–776. doi:10.4202/app.00292.2016

Li, Q., Gong, Y.-X., and Wang, Y.-Q. (2017). New dipodid rodents from the late Eocene of Erden Obo (Nei Mongol, China). *Hist. Biol.* 29, 692–703. doi:10.1080/08912963.2016.1232406

Licht, A., Métais, G., Coster, P., İbilioğlu, D., Ocakoğlu, F., Westerweel, J., et al. (2022). Balkanatolia: the insular mammalian biogeographic province that partly paved the way to the Grande Coupure. *Earth Sci. Rev.* 226, 103929. doi:10.1016/j.earscirev.2022.103929

Maridet, O., and Ni, X. (2013). A new cricetid rodent from the early Oligocene of Yunnan, China, and its evolutionary implications for early Eurasian cricetids. *J. Vert. Paleontol.* 33, 185–194. doi:10.1080/02724634.2012.710283

Meng, J., and McKenna, M. C. (1998). Faunal turnovers of Palaeogene mammals from the Mongolian Plateau. *Nature* 394 (6691), 364–367. doi:10.1038/28603

Métais, G., Coster, P., Licht, A., Ocakoğlu, F., and Beard, K. C. 1993. Additions to the late Eocene Süngülü mammal fauna in Easternmost Anatolia and the Eocene-Oligocene transition at the periphery of Balkanatolia. *C. R. Palevol.* (In press).

Premoli Silva, I., and Jenkins, D. G. (1993). Decision on the Eocene-Oligocene boundary stratotype. *Episodes* 16 (3), 379–382. doi:10.18814/epiiugs/1993/v16i3/002

Speijer, R. P., Pälike, H., Hollis, C. J., Hooker, J. J., and Ogg, J. G. (2020). "The Paleogene Period," in *The Geologic Time Scale 2020*. Editors F. M. Gradstein, J. G. Ogg, M. D. Schmitz, and G. M. Ogg (Amsterdam: Elsevier BV), 1087–1140. doi:10.1016/B978-0-12-824360-2.00028-0

Stehlin, H. G. (1909). Remarques sur les faunules de mammifères de l'Eocène et de l'Oligocène du Bassin de Paris. *Bull. Soc. Géol. Fr.* 4 (9), 488–520.

Wang, Y.-Q., Meng, J., Beard, K. C., Li, Q., Ni, X., Gebo, D. L., et al. (2010). Early Paleogene stratigraphic sequences, mammalian evolution and its response to environmental changes in Erlian Basin, Inner Mongolia, China. *Sci. China Earth Sci.* 53, 1918–1926. doi:10.1007/s11430-010-4095-8

Wang, Y.-Q., Meng, J., and Jin, X. (2012). Comments on Paleogene localities and stratigraphy in the Erlian Basin, Nei Mongol, China. *Vert. Palasiat.* 50, 181–203.

Wasiljeff, J., and Zhang, Z.-Q. (2022). Stratigraphical significance of Ulantatal sequence (Nei Mongol, China) in refining the latest Eocene and Oligocene terrestrial regional stages. *Vert. Palasiat.* 60, 42–53. doi:10.19615/j.cnki.2096-9899.210716

Wasiljeff, J., Kaakinen, A., Salminen, J. M., and Zhang, Z.-Q. (2020). Magnetostratigraphic constraints on the fossiliferous Ulantatal sequence in Inner Mongolia, China: implications for Asian aridification and faunal turnover before the Eocene–Oligocene boundary. *Earth Planet. Sci. Lett.* 535, 116125. doi:10.1016/j.epsl.2020.116125

Xu, R., Zhang, Z., Li, Q., and Wang, B. (2023). New material of *Karakoromys* (Ctenodactylidae, Rodentia) from Late Eocene-Early Oligocene of Ulantatal (Nei Mongol): taxonomy, diversity, and response to climatic change. *Diversity* 15, 744. doi:10.3390/d15060744

Zachos, J. C., Sloan, L., Thomas, E., and Billups, K. (2001). Trends, rhythms, and aberrations in global climate 65 Ma to present. *Science* 292, 686–693. doi:10.1126/science.1059412

Zhang, Z.-Q., Liu, Y., Wang, L.-H., Kaakinen, A., Wang, J., Mao, F.-Y., et al. (2016). Lithostratigraphic context of Oligocene mammalian faunas from Ulantatal, Nei Mongol, China. *C. R. Palevol.* 15, 903–910. doi:10.1016/j.crpv.2015.05.012

frontiers | Frontiers in Ecology and Evolution

TYPE Original Research
PUBLISHED 08 September 2022
DOI 10.3389/fevo.2022.955779

OPEN ACCESS

EDITED BY
K. Christopher Beard,
University of Kansas, United States

REVIEWED BY
Pauline Coster,
National Geologic Nature Reserve of Luberon, France
Wilma Wessels,
Utrecht University, Netherlands

*CORRESPONDENCE
Qian Li
liqian@ivpp.ac.cn

SPECIALTY SECTION
This article was submitted to Paleontology, a section of the journal Frontiers in Ecology and Evolution

RECEIVED 29 May 2022
ACCEPTED 05 August 2022
PUBLISHED 08 September 2022

CITATION
Li Q, Li Q, Xu R and Wang Y (2022) Rodent faunas, their paleogeographic pattern, and responses to climate changes from the early Eocene to the early Oligocene in Asia. *Front. Ecol. Evol.* 10:955779. doi: 10.3389/fevo.2022.955779

Rodent faunas, their paleogeographic pattern, and responses to climate changes from the early Eocene to the early Oligocene in Asia

Qian Li[1,2]*, Qi Li[1,3], Rancheng Xu[1,4] and Yuanqing Wang[1,2,4]

[1]Key Laboratory of Vertebrate Evolution and Human Origins of Chinese Academy of Sciences, Institute of Vertebrate Paleontology and Paleoanthropology, Chinese Academy of Sciences, Beijing, China, [2]CAS Center for Excellence in Life and Paleoenviroment, Beijing, China, [3]Centre for Vertebrate Evolutionary Biology, Yunnan University, Kunming, China, [4]College of Earth and Planetary Sciences, University of Chinese Academy of Sciences, Beijing, China

Rodents are an important component in Paleogene terrestrial ecosystems. Their evolution and faunal turnover have likely been influenced and triggered by global climate change. Here, we compiled rodent faunas from the early Eocene to the early Oligocene in Asia to discuss rodent faunal turnover and its correlation with paleogeographic and paleoclimate changes. Successive rodent faunas from the early Eocene to the early Oligocene are recorded in East Asia, and rodent faunal turnover is obviously affected by paleoclimatic changes. During the Ulangochuian (after the middle Eocene climatic optimum), when temperatures declined slowly, the East Asian rodent fauna showed a clear decline in generic diversity and a transformation from ctenodactyloid-dominant to cricetid–dipodid-dominant faunas. During the Eocene–Oligocene transition (EOT) and global cooling, the East Asian rodent fauna exhibited a considerably high generic diversity of cricetids, dipodids, and ctenodactylids. The low temperatures during the Ulangochuian and Ergilian in East Asia served as a habituation ground for the cricetids and dipodids, which became preadapted for the EOT, successfully helping rodents become dominant faunas after EOT. The rodent faunas in South Asia formed a relatively unique group in much of the Eocene and early Oligocene; sometimes, they were closer to European or African than to Asian rodents. The greatly different paleoenvironment probably caused striking differences between the rodent faunas in South Asia and East Asia.

KEYWORDS

Paleogene, climate change, rodent fauna, East Asia, South Asia

Introduction

Today, rodents are the most diverse and abundant terrestrial mammals. Rodents constitute over half the species of living mammals, and their fossil forms are also extremely diverse. Rodents are found worldwide, except for Antarctica and some oceanic

islands, and they exhibit a number of different lifestyles and locomotor behaviors. While generalized rodent adaptation is terrestrial, various forms are more specialized for climbing, gliding, swimming, or digging. Because of their large populations and short gestation periods, rodents have more advantages than other mammals in fauna in terms of biostratigraphic comparison and the relationship between mammal evolution and climate change.

The rodent fossil record has expanded at a significant pace, and fossils are increasingly discovered in regions that have been previously less known for fossils. In Asia, the complex rodent evolutionary history began during the early Eocene, from which the oldest fossils have been found (Li et al., 1989; Meng and Li, 2010; Li and Meng, 2015). The Paleogene is a key period for the origin and evolution of rodents, and the paleoclimate had multiple changes during the Paleogene (Westerhold et al., 2020), such as the global cooling event during the Eocene–Oligocene transitional period (Meng and McKenna, 1998; Kraatz and Geisler, 2010; Zhang et al., 2012; Sun et al., 2014); thus, we focus on rodent fossil records in Asia from the early Eocene to the early Oligocene. Furthermore, by taking advantage of an updated Cenozoic timescale in Asia (Romer, 1966; Luterbacher et al., 2004; Vandenberghe et al., 2012; Wang et al., 2019; Speijer et al., 2020), we use all available rodent faunal data and analyze rodent composition and diversity at the genus level, noting the different rodent assemblages and faunal turnovers. We discuss the possible relationships between the rodent evolution and faunal turnover and paleoclimatic changes. In addition, because different rodent assemblages also appeared in different areas of Asia during the same period, we consider the possible relationships between faunal dispersal and paleogeographic transformation.

Methods

Biochronology

Following the principle of North American land mammal ages, Romer (1966) proposed some related Asian Paleogene land mammal ages on the basis of mammalian faunas from different stratigraphic levels, which have formed the foundation for further Asian Paleogene chronostratigraphic study (Wang et al., 2019). These land mammal ages have often been used in discussing intercontinental biostratigraphic correlation and mammalian dispersals. Now, the Bumbanian, Arshantan, Irdinmanhan, Sharamurunian, Ulangochuian, and Ergilian ages in the Eocene, and the Hsandagolian age in the Oligocene have been adopted as the Asian Paleogene land mammal ages in the geologic time scales (Luterbacher et al., 2004; Vandenberghe et al., 2012; Speijer et al., 2020).

For many years, the Ulangochuian land mammal age that is currently used in the Chinese Paleogene land mammal age sequence was equivalent to both the Ulangochuian and Ergilian Asian land mammal ages (Tong et al., 1995; Vandenberghe et al., 2012). A recent investigation in the Erlian Basin, Nei Mongol, revealed that deposits between those with typical Ulangochuian and early Oligocene mammal faunas contain fossil mammals that are correlated to the Mongolian Ergilian fauna; thus, the Baiyinian land mammal age was proposed as the equivalent of the Ergilian in the Chinese Paleogene land mammal age sequence (Wang et al., 2019).

Here, these Asian Paleogene land mammal ages are used to indicate the evolution and turnover of rodent faunas in more detail. The ages of fossil localities are inferred based on the latest biostratigraphic, magnetostratigraphic, and radiometric dating.

Distribution of localities

Known rodent fossils are widely distributed in different areas of Asia, and the different mammalian fossil compositions may have been caused by paleogeographic patterns or may indicate different habitat conditions. The present study considers 35 localities that are biostratigraphically dated from the early Eocene to the early Oligocene (Appendix Tables 1–3) and assembled into three regions of Asia: East Asia (China and Mongolia), Central Asia (Kyrgyzstan and Kazakhstan), and South Asia (India, Pakistan, Thailand, and Myanmar) (Figure 1).

Taxonomy

Known rodent fossils were classified into different rodent families, and the taxonomic system of the family that was adopted in our analysis is as follows: Alagomyidae, Orogomyidae (Dashzeveg, 1990b), Aplodontidae (Wood, 1980), Anomaluroidea (Marivaux et al., 2005), Archetypomyidae (Meng et al., 2007), Castoridae, Sciuridae (McKenne and Bell, 1997), Ctenodactylidae (Wang, 1997a, 2001b), Cricetidae (Wang et al., 2020), Cylindrodontidae (Wood, 1980; Wang, 2019), Diatomyidae (Mein and Ginsburg, 1997), Dipodidae (Qiu and Wang, 2019), Eomyidae (Fejfar et al., 1998), Ischromyidae (Anderson, 2008), Tsaganomyidae (Wang, 2001a), and Zelomyidae (Dawson et al., 2003a).

Regarding ctenodactyloids, recent phylogenetic analysis indicated that some families or subfamilies, such as Cocomyinae, Advenimurinae (Dashzeveg, 1990a), Tamquammyidae (Averianov, 1996; Tong, 1997), Yuomyidae (Dawson et al., 1984; Tong, 1997), and Chapattimyidae (Averianov, 1996), are probably paraphyletic (Li and Meng, 2015). Because of the poor preservation of some early ctenodactyloid rodents and the complicated history of taxonomic studies on the group, it is extremely difficult to conduct a thorough phylogenetic analysis of ctenodactyloids. Some researchers have suggested the use of Ctenodactyloidea without reference to a specific family for the

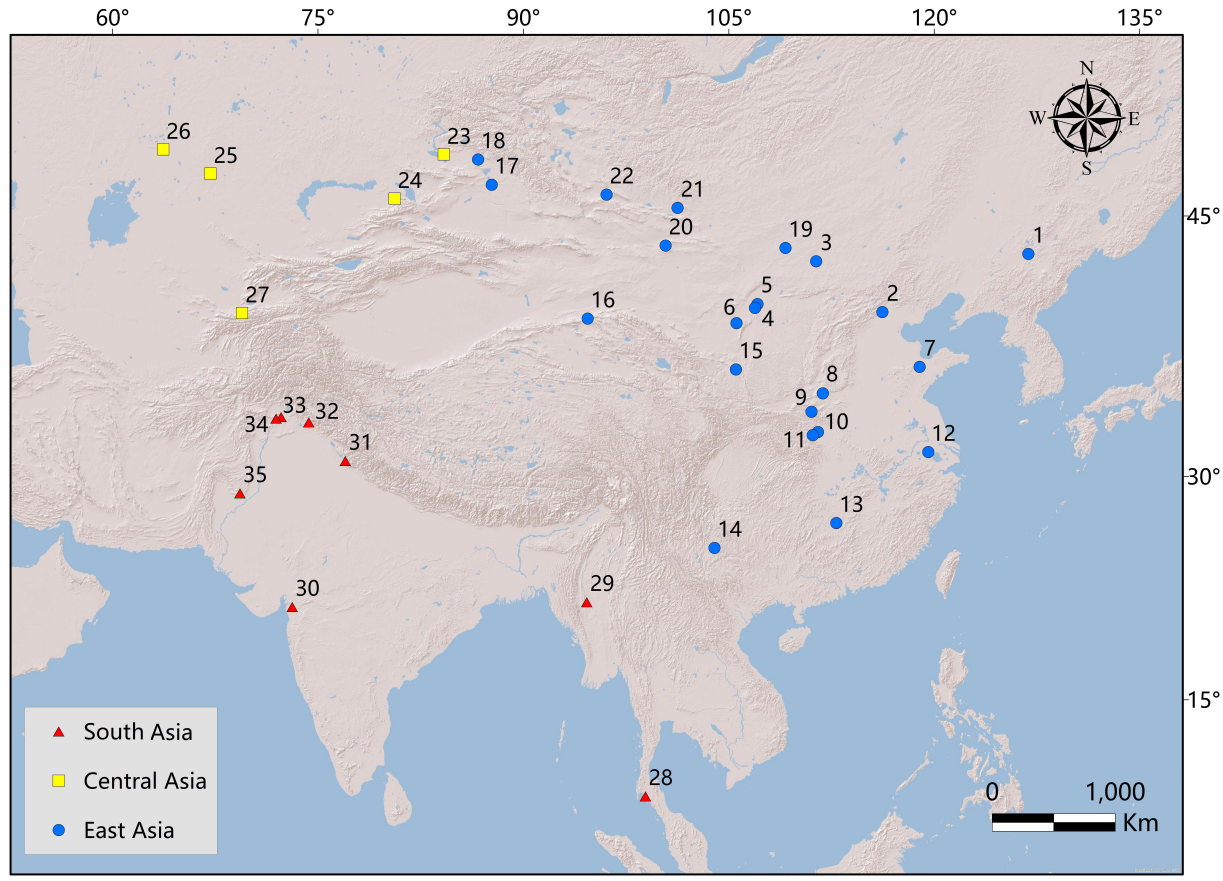

FIGURE 1
Principal Paleogene rodent localities of Asia are drawn in ArcMap10.3. Blue circles represent localities of East Asia, yellow squares represent localities of Central Asia, and red triangles represent localities of South Asia. Localities 1-17 are from China: 1. Huadian; 2. Changxindian; 3. Erlian Basin; 4. Qianlishan; 5. Saint Jacques; 6. Ulantatal; 7. Wutu; 8. Yuanqu; 9. Lushi; 10. Liguanqiao; 11. Danjiangkou; 12. Shanghuang; 13. Lingcha; 14. Caijiachong; 15. Haiyuan; 16. Danghe; 17 Ulungur River area; and 18. Burqin. Localities 19-22 are from Mongolia: 19. eastern Gobi Desert; 20. Nemegt Basin; 21. Valley of Lakes; and 22. Shine Us. Localities 23-26 are from Kazakhstan: 23. Zaysan; 24. Shinzhaly; 25. Kyzyl-Kak; and 26. Chelkar-Teniz; 27. Andarak 2 (Kyrgyzstan); 28. Krabi (Thailand); and 29. Pondaung (Myanmar). Localities 30–32 are from India: 30. Vastan; 31. Subathu; and 32. Kalakot. Localities 33–35 are from Pakistan: 33. Ganda Kas; 34. Chorlakki; and 35. Bugti Hills.

Eocene genera Dashzeveg and Meng, 1998; Li and Meng, 2015). Here, we also followed this opinion; most Eocene genera of ctenodactyloids included Ctenodactyloidea. Ctenodactylidae as a monophyletic is a generally accepted view; here, late Eocene *Karakoromys* and Oligocene ctenodactylids were included in Ctenodactylidae (Wang, 1997a, 2001b).

Indeterminate taxon identifications and taxonomic modifications, such as "cf." or "?", or some cases of "sp.", were included in our analyses as a record.

Diversity and sampling biases

The simplest method to count the number of taxa to measure biodiversity may produce biases that distort the diversity pattern due to the different preservation and sampling intensities of various fossils. The rarefaction method is widely used in paleontology for removing biases (Gotelli and Colwell, 2001; Shen et al., 2004; Huang, 2012); here, paleobiological biodiversity curves were corrected using rarefaction by PAST software (Hammer et al., 2001).

Results

Bumbanian rodent assemblage

Early Eocene Bumbanian rodent fossil assemblages are present in China, Mongolia, and India. In China, the Bumbanian rodent fossil localities are present in multiple regions, including Hunan, Hubei, Nei Mongol, Shandong, and Henan (Li, 1963; Dawson et al., 1984; Li et al., 1989, 2018; Hu, 1995; Tong, 1997; Guo et al., 2000; Wible et al., 2005; Tong and Wang, 2006; Meng and Li, 2010; Li and Meng, 2015). In addition, abundant rodent

fossils are found in the Bumban Member of the Naran-Bulak Formation of the Tsagan Khushu locality in the Nemegt Basin of Mongolia (Shevyreva, 1989; Dashzeveg, 1990a,b), and an ischyromyid rodent, *Meldimys*, is recorded in the lower Eocene Vastan lignite mine of western India (Rana et al., 2008); this occurrence is the oldest record of a rodent from India.

The Bumbanian rodent assemblages from China and Mongolia are similar in the dominance of original ctenodactyloids, and original rodents such as *Alagomys* are also present (Figure 2) (Appendix Table 1). Ctenodactyloid rodents in Bumbanian, as the oldest known rodents with modern features in Asia, already have a high diversity and are represented by different ctenodactyloid genera known primarily from China and Mongolia.

Except for ctenodactyloids, other basal rodent families are present in China and Mongolia. *Alagomys* is from the Erlian Basin of Nei Mongol of China and the Nemegt Basin of Mongolia. However, the validity of the familial association of *Alagomys* is still unknown. Meng and Wyss (2001) excluded *Alagomys* from the Rodentia, but others pointed out that *Alagomys* is close to true rodents and is generally considered the most primitive rodent (Dawson, 2015). Based on the similarities of *Alagomys* and the original ctenodactyloids and cylindrodontids, we also adopted *Alagomys* in Rodentia and Alagomyidae (Dashzeveg, 1990b). *Archetypomys* is a primitive rodent and occupies an intermediate phylogenetic position between alagomyids and rodents of modern features. Primitive ischyromyids, such as *Actioparamys* and *Taishanomys*, are also present in the Bumbanian rodent assemblage from China. *Orogomys* from the Nemegt Basin of Mongolia was classified as Orogomyidae (Dashzeveg, 1990b).

Arshantan rodent assemblage

The Arshantan rodent assemblages are known in East, Central, and South Asia. In East Asia, Arshantan rodents appeared in the Erlian Basin of Nei Mongol and in the Junggar Basin of Xinjiang, China (Meng et al., 2001; Li and Meng, 2010, 2015; Li et al., 2018; Li, 2019). The ∼2,900 Arshantan rodent specimens collected from the Erlian Basin represent at least 323 individuals, as counted by the minimum number of individuals (MNI), and rodents from the Erlian Basin have an absolute advantage in both number and species diversity. In Central Asia, abundant rodents are known at the Andarak 2 locality in Kyrgyzstan (Averianov, 1996) and the Zaysan Depression in eastern Kazakhstan (Shevyreva, 1984, 1996). The South Asian Arshantan rodents were described in the lower middle part of the Subathu Formation of the type area in Himachal Pradesh, northwestern sub-Himalaya, India (Gupta and Kumar, 2015).

In the Arshantan rodents, whether in East Asia, Central Asia, or South Asia, ctenodactyloids are a dominant element (Figure 3). In China, ctenodactyloids contain the primitive ctenodactyloid *Tamquammys*, *Chenomys*, *Simplicimys*, and *Advenimus*. Among them, *Tamquammys*, *Advenimus*, and *Chenomys* were present in the Bumbanian and in the Arshantan assemblage.

In Central Asia, ctenodactyloid rodents have high generic richness and are clearly different from East and South Asian ctenodactyloids in genera (Appendix Tables 1–3). Only *Advenimus* is present in East and Central Asia, which may suggest that some faunal exchanges occurred between East and Central Asia during the Arshantan. Only ctenodactyloids *Subathumys*, *Birbalomys*, and *Chapattimys* are present in South Asia. Except for various ctenodactyloids, in East Asia, the primitive myodont *Erlianomys* (Li and Meng, 2010), the basal cylindrodontid *Gobiocylindrodon* (Li et al., 2019), the primitive rodent *Archetypomys*, and some ischyromyid fossils (Li, 2016) from the Arshantan rodent assemblage are present (Figure 3). In Central Asia, the ischyromyids *Mneiomys*, *Paramys*, and *Abrosomys* were found in the Zaysan depression in Kazakhstan (Shevyreva, 1984, 1996).

The ctenodactyloids in Central Asia were classified as Chapattimyidae or Tamquammyidae by Averianov (1996) and Shevyreva (1984, 1989), and South Asian ctenodactyloids were included in Chapattimyidae (Gupta and Kumar, 2015). The phylogenetic analysis of these families indicated that they are not monophyletic (Li and Meng, 2015). Resolving phylogenetic problems is difficult and beyond the scope of this study. However, the P4/p4 morphology, either molariform or nonmolariform, has been frequently emphasized as an important characteristic in ctenodactyloid rodents. The ctenodactyloids classified as yuomyids and chapattimyids are distinguished from other ctenodactyloids by their molariform P4/p4 morphology. Recently, the characteristics of the molariform P4/p4 morphology have also been further clarified by Li and Meng (2015). According to the P4/p4 morphology, in the Arshantan, most East Asian ctenodactyloids present nonmolariform premolars, and the ctenodactyloids with molariform premolars are more commonly found in Central and South Asia. Gupta and Kumar (2015) described *Subathymys* from the Subathu Formation of India and pointed out that chapattimyids originated in the sub-Himalayan region during the Ypresian. According to the aforementioned description, ctenodactyloids with molariform premolars quite possibly originated from South Asia; they moderately diversified in Arshantan and spread rather quickly into Central Asia.

In summary, the Arshantan rodent assemblages in East, Central, and South Asia are distinct, and they rarely have the same genera.

Irdinmanhan rodent assemblage

The middle Eocene Irdinmanhan rodent assemblage is found in China in East Asia, eastern Kazakhstan in Central

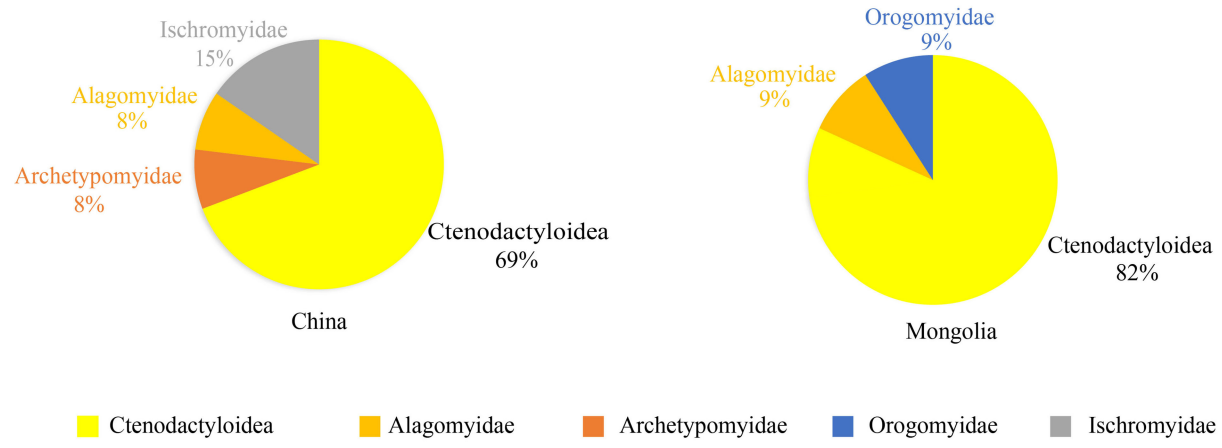

FIGURE 2
Diagrams of the Bumbanian rodent composition from China and Mongolia in East Asia (in percentage of genera).

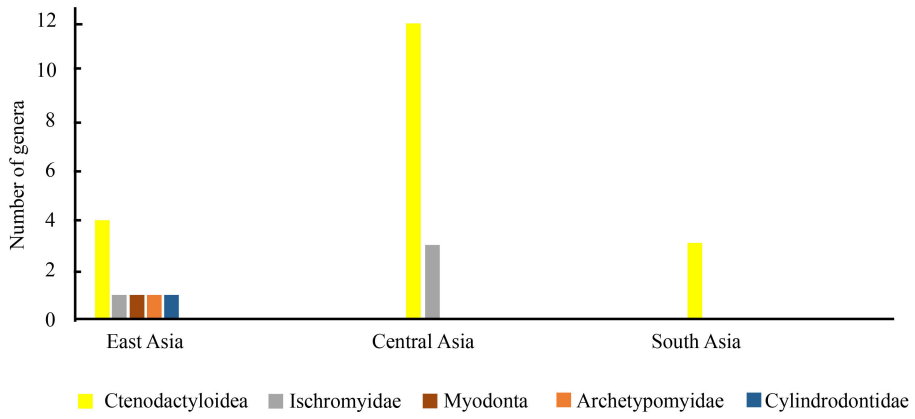

FIGURE 3
Diagram of the Arshantan rodent compositions in East, Central, and South Asia.

Asia, and Pakistan and India in South Asia. In China, the Irdinmanhan rodent fossil localities are known in Nei Mongol, Henan, Jiangsu, and Shanxi (Li, 1963, 2012; Tong, 1997; Dawson et al., 2003a, 2010; Li and Meng, 2013, 2015; Li et al., 2016, 2018; Fostowicz-Frelik et al., 2021). Irdinmanhan rodents are found in the Kolpak Formation of the Shinzhaly River in eastern Kazakhstan (Emry et al., 1998b). In South Asia, Irdinmanhan rodents have been recorded in the upper part of the Subathu Formation in India (Sahni and Khare, 1973; Sahni and Srivastava, 1976; Kumar et al., 1997a,b; Gupta and Kumar, 2015), the Kuldana Formation of the Ganda Kas area, and the Mami Khel Formation of the Chorlakki area in Pakistan (Hussain et al., 1978; Hartenberger, 1982; Dawson et al., 1984; Thewissen et al., 2001).

In East Asia, the Irdinmanhan rodent assemblage has more derived members than the Bumbanian and Arshantan rodent assemblages, such as cricetids, dipodids, zelomyids, and ? diantomyids (Appendix Table 1). The rodent faunas in some localities of the Erlian Basin in Nei Mongol and the Shipigou locality in Henan have been studied in detail based on the MNI (Tong, 1997; Li, 2016). The generic rodent number in Henan is the highest in China. Ctenodactyloids are major components in Henan and Nei Mongol, and cricetids, ischyromyids, and cylindrodontids are moderately diversified in the Irdinmanhan rodent assemblage (Figure 4). The few fossils of Zelomyidae and ? Diatomyidae appeared in the fissure D in the Shanghuang fissure in Liyang, Jigansu, and Huoshipou of the Yuanqu Basin, Shanxi (Dawson et al., 2003a, 2010).

The Irdinmanhan rodents in Kazakhstan are similar to those in China, and they also contain ctenodactyloids, dipodids, and cricetids. Ctenodactyloid *Saykanomys* and cricetid *Pappocricetodon* are present in China and Kazakhstan. In

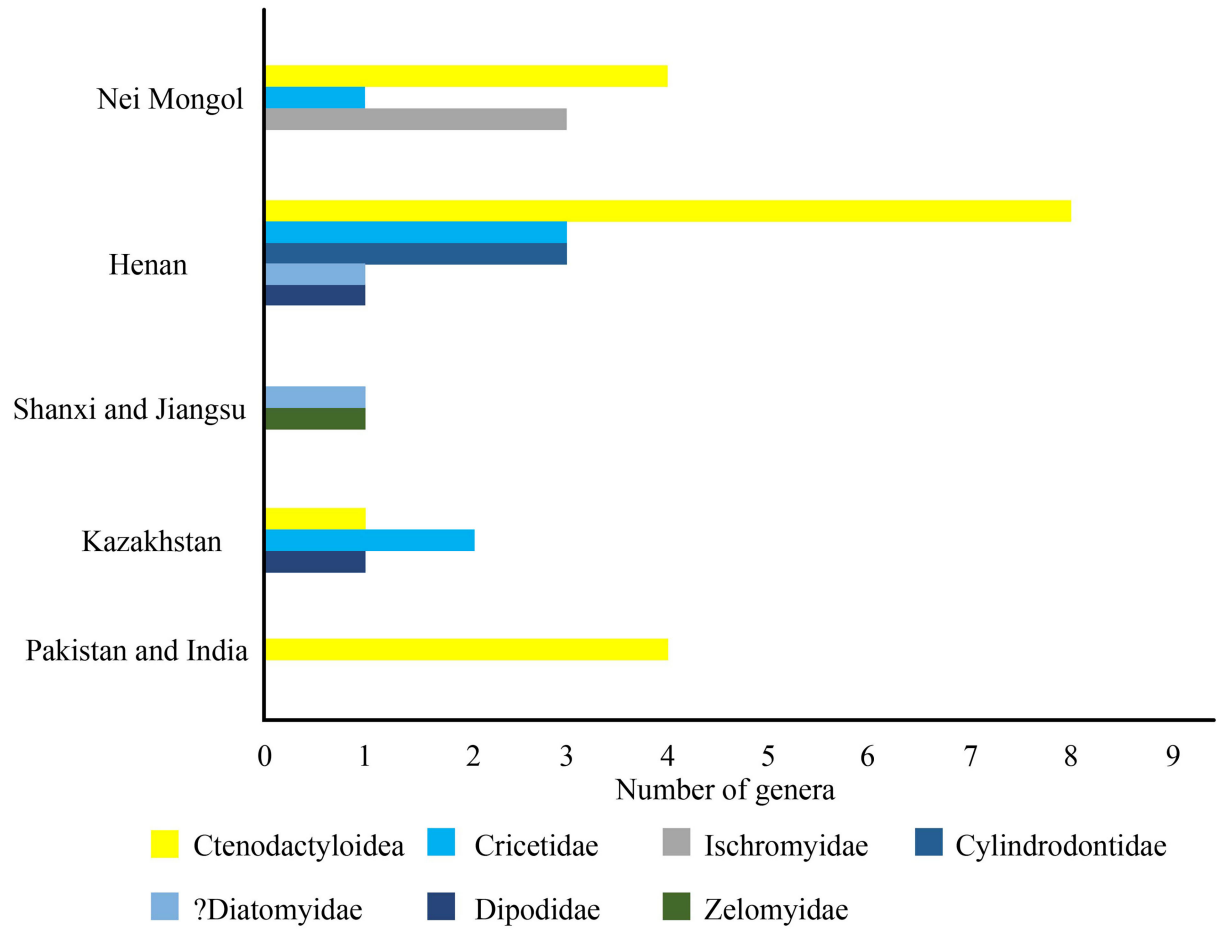

FIGURE 4
Diagram of the Irdinmanhan rodent compositions in East, Central, and South Asia.

South Asia, the Irdinmanhan rodent assemblage is distinctly different from the rodent assemblage in East and Central Asia and is characterized by only ctenodactyloids that were classified as Chapattimyidae (Gupta and Kumar, 2015). The Irdinmanhan rodents in India and Pakistan are very similar; the dominant elements in these areas are *Birbalomys* and *Chapattimys*, which first appeared in the Arshantan rodent assemblage in India (Gupta and Kumar, 2015), extended to the Irdinmanhan assemblage and showed high species diversity.

Sharamurunian rodent assemblage

The middle Eocene Sharamurunian rodent fossil localities are in Nei Mongol, Shanxi, Jilin, Jiangsu, and Henan in China (Dawson, 1968; Wang and Dawson, 1994; Tong, 1997; Wang et al., 1998; Meng et al., 1999; Dawson et al., 2003a; Li et al., 2016; Li, 2018, 2019). The Sharamurunian of the Asian Paleogene land mammal age proposed by Romer (1966) was derived from the Paleogene mammal fauna found in the Ula Usu locality of the Erlian Basin, Inner Mongolia. Studies on Sharamurunian rodent fossils in the classic locality are very limited (Li, 1975). Recently, abundant rodent fossils were found in the Ula Usu locality, and a detailed study of these fossils has been carried out.

In known localities, many rodent fossils of the Shanghe-Zhaili fauna in the Yuanqu Basin of Shanxi and the Erlian Basin of Nei Mongol are present, showing a variety of genera and species. The Sharamurunian rodent assemblages in the Yuanqu and Erlian Basins show similarities in family composition; they all contain ctenodactyloids, cricetids, dipodids, and ischyromyids, and many genera are present in both localities (Table 1). However, zelomyids and cylindrodontids are present in the Yuanqu and Erlian basins, respectively. The ctenodactyloids in the Yuanqu Basin show higher generic richness than those in the Erlian Basin, and *Gobiomys* is the

dominant ctenodactyloid genus in the Erlian Basin. Detailed analysis of the rodent fauna of the Sharamurunian in the Yuanqu and Erlian basins has been carried out based on the MNI. The results showed that cricetids and dipodids are dominant in the Yuanqu Basin, but in the Erlian Basin, ctenodactyloids and dipodids are dominant and secondary, respectively (Tong, 1997).

In other localities, such as Huadian in Jilin, Shanghuang fissure fillings in Jiangsu, and Lushi in Henan, only zelomyids of the Sharamurunian rodent fauna have been discovered in these areas (Dawson et al., 2003a).

In addition to China, a few Sharamurunian rodent materials have been found in South Asia. The Pondaung Formation of central Myanmar has yielded one of the most diversified Eocene land mammal faunas in South Asia. Geochronological evidence has definitely established a late middle Eocene age for the mammal-bearing strata of the Pondaung Formation, and both fission track analyses of zircon grains and paleomagnetic studies of strata from the Pondaung area suggest an age of approximately 40 Ma (Tsubamoto et al., 2002; Khin et al., 2014; Jaeger et al., 2019). Therefore, the age of the Pondaung fauna corresponds to the Sharamurunian, based on biostratigraphy, nannoplankton assemblage, and magnetostratigraphic and radiometric dating. Some rodent specimens from the Pondaung Formation have been reported and included in the rodent superfamily Anomaluroidea, which is currently limited to tropical and subtropical forests of western and central Africa (Tsubamoto et al., 2000; Dawson et al., 2003b; Marivaux et al., 2005). The rodent *Pondaungimys* from the Pondaung Formation is similar to *Nementchamys*, an anomaluroid from the late middle Eocene strata of Algeria. The close relationship between *Pondaungimys* and *Nementchamys* emphasizes the widespread South Asian–North African distribution of anomaluroid rodents, thus suggesting communication between South Asia and Africa during the Sharamurunian (Marivaux et al., 2005).

Ulangochuian rodent assemblage

Of the reported Ulangochuian rodents in East Asia, localities restricted to the redefined Ulangochuian land mammal age mainly include Nei Mongol and Yunnan in China (Wang, 1985, 2001a; Wang and Meng, 1986; Li, 2018, 2019, 2021).

In Nei Mongol, Ulangochuian rodents were reported in the Lower White to Middle White beds of the Erden Obo section in the Erlian basin, Nei Mongol (Li, 2018, 2019, 2021). The classic Houldjin site in the Erlian Basin is another important locality. A recent investigation showed that the reported Houldjin fauna was represented by a mixed assemblage due to reworking (Wang, 2008; Wang et al., 2009); thus, here, we do not include these fossils. The rodent in the lower part of the Chijiachong Formation of Qujing, Yunnan, was considered as the Ulangochuian rodent (Wang, 1985, 2001a; Wang and Meng, 1986; Maridet and Ni, 2013).

The Ulangochuian rodent assemblage in Yunnan and Nei Mongol contains ctenodactyloid, cricetid, and dipodid rodents, and the cylindrodontid rodents are present only in Nei Mongol (Figure 5). In both localities, ctenodactyloids are moderately diversified and show different generic compositions, but *Gobiomys* in Nei Mongol and *Youngomys* in Yunnan are a sister group in the phylogenetic analysis (Wang, 2001c). However, some genera appear in both localities during the Ulangochuian, such as cricetid *Eocricetodon*, dipodid *Allosminthus*, *Sinosminthus*, and *Heosminthus*.

Ergilian rodent assemblage

Late Eocene Ergilian rodent faunas are found in China and Mongolia in East Asia, Kazakhstan in Central Asia, and Thailand in South Asia.

Based on the biostratigraphic correlation, the age of the Upper Red beds of the Erden Obo section in the Erlian Basin, Nei Mongol, China, is the Ergilian land mammal age (Li, 2018). Ulantatal in Nei Mongol is another important site. Recently, Wasiljeff et al. (2020) derived a chronostratigraphic framework for the Ulantatal sequence, using paleomagnetic reversal stratigraphy and biostratigraphic correlation, and the time spanned by the strata was 35 to 27 Ma (from the latest Eocene to late Oligocene). The rodents in the lower part of the Kekeamu section in Ulantatal were representative of the latest Eocene (Wasiljeff and Zhang, 2022). In Mongolia, the Ergilian rodents were reported in the Ergilin Dzo Formation in the eastern Gobi Desert of Mongolia (Dashzeveg, 1993). The Zaysan Basin, eastern Kazakhstan, has a sedimentary section that includes strata spanning the Eocene–Oligocene boundary. The upper part of the Aksyir svita contains mammals, including abundant rodents that typically occur in the Ergilin Dzo fauna of Mongolia (Emry et al., 1998a).

The East and Central Asian Ergilian assemblage consists of ctenodactyloids, cricetids, dipodids, and cylindrodontids, and cricetids and dipodids are dominant. The rodent genera from Kazakhstan are all present in China and Mongolia in East Asia (Figure 6). In East Asia, the composition and dominant taxa of the Ergilian rodent assemblage are also similar to those of the Ulangochuian rodent faunas (Appendix Table 1). Ctenodactyloid *Gobiomys*, dipodid *Allosminthus*, *Heosminthus*, and *Sinosminthus* are present in the Ulangochuian and in the Ergilian assemblages.

In South Asia, *Baluchimys krabiense* has been found in the late Eocene strata in the Krabi Basin, Thailand. The striking affinities between *B. krabiense* and the late Eocene African *P. algeriensis* suggest faunal exchanges between South Asia and Africa during the Eocene (Marivaux et al., 2000).

TABLE 1 Sharamurunian rodent assemblages in China.

		Nei Mongol	Shanxi	Jilin	Jiangsu	Henan
Ctenodactyloidea	*Gobiomys*	√				
	Yuomys	√	√			
	Xueshimys		√			
	Zodiomys		√			
	Anadianomys		√			
	Protataromys		√			
Dipodidae	*Primisminthus*	√	√			
	Allosminthus	√	√			
	cf. *Sinosminthus*		√			
Cylindrodontidae	*Gobiocylindrodon*	√				
	Proardynomys	√				
Cricetidae	*Pappocricetodon*	√	√			
	Raricricetodon		√			
Ischyromyidae	*Eosischyromys*	√				
	Hulgana	√	√			
Zelomyidae	*Andersomys*		√			
	Zelomys			√		
	Haozi					√
	Suomys				√	

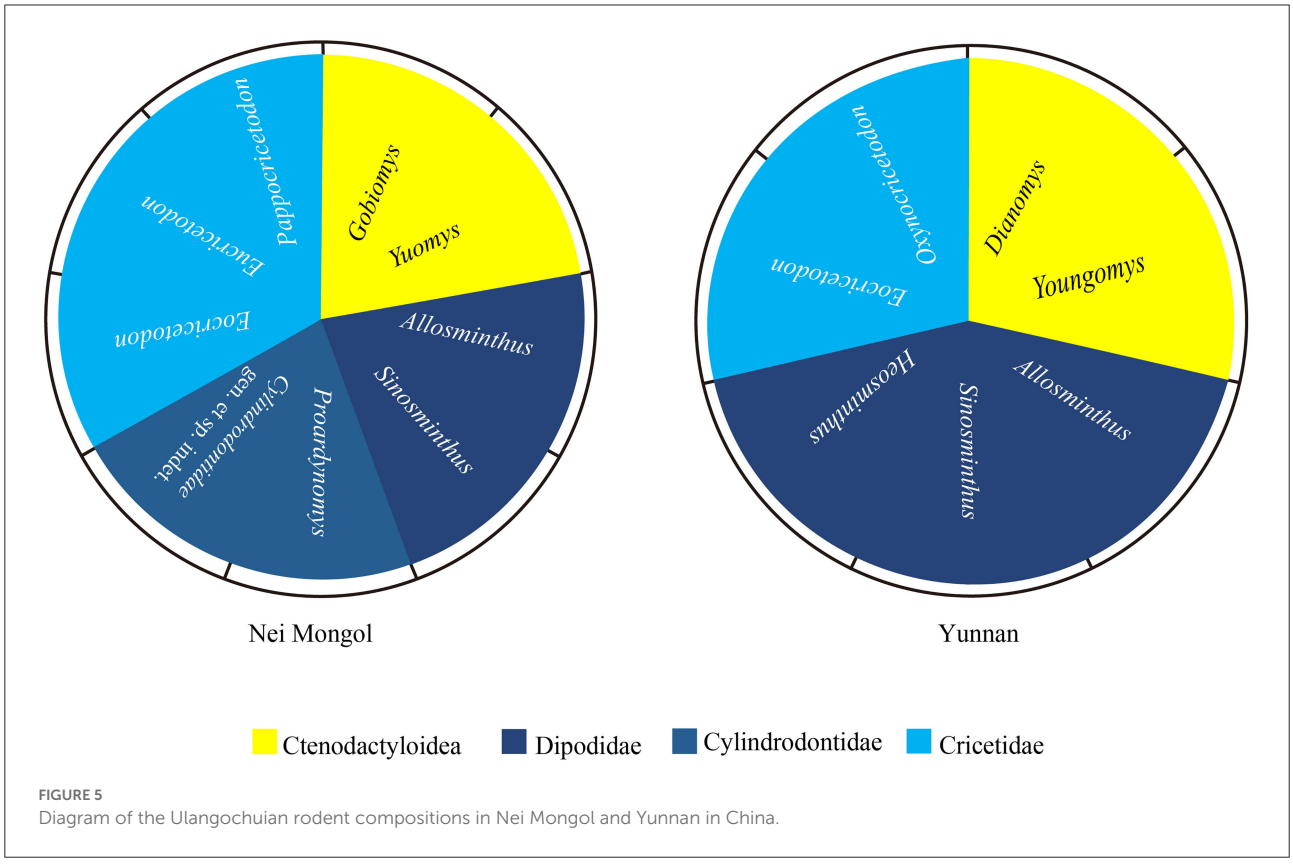

FIGURE 5
Diagram of the Ulangochuian rodent compositions in Nei Mongol and Yunnan in China.

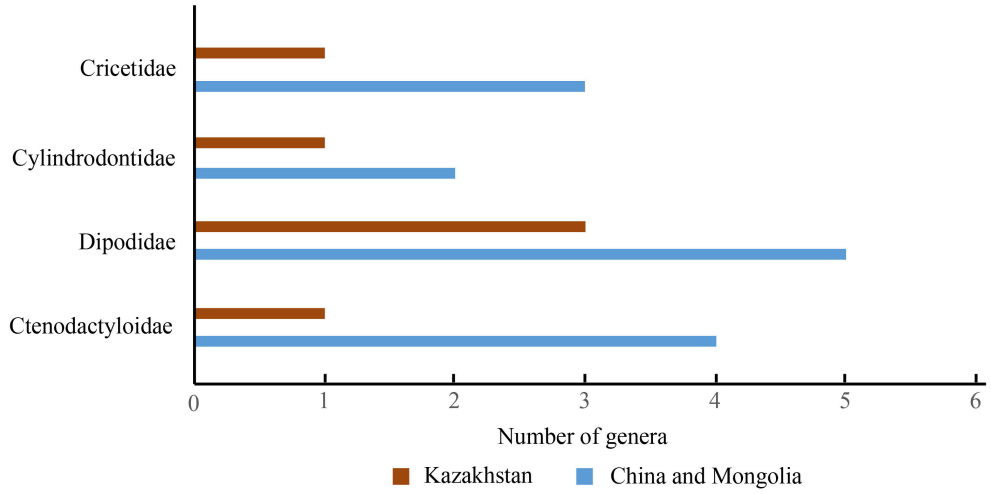

FIGURE 6
Diagram of the Ergilian rodent compositions in China and Mongolia in East Asia, and Kazakhstan in Central Asia.

Hsandagolian rodent assemblage

The Hsandagolian age corresponds to the Rupelian Stage and the lower part of the Chattian Stage (Speijer et al., 2020); thus, Hsandagolian includes the early Oligocene and part of the late Oligocene. Hsandagolian mammalian fossils are distributed in China, Mongolia, and Pakistan in Asia. In China, the Hsandagolian rodent mammals are found in the Ulantatal area, the "Upper White" beds of the Erlian Basin, Saint Jacques area and Qianlishan district in Nei Mongol (Wang, 1987; Wang and Emry, 1991; Wang and Qiu, 2003; Gomes Rodrigues et al., 2014; Li, 2018, 2021), the Burqin Basin in the northern area of Xinjiang (Wu et al., 2004; Ye et al., 2005), the Qingshuiying Formation in Haiyuan in Ningxia (Wang et al., 1994), the lower part of the Paoniuquan Formation in the Danghe Basin of Gansu (Wang and Qiu, 2004), and the upper part of the Caijiachong Formation in Qujing in Yunnan (Maridet and Ni, 2013; Li et al., 2017). The Oligocene deposits of the Ulantatal area in Nei Mongol contain rich rodent fossils, and a review of the rodent list was provided (Gomes Rodrigues et al., 2014). Based on earlier research in the area, the Ulantatal sequence was considered to be constrained to the Oligocene (Wang, 1997b; Gomes Rodrigues et al., 2014). Recently, Wasiljeff et al. (2020) redefined the stratigraphy and suggested that the Ulantatal Formation spans from the latest Eocene to the late Oligocene. Here, the Hsandagolian rodent assemblage in the Ulantatal area has been revised based on the latest work. The abundant Hsandagolian rodent fossils are mainly distributed in northern China, but few materials have been reported in South China.

Cenozoic sediments of the Valley of Lakes are rich in fossils that provide unique evidence of mammal evolution in Mongolia. The strata are intercalated with basalt flows, and $^{40}Ar/^{39}Ar$ data of the basalts frame the time of sediment deposition and mammal evolution and enable a composite age chronology for the Valley of Lakes area. Based on the radiometric ages of basalt and magnetostratigraphic data, the ages of Mongolian biozones A-C range from 33 to 25.6 Ma and correspond to the Hsandagolian (Daxner-Höck et al., 2010; Kraatz and Geisler, 2010). A total of 70 fossil beds in the Taatsiin Gol and Taatsiin Tsagaan Nuur areas in the Valley of Lakes yielded more than 19,000 mammal fossils, and rodent species composed 50% of the 175 mammal species in the study area (Daxner-Höck et al., 2017). Recently, a rich and diverse fossil assemblage in the Shine Us locality in southwestern Mongolia was described (Daxner-Höck et al., 2019).

The compositions of the Hsandagolian rodent assemblage in China and Mongolia are similar, and they include diverse small- to middle-sized rodents, such as dipodids, cricetids, ctenodactylids, cylindrodontids, eomyids, and large body-sized rodent tsaganomyids (Figure 7). Many genera in the Hsandagolian rodent assemblage are present in both Mongolia and China. In addition, in the Hsandagolian assemblage, castorids are found in China, and scuirids are present in Mongolia. In the Hsandagolian rodent assemblage in East Asia, cricetids, dipodids, and ctenodactylids are dominant, and some rodents are the earliest records of their family in China or Mongolia, such as Tsaganomyidae, Castoridae, and Aplodontidae.

The Asian record of the Dipodidae and Cricetidae dates back to the middle Eocene, where those families diversified and played a dominant role in Oligocene rodent communities. Recently, some dipodids and cricetids have been reported in European Oligocene strata (de Bruijn et al., 2019; Wessels et al., 2020), and these materials are the nearest fossil relatives to

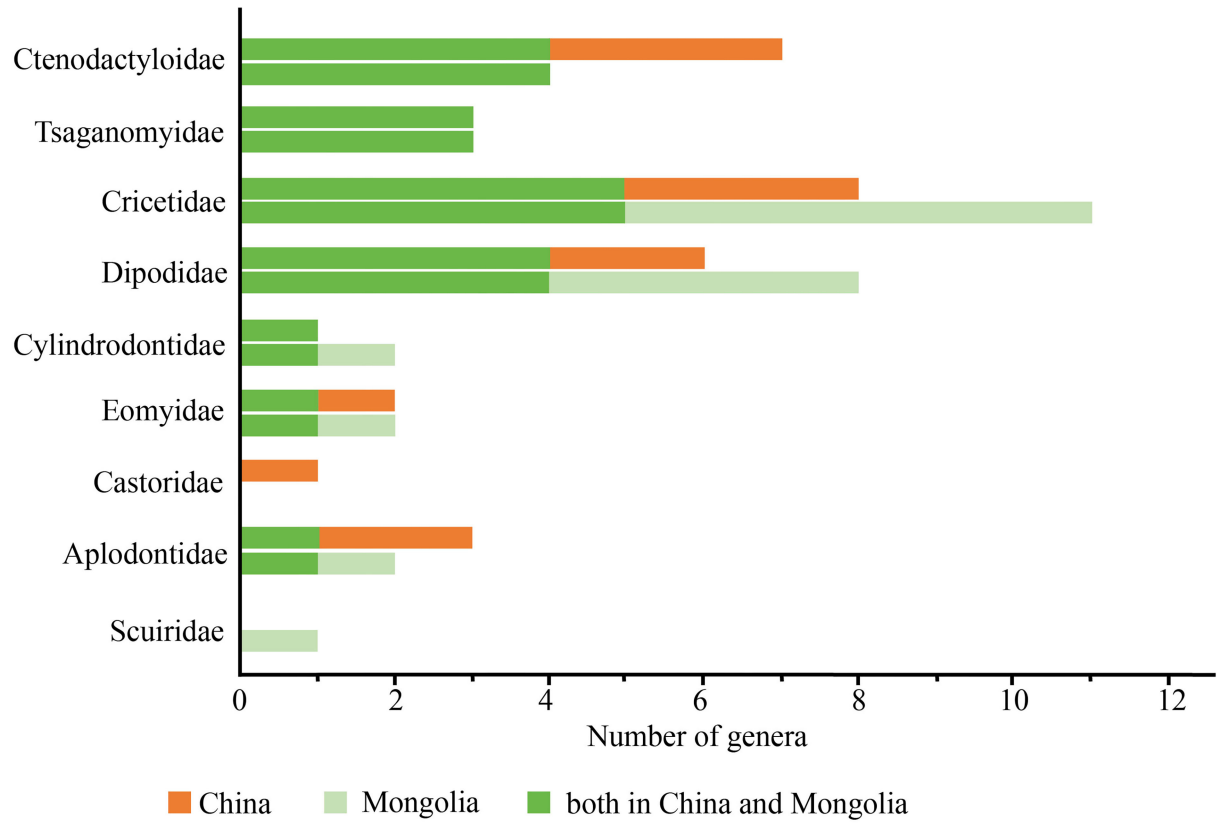

FIGURE 7
Diagrams of the Hsandagolian rodent composition in China and Mongolia.

those in Asian. As a result, dipodids and cricetids immigrated from Asia to Europe in the early Oligocene, and rodent faunal exchange over a large area was possible during the period, such as Dipodidae and cricetid Pappocricetodontinae.

A few rodent materials in Kazakhstan have been reported by Shevyreva (1971), and they are described as *Karakoromys* and *Prosciurus*. In the southwestern Sulaiman geological province (Balochistan, Pakistan), terrestrial detrital facies from the Bugti Hills region have yielded rich tertiary vertebrate faunas. The age of the lower Chitarwata Formation in the Bugti Hills is still controversial (Métais et al., 2017), but the rodents and the perissodactyls from the lower Chitarwata Formation clearly suggest an early Oligocene age (Marivaux et al., 1999; Welcomme et al., 2001; Marivaux and Welcomme, 2003; Métais et al., 2009; Antoine et al., 2013), which is correlative with the MP21-22 bio-horizons in Europe. The Bugti rodent fauna did not consist only of buluchimyines that were initially interpreted as a subfamily of the ctenodactyloid Chappatimyidae (sciurognathous) by Flynn et al. (1986) and yielded dipodids, anomaluroids, sciuroids, diatomyids, and typical early Oligocene cricetids (Appendix Table 3). Recently, a phylogenetic analysis showed no support for the monophyly of a baluchimyine clade, so "baluchimyines" were reinterpreted as Hystricognathi *incertae sedis*, and the phylogenetic results supported that "baluchimyines" and tsaganomyids were representatives of an initial phase of the diversification of hystricognathous rodents in Asia (Marivaux et al., 2002). The Pakistan Hsandagolian rodent fauna is significantly different from that in China and Mongolia; only Cricetidae and Dipodidae at the family level are common elements in East and South Asian rodent faunas, but the genera of these two families are different.

Discussion

South Asian rodent faunas

Using the updated Paleogene timescale in Asia (Wang et al., 2019; Speijer et al., 2020), we compiled a list of Asian rodent genera from the early Eocene to the early Oligocene (Appendix Tables 1–3). In general, the most complete rodent record from the early Eocene to the early Oligocene in Asia is recorded in East Asia, followed by South Asia, and there

are fewer Central Asian rodent records. Central Asia and East Asia share many common elements at the levels of rodent families and genera, but the rodent faunas in South Asia show unique characteristics.

In the Bumbanian ischyromyid *Meldimys* from India, which is close to the European ischormyids, the chapattimyids of Ctenodactyloidea are the only rodent group during the Arshantan and Irdinmanhan (Thewissen et al., 2001; Gupta and Kumar, 2015). In recent years, studies have suggested that some mammals from the Indian subcontinent and Asia mainland, such as perissodactyls and primates, have close phylogenetic connections at the genus level (Rose et al., 2009; Missiaen and Gingerich, 2012, 2014). These facts indicate that there was no impassable geographic barrier for the early Eocene mammals on the two patches of land. Ni et al. (2020) also pointed out that before the Sharamurunian of the Eocene, the mammalian faunas on the Indian subcontinent formed a relatively isolated group and were different from those on the Asian mainland. A recent study suggested the probable presence of strong seasonal rainfall similar to the modern South Asian monsoon in early Eocene India (Spicer et al., 2016; Ding et al., 2017). Obviously, the paleoenvironment in South Asia was different from the environment in East and Central Asia during the early Eocene. Therefore, before the Sharamurunian of the Eocene, the rodent faunas in South Asia formed a relatively isolated group and included some endemic species probably because the difference was caused by different paleoenvironments.

In the Sharamurunian assemblage, the anomaluroid *Pondaungimys* was found in Myanmar (Dawson et al., 2003b; Marivaux et al., 2005), and Hystricognathi *Baluchimys* was reported in the Ergilian in Thailand (Marivaux et al., 2000). They had close phylogenetic relationships with rodents from Africa and suggest the occurrence of faunal exchanges between South Asia and Africa during the Sharamurunian and Ergilian. Recent research has shown that since the Sharamurunian of the Eocene, the mammalian faunas in South and East Asia have started to mix together (Ni et al., 2020), but rodent faunas have not exhibited this situation. Rodent fossils from South Asia are present only in limited locations, and only a few specimens are present, so more complete and numerous specimens are needed to assess the rodent relationship between South and East Asia.

The Hsandagolian rodents from East Asia are mainly concentrated in the northern areas of East Asia (northern China and southern Mongolia). The Hsandagolian rodent faunas in South Asia are significantly different from those in China and Mongolia. Ni et al. (2016) suggested that the Indian subcontinent and Yunnan maintained large areas of tropical jungle habitats in the early Oligocene (Ni et al., 2016). Pound and Salzmann (2017) used an extensive palynological dataset and presented global vegetation and terrestrial temperature reconstructions for the Eocene–Oligocene transition (EOT). As a result, at the boundary of the Eocene and Oligocene, the reconstructed terrestrial temperatures showed a decline in the mean annual temperature ranges in the area that included northern China and southern Mongolia; by contrast, no change in temperature was reconstructed for India and tropical Asia. In addition, recent paleoclimate research has suggested that the Central Asian (Mongolia and northern China) steppe desert has existed since at least the Eocene (Barbolini et al., 2020). Obviously, during the early Oligocene, the paleoenvironment was different between South Asia and northern China and southern Mongolia, and the striking difference in the paleoenvironment probably caused the difference in rodent faunas.

East Asian rodent succession from the early Eocene to the early Oligocene and responses to paleoclimatic changes

In general, from the early Eocene to the early Oligocene, rodent faunas in East Asia have obvious succession, and generic rodent diversity fluctuated in relation to paleoclimatic changes. At the beginning of the early Eocene, ctenodactyloid rodents were the dominant elements and moderately diverged as early as the earliest Eocene during the Paleocene–Eocene thermal maximum (PETM) (Figures 8, 9, Table 2). An abrupt increase in diversity during the Irdinmanhan and Sharamurunian is likely related to the rising temperatures of the middle Eocene climatic optimum. Cricetids and dipodids were first found in the Irdinmanhan and Sharamurunian and had some diversity.

A conspicuous event occurred between the Sharamurunian and the Ulangochuian; the generic diversity of rodents was reduced (Figure 9), and the ctenodactyloid-dominant rodent faunas were gradually replaced by the cricetid–dipodid-dominant faunas (Figure 8). Based on the MNI, the rodent assemblages of the Erden Obo section in Nei Mongol also showed a transformation from ctenodactyloid-dominant to cricetid–dipodid-dominant faunas in the Eocene Ulangochuian (Li, 2018). Similarly, perissodactyls and the entire mammalian fauna from China showed a similar abrupt decrease after the Sharamurunian in terms of the number of both species and genera (Wang et al., 2007; Bai et al., 2020). Bai et al. (2020) named the event the "Ulan Gochu Decline", and the event was comparable to the contemporaneous post-Uintan decline of the North American land fauna (Berggren and Prothero, 1992) and probably related to the sustained cooling following the middle Eocene climatic optimum (MECO).

The Asian mammalian faunal turnover during the EOT was known as the "Mongolian remodeling", with the perissodactyl-dominant fauna replaced by the rodent/lagomorph-dominant fauna, and it was a turnover that was attributed to the dramatic drop in temperature at the end of the Eocene (Meng and McKenna, 1998). Perissodactyls in China showed a

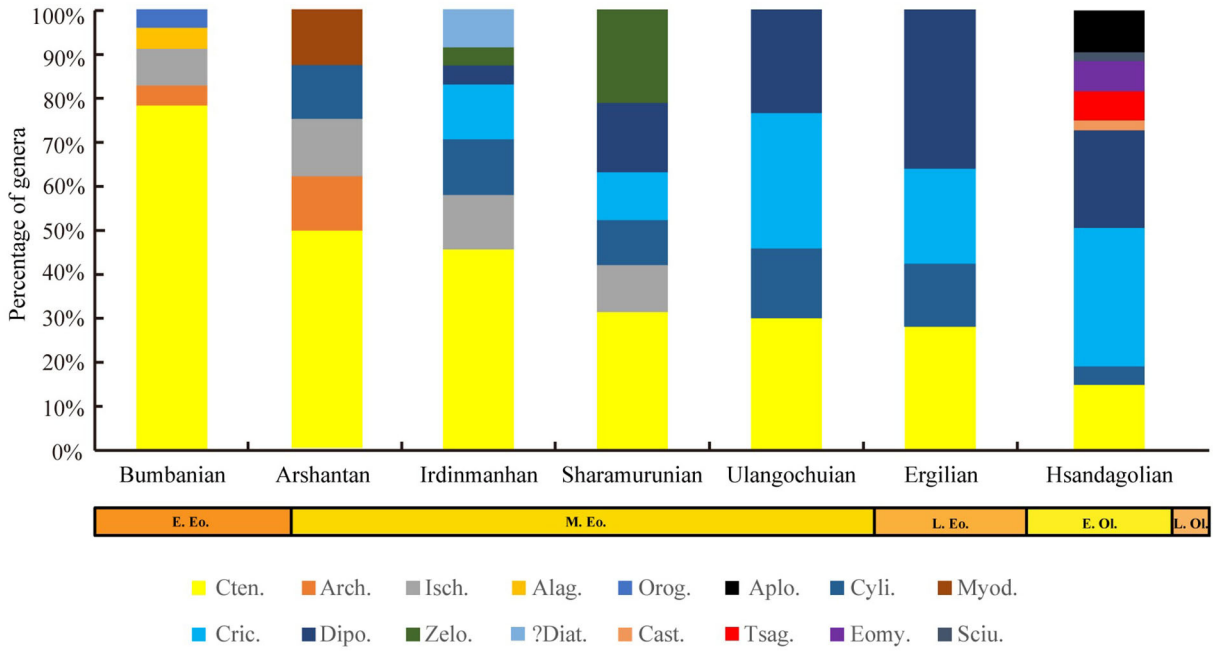

FIGURE 8
East Asian rodent composition from the early Eocene to the early Oligocene. Aplo., Aplodontidae; Arch., Archetypomyidae; Alag., Alagomyidae; Cast., Castoridae; Cten., Ctenodactyloidea; Cric., Cricetidae; Cyli., Cylindrodontidae; Diat., Diatomyidae; Dipo., Dipodidae; Eomy., Eomyidae; Isch., Ischromyidae; Myod., Myodonta; Sciu., Sciuridae; Tsag., Tsaganomyidae; Orog., Orogomyidae; Zelo., Zelomyidae.

decrease in terms of generic number during the EOT, but the decline was not as obvious as in the "Ulan Gochu Decline" (Bai et al., 2020). However, during the EOT, the generic diversity of rodents obviously increased (Figure 9), cricetid–dipodids were still dominant elements in rodent faunas (Figure 8), and the generic diversity of cricetids and dipodids also obviously increased compared with than that in the Ulangochuian and Ergilian.

In summary, the Eocene rodent faunas in East Asia showed two different changes in diversity, which may be related to global climatic declines. The first change occurred after the MECO when temperatures declined slowly and manifested as a clearly decreased diversity of rodents and a transformation from ctenodactyloid-dominant to cricetid–dipodid-dominant faunas. The second change occurred at the EOT and may have been a response to the sudden global drop in temperature; the change was manifested as a high generic diversity of cricetids, dipodids, and ctenodacylids and the appearance of rodent families such as Tsaganomyidae, Castoridae, and Eomyidae.

Based on the aforementioned discussion, after the dramatic drop in temperature, rodents became the dominant element in the Oligocene mammal fauna, but not overnight. The low temperatures during the Ulangochuian and Ergilian in East Asia served as a habituation ground for the cricetids and dipodids, which became preadapted for the EOT, successfully helping the rodent become the dominant fauna after the EOT.

Conclusion

Successive Asian rodent faunas from the early Eocene to the early Oligocene are recorded in East Asia, and the rodent records in Central and South Asia are incomplete. Central Asia and East Asia share many common elements at the rodent family and genus levels. The rodent faunal turnover in East Asia was obviously affected by paleoclimatic changes. During the Irdinmanhan and Sharamurunian, East Asian rodent faunas showed an increase in the diversity of genera and families, which may be related to the rising temperatures of the mid-Eocene climatic optimum. In the Ulangochuian (after the MECO), when temperatures declined slowly, the rodent fauna showed a clear decline in the diversity at the genus level and a transformation from ctenodactyloid-dominant to cricetid–dipodid-dominant faunas. During the Eocene–Oligocene transition (EOT) and global cooling, the East Asian rodent fauna is shown by the considerably high generic diversity of cricetids, dipodids, and ctenodactylids. The low temperatures during the Ulangochuian and the Ergilian in East Asia served as a habituation ground for the cricetids and dipodids, which became preadapted for the EOT, successfully helping the rodent as the dominant fauna after the EOT.

Before the Sharamurunian of the Eocene and the early Oligocene, the South Asian rodent faunas showed unique characteristics, and the striking differences between the rodent

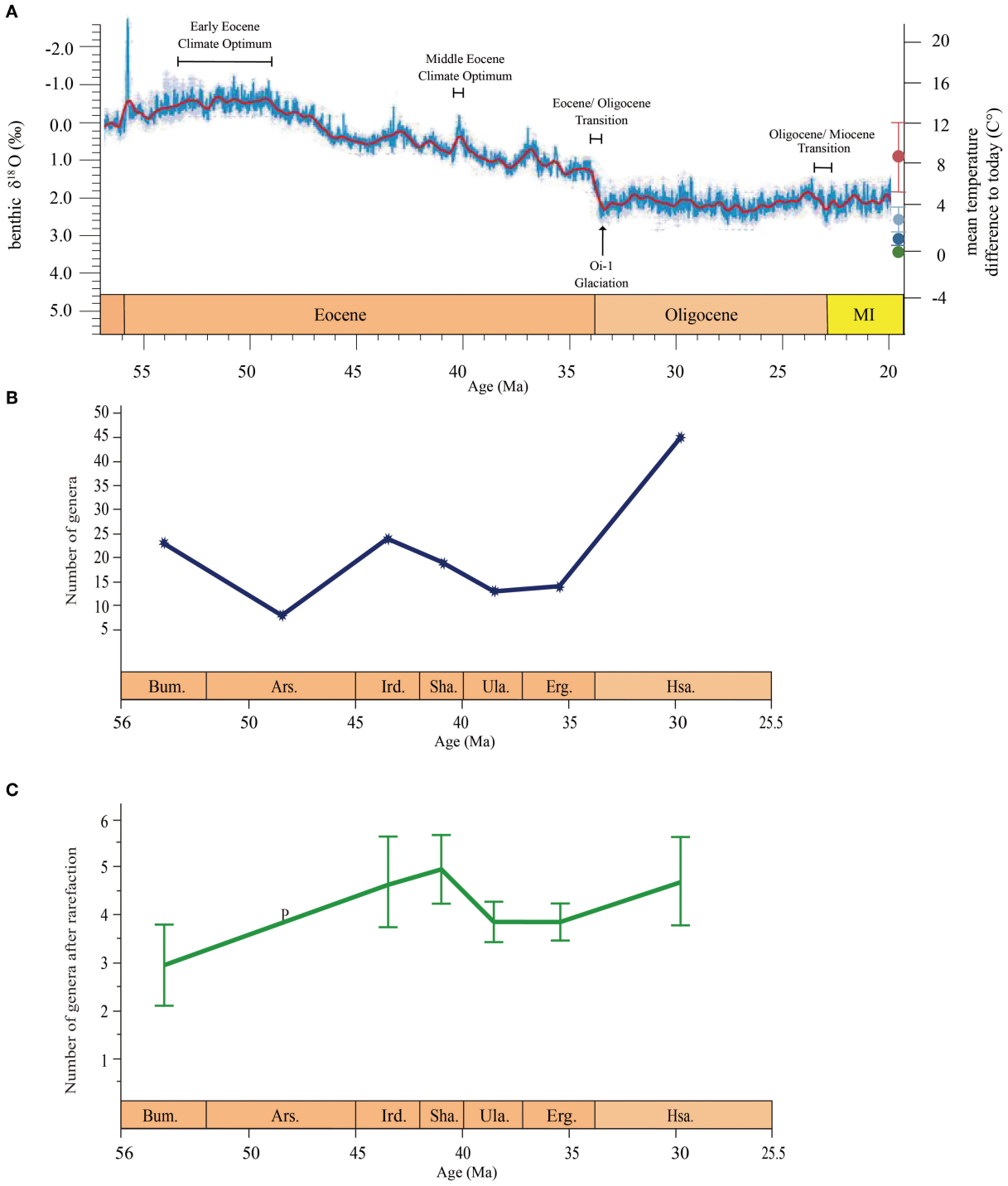

FIGURE 9
(A,B) East Asian rodent genus-level diversity from the early Eocene to the early Oligocene in relation to global climatic change (modified from Westerhold et al., 2020). **(C)** Rodent diversity trajectory based on rarefaction estimates of genus richness for each series at a sample size of five genus occurrences. Error bars depict 95% confidence intervals around the estimates. Bum., Bumbanian; Ars., Arshantan; Ird., Irdinmanhan; Sha., Sharamurunian; Ula., Ulangochuian; Erg., Ergilian; Hsa., Hsandagolian.

TABLE 2 Generic numbers of different rodent groups from early Eocene to early Oligocene in East Asia.

	Bumbanian	Arshantan	Irdinmanhan	Sharamurunian	Ulangochuian	Ergilian	Hsandagolian
Cten.	18	4	11	6	4	4	7
Arch.	1	1					
Isch.	2	1	3	2			
Alag.	1						
Orog.	1						
Cyli.		1	3	2	2	2	2
Myod.		1					
Cric.			3	2	4	3	14
Dipo.			1	3	3	5	10
Zelo.			1	4			
?Diat.		2	2				
Cast.							1
Tsag.							3
Eomy.							3
Scui.							1
Aplo.							4
Sum	23	10	24	19	13	14	45
N. Loc.	6	2	5	6	2	3	10

Aplo, Aplodontidae; Arch, Archetypomyidae; Alag, Alagomyidae; Cast, Castoridae; Cten, Ctenodactyloidea; Cric, Cricetidae; Cyli, Cylindrodontidae; Diat, Diatomyidae; Dipo, Dipodidae; Eomy, Eomyidae; Isch, Ischromyidae; Myod, Myodonta; Sciu, Sciuridae; Tsag, Tsaganomyidae; Orog, Orogomyidae; Zelo, Zelomyidae; N. Loc., the number of localities.

faunas in South Asia and those in East Asia were probably the result of different paleoenvironmental habitats. In the Sharamurunian and Ergilian, rodents in South Asia have close phylogenetic relationships with rodents from Africa and suggest the occurrence of faunal exchanges between South Asia and Africa.

Data availability statement

The original contributions presented in the study are included in the article/Supplementary material, further inquiries can be directed to the corresponding author.

Author contributions

QiaL designed the study and wrote the manuscript. QiL and RX analyzed the data. YW helped revise the manuscript and gave some useful suggestions. All authors contributed to the manuscript and approved the submitted version.

Funding

This research was funded by the National Natural Science Foundation of China (Grant 42072023) and the Strategic Priority Research Program of Chinese Academy of Sciences (XDB26000000). The fieldwork was also supported by the Special Fund for Fossil Excavation and Preparation, CAS.

Acknowledgments

We thank Jin Meng, Bin Bai, Xun Jin, Ping Li, K. C. Beard, D. L. Gebo, Xijun Ni, Wei Chen, Wei Zhou, Wei Gao, and Shijie Li for their assistance in the fieldwork. Wang Bian helped improve English in the text. We are grateful to the editors and reviewers for their constructive comments on our manuscript.

Conflict of interest

The authors declare that the research was conducted in the absence of any commercial or financial relationships that could be construed as a potential conflict of interest.

Publisher's note

Supplementary material

The Supplementary Material for this article can be found online at: https://www.frontiersin.org/articles/10.3389/fevo.2022.955779/full#supplementary-material

References

Anderson, D. (2008). "Ischyromidae," in *Evolution of Tertiary Mammals of North American*, eds. C. M. Janis, G. F. Gunnell, and M. D. Uhen (New York: Cambridge University press) 311–325.

Antoine, P. O., Métais, G., Orliac, M. J., Crochet, J. Y., Flynn, L. J., Marivaux, L., et al. (2013). "Mammalian Neogene biostratigraphy of the Sulaiman Province, Pakistan," in *Fossil Mammals of Asia*, eds. X. Wang, L. J. Flynn, and M. Fortelius (San Francisco: California University Press), 400–422. doi: 10.7312/columbia/9780231150125.003.0016

Averianov, A. O. (1996). Early Eocene Rodentia of Kyrgyzstan. *Bull. Mus. Natl. Hist. Nat.* 18C, 663–671. doi: 10.1127/njgpm/1996/1996/739

Bai, B., Meng, J., Janis, C. M., Zhang, Z. Q., and Wang, Y. Q. (2020). Perissodactyl diversities and responses to climate changes as reflected by dental homogeneity during the Cenozoic in Asia. *Ecol. Evol.* 00, 1–23. doi: 10.1002/ece3.6363

Barbolini, N., Woutersen, A., Dupont-Nivet, G., Silvestro, D., Tardif, D., Coster, P. M. C., et al. (2020). Cenozoic evolution of the steppe-desert biome in Central Asian. *Sci. Adv.* 6, eabb8227. doi: 10.1126/sciadv.abb8227

Berggren, W. A., and Prothero, D. R. (1992). "Eocene-Oligocene climatic and biotic evolution: An overview." in *Eocene–Oligocene climatic and biotic evolution*, eds. W. A. Berggren, and D. R. Prothero (Princeton, NJ: Princeton University Press), 1–28. doi: 10.1515/9781400862924.1

Dashzeveg, D. (1990a). The earliest rodents (Rodentia, Ctenodactyloidea) of Central Asia. *Acta Zool. Cracov.* 33, 11–35.

Dashzeveg, D. (1990b). New trends in adaptive radiation of Early Tertiary rodents (Rodentia, Mammalia). *Acta Zool. Cracov.* 33, 37–44.

Dashzeveg, D. (1993). A synchronism of the main mammalian faunal events near the Eocene–Oligocene boundary. *Ter. Res.* 14, 141–149.

Dashzeveg, D., and Meng, J. (1998). New Eocene ctenodactyloid rodents from the eastern Gobi desert of Mongolia and a phylogenetic analysis of ctenodactyloids based on dental features. *Am. Muse. Novit.* 3246, 1–20.

Dawson, M. R. (1968). Oligocene rodents (Mammalia) from East Mesa, Inner Mongolia. *Am. Muse. Novit.* 2324, 1–12.

Dawson, M. R. (2015). "Emerging perspectives on some Paleogene sciurognath rodents in Laurasia: the fossil record and its interpretation," in *Evolution of the Rodents: Advances in Phylogeny, Functional Morphology and Development*, eds. P. G. Cox and L. Hautier (Cambridge: Cambridge University Press), 70–86. doi: 10.1017/CBO9781107360150.004

Dawson, M. R., Huang, X. S., Li, C. K., and Wang, B. Y. (2003a). Zelomyidae, a new family of Rodentia (Mammalia) from the Eocene of Asia. *Vert. PalAsiat.* 41, 249–270.

Dawson, M. R., Li, C. K., and Qi, T. (1984). Eocene ctenodactyloid rodents (Mammalia) of eastern and central Asia. *Carnegie Mus. Na.t Hist. Special Publ.* 9, 138–150.

Dawson, M. R., Li, C. K., and Qi, T. (2010). The diatomyidae (Mammalia, Rodentia) and bilophodonty in Middle Eocene Asian rodents. *Vert. PalAsiat.* 48, 328–335.

Dawson, M. R., Tsubamoto, T., Takai, M., Egi, N., Tun, S. T., and Sein, C. (2003b). Rodents of the family Anomaluridae (Mammalia) from Southeast Asia (middle Eocene, Pondaung Formation, Myanmar). *Ann. Carnegie Mus.* 72, 203–213. doi: 10.5962/p.215090

Daxner-Höck, G., Badamgarav, D., Barsbold, R., Bayarmaa, B., Erbajeva, M., Göhlich, U. B., et al. (2017). Oligocene stratigraphy across the Eocene and Miocene boundaries in the Valley of Lakes (Mongolia). *Palaeobio. Palaeoenv.* 97, 111–218. doi: 10.1007/s12549-016-0257-9

Daxner-Höck, G., Badamgarav, D., and Erbajeva, M. (2010). Oligocene stratigraphy based on a sediment-basalt association in Central Mongolia (Taatsiin Gol and Taatsiin Tsagaan Nuur Area, Valley of Lakes): review of a Mongolian-Austrian project. *Vert. PalAsiat.* 48, 348–366.

Daxner-Höck, G., Erbajeva, M. A., Göhlich, U. B., Lopez-Guerrero, P., Narantsetseg, T., Mennecart, B., et al. (2019). The Oligocene vertebrate assemblage of Shine Us (Khaliun Basin, south western Mongolia). *Ann. Naturhist. Mus. Wien, Serie A.* 121, 195–256.

de Bruijn, H., Marković, Z., Wessels, W., and van de Weerd, A. A. (2019). Pappocricetodontinae (Rodentia, Muridae) from the Paleogene of south-east Serbia. *Palaeobio. Paleoenv.* 99, 511–526. doi: 10.1007/s12549-018-0343-2

Ding, L., Spice, R. A., Yang, J., Xu, Q., Cai, F., Li, S., et al. (2017). Quantifying the rise of the Himalaya orogen and implications for the South Asian monsoon. *Geology.* 45: 215–218. doi: 10.1130/G38583.1

Emry, R. J., Lucas, S. G., Tyutkova, L. A., and Wang, B. Y. (1998a). The Ergilian-Shandgolian (Eocene-Oligocene) transition in the Zaysan Basin, Kazakstan. *Bull. Carnegie Mus. Nat. Hist.* 34, 298–312.

Emry, R. J., Tyutkova, L. A., Lucas, S. G., and Wang, B. Y. (1998b). Rodents of the middle Eocene Shinzhaly fauna of Eastern Kazakstan. *J. Vert. Pale.* 18, 218–227. doi: 10.1080/02724634.1998.10011045

Fejfar, O., Rummel, M., and Tomida, Y. (1998). "New eomyid genus and species from the Early Miocene (MN zones 3-4) of Europe and Japan related to *Apeomys* (Eomyidae, Rodentia, Mammalia)." In: *Advances in Vertebrate Paleontology and Geochronology*, eds. Tomida, Y., Flynn, L. J., Jacpbs, I. I. (Tokyo: Nat Sci Mus Monographs), 14, 123–143.

Flynn, L. J., Jacobs, L. L., and Cheema, I. U. (1986). Baluchimyinae. A new Ctenodactyloid Rodent subfamily from the Miocene of Baluchistan. *Am. Muse. Novit.* 2841, 1–58.

Fostowicz-Frelik, L., López-Torres, S., and Li, Q. (2021). Tarsal morphology of ischyromyids rodents from the middle Eocene of China gives an insight into the group's diversity in Central Asia. *Sci. Rep.* 11:11543. doi: 10.1038/s41598-021-90796-1

Gomes Rodrigues, H., Marivaux, L., and Vianey-Liaud, M. (2014). Rodent paleocommunities from the Oligocene of Ulantatal (Inner Mongolia, China). *Palaeovertebrata.* 38, 1–12. doi: 10.18563/pv.38.1.e3

Gotelli, N. J., and Colwell, R. K. (2001). Quantifying biodiversity: procedures and pitfalls in the measurement and comparison of species richness. *Ecol. Lett.* 4, 379–391. doi: 10.1046/j.1461-0248.2001.00230.x

Guo, J. W., Wang, Y., and Yang, X. A. (2000). A new early Eocene ctenodactyloid rodent (Rodentia, Mammalia) and the associated mammalian fossils from Danjiangkou, Hubei. *Vert. PalAsiat.* 38, 303–313.

Gupta, S., and Kumar, K. (2015). Early Eocene rodents (Mammalia) from the Subathu Formation of type area (Himachal Pradesh), NW sub-Himalaya, India: Palaeobiogeographic implications. *J. Earth Syst. Sci.* 124, 1201–1221. doi: 10.1007/s12040-015-0607-4

Hammer, Ø., Harper, D. A. T., and Ryan, P. D. (2001). PAST: Palaeontological statistics software package for education and data analysis. *Pala. Elec.* 4, 1–9.

Hartenberger, J. L. (1982). A review of the Eocene rodents of Pakistan. *Contrib. Mus. Paleontol. Univ. Michigan.* 26, 19–35.

Hu, Y. M. (1995). New late early Eocene ctenodactyloid rodents (Rodentia, Mammalia) from Danjiangkou, Hubei. *Vert. PalAsiat.* 33, 24–38.

Huang, B. (2012). Rarefaction and its application to the study of diversity of palaeocommunities. *Acta Palae. Sin.* 51, 200–208.

Hussain, S. T., de Bruijn, H., and Leinders, J. M. (1978). Middle Eocene rodents from the Kala Chitta Range (Punjab, Pakistan). *Proc. Konink. Nederl. Akad. Wetensch. Ser. B.* 81, 74–112.

Jaeger, J.-J., Chavasseau, O., Lazzari, V., Soe, A. N., Sei, C., Maitre, A. L., et al. (2019). New Eocene primate from Myanmar shares dental characters with African Eocene crown anthropoids. *Nature Comm.* 10, 3511. doi: 10.1038/s41467-019-11295-6

Khin, Z., Meffre, S., Takai, M., Suzuki, H., Burret, C., Htike, T., et al. (2014). The oldest anthropoid primates in SE Asia: Evidence from LA-ICP-MS U-Pb zircon age in the Late Middle Eocene Pondaung Formation, Myanmar. *Gondwana Res.* 26, 122–131. doi: 10.1016/j.gr.2013.04.007

Kraatz, P., and Geisler, J. H. (2010). Eocene-Oligocene transition in Central Asia and its effects on mammalian evolution. *Geology.* 38, 111–114. doi: 10.1130/G30619.1

Kumar, K., Loyal, R. S., and Srivastava, R. (1997a). Eocene rodents from new localities in Himachal Pradesh, northwest Himalaya, India: Biochronologic implications. *J. Geol. Soc. India.* 50, 461–474.

Kumar, K., Srivastava, R., and Sahni, A. (1997b). Middle Eocene rodents from the Subathu Group, northwest Himalaya. *Palaeovertebrata.* 26, 83–128.

Li, C. K. (1963). Paramyid and scuiravids from North China. *Vert. PalAsiat.* 7, 151–160.

Li, C. K. (1975). *Yuomys*, a new ischyromyoid rodent genus from the Upper Eocene of North China. *Vert. PalAsiat.* 13, 58–70.

Li, C. K., Zheng, J. J., and Ting, S. Y. (1989). "The skull of *Cocomys lingchaensis*, an Early Eocene ctenodactyloid rodent of Asia," in *Papers on Fossil Rodents in Honor of Albert Elmer Wood*, eds. C. C. Black, and M. R. Dawson (Los Angeles, NHMLAC Press), 179–192.

Li, L. Z., Ni, X. J., Lu, X. Y., and Li, Q. (2017). First record of Cricetops rodent in the Oligocene of southwestern China. *Hist. Biol.* 29, 488–494. doi: 10.1080/08912963.2016.1196686

Li, Q. (2012). Middle Eocene cricetids (Rodentia, Mammalia) from the Erlian Basin, Nei Mongol, China. *Vert. PalAsiat*. 50, 237–244.

Li, Q. (2016). Eocene fossil rodent assemblages from the Erlian Basin (Inner Mongolia, China): Biochronological implications. *Palaeoworld*. 25, 95–103. doi: 10.1016/j.palwor.2015.07.001

Li, Q. (2018). Additional cricetid and dipodid rodent material from the Erden Obo section, Erlian Basin (Nei Mongol, China) and its biochronological implications. *Palaeoworld*. 27, 490–505. doi: 10.1016/j.palwor.2018.09.003

Li, Q. (2019). Eocene ctenodactyloid rodent assemblages and diversification from Erden Obo, Nei Mongol, China. *Hist. Biol.* 31, 813–823. doi: 10.1080/08912963.2017.1395422

Li, Q. (2021). Additional tsaganomyid, cylindrodontid and ctenodactyloid rodent materials from the Erden Obo section, Erlian Basin (Nei Mongol, China). *Vert. PalAsiat*. 59, 1–18.

Li, Q., Mao, F. Y., and Wang, Y. Q. (2018). First record of Eocene fossil rodent assemblages from the lower part of the Erden Obo section, Erlian Basin (Nei Mongol, China) and its biochronological implications. *Palaeobio. Paleoenv*. 98, 259–276. doi: 10.1007/s12549-017-0303-2

Li, Q., and Meng, J. (2010). *Erlianomys combinatus*, a primitive myodont rodent from the Eocene Arshanto Formation, Nuhetingboerhe, Nei Mongol, China. *Vert. PalAsiat*. 48, 133–144.

Li, Q., and Meng, J. (2013). Eocene ischyromyids (Rodentia, Mammalia) from the Erlian Basin, Nei Mongol, China. *Vert. PalAsiat*. 51, 289–304.

Li, Q., and Meng, J. (2015). New ctenodactyloid rodents from the Erlian Basin, Nei Mongol, China, and the phylogenetic relationships of Eocene Asian ctenodactyloids. *Am. Muse. Novit*. 3828, 1–58. doi: 10.1206/3828.1

Li, Q., Wang, Y. Q., and Fostowicz-Frelik, Ł. (2016). Small mammal fauna from Wulanhuxiu (Nei Mongol, China) implies the Irdinmanha-Sharamurunian (Eocene) faunal turnover. *Acta Palaeontol. Pol.* 61, 759–776. doi: 10.4202/app.00292.2016

Li, Q., Wang, Y. Q., Mao, F. Y., and Meng, J. (2019). A new Eocene cylindrodontid rodent from the Erlian Basin (Nei Mongol, China) and its implications for phylogeny and biochronolog. *J. Vert. Paleont.* 39, 5,e1680990. doi: 10.1080/02724634.2019.1680990

Luterbacher, H. P., Ali, J. R., Brinkhuis, H., Gradstein, F. M., Hooker, J. J., Monechi, S., et al. (2004). "The Paleogene Period", in *A Geological Time Scale 2004*, eds. F. M. Gradstein, J. G. Ogg, and A. Smith (Cambridge: Cambridge University Press) 384–408. doi: 10.1017/CBO9780511536045.021

Maridet, O., and Ni, X. J. (2013). A new cricetid rodent from the early Oligocene of Yunnan, China, and its evolutionary implications for early Eurasian cricetids. *J. Vert. Paleon.* 33, 185–194. doi: 10.1080/02724634.2012.710283

Marivaux, L., Benammi, M., Ducrocq, S., Jaeger, J. J., and Chaimanee, Y. (2000). A new baluchimyine rodent from the Late Eocene of the Krabi Basin (Thailand): palaeobiogeographic and biochronologic implications. *Earth Planet Sci*. 331, 427–433. doi: 10.1016/S1251-8050(00)01427-0

Marivaux, L., Ducrocq, S., Jaeger, J. J., Marandat, B., Sudre, J., Chaimanee, Y., et al. (2005). New remains of *Pondaungimys anomaluropsis* (Rodentia, Anomaluroidae) from the latest Middle Eocene Pondaung Formation of central Myanmar. *J. Vert. Paleon*. 25, 214–227. doi: 10.1671/0272-4634(2005)025[0214:NROPAR]2.0.CO;2

Marivaux, L., Vianey-Liaud, M., and Welcomme, J. L. (1999). Première découverte de Cricetidae (Rodentia, Mammalia) oligocènes dans le synclinal sud de Gandoï (Bugti Hills, Balouchistan, Pakistan). *CR l'Acad. Sci. Paris, Ser. IIa*. 329, 839–844. doi: 10.1016/S1251-8050(00)88640-1

Marivaux, L., Vianey-Liaud, M., Welcomme, J. L., and Jaeger, J. J. (2002). The role of Asia in the origin and diversification of hystricognathous rodents. *Zool. Scr.* 31, 225–239. doi: 10.1046/j.1463-6409.2002.00074.x

Marivaux, L., and Welcomme, J. L. (2003). New diatomyid and baluchimyine rodents from the Oligocene of Pakistan (Bugti Hills, Balochistan): systematic and paleobiogeographic implications. *J. Vertebr. Paleontol.* 23, 420–434. doi: 10.1671/0272-4634(2003)023[0420:NDABRF]2.0.CO;2

McKenne, M. C., and Bell, S. K. (1997). *Classification of Mammals Above the Species Level*. New York: Columbia University Press.

Mein, P., and Ginsburg, L. (1997). Les mammiféres du gisement miocéne inférieur de Li Mae Long, Thailande. *Geodiversitas*. 19, 783–844

Meng, J., and Li, C. K. (2010). New rodents from the earliest Eocene of Nei Mongol, China. *Vert. PalAsiat*. 48, 390–401.

Meng, J., Li, C. K., Ni, X. J., Wang, Y. Q., and Beard, K. C. (2007). A new Eocene rodent from the lower Arshanto Formation in the Nuhetingboerhe (Camp Margetts) area, Inner Mongolia. *Am. Muse. Novit*. 3569, 1–18. doi: 10.1206/0003-0082(2007)536[1:ANERFT]2.0.CO;2

Meng, J., and McKenna, M. C. (1998). Faunal turnovers of Palaeogenemammals from the Mongolian plateau. *Nature*. 394, 364–367. doi: 10.1038/28603

Meng, J., Wu, W. Y., and Ye, J. (2001). A new species of *Advenimus* (Rodentia, Mammalia) from the Eocene of northern Junggar Basin of Xinjiang, China. *Vert. PalAsiat*. 39, 185–196.

Meng, J., and Wyss, A. R. (2001). The morphology of *Tribosphenomys* (Rodentiaformes, Mammalia): phylogenetic implications for basal Glires. *J. Mammal Evol.* 8, 1–71. doi: 10.1023/A:1011328616715

Meng, J., Ye, J., and Huanag, X. S. (1999). Eocene mammals from the Bayan Ulan of Nei Mongol (Inner Mongolia) and comments on related stratigraphy. *Vert PalAsiat*. 37, 165–174.

Métais, G., Antoine, P. O., Baqri, S. R. H., Crochet, J. Y., De Franceschi, D., Marivaux, L., et al. (2009). Lithofacies, depositional environments, regional biostratigraphy and age of the chitarwata formation in the Bugti Hills, Balochistan, Pakistan. *J. Asian Earth Sci.* 34, 154–167. doi: 10.1016/j.jseaes.2008.04.006

Métais, G., Mennecart, B., and Roohi, G. (2017). A new assemblage of stem pecoran ruminants from the Oligocene Chitarwata Formation, Bugti Hills, Baluchistan, Pakistan: Paleoenvironmental and paleobiogeographic implications. *J. Asian Earth Sci.* 136, 40–49. doi: 10.1016/j.jseaes.2016.09.009

Missiaen, P., and Gingerich, P. D. (2012). New Early Eocene tapiromorph perissodactyls from the Ghazij Formation of Pakistan, with implications for mammalian biochronology in Asia. *Acta Palaeontol. Pol.* 57, 21–34. doi: 10.4202/app.2010.0093

Missiaen, P., and Gingerich, P. D. (2014). New basal perissodactyla (Mammalia) from the lower Eocene Ghazij Formation of Pakistan. *Contrib. Muse. Paleont. Univ. Michigan* 32, 139–160.

Ni, X. J., Li, Q., Li, L. Z., and Beard, K. C. (2016). Oligocene primates from China reveal divergence between African and Asian primate evolution. *Science*. 352(6286), 673–677. doi: 10.1126/science.aaf2107

Ni, X. J., Li, Q., Zhang, C., Samiullah, K., Zhang, L. M., Yang, Y. H. S., et al. (2020). Paleogene mammalian fauna exchanges and the paleogeographic pattern in Asia. *Sci. China Earth Sci*. 63, 202–211. doi: 10.1007/s11430-019-9479-1

Pound, M. J., and Salzmann, U. (2017). Heterogeneity in global vegetation and terrestrial climate change during the late Eocene to early Oligocene transition. *Sci. Rep.* 7, 43386. doi: 10.1038/srep43386

Qiu, Z. D., and Wang, B. Y. (2019). "Dipodidae," in *Palaeovertebrata Sinica, VIII, Basal Synapsids and Mammals, Fascicle 5(2), Glires II: Rodentia I,* eds. Z. X. Qiu, and C. K. Li (Beijing: Science Press), 242–325.

Rana, R. S., Kumar, K., Escarguel, G., Sahni, A., Rose, K. D., Smith, T., et al. (2008). An ailuravine rodent from the lower Eocene Cambay Formation at Vastan, western India, and its palaeobiogeographic implications. *Acta Palaeontol. Pol.* 53, 1–14. doi: 10.4202/app.2008.0101

Romer, A. S. (1966). *Vertebrate Paleontology*. Chicago and London: University of Chicago Press.

Rose, K. D., Rana, R. S., Sahni, A., Kumar, K., Missiaen, P., et al. (2009). Early Eocene Primates from Gujarat, India. *J. Human Evol.* 56, 366–404. doi: 10.1016/j.jhevol.2009.01.008

Sahni, A., and Khare, S. K. (1973). Additional Eocene mammals from the Subathu Formation of Jammu and Kashmir. *J. Palaeontol. Soc. India*. 17, 31–49.

Sahni, A., and Srivastava, V. C. (1976). Eocene rodents and associated reptiles from the Subathu Formation of northwestern India. *J. Paleontol.* 50, 922–928.

Shen, S. Z., Zhang, H., and Li, W. Z. (2004). An introduction of methods for removing biases in establishing biodiversity patterns from fossil records. *Acta Palae. Sin.* 43, 433–441.

Shevyreva, N. S. (1971). New Middle Oligocene rodents of Kazakhstan and Mongolia. *Bull. Aca. Sci. SSR*.130, 70–86.

Shevyreva, N. S. (1984). "New rodents from the Early Eocene of the Zaisan Depression," in *Floras and Faunas of the Zaisan Depression*, eds. L. S. Daweta, and S. Wele (AH GSSR), 77–114 (in Russian)

Shevyreva, N. S. (1989). New rodents (Ctenodactyloidea, Rodentia, Mammalia) from the Lower Eocene of Mongolia. *J. Paleontolo.* 3, 60–72.

Shevyreva, N. S. (1996). New rodents (Rodentia, Mammalia) from the Lower Eocene of the Zaisan Depression (Eastern Kazakhstan). *J. Paleontolo*. 30, 81–94.

Speijer, R. P., Pälike, H., Hollis, C. J., Hooker, J. J., and Ogg, J. G. (2020). "The Paleogene Period," in *Geologic Time Scale 2020*, eds. F. M. Gradstein,

J.G. Ogg, M.D. Schmitz, and G.M. Ogg (Oxford: Elsevier BV), 1087–1140. doi: 10.1016/B978-0-12-824360-2.00028-0

Spicer, R. A., Yang, J., Herman, A. B., Kodrul, T., Maslova, N., Spicer, T. E. V., et al. (2016). Asian Eocene monsoons as revealed by leaf architectural signatures. *Earth Planet. Sc. Lett.* 449, 61–68. doi: 10.1016/j.epsl.2016.05.036

Sun, J. M., Ni, X. J., Bi, S. D., Wu, W. Y., Ye, J., Meng, J., et al. (2014). Synchronous turnover of flora, fauna, and climate at the Eocene-Oligocene boundary in Asia. *Sci. Rep*. 4, 7463. doi: 10.1038/srep07463

Thewissen, J. G. M., Williams, E. M., and Hussain, S. T. (2001). Eocene mammal faunas from northern Indo-Pakistan. *J. Vert. Paleontol.* 21, 347–366. doi: 10.1671/0272-4634(2001)021[0347:EMFFNI]2.0.CO;2

Tong, Y. S. (1997). Middle Eocene small mammals from Liguanqiao Basin of Henan Province and Yuanqu Basin of Shanxi Province, Central China. *Paleont. Sin. New Ser. C.* 26, 1–256.

Tong, Y. S., and Wang, J. W. (2006). Fossil Mammals from the Early Eocene Wutu Formation of Shandong Province, Central China. *Paleont. Sin. New Ser. C.* 28, 1–195.

Tong, Y. S., Zheng, S. H., and Qiu, Z. D. (1995). Cenozoic mammal ages of China. *Vert. PalAsiat*. 33, 290–314.

Tsubamoto, T., Egi, N., Takai, M., Shigehara, N., Aung, A. K., Thein, T., et al. (2000). A preliminary report on the Eocene mammals of the Pondaung fauna, Myanmar. *Asian Paleoprimatology*. 1, 29–101.

Tsubamoto, T., Takai, M., Shigehara, N., Egi, N., Thura, T. S., Aung, K. A., et al. (2002). Fission-track zircon age of the Eocene Pondaung Formation, Myanmar. *J. Hum. Evol*. 42, 361–369. doi: 10.1006/jhev.2001.0543

Vandenberghe, N., Hilgen, F. L., and Speijer, R. P. (2012). "The Paleogene Period," *in The Geologic Time Scale 2012,* eds. F. M. Gradstein, J. G. Ogg, M. D. Schmitz, and G. M. Ogg (Oxford: Elsevier BV), 855–922. doi: 10.1016/B978-0-444-59425-9.00028-7

Wang, B. Y. (1985). Zapodidae (Rodentia, Mammalia) from the Lower Oligocene of Qujing, Yunnan, China. *Mainz. Geowiss. Mitt*. 14, 345–367.

Wang, B. Y. (1987). Discovery of Aplodontidae (Rodentia, Mammalia) from middle Oligocene of Nei Mongol, China. *Vert. PalAsiat*. 25(1), 32–45.

Wang, B. Y. (1997a). The Mid-Tertiary Ctenodactylidae (Rodentia, Mammalia) of eastern and central Asia. *Bul. Am. Mus. Nat. Hist*. 234: 1–88.

Wang, B. Y. (1997b). Chronological sequence and subdivision of Chinese Oligocene mammalian faunas. *J. Stratigr*. 21, 183–191.

Wang, B. Y. (2001a). Late Eocene ctenodactyloids (Rodentia, Mammalia) from Qujing, Yunnan, China. *Vert. PalAsiat*. 39, 24–42.

Wang, B. Y. (2001b). On Tsaganomyidae (Rodentia, Mammalia) of Asia. *Am. Muse. Novit*. 3317, 1–50. doi: 10.1206/0003-0082(2001)317<0001:OTRMOA>2.0.CO;2

Wang, B. Y. (2001c). Eocene ctenodactyloids (Rodentia, Mammalia) from Nei Mongol, China. *Vert. PalAsiat*. 39, 98–114

Wang, B. Y. (2008). Additional rodent material from Houldjin Formation of Erenhot, Nei Mongol, China. *Vert. PalAsiat*. 46(1), 21–30.

Wang, B. Y. (2019). "Cylindrodontidae," in *Palaeovertebrata Sinica, VIII, Basal Synapsids and Mammals, Fascicle 5(2), Glires II: Rodentia I*, eds. Z. X. Qiu, and C. K. Li (Beijing: Science Press), 449–478

Wang, B. Y., and Dawson, M. R. (1994). A primitive cricetid (Mammalia: Rodentia) from the Middle Eocene of Jiangsu Provinces, China. *Ann. Carnegie Mus.* 63, 239–256. doi: 10.5962/p.215814

Wang, B. Y., and Emry, R. J. (1991). Eomyidae (Rodentia: Mammalia) from the Oligocene of Nei Mongol, China. *J. Vert. Paleontol.* 11, 370–377. doi: 10.1080/02724634.1991.10011404

Wang, B. Y., and Meng, J. (1986). *Eucricetodon* (Rodentia, Mammalia) from the Lower Oligocene of Qujing, Yunnan, China. *Vert. PalAsiat*. 24(2), 110–120.

Wang, B. Y., and Qiu, Z. X. (2003). Note on Early Oligocene Ursids (Carnivora, Mammalia) from Saint Jacques, Nei Mongol, China. *Bull. Am. Mus. Nat. Hist*. 279, 116–124. doi: 10.1206/0003-0090(2003)279<0116:C>2.0.CO;2

Wang, B. Y., and Qiu, Z. X. (2004). Discovery of early Oligocene mammalian fossils from Danghe are, Gansu, China. *Vert. PalAsiat*. 42, 130–143.

Wang, B. Y., Qiu, Z. X., Zhang, Q. Z., Wu, L. J., and Ning, P. J. (2009). Large mammals found from Houldjin Formation near Erenhot, Nei Mongol, China. *Vert. PalAsiat.* 47, 85–110.

Wang, B. Y., Wu, W. Y., and Qiu, Z. X. (2020). "Cricetidae," in *Palaeovertebrata Sinica, VIII, Basal Synapsids and Mammals, Fascicle 5(2), Glires II: Rodentia II,* eds. Z. X. Qiu, and C. K. Li (Beijing: Science Press) 12–151.

Wang, B. Y., Yan, Z. Q., Lu, Y. J., and Chen, G. X. (1994). Discovery of two mid-Tertiary mammalian faunas from Haiyuan, Ningxia, China. *Vert. PalAsiat*. 32, 285–296.

Wang, B. Y., Zhai, R. J., and Dawson, M. R. (1998). Discovery of Ischyromyinae (Rodentia, Mammalia) from the middle Eocene of North China. *Vert. PalAsiat.* 36, 1–12.

Wang, Y. Q., Li, Q., Bai, B., Jin, X., Mao, F. Y., and Meng, J. (2019). Paleogene integrative stratigraphy and timescale in China. *Sci. China Earth Sci.* 62, 287–309. doi: 10.1007/s11430-018-9305-y

Wang, Y. Q., Meng, J., Ni, X. J., and Li, C. K. (2007). Major events of Paleogene mammal radiation in China. *Geol. J.* 42, 415–430. doi: 10.1002/gj.1083

Wasiljeff, J., Kaakinen, A., Salminen, J. M., and Zhang, Z. Q. (2020). Magnetostratigraphic constraints on the fossiliferous Ulantatal sequence in Inner Mongolia, China: implications for Asian aridification and faunal turnover before the Eocene–Oligocene boundary. *Earth Planet. Sci. Lett*. 535, 116–125. doi: 10.1016/j.epsl.2020.116125

Wasiljeff, J., and Zhang, Z. Q. (2022). Stratigraphical significance of Ulantatal sequence (Nei Mongol, China) in refining the latest Eocene and Oligocene terrestrial regional stages. *Vert PalAsiat*. 60, 42–53. doi: 10.19615/j.cnki.2096-9899.210716

Welcomme, J. L., Benammi, M., Crochet, J. Y., Marivaux, L., Métais, G., Antoine, P. O., et al. (2001). Himalayan Forelands: palaeontological evidence for Oligocene detrital deposits in the Bugti Hills (Balochistan, Pakistan). *Geol. Mag.* 138, 397–405. doi: 10.1017/S0016756801005428

Wessels, W., van de Weerd, A. A., de Bruijn,. H., and Marković, Z. (2020). Dipodidea (Mammalia, Rodentia) from the Paleogene of south-east Serbia. *Palaeobio. Paleoenv*. 100, 841–848. doi: 10.1007/s12549-019-00392-5

Westerhold, T., Marwan, N., Drury, A. J., Liebrand, D., Agnini, A., Anagnostou, E., et al. (2020). An astronomically dated record of Earth's climate and its predictability over the last 66 million years. *Sci.* 369, 1383–1387. doi: 10.1126/science.aba6853

Wible, J. R., Wang, Y. Q., Li, C. K., and Dawson, M. R. (2005). Cranial anatomy and relationships of a new ctenodactyloid (Mammalia, Rodentia) from the Early Eocene of Hubei Province, China. *Ann. Carnegie Mus.* 74, 91–150. doi: 10.2992/0097-4463(2005)74[91:CAAROA]2.0.CO;2

Wood, A. E. (1980). The Oligocene rodents of North America. *Trans. Am. Philos. Soc*. 70, 1–68. doi: 10.2307/1006314

Wu, W. Y., Meng, J., Ye, J., and Ni, X. J. (2004). *Propalaeocastor* (Rodentia, Mammalia) from the Early Oligocene of Burqin Basin, Xinjiang. *Am Mus Novit*. 3461, 1–16. doi: 10.1206/0003-0082(2004)461<0001:PRMFTE>2.0.CO;2

Ye, J., Meng, J., Wu, W. Y., and Ni, X. J. (2005). Late Eocene-early Oligocene lithological and biological Stratigraphy in the Burqin region of Xinjiang. *Vert. PalAsiat*. 43, 49—60.

Zhang, R., Kravchinsky, V. A., and Yue, L. P. (2012). Link between global cooling and mammalian transformation across the Eocene-Oligocene boundary in the continental interior of Asia. *Int. J. Earth Sci.* 101, 2193–2200. doi: 10.1007/s00531-012-0776-1

frontiers | Frontiers in Earth Science

TYPE Original Research
PUBLISHED 12 January 2023
DOI 10.3389/feart.2022.1004509

OPEN ACCESS

EDITED BY
Grégoire Métais,
Centre National de la Recherche Scientifique (CNRS), France

REVIEWED BY
Lawrence John Flynn,
Harvard University, United States
Wilma Wessels,
Utrecht University, Netherlands

*CORRESPONDENCE
Qiang Li,
liqiang@ivpp.ac.cn
Xijun Ni,
nixijun@ivpp.ac.cn

†These authors have contributed equally to this work

SPECIALTY SECTION
This article was submitted to Paleontology, a section of the journal Frontiers in Earth Science

RECEIVED 27 July 2022
ACCEPTED 28 December 2022
PUBLISHED 12 January 2023

CITATION
Li Q, Ni X, Stidham TA, Qin C, Gong H and Zhang L (2023), Two large squirrels (Rodentia, Mammalia) from the Junggar Basin of northwestern China demonstrate early radiation among squirrels and suggest forested paleoenvironment in the late Eocene of Central Asia.
Front. Earth Sci. 10:1004509.
doi: 10.3389/feart.2022.1004509

Two large squirrels (Rodentia, Mammalia) from the Junggar Basin of northwestern China demonstrate early radiation among squirrels and suggest forested paleoenvironment in the late Eocene of Central Asia

Qiang Li[1,2,3]*†, Xijun Ni[1,2,3]*†, Thomas A. Stidham[1,2,3], Chao Qin[1,3], Hao Gong[1,3] and Limin Zhang[1,3]

[1]Key Laboratory of Vertebrate Evolution and Human Origins of Chinese Academy of Sciences, Institute of Vertebrate Paleontology and Paleoanthropology, Chinese Academy of Sciences, Beijing, China, [2]CAS Center for Excellence in Life and Paleoenvironment, Beijing, China, [3]College of Earth and Planetary Sciences, University of Chinese Academy of Sciences, Beijing, China

Fossil evidence is indispensable for studying the derivation, divergence, and dispersal of squirrels as they responded to global Cenozoic climatic and paleoenvironmental change. Among these fossil records, the earliest known definitive fossil squirrels in Eurasia occur after the Eocene/Oligocene Boundary and are slightly younger than the oldest records in North America. Here, we report the discovery of two new extinct large squirrel species from the late Eocene of the Junggar Basin in northwestern China. The dental morphologies of these new taxa represent tree and flying morphotypes, and their estimated body masses are approximately 1.2 kg and 2.6 kg, respectively. In addition, these extinct lineages push the age of the first appearance of Sciuridae in northern Asia into the late Eocene. Together with *Douglassciurus* and *Oligospermophilus* from North America, these two new squirrels from the Junggar Basin are the earliest records of sciurids, and analysis of their teeth clearly demonstrates that the three principle morphotypes of sciurids (flying, ground, and tree squirrels) had diverged from one another by the late Eocene. That proposed late Eocene divergence among the major groupings of sciurids is consistent with some molecular clock analyses and helps to document that macroevolutionary timing and pattern. Comparison with modern squirrel analogs for body masses over 1 kg points to these early Chinese species as having occupied forested habitats, and that hypothesis is congruent with published palynological studies. Furthermore, these two new squirrel taxa from Jeminay provide new data to evaluate the examination of the long-term aridification of Central Asia.

KEYWORDS

body mass, forest paleohabitat, Junggar Basin, late Eocene, morphotype, Sciuridae

Introduction

Squirrels are a rodent group with small- to medium-sized bodies in the family Sciuridae, which is the fourth most diverse family of living mammals, consisting of 58 genera and ~285 extant species (Thorington and Hoffmann, 2005; Thorington et al., 2012). The fossil squirrels have been allocated to more than 35 extinct genera (McKenna and Bell, 1997; Fossilworks Group, 2022). Previous work has revealed that the geographic distribution and diversification of both fossil and living sciurids were affected significantly by global climate change during the Cenozoic (Mercer and Roth, 2003) and that the evolution of arboreality possibly aided the divergence of the arboreal group from their hypothetical terrestrial/fossorial ancestors (Steppan et al., 2004). Known fossil records point to the late Eocene as a critical period for the derivation, early divergence, and radiation of sciurids (Goodwin, 2008; Fabre et al., 2012). This temporal interval coincides with the global climatic shift from greenhouse to icehouse climates during the Eocene–Oligocene Transition (EOT) (Zachos et al., 2001; Liu et al., 2009; Hren et al., 2013; Hutchinson et al., 2021), and that climate change possibly initiated or enhanced the aridification of the Asian continental interior in combination with the uplift of the Tibetan Plateau and retreat of Paratethys (e.g., Dupont-Nivet et al., 2007; Abels et al., 2011; Miao et al., 2012; Miao et al., 2013; Bosboom et al., 2014; Fang et al., 2015; Sun and Windley, 2015; Li et al., 2018). As a consequence, the Eocene–Oligocene climatic shift led to the large-scale extinction of marine invertebrates and terrestrial floristic and faunal turnover (e.g., Collinson et al., 1981; Prothero and Emry, 1994; Prothero et al., 2003; Hooker et al., 2004; Retallack et al., 2004), such as the Grande Coupure in Europe and the Mongolian Remodelling in North Asia (Stehlin, 1910; Meng and McKenna, 1998).

Sciurids have been considered to have originated in North America on the eve of the EOT, with the representatives *Douglassciurus jeffersoni* known at about 36.6 Ma (Douglass, 1901; Emry and Korth, 1996; Emry and Korth, 2001) or *D. oaxacaensis* at about 40 Ma (Ferrusquia-Villafranca et al., 2018). From that hypothetical origin, squirrels are thought to have dispersed into Europe and South Asia soon after the EOT, as documented by fossils of *Oligopetes* (Vianey-Liaud, 1974; Heissig, 1979; Vianey-Liaud, 1985; De Bruijn and Ünay, 1989; Welcomme et al., 2001). Squirrels appear to have immigrated rather late to North Africa in the Miocene and to South America in the Pleistocene (De Bruijn, 1999). The Eurasian *Oligopetes* has been presumed to be a Grande Coupure immigrant (Dawson, 2003; Heissig, 2003). However, a large temporal gap exists between the EOT and the first appearance of Sciuridae in the Mongolian Remodelling of North Asia (Meng and McKenna, 1998). In recent years, the Paleogene records of sciurids in North Asia have continued to grow, and they have demonstrated that squirrels were rather diverse in the early Oligocene (Minjin, 2004; Wang and Qiu, 2004; Wang and Dashzeveg, 2005; Maridet et al., 2014). In addition, fossils have suggested that sciurids also might date back to the late Eocene (Wang, 2008). In fact, we can confirm Eocene occurrence in northern Asia through the recognition of two new fossil species of large arboreal squirrels from late Eocene sediments of the Junggar Basin in northwestern China. These fossils and the taxa they represent greatly aid in improving our understanding of the derivation, early divergence, and spatiotemporal distribution of sciurids, and they support the occurrence of forested paleohabitat in the late Eocene of Central Asia.

All of the extant and extinct squirrel species comprise a monophyletic Sciuridae, which is the sister group to Aplodontidae (Huchon and Douzery, 2001; DeBry, 2003; Montgelard et al., 2008; Blanga-Kanfi et al., 2009; Fabre et al., 2012). Traditionally, Sciuridae were split into the two subfamilies which are the Pteromyinae (the flying squirrels with their gliding membrane) and Sciurinae (the non-flying tree and ground squirrels) (e.g., Simpson, 1945; Hoffmann et al., 1993; Thorington et al., 2002). Based on dental and mandibular morphologies, De Bruijn, (1999) recognized three morphotypes among the squirrels that include "ground," "tree," and "flying" squirrels, and he elevated Pteromyinae and Sciurinae to the family level, raising the Sciuridae to superfamily rank. Qiu (2019) summarized the known 32 genera of sciurid fossils in China and divided them into four subfamilies. In that taxonomy (Qiu, 2019), flying squirrels are still treated as an independent subfamily, Pteromyinae. However, molecular phylogenetic studies refined the higher level systematic arrangement of the Sciuridae and its extant lineages of five subfamilies: Ratufinae, Sciurillinae, Sciurinae, Callosciurinae, and Xerinae (Mercer and Roth, 2003; Steppan et al., 2004). In this treatment, the "flying squirrels" are monophyletic (Thorington, 1984; Oshida et al., 1996) and are treated as a tribe within the subfamily Sciurinae (Mercer and Roth, 2003; Steppan et al., 2004; Thorington and Hoffmann, 2005; Fabre et al., 2012). In addition to the five living subfamilies, there are two extinct subfamilies. One is the subfamily Cedromurinae proposed by Korth and Emry (1991) for the two extinct genera *Cedromus* Wilson (1949) and *Oligospermophilus* Korth (1987) from the late Eocene to late Oligocene of North America. This clade was subsequently accepted by some paleontologists (McKenna and Bell, 1997; Wang and Dashzeveg, 2005; Goodwin, 2008). The other is the subfamily Aepyosciurinae erected by Wang and Qiu (2003) for a specialized sciurid group with unilaterally hypsodont and lophodont cheek teeth. At present, it includes only genus *Aepyosciurus* and is restricted in the late Neogene and Quaternary (early Pliocene to early Pleistocene) of the Tibetan Plateau and North China (Wang and Qiu, 2003; Qiu et al., 2005; Cai et al., 2013; Wang et al., 2013; Li et al., 2014). Based on their dental morphologies, the two new species in this text from Jeminay, northwestern China, should be placed in the subfamily Sciurinae.

Materials and methods

Fossil sites

The new sciurid fossil specimens were discovered in Jeminay County in the northwestern part of the Xinjiang Uygur Autonomous Region of China. The new fossil sites are located in a gully west of the village of Xiaerhete, which is ~10 km south of the Irtysh River and 6 km northwest of the county seat of Jeminay County, close to the China–Kazakhstan border. The Jeminay area has produced middle Eocene fossil plants including *Taxodium* sp., *Ampelopsis* sp., *Populus* sp., and *Corylus* sp. and mammals including *Triplopus* sp., *Triplopus jeminaiensis*, *Lophialetes* sp., and Hyaenodontidae gen. et sp. indet. (Wang F. Y., 1984; Jin, 2000). Jin (2000) considered the Cenozoic sediments in Jeminay area and along the Irtysh River as an eastern extension of the neighboring deposits in the Zaysan Basin of Kazakhstan. The squirrel fossils derive from two extremely close sites (XJ20140619LQ03 and XJ20140626NI01, N47°28′, E86°47′, elevation 869 m) and from almost the same layer

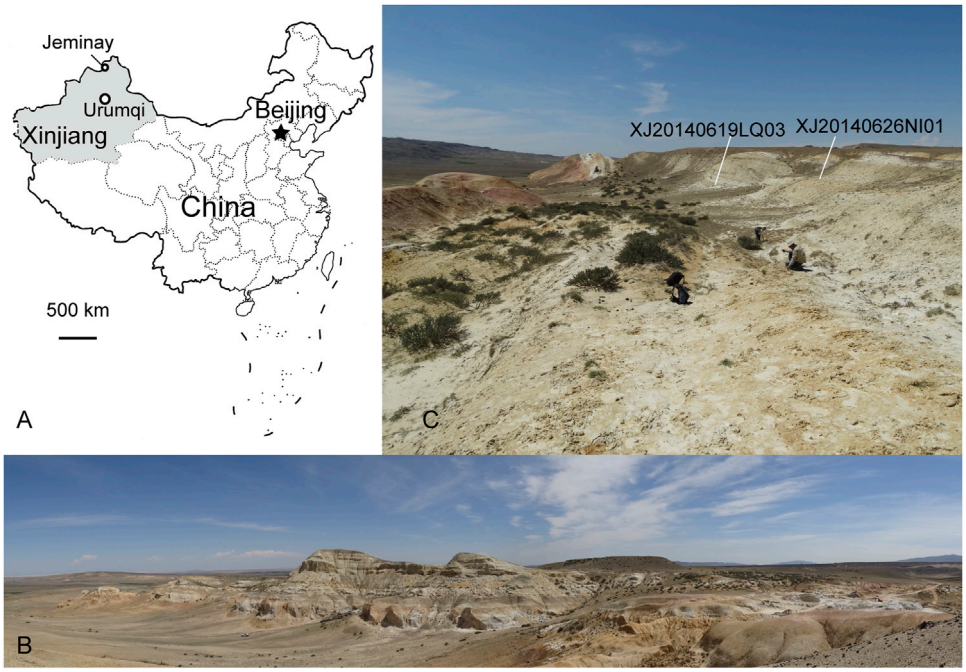

FIGURE 1
Late Eocene sciurid sites in Jeminay, northwestern Xinjiang, China. **(A)** Map showing the fossil sites located at Jeminay, Xijiang Uygur Autonomous Region, northwestern China; **(B)** panoramic view of the fossiliferous profile of the Keziletuogayi Formation that produced the additional material of fossil squirrels (photo taken by the first author QL on 20 June 2014); **(C)** a close-up view of the stratigraphy yielding the fossil squirrels.

(only a half-meter interval of two sites) consisting of ~5 m of yellowish fluvial sandstone, grayish white siltstone, and sandy mudstone of the Keziletuogayi Formation (Figure 1). A large anseriform fossil (cf. Romainvilliinae) was previously discovered and reported from this same layer (Stidham and Ni, 2014). Lithologically, the squirrel fossil layer can be correlated to the Keziletuogayi Formation yielding an A3 mammalian zone fauna from the nearby Keziletuogayi section. Paleomagnetic dating of that interval provides an age range of 34.0–35.0 Ma (Sun et al., 2014). The associated mammals from the Keziletuogayi section include Brontotheriidae, Amynodontinae, *Cadurcodon* cf. *C. ardynensis*, and *Ardynomys vinogradov*, and that fauna also confirms its late Eocene age.

Material

The fossil squirrel specimens include four enamel caps of one upper and three lower molars, collected by wet-sieving technique in 2014. The other rodent specimens are as yet unstudied. All specimens are housed at the Institute of Vertebrate Paleontology and Paleoanthropology (IVPP), Chinese Academy of Sciences, Beijing.

Comparative sample

For comparative purposes, we discuss all known late Eocene and early-late Oligocene sciurid genera (16 taxa). The following is a list of these genera.

Asian forms include *Sciurus* sp., *Oligosciurus*, *Kherem*, Marmotini gen. et sp. indet., and *Plesiosciurus* aff. *sinensis*. The specimens of *Sciurus* sp. reported by Bohlin (1946) include a right M3 (T. b. 202) and a right m2 (T. b. 593) from the late Oligocene Taben-buluk Basin of Gansu Province, China. *Oligosciurus* (Wang and Qiu, 2004) (type and only species: *O. dangheensis*) is based on the topotype jaw (IVPP V13556) from the lower Oligocene Paoniuquan Formation in the Danghe region of Gansu Province, China. The topotype belongs to an ontogenetically old individual with a heavily worn m1 and m2. *Kherem* (Minjin, 2004) comprises two members, *K. hsandgoliensis* (the type species) and *K. asiatica*, both of which were discovered in the Hsanda Gol Formation (early Oligocene) of the Valley of Lakes area, Mongolia (Minjin, 2004; Wang and Dashzeveg, 2005). *Kherem* was once assigned to the subfamily Cedromurinae recognized by Korth and Emry, (1991) (Wang and Dashzeveg, 2005). Recently, Maridet et al. (2014) treated *K. asiatica* as a synonym of *K. hsandgoliensis*, assigned *Kherem* to the subfamily Xerinae, and expanded the former temporal range from early Oligocene through early middle Miocene. We agree with Maridet et al. (2014) that *K. asiatica* is synonymous with *K. hsandgoliensis*. The material referred to as Marmotini gen. et sp. indet. described by Wang (2008) comprises a broken M1/2 (IVPP V 15003) from the Upper Eocene Houldjin Formation of Erenhot, Inner Mongolia, China. Its attribution to Sciuridae is doubtful. The specimens of *Plesiosciurus* aff. *sinensis* (Qiu and Lin, 1986) were discovered in Toglorhoi, Unkheltseg, Hotuliin Teeg, Ulann Tolgoi, and Loh (early Late Oligocene to early Middle Miocene) of the Valley of Lakes, Mongolia (Maridet et al., 2014, p. 274).

European forms include *Palaeosciurus*, *Heteroxerus*, and *Oligopetes*. *Palaeosciurus* Pomel, 1853 comprises five European species: *P. feignouxi* (type species), *P. fissurae* (Dehm, 1950), *P. goti* (Vianey-Liaud, 1974), *P. sutteri* (Ziegler and Fahlbusch, 1986), and *P. ultimus* (Mein and Ginsburg, 2002), and a Chinese species *P. jiangi*

(Qiu, 2015). This genus ranges temporally from the earliest Oligocene to the early Miocene in Eurasia (de Bruijn, 1999; Qiu, 2015). *Palaeosciurus goti* from Mas de Got of France (MP22) was once regarded as the earliest sciurid in Europe (Vianey-Liaud, 1985). *Heteroxerus* Schaub (in Stehlin and Schaub, 1951, p. 200) (type species: *H. hürzeleri*) is a member of Xerini and ranges from the early Oligocene through the late Miocene in Europe (McKenna and Bell, 1997). Its holotype is a fragmentary lower dentition with m1-2 (Stehlin and Schaub, 1951, p. 201, figure 300). *Oligopetes* (Heissig, 1979) is the hitherto earliest known record of flying squirrels. It consists of three species, *O. radialis* (type species), *O. lophulus*, and *O. obtusus*, which all derive from the fissure fillings of Suevium (lower to middle Oligocene).

North American forms include *Protospermophilus*, *Cedromus*, *Miospermophilus*, *Miosciurus*, *Protosciurus*, *Oligospermophilus*, *Nototamias*, and *Douglassciurus*. *Protospermophilus* (Gazin, 1930) contains of a total of six species: *P. quatalensis* (type species), *P. wortmani*, *P. kelloggi*, *P. angusticeps*, *P. oregonensis*, and *P. malheurensis* (Cope, 1879; Gazin, 1930; Gazin, 1932; Matthew and Mook, 1933; Downs, 1956; Black, 1963). Temporally, they span from the early Arikareean to late Clarendonian NALMA (late Oligocene to late Miocene) (Goodwin, 2008). The genotype *P. quatalensis* is present in the Cuyama Basin (late Miocene) of California (USA). *Cedromus* (Wilson, 1949) consists of the type species *Cedromys wardi* and *C. wilsoni* (Korth and Emry, 1991). *Cedromus* ranges from the early Orellan to the late Whitneyan NALMA (early Oligocene to early Late Oligocene) (Goodwin, 2008). *Miospermophilus* (Black, 1963) comprises three species, namely, *M. bryanti* (type sepcies), *M. wyomingensis*, and the questionable *M. lavertyi* (Wilson, 1960; Black, 1963; Dalquest et al., 1996), and it spans from the early Arikareean to the late Clarendonian NALMA (late Oligocene to late Miocene) (Goodwin, 2008). *Miosciurus* (Black, 1963) contains one species, *M. ballovianus* (Cope, 1881). *Miosciurus ballovianus* is an early Arikareean NALMA (late Oligocene) sciurid from the United States, and thus far it has been found only in the "*Diceratherium* beds" (probably Turtle Cove Member, see Albright et al., 2008) of the John Day Formation of Oregon. *Protosciurus* (Black, 1963) includes *P. condoni* (type species), *P. mengi*, *P. rachelae*, and *P. tecuyensis* (Bryant, 1945). The genus ranges from early Orellan to early Hemingfordian NALMA (early Oligocene to late early Miocene), and it may have survived into the early Barstovian NALMA (early middle Miocene) (Goodwin, 2008). *Oligospermophilus* (Korth, 1987) (type and only species: *O. douglassi*), typical of the Orella Member of the Brule Formation (early Oligocene), Prairie Dog Creek of Nebraska (USA), was assigned originally to *Protosciurus* (Korth, 1981). *Nototamias* (Pratt and Morgan, 1989) is a chipmunk-sized sciurid with a *Tamias*-like upper dental pattern. Chronologically, it spans from the early Arikareean to the late Clarendonian NALMA (late Oligocene to late Miocene), similar to *Protospermophilus* (Goodwin, 2008). It comprises three species: *N. hulberti* (type species), *N. quadratus*, and *N. ateles* (Hall, 1930; Pratt and Morgan, 1989; Korth, 1992). *Douglassciurus* is a replacement name for *Douglassia* Emry and Korth (1996) (Emry and Korth, 2001). This genus consists of four species: *D. jeffersoni* (late Eocene), *D. sapphirus* (late Oligocene), *D. bjorki* (middle Oligocene), and *D. oaxacaensis* (late middle Eocene) (Douglass, 1901; Korth, 2009; Korth, 2014; Ferrusquia-Villafranca et al., 2018). The type species is *D. jeffersoni* from the Chadronian NALMA (late Eocene) Pipestone Springs Formation, Montana (USA), and it was originally referred to the genus *Sciurus* by Douglass (1901). Its generic and familial allocations were uncertain for a long time, attributed to *Prosciurus* (Matthew, 1903) of the Aplodontidae (Osborn and Matthew, 1909; Wood, 1937) or to *Cedromus* or *Protosciurus* of the Sciuridae (Wood, 1962; Black, 1963; Wood, 1980; Emry and Thorington, 1982).

Site and institutional abbreviations

IVPP, The Institute of Vertebrate Paleontology and Paleoanthropology, Chinese Academy of Sciences, Beijing (China); MP, European Paleogene mammal faunal zones; XJ, prefix to Xinjiang of field localities of the IVPP; T.b., Taben-buluk area (Gansu Province, China) in Bohlin's (1946) pioneering work.

Measurements and nomenclature

Specimens were measured using an Olympus SZX7 microscope with a precision of +/− 0.01 mm. The length is defined as the anteroposterior chord. The width is defined along the chord perpendicular to the length. The dental terminology (Figure 2) is mostly adopted from Qiu (1996) and Qiu, (2019) except for our usage of "anterobuccal cingulid" to replace their "anterobuccal cingulum" on m1/2 and additions of "anterobuccal sinusid" and "protocone crest." The protocone crest is "a short crest extending anterobuccally from the protocone into the valley between the anterior cingulum and the protoloph" defined by Emry and Korth (1996), and it is equal to the "protostyl" used by Heissig (1979).

CT scanning and reconstruction

The specimens were CT-scanned using the 100 kv Micro–CT in the Key Laboratory of Vertebrate Evolution and Human Origins of the Chinese Academy of Sciences. The 3D virtual reconstruction was made with VGSTUDIO (Version 2.0, genuine authorized) software (Volume Graphics) installed in the computers of the laboratory following the standard procedure introduced by Ni et al. (2012).

Body mass estimation

Following Freudenthal and Martín-Suárez (2013), we first calculated the length of the lower tooth row using one of their regression equations (ln (LRsum)=0.51×ln (L×W of m1)+1.25) applied to the Sciuridae (Freudenthal and Martín-Suárez (2013), p.7). Then, we substituted the tooth row length into their other equation (ln (mass) = 3.023ln (row)−0.993) to obtain a body mass estimate (Freudenthal and Martín-Suárez (2013), p.8).

Systematic Paleontology

Order Rodentia Bowdich, (1821).

Family Sciuridae (Fischer de Waldheim, 1817)
Subfamily Sciurinae (Fischer de Waldheim, 1817)
Genus *Junggarisciurus* gen. nov.
Junggarisciurus *jeminaiensis* sp. nov.
Figures 3A1–5, B1–5, C1–5

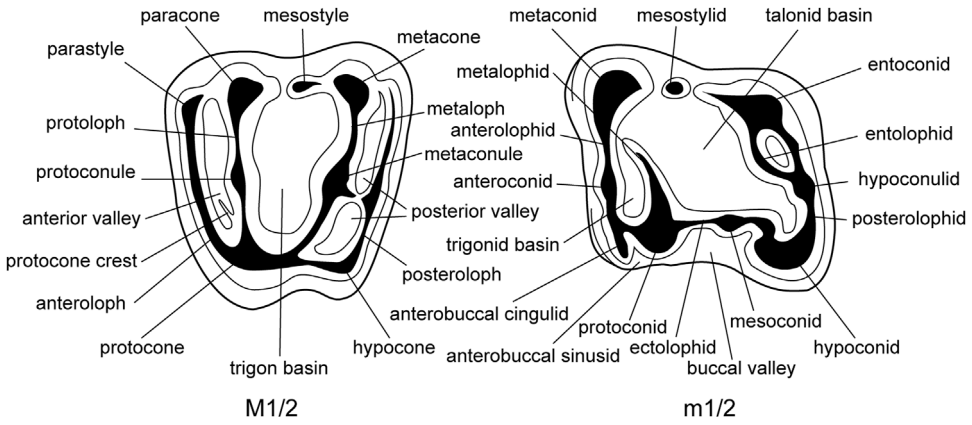

FIGURE 2
Dental nomenclature of the Sciuridae molars (cited from Qiu, 1996; Qiu, 2019).

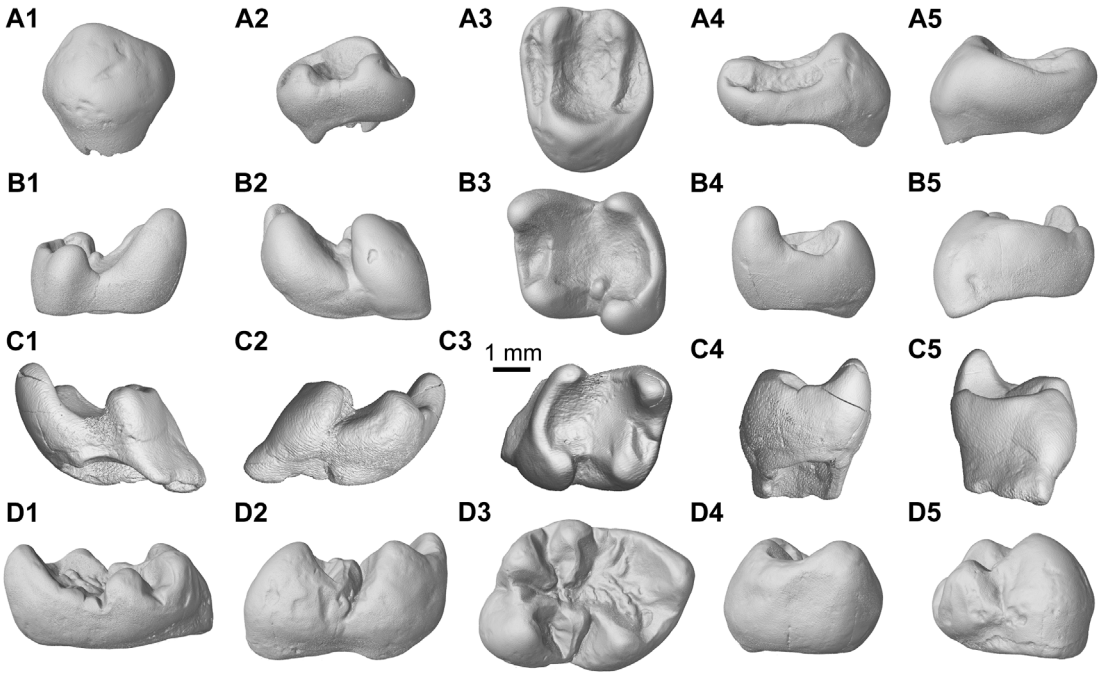

FIGURE 3
3D virtual reconstruction of the molars of *Junggarisciurus jeminaiensis* gen. et. sp. nov. and *Eopetes irtyshensis* gen. et. sp. nov. **(A1–A5)** IVPP V23185, holotype of *J. jeminaiensis*, left M1/2; **(B1–B5)** IVPP V23186, left m1/2; **(C1–C5)** IVPP V23280, paratype, right m1/2; **(D1–D5)** IVPP V31378, holotype of *E. irtyshensis*, right m1/2.1, lingual view; 2, buccal view; 3, occlusal view; 4, anterior view; 5, posterior view. All in the same scale (bar equals 1 mm).

Etymology. "Junggar," Mongolian, referring to the Junggar Basin, the provenance of this new taxon; "sciurus" is from Greek *skiourus* (squirrel); "Jeminay," Mongolian, is the nearby county seat of the fossil sites.

Holotype. IVPP V23185, an isolated left M1/2 (Figures 3A1–5), collected from IVPP field site XJ20140619LQ03.

Paratype. IVPP V23280, a right m1/2 (Figures 3C1–5), collected from IVPP field site XJ20140619LQ03.

Referred specimen. IVPP V23186, a left m1/2 (Figures 3B1–5), collected from IVPP field site XJ20140626NI01.

Type Locality and Age. Jeminay, northwestern Xinjiang Uygur Autonomous Region, China, the Keziletuogayi Formation, late Eocene, 34.0–35.0 Ma.

Generic diagnosis

A large-sized sciurid. Molars are brachydont with incipient rugose floor in the trigon and talonid basins. M1/2 outline is quadrate; protocone is

anteroposteriorly expanded; hypocone is absent; protoconule, metaconule, and mesotyle are indistinct; anterocone is reduced; protoloph and metaloph are complete and nearly parallel; metaloph is constricted at its junction with protocone; and protocone crest and ectoloph are absent. The m1/2 outline is more rectangular, metaconid is sharp, entoconid is well-delimited, mesoconid is developed or indistinct, hypoconulid and mesostylid are absent, trigonid basin is wide and enclosed by complete metalophid, talonid basin is incompletely enclosed with two notches near the center of the buccal and lingual sides, anterobuccal cingulid and entolophid are absent, anterobuccal sinusid at the junction of the protolophid is absent, ectolophid is weak and discontinuous, posterolophid is continuous and connected to entoconid. Slightly larger than *Protosciurus condoni* and remarkably larger than other known late Eocene–Oligocene sciurids. Furthermore, *Junggarisciurus jeminaiensis* differs from *Kherem* of Xerinae and *Palaeosciurus*, *Oligopetes*, *Protospermophilus*, *Miospermophilus*, *Protosciurus*, *Nototamias*, *Douglassciurus*, *Plesiosciurus* aff. *sinensis*, and Marmotini gen. et sp. of Sciurinae in its protoloph parallel to the metaloph on M1/2. Furthermore, it differs from *Kherem* and *Heteroxerus* of Xerinae and *Oligopetes*, *Miospermophilus*, and *Miosciurus* of Sciurinae in the absence of an anterobuccal sinusid on m1/2. It differs from *Sciurus* sp. (Sciurinae) in its less quadrate outline and well-developed metalophid, trigonid basin, and entoconid on m1/2. Compared to the taxa of Cedromurinae, it differs from *Cedromus* in its less developed or absent anteroconid, entolophid, and ectolophid on m1/2. It differs from *Oligospermophilus* by having more rounded corners, an absence of a hypocone and mesostyle on M1/2, and a less developed anteroconid, an entoconid merged into the posterolophid, and the absence of a mesostylid on m1/2. It differs from *Oligosciurus* in the presence of a mesostylid and mesoconid, a wide trigonid, a narrow buccal valley, and absence of an entolophid.

Specific diagnosis

Same as that of the generic diagnosis.

Measurements (in mm)

M1/2 (IVPP V23185): length × width = 3.63 × 4.75; m1/2 (IVPP V23186): 4.30 × 3.95; m1/2 (IVPP V23280): 4.15 × 3.90.

Description

The holotype M1/2 (Figures 3A1–5) has a quadrate outline that is wider than long. There are three marginal cusps and four lophs, which form a wide and deep middle and two narrow and shallow marginal depressions with an incipient rugose surface. The lingual main cusp is far higher than the buccal. Tooth anterior and buccal walls are less curved, while the posterior and lingual are rather rounded. The protocone is conspicuously large and anteroposteriorly expanded. The hypocone is absent. The paracone and metacone are small and nearly the same size. The anterocone is reduced and inconspicuous, merging with the anteroloph. Both the protoconule and metaconule are absent. No distinct parastyle, protoconule, or metaconule is present. The mesostyle is extremely small and inconspicuous. Both the protoloph and metaloph are complete, nearly parallel to each other, and extend slightly anterolingually toward the protocone. The protoloph is strong, and the metaloph is constricted distinctly at its junction with the protocone. The anteroloph and posteroloph are lower than the protoloph and metaloph. A protocone crest similar to that of *Douglassciurus jeffersoni* (see Emry and Korth, 1996) and an ectoloph resembling *Oligopetes* (Heissig, 1979) are not present. The trigon basin is deep and wide. The anterior valley is slightly narrower than the posterior. No roots are preserved.

The m1/2s (Figures 3B1–5, C1–5) have a nearly rectangular outline and are slightly anterobuccal-posterolingually compressed. There are four marginal cusps and three transverse lophs, surrounding a small, shallow anterior trigonid basin and a large, deep posterior talonid basin with a less rugose floor compared to *Oligopetes* and *Palaeosciurus*. The two anterior cusps project more than the two posterior cusps. The anterolingual metaconid is the highest and positioned slightly more anteriorly than the protoconid. The lingual entoconid is situated opposite of the buccal hypoconid, and it is well-delimited at lingoposterior corner of the tooth. The mesoconid is well developed on the referred specimen (IVPP V23186) but indistinct on the paratype (IVPP V23280). The anteroconid can be observed on the IVPP V23280 but merges with the anterolophid of the IVPP V23186. The hypoconulid and mesostylid are both absent. The metalophid is complete and encloses the trigonid basin. The ectolophid is weak and discontinuous. The posterolophid is strong and continuous, and it connects the hypoconid and entoconid. No entolophid (or hypolophid) is present. The buccal and lingual valleys are present as deep notches of external margin of the talonid basin. The anterobuccal cingulid is absent. There is no trace of an anterobuccal sinusid between anterolophid and protoconid. No roots are preserved.

Remarks

The Jeminay sample generally resembles that of living Sciurini, particularly *Sciurus*, by having a quadrate outline, a complete protoloph and metaloph, an absent metaconule on M1/2, a developed metalophid enclosing the trigonid basin, and a conspicuous entoconid on m1/2. It seems reasonable to refer the m1/2 to the tree squirrels (Qiu, 2019). However, it differs from *Sciurus* in its larger tooth size and having a transverse metalophid parallel to the anterolophid, a larger trigonid basin in contrast to that of *Sciurus*, and a V-shaped notch between the metaconid and entoconid on m1/2. For further comparative purposes, we discuss all known late Eocene and early-late Oligocene sciurid genera (16 taxa, above). The Jeminay sample differs from these taxa in both its dental size and morphology (see Generic diagnosis).

Genus *Eopetes* gen. nov.

Eopetes irtyshensis sp. nov.

Figures 3D1–5.

Etymology. "Eo-," Greek, means dawn; "petes" is derived from the Sanskrit "patara" meaning flying; "Irtysh," Mongolian, refers the Irtysh River near the holotype locality.

Holotype. IVPP V31378, an isolated right m1/2 (Figures 3D1–5), collected from IVPP field site XJ20140619LQ03.

Type Locality and Age. Jeminay, northwestern Xinjiang Uygur Autonomous Region, China, the Keziletuogayi Formation, late Eocene, 34.0–35.0 Ma.

Generic diagnosis

A large-sized sciurid. Lower molar brachydont with rugose floor and extra ridges in the talonid basin. Entoconid, hypoconulid,

mesoconid, and ectomesolophid well-developed. Entoconid relatively isolated. No anterobuccal cingulid or sinusid. Protolophid low and extending posterolingually. Metastylid and mesostylid well developed. Trigonid basin posteriorly open. Compared to taxa of flying squirrels, it differs from *Oligopetes* by the presence of well-developed entoconid and hypoconulid and the absence of anterobuccal cingulid and anterobuccal sinusid and having a crowded talonid basin. It differs from *Parapetaurista*, *Miopetaurista*, *Hylopetodon*, *Yunopterus*, *Hylopetes*, *Pteromys*, *Petaurista*, and *Aeretes* in the absence of an anterobuccal cingulid and sinusid, a limited talonid basin, and a robust hypoconulid. It differs from *Belomys*, *Trogopterus*, and the *Pliopetaurista* in lophs being conspicuously weaker than the cusps.

Species diagnosis

Same as that of the generic diagnosis.

Measurements (mm)

The holotype m1/2 (IVPP V31378), length × width = 5.8 × 4.6.

Description and comparison

The tooth is brachydont with heavily built cusps and extra ridges. It has a rhomboid occlusal outline with projecting anterolingual metaconid and posterobuccal hypoconid corners. The metaconid is the highest of the main cusps, and it is situated further anteriorly than the protoconid. Posterior to the lingual part of the metaconid, the metastylid is present and has a short transverse ridge. No anterobuccal cingulid is present. The anteroconid is situated between the metaconid and the protoconid, is much lower than them, and is connected to them through thin ridges. The protoconid is subtriangular in outline, and it is separated from the posterior mesoconid. The trigonid is open posteriorly. The protolophid is low and wavy, derives from the anterolingual part of the protoconid, and extends posterolingually into the talonid basin, failing to reach the entoconid. The mesoconid is prominent, subtriangular in shape, and as high as the entoconid. The ectomesolophid is derived from the mesoconid, tapers buccally, slopes ventrally, and interrupts the buccal valley (=hypoflexid) by an anterior narrow groove and a posterior enclosed fossa surrounded by the ectolophid, hypoconid, mesoconid, and ectomesolophid. The mesostylid is present on the lingual margin, and it is situated between the metastylid and entoconid. The entoconid is nearly isolated and opposite the mesoconid. The entolophid is short and bulging and is buccally contracted. The ectolophid is short and longitudinally links the mesoconid and the hypoconid. The hypoconid has a long anterobuccal crest and a short posterior arm with an extra cuspid. A notch exists between the posterior side of the hypoconid and hypoconulid. The hypoconulid is triangular in shape, lower than the hypoconid, higher than the entoconid, and as large as the entoconid. The hypoconulid is separated from the entoconid. The anterior part of the talonid basin has a wrinkled surface, but the posterior part is occupied by the heavily built entoconid and hypoconulid. The space demarcated by the entoconid, hypoconulid, and ectolophid is quite limited.

This m1/2 has a complicated occlusal structure, with a rugose talonid surface, extra ridges, and a prominent entoconid. It seems reasonable to refer the m1/2 to the grouping of flying squirrels (Qiu, 2019). The m1/2 has a heavily built entoconid, hypoconulid, and meseoconid, and it lacks an anterobuccal cingulid or sinusid. That morphology resembles that of some genera of flying squirrels, such as the extant *Belomys* and *Trogopterus* and the fossil *Pliopetaurista*, but the morphology differs from other flying squirrels in the absence of an anterobuccal cingulid and sinusid, a limited talonid basin, and a robust hypoconulid (Qiu, 2019). Furthermore, the morphology of this m1/2 is so unique as to distinguish it from other Oligocene flying squirrels such as *Oligopetes* or the living representatives through its lophs being conspicuously weaker than the cusps. Although this taxon is represented currently by only one lower tooth, it is worth erecting a new genus and species for it given its large size and unique morphology.

Results

Derivation and early divergence of sciurids

The family Sciuridae is generally thought to have derived from the Ischyromyidae (including Paramyinae) in North America (Matthew, 1910; Wilson, 1949; Wood, 1962; Black, 1963; Emry and Thorington, 1984; Korth, 1984; Emry and Korth, 1996). Korth and Emry (1991) proposed that the Sciuridae possibly shares with the Aplodontidae a common ancestor that arose from a *Reithroparamys*-like ischyromyid with the Aplodontidae. Their view was accepted by many researchers (Korth, 1994; Emry and Korth, 1996; Mercer and Roth, 2003; Goodwin, 2008) but is still questioned by a few (de Bruijn, 1999; Heissig, 2003). *Junggarisciurus jeminaiensis* from the Junggar Basin is easily distinguished from *Reithroparamys* or other ischyromyids, and it displays conspicuous dental features, such as the lack of a hypocone, protoconule, and metaconule on M1/2, the absence of an anterobuccal sinusid at the junction of the anteroconid and protoconid, an inconspicuous ectolophid, the absence of an entoconid crest, and a joining of the entoconid and posterolophid on m1/2 (Wood, 1962). It seems that there is no close affiliation between the sciurid *J. jeminaiensis* and the ischyromyid *Reithroparamys*. *Junggarisciurus jeminaiensis* shares some characters with the ischyromyid *Hulgana ertnia*, which was erected based on the material collected from the Upper Eocene "Ulan Gochu" beds at Jhama Obo, East Mesa, Inner Mongolia (China) (Dawson, 1968). The shared characteristics include large size, deep talonid basin relative to the main cusps, outline of the lower molar rhomboid, indistinct conules, and absent hypocone, style (id)s, and hypolophid. However, *Hulgana ertnia*'s P4-M2 have an anterolingual protrusion of the protocone with crests converging on the protocone and a concavity at the lingual-posterior of the protocone, and its lower molars have incompletely enclosed the trigonid and lack a mesoconid. Furthermore, on the buccal side the mandible of *H. ertnia*, the apex of the masseteric ridges is situated far posteriorly (posterior to m2), but that of the Sciuridae is placed anteriorly (m1 or posterior p4) (Qiu, 2019). Unfortunately, the specimen of *Junggarisciurus jeminaiensis* has no jaw, so the situation of the apex of the masseteric ridges of this species is unknown. *Eopetes irtyshensis* has a special dental morphology on m1/2 with crenulations and stylids, the presence of a robust entoconid, hypoconulid, and mesoconid, and the absence of an anterobuccal sinusid, resembling that of some flying squirrels, particularly the extant *Belomys* and *Trogopterus* and extinct

10.3389/feart.2022.1004509

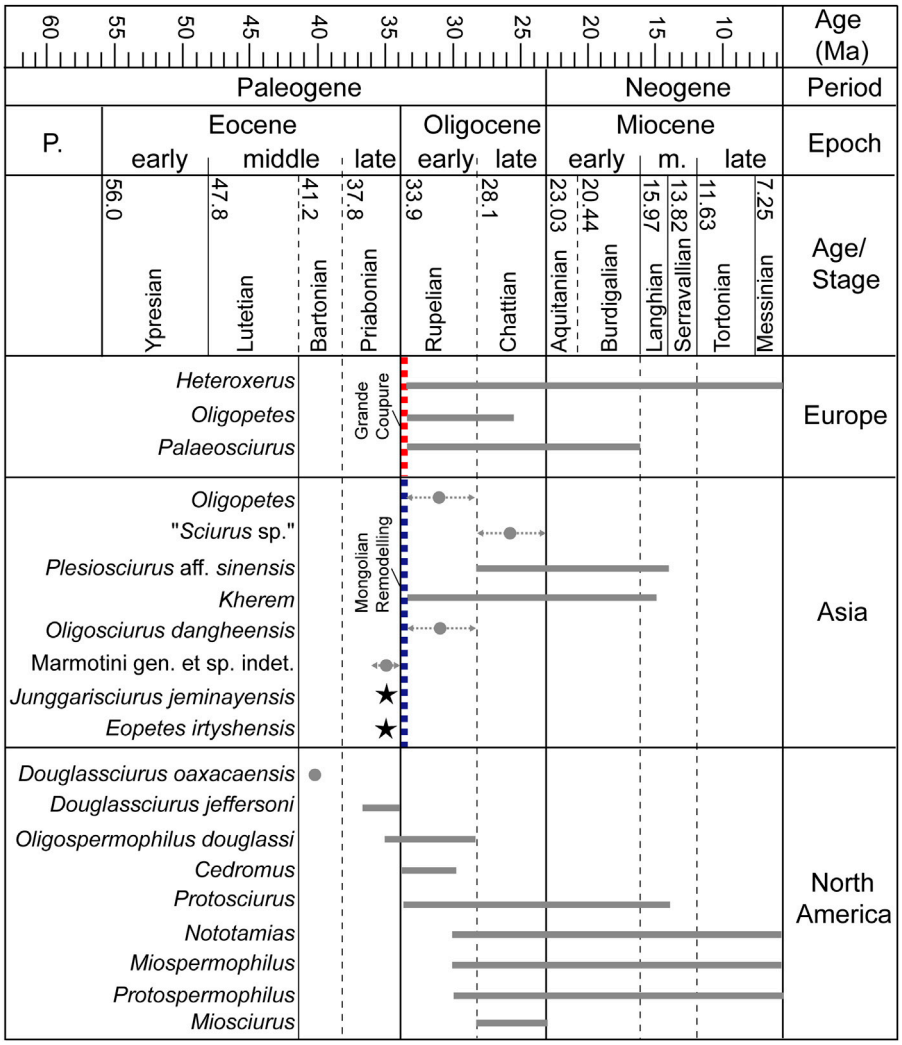

FIGURE 4
Chronologic ranges of Eocene to Oligocene sciurids from North America, Asia, and Europe. The fossil records of sciurids span the Eocene/Oligocene boundary in both North America and Asia but appear later in the early Oligocene of Europe. *Douglassciurus oaxacaensis* is the earliest member of sciurids in late middle Eocene, *Junggarisciurus jeminaiensis*, *Eopetes irtyshensis*, *Douglassciurus jeffersoni,* and *Oligospermophilus douglassi* form the second earliest confident records of sciurids in the late Eocene. Red dashed line, Grande Coupure; blue dashed line, Mongolian Remodelling; gray dot with dashed arrowed line, estimated date; asterisks, *J. jeminaiensis* and *E. irtyshensis* from Jeminay, northwestern Xinjiang, China. Abbreviations: *P.*, Paleogene; m., middle Miocene.

Pliopetaurista (Qiu, 2019). *Eopetes irtyshensis* differs from *Reithroparamys* or other ischyromids in having a robust hypoconulid, a weaker metalophid, and an entolophid extending toward the mesoconid. It seems that the Sciuridae were not derived directly from any known ischyromids. In fact, there is still a large time gap between the records of latest ischyromids (early middle Eocene) and the earliest sciurids (late Eocene) (Tong and Li, 2019).

Mercer and Roth (2003) used the age of *Douglassicurus* (36 Ma) as the calibration of their molecular-clock tree of sciurids, which yielded an estimated divergence date of 50 Ma for the node joining *Aplodontia* and Sciuridae. It seems that we should explore for the origins of sciurids in the middle or even early Eocene (the interval of 50–36 Ma) of North America or Asia. Recent discovery of *Douglassciurus oaxacaensis* from late middle Eocene (about 40 Ma) Oaxaca, Mexico, seems to prove this judgment. Mercer and Roth (2003) also estimated that the divergence of the five major clades of squirrels had arisen penecontemporaneously with the EOT. These late Eocene squirrels from Jeminay lived in northwestern China at about 35–34 Ma in the late Eocene. The discovery of *Junggarisciurus jeminaiensis* and *Eopetes irtyshensis* provides a minimum age of calibration for the Sciurinae crown group fairly close to the molecular clock estimated late Eocene 36 Ma split. Based on the fossil-calibrated molecular-clock phylogeny of modern squirrel genera by Mercer and Roth (2003); Roth and Mercer (2008) further investigated the macroevolutionary processes among the linages since the origin of the Sciuridae. Roth and Mercer (2008) described the diversification of squirrels as taking place in three phases: initial (36–30 Ma); intervening (30–7 Ma); and recent (~7 Ma to present) phases. Their results show that the initial phase of squirrel evolution was a rapid burst of diversification (Roth and Mercer, 2008). The two new taxa from Jeminay indicate that there were at least two genera of Sciurinae that occurred in late Eocene Asia.

TABLE 1 Measurements (in mm) of M1/2s and m1/2s of late Eocene-Oligocene sciurids. a.-p., anteroposterior length; tr., maximum transverse width. Measurements of taxa 2–10 and 12–21 derive from the references listed in this table, and those of taxon 11 are estimated from the illustration by Stehlin and Schaub (1951, p. 201). All sources are in the References.

		M1/2		m1/2	
	Taxa (references)	Range of a.-p.	Range of tr.	Range of a.-p.	Range of tr.
1	*Junggarisciurus jeminaiensis* (this text)	3.63	4.75	4.15–4.30	3.90–3.95
2	*Eopetes irtyshensis* (this text)	-	-	5.8	4.6
3	*Oligosciurus dangheensis* (Wang and Qiu, 2004)	-	-	1.60–1.80	1.80–2.0
4	*Kherem hsandgoliensis* (Minjin, 2004)	-	-	1.85–2.10	1.96–2.10
5	*Kherem hsandgoliensis* (Wang and Dashzeveg, 2005)	2.20–2.30	3.10	2.10–2.50	2.30–2.70
6	*Kherem hsandgoliensis* (Maridet et al., 2014)	1.99–2.11	2.51–2.60	2.53–2.59	2.58–2.65
7	*Sciurus* sp. (Bohlin, 1946)	-	-	1.70	1.80
8	Marmotini gen. et sp. indet. (Wang, 2008)	2.10	2.10	-	-
9	*Plesiosciurus* aff. *sinensis* (Maridet et al., 2014)	1.42	1.70–1.82	1.58–1.66	1.50–1.63
10	*Palaeosciurus goti* (Vianey–Liaud, 1974)	1.50–1.83	1.81–2.07	1.65–1.99	1.61–2.01
11	*Oligopetes radialis* (Heissig, 1979)	1.70–2.0	2.05–2.20	1.75–1.90	1.70–1.90
12	*Heteroxerus hürzeleri* (Stehlin and Schaub, 1951)	-	-	1.64–1.87	1.84–1.95
13	*Douglassciurus jeffersoni* (Emry and Korth, 1996)	2.63–3.01	3.45–3.90	2.52–3.10	2.82–3.33
14	*Douglassciurus sapphirus* (Korth, 2009)	1.77–1.90	2.23–2.28	1.84–1.92	1.94–2.25
15	*Douglassciurus bjorki* (Korth, 2014)	2.22–2.75	2.76–3.29	2.12–?	2.24–?
16	*Douglassciurus oaxacaensis* (Ferrusquia-Villafranca et al., 2018)	-	-	1.65–1.91	1.63–1.69
17	*Oligospermophilus douglassi* (Korth, 1987)	1.92–2.19	2.32–2.64	-	-
18	*Cedromus wardi* (Korth and Emry, 1991)	-	-	2.47–2.71	2.70–2.79
19	*Cedromus wilsoni* (Korth and Emry, 1991)	2.17–2.30	2.83–3.0	2.15–2.32	2.37–2.75
20	*Protosciurus condoni* (Black, 1963)	3.40–3.60	3.80–4.0	3.30–3.60	3.40–3.80
21	*Protosciurus mengi* (Black, 1963)	-	-	2.50–2.80	2.70–3.10
22	*Protospermophilus quatalensis* (Gazin, 1930)	2.20–2.30	2.60–2.70	2.0–2.40	2.30–2.70
23	*Miospermophilus bryanti* (Black, 1963)	1.50–1.75	2.0–2.20	1.60–1.80	1.80–2.0
24	*Miosciurus ballovianus* (Black, 1963)	1.50	1.70	1.50–1.60	1.50–1.70
25	*Nototamias hulberti* (Pratt and Morgan, 1989)	1.0–1.30	1.20–1.56	0.98–1.28	1.24–1.61

Squirrels have been divided typically into three morphotypes (ground, tree, and flying) based on their dental and jaw morphologies (e.g., De Bruijn, 1999; Qiu, 2019). *Junggarisciurus jeminaiensis* belongs to the tree squirrel morphotype because it possesses a less rugose surface of the trigon and talonid basins, a complete metaloph, a nearly parallel protoloph and metaloph of M1/2, and a well-delimited entoconid of m1/2. The morphology of *Eopetes irtyshensis* is consistent with that of a typical flying squirrel because it exhibits a complicated dental pattern with a distinct rugose floor of the talonid basin, extra ridges and stylids, and a prominent entoconid. Of the known records, North America is possibly the birthplace of squirrels. *Douglassciurus oaxacaensis* from late middle Eocene (about 40 Ma) in Oaxaca, southeastern Mexico, is possibly the earliest squirrel (Ferrusquia-Villafranca et al., 2018). Due to the lack of upper molars, the morphotype of *D. oaxacaensis* is uncertain. Four late Eocene species, *Douglassciurus jeffersoni* and *Oligospermophilus douglassi* from North America and *Junggarisciurus jeminaiensis* and *Eopetes irtyshensis* from Central Asia, are the second earliest records of the Sciuridae (Figure 4). These fossil records demonstrate that by the late Eocene, the sciurids had diverged into the three principle morphotypes, represented by the earliest flying squirrel *Eopetes irtyshensis* from northwestern China (this text), the earliest ground squirrel *Oligospermophilus douglassi* from North America (Korth, 1987), and the earliest tree squirrels *Douglassciurus jeffersoni* from North America (Emry and Korth, 1996) and *Junggarisciurus jeminaiensis* from Jeminay, northwestern China (this text).

After the Eocene/Oligocene boundary, members of Sciuridae rapidly spread into Europe and flourished across the Holarctic region during the Oligocene. That radiation is demonstrated by the occurrence of eight genera in the early Oligocene, represented by *Heteroxerus* (ground) and *Palaeosciurus* (tree) in Europe, *Oligopetes*

(flying) in Europe and South Asia, *Kherem* (ground) and *Oligosciurus* (tree) in North Asia, and *Oligospermophilus* (ground), *Cedromus* (ground) and *Protosciurus* (tree) in North America (Figure 4). With the oldest sciurid records from Asia and North America predating the first occurrences in Europe, it would seem that sciurids are a component of the European Grand Coupure. Without a phylogenetic context, it is not presently possible to determine if the first sciurids in Europe came from Asia or North America. However, a hypothesis of an Asian origin for those dispersers would seem more likely given the preponderance of mammalian lineages known to have dispersed from Asia to Europe at the start of the Oligocene (coincident with climatic changes and the loss of seaway barriers). In parallel, the published bird (Anatidae: cf. Romainvilliinae) from the same bed as these new sciurid taxa represents an Asian record (late Eocene) predating the group's first appearance in Europe (Oligocene) as another indicator of potential central-Asia-to-Europe dispersal (Stidham and Ni, 2014).

Body mass estimation and paleohabitat

The large size of these fossils is a striking feature of the two new fossil sciurid taxa from Jeminay, northwestern China. The smaller *Junggarisciurus jeminaiensis* is slightly larger than *Protosciurus condoni* and remarkably larger than the 22 other Eocene-to-Oligocene compared taxa in Table 1. To understand the rodents' paleoecological roles, we estimated their body mass from these isolated cheek teeth using published methods (e.g., Legendre, 1989; Hopkins, 2008; Goodwin and Bullock, 2012; Freudenthal and Martín-Suárez, 2013). Following the regression equations of Freudenthal and Martín-Suárez (2013, p.7 and p. 8, see Body mass estimation in Materials and methods in this text), we calculated that the average body masses of *Junggarisciurus jeminaiensis* and *Eopetes irtyshensis* were ~1.2 kg and 2.6 kg, respectively. Among living squirrels, the majority of taxa have average body weights less than 1.0 kg. Only a few are over 1.0 kg, including a tree squirrel *Rheithrosciurus macrotis*, several flying squirrels *Ratufa*, *Petaurista*, *Petinomys crinitus*, and *Aeromys tephromelas*, and most species of ground squirrels *Cynomys* and *Marmota* (Thorington and Heaney, 1981; Ernest, 2003; Hayssen, 2008; Jones et al., 2009; Thorington et al., 2012; Freudenthal and Martín-Suárez, 2013). *Marmota* has an extreme body mass ranging up to 8.0 kg, but *Cynomys* is normally less than 2 kg. Both of them are well adapted to their fossorial steppe environments. The other large living tree and flying squirrels (body mass concentrated in the range of 1–2 kg) all dwell in forests, ranging across tropical rainforest, subtropical deciduous, mixed deciduous and moist evergreen, coniferous and broadleaf, montane and riparian forests. Forests supply large tree or flying squirrels with diverse foods, including seeds, fruits, nuts, bark, insects, and even bird eggs (Thorington et al., 2012). Emry and Thorington (1984) considered that the large tree squirrels should have relatively few competitors, other than birds, for the rich source of nutrients in the forest.

Compared to the monsoon-dominated climatic pattern after the Oligocene–Miocene Transition (OMT), the Paleogene climate of China is considered to have displayed a typical zonal pattern (Wang F. Y., 1984; Sun and Wang, 2005; Guo et al., 2008). During the Eocene and Oligocene, the Junggar Basin is hypothesized to have been situated in a warm-temperate zone (Wang P. X., 1984) or in a subtropical humid vegetation zone of northern China (Sun and Wang, 2005) and to have had a humid environment, contrasting with the arid or semi-arid belt of Guo et al. (2008). In the late Eocene Irtysh River area, fossil pollen assemblages are dominated by coniferous plants like *Pinuspollenites*, *Piceaepollenites*, *Abiespollenites*, and *Podocarpidites*, and broadleaved taxa such as *Betulaepollenites*, *Quercoidites*, *Ulmipollenites*, and *Juglanspollenites*, pointing to a mixed coniferous and broadleaved forest paleoenvironment (Sun et al., 2014). The occurrence of the large tree squirrel *Junggarisciurus jeminaiensis* and the flying squirrel *Eopetes irtyshensis* helps to support this palynological hypothesis of the existence of a forested paleoenvironment in the late Eocene Irtysh River area rather than arid conditions.

Conclusion and perspectives

Based on the large dimensions and unusual morphology of these isolated molar fossils, we erect two new fossil genera and species of squirrels from the late Eocene of the Jeminay area of the Junggar Basin in northwestern China. *Junggarisciurus jeminaiensis* displays molars with a "tree squirrel" morphotype, and *Eopetes irtyshensis* has a lower molar with a "flying squirrel" morphotype. These fossils and taxa are first two confirmed representatives of sciurids in the late Eocene of North Asia and they extend the first appearance of squirrels into the Eocene of Asia.

The impressive size of these two new species from the Junggar Basin leads to estimated body masses of *Junggarisciurus jeminaiensis* and *Eopetes irtyshensis* being ~1.2 kg and 2.6 kg, respectively. All of the extant species of tree or flying morphotype squirrels over 1 kg inhabit forested habitats, and it would seem likely to regard *J. jeminaiensis* and *E. irtyshensis* as having lived in late Eocene forests of Central Asia, consistent with the palynologic analysis by Sun et al. (2014). That interpretation of a forested habitat in the late Eocene of Central Asia will feed into future work investigating the process and pattern of aridification of Central Asia.

Data availability statement

The datasets presented in this study can be found in online repositories. The names of the repository/repositories and accession number(s) can be found in the article/Supplementary Material.

Author contributions

XN and QL led and CQ and HG participated in the fieldwork in the Jeminay area for correlating the stratigraphy and collecting fossils. QL digitized the fossil specimens. QL, XN, and TS wrote the manuscript draft. All authors discussed and revised the manuscript.

Funding

This work was supported by the Strategic Priority Research Program of Chinese Academy of Sciences, under Grant Nos XDB26000000 and XDA2007203.

Acknowledgments

The authors are indebted to the assistance of Lvzhou Li, Xiaoyu Lu, and Shubing Fu of the IVPP who undertook the fieldwork in the Jeminay area. The authors thank Dr. Yemao Hou of the IVPP for his help with CT

scanning and Dr. Xiaoming Wang of the Natural History Museum of California for his advice and comments on the first draft of the manuscript.

Conflict of interest

The authors declare that the research was conducted in the absence of any commercial or financial relationships that could be construed as a potential conflict of interest.

Publisher's note

All claims expressed in this article are solely those of the authors and do not necessarily represent those of their affiliated organizations, or those of the publisher, the editors, and the reviewers. Any product that may be evaluated in this article, or claim that may be made by its manufacturer, is not guaranteed or endorsed by the publisher.

References

Abels, H. A., Dupont-Nivet, G., Xiao, G. Q., Bosboom, R., and Krijgsman, W. (2011). Step-wise change of asian interior climate preceding the Eocene–Oligocene Transition (EOT). *Palaeogeogr. Palaeocl.* 299, 399–412. doi:10.1016/j.palaeo.2010.11.028

Albright, L. B., Woodburne, M. O., Fremd, T. J., Swisher, C. C., MacFadden, B. J., and Scott, G. R. (2008). Revised chronostratigraphy and biostratigraphy of the John Day Formation (Turtle Cove and kimberly memmbers), Oregon, with implications for updated calibration of the Arikareean North American Land Mammal Age. *J. Geol.* 116, 211–237.

Black, C. C. (1963). A review of the North American tertiary Sciuridae. *Bull. Mus. Comp. Zool.* 130, 109–248.

Blanga-Kanfi, S., Miranda, H., Penn, O., Pupko, T., DeBry, R., and Huchon, D. (2009). Rodent phylogeny revised: Analysis of six nuclear genes from all major rodent clades. *BMC Evol. Biol.* 9, 71. doi:10.1186/1471-2148-9-71

Bohlin, B. (1946). The fossil mammals from the tertiary deposit of taben-buluk, western kansu. Part II: Simplicidentata, carinvora, artiodactyla, perissodactyla, and primates. *Palaeont. Sin. N. Ser. C* 8b, 1–259.

Bosboom, R., Dupont-Nivet, G., Grothe, A., Brinkhuis, H., Villa, G., Mandic, O., et al. (2014). Timing, cause and impact of the late Eocene stepwise sea retreat from the Tarim Basin (west China). *Palaeogeogr. Palaeocl.* 403, 101–118. doi:10.1016/j.palaeo.2014.03.035

Bowdich, T. E. (1821). *An analysis of the natural classifications of mammalia, for the use of students and travellers*. Paris: J. Smith.

Bryant, M. D. (1945). Phylogeny of nearctic Sciuridae. *Am. Midl. Nat.* 33, 257–390. doi:10.2307/2421337

Cai, B. Q., Zheng, S. H., Liddicoat, J. C., and Li, Q. (2013). "Chapter 8. Review of the litho-, bio–, and chronostratigraphy in the Nihewan Basin, Hebei, China," in *Fossil Mammals of Asia, Neogene Biostratigraphy and Chronology*. Editors X. M. Wang, L. J. Flynn, and M. Fortelius (New York: Columbia University Press), 218–242.

Collinson, M. E., Fowler, K., and Boulter, M. C. (1981). Floristic changes indicate a cooling climate in the Eocene of southern England. *Nature* 291, 315–317. doi:10.1038/291315a0

Cope, E. D. (1881). On the Nimravidae and Canidae of the Miocene period of NorthNorth America. *Bull. U.S. Geol. Geogr. Surv. Ter.* 6, 165–181.

Cope, E. D. (1879). Second contribution to a knowledge of the Miocene fauna of Oregon. *Paleontol. Bull.* 31, 1–7.

Dalquest, W. W., Baskin, J. A., and Schultz, G. E. (1996). "Fossil mammals from a late Miocene (Clarendonian) site in Beaver County, Oklahoma," in *Contributions in mammalogy: A memorial volume honoring Dr.* Editors J. Knox JonesJr., H. H. Genoways, and R. J. Baker (Lubbock: Museum of Texas Technical University), 107–137.

Dawson, M. R. (1968). Oligocene rodents (mammalia) from East Mesa, Inner Mongolia. *Am. Mus. Novit.* 2324, 1–12.

Dawson, M. R. (2003). Paleogene rodents of Eurasia. *Deinsea* 10, 97–126.

De Bruijn, H. (1999). "Superfamily Sciuroidea," in *The Miocene land mammals of Europe*. Editors G. E. Rössner and K. Heissig (München: Verlag Dr. Friedrich Pfeil), 271–280.

De Bruijn, H., and Ünay, E. (1989). Petauristinae (mammalia, Rodentia) from the Oligocene of Spain, Belgium, and Turkish thrace. *Nat. Hist. Mus. L.A. Sci. Ser.* 33, 139–145.

DeBry, R. (2003). Identifying conflicting signal in a multigene analysis reveals a highly resolved tree: The phylogeny of Rodentia (mammalia). *Syst. Biol.* 52, 604–617. doi:10.1080/10635150390235403

Dehm, R. (1950). Die Nagetiere aus dem Mittel-Miozän (Burdigalium) von Wintershof–West bei Eichstätt in Bayern. *N. Jb. Min. Geol. Paläont. Abh. B* 90, 321–428.

Douglass, E. (1901). Fossil mammalia of the White River beds of Montana. *Trans. Am. Philos. Soc.* 20, 237–279. doi:10.2307/1005478

Downs, T. (1956). The Mascall Fauna from the Montana territory. *Univ. Calif. Publ. Geol. Sci.* 31, 199–354.

Dupont-Nivet, G., Krijgsman, W., Langereis, C. G., Abels, H. A., Dai, S., and Fang, X. M. (2007). Tibetan Plateau aridification linked to global cooling at the Eocene–Oligocene transition. *Nature* 445, 635–638. doi:10.1038/nature05516

Emry, R. J., and Korth, W. W. (2001). *Douglassciurus*, new name for *Douglassia* Emry and Korth, 1996, not *Douglassia* bartsch, 1934. *J. Vertebr. Paleontol.* 21, 400. doi:10.1671/0272-4634(2001)021[0400:dnnfde]2.0.co;2

Emry, R. J., and Korth, W. W. (1996). The Chadronian squirrel "*Sciurus*" *jeffersoni* Douglass, 1901: A new generic name, new material, and its bearing on the early evolution of Sciuridae (Rodentia). *J. Vertebr. Paleontol.* 16, 775–780. doi:10.1080/02724634.1996.10011366

Emry, R. J., and Thorington, R. W., Jr. (1982). Descriptive and comparative osteology of the oldest fossil squirrel, *Protosciurus* (Rodentia: Sciuridae). *Smithson. Contrib. Paleobiol.* 47, 1–35. doi:10.5479/si.00810266.47.1

Emry, R. J., and Thorington, R. W., Jr. (1984). "The tree squirrel *Sciurus* as a living fossil," in *Living Fossils*. Editors N. Eldredge and S. Stanley (New York: Springer-Verlag), 23–31.

Ernest, S. K. M. (2003). Life history characteristics of placental nonvolant mammals. *Ecology* 84, 3402. doi:10.1890/02-9002

Fabre, P. H., Hautier, L., Dmitrov, D., and Douzery, E. J. P. (2012). A glimpse on the pattern of rodent diversification: A phylogenetic approach. *BMC Evol. Biol.* 12, 88–19. doi:10.1186/1471-2148-12-88

Fang, X. M., Zan, J. B., Appel, E., Lu, Y., Song, C. H., Dai, S., et al. (2015). An Eocene-Miocene continuous rock magnetic record from the sediments in the Xining Basin, NW China: Indication for cenozoic persistent drying driven by global cooling and Tibetan Plateau uplift. *Geophys. J. Int.* 201, 78–89. doi:10.1093/gji/ggv002

Ferrusquia-Villafranca, I., Flynn, L. J., Ruiz-Gonzalez, J. R., Torres-Hernandez, J. R., and Martinez-Hernandez, E. M. (2018). New Eocene rodents from northwestern Oaxaca, southeastern Mexico, and their paleobiological significance. *J. Vert. Pal.*, e1514615. doi:10.1080/02724634.2018.1514615

Fischer de Waldheim, G. (1817). Adversaria zoologica. *Mem. Soc. Nat. Moscou* 5, 357–446.

Fossilworks Group (2022). Available at: http://www.fossilworks.org (Accessed June 25, 2022).

Freudenthal, M., and Martin-Suárez, E. (2013). Estimating body mass of fossil rodents. *Scr. Geol.* 145, 1–130.

Gazin, C. L. (1932). A Miocene mammalian fauna from southeastern Oregon. *Carnegie Inst. Wash. Publ.* 418, 36–86.

Gazin, C. L. (1930). *A Tertiary Vertebrate Fauna from the Upper Cuyama Drainage Basin*, 404. California: Carnegie Inst. Wash. Publ, 55–76.

Goodwin, T. H., and Bullock, K. M. (2012). Estimates of body mass for fossil giant ground squirrels, genus *Paenemarmota*. *J. Mamm.* 93, 1169–1177. doi:10.1644/11-mamm-a-312.3

Goodwin, T. H. (2008). "Chapter 21 Sciuridae," in *Evolution of tertiary mammals of North America, volume 2: Small mammals, xenarthrans, and marine mammals*. Editors C. M. Janis, G. F. Gunnell, and M. D. Uhen (New York: Cambridge University Press), 355–376.

Guo, Z. T., Sun, B., Zhang, Z. S., Peng, S. Z., Xiao, G. Q., Ge, J. Y., et al. (2008). A major reorganization of Asian climate by the early Miocene. *Clim. Past.* 4, 153–174. doi:10.5194/cp-4-153-2008

Hall, E. R. (1930). Rodents and lagomorphs from the Barstow beds of southern California. *Univ. Calif. Publ. Geol. Sci.* 19, 313–318.

Hayssen, V. (2008). Patterns of body and tail length and body mass in Sciuridae. *J. Mamm.* 89, 852–873. doi:10.1644/07-mamm-a-217.1

Heissig, K. (1979). Die frühestern Flughörnchen und primitive Ailuravinae (Rodentia, Mammalia) aus dem suddeutschen Oligozän. *Mitt. Bayer. Staatssamml. Paläontol. Hist. Geol.* 19, 139–169.

Heissig, K. (2003). Origin and early dispersal of the squirrels and their relatives. *Deinsea* 10, 277–286.

Hoffmann, R. S., Anderson, C. G., Thorington, R. W., Jr., and Heaney, L. R. (1993). "Family Sciuridae," in *Mammal Species of the World*. Editors D. E. Wilson and D. M. Reeder (Washington: Smithsonian Institution Press), 419–465.

Hooker, J. J., Collinson, M. E., and Sille, N. P. (2004). Eocene–Oligocene mammalian faunal turnover in the hampshire basin, UK: Calibration to the global time scale and the major cooling event. *J. Geol. Soc.* 161, 161–172. doi:10.1144/0016-764903-091

Hopkins, S. B. (2008). Reassessing the mass of exceptionally large rodents using toothrow length and area as proxies for body mass. *J. Mamm.* 89, 232–243. doi:10.1644/06-mamm-a-306.1

Huchon, D., and Douzery, E. (2001). From the old world to the new world: A molecular chronicle of the phylogeny and biogeography of hystricognath rodents. *Mol. Phylogenet. Evol.* 20, 238–251. doi:10.1006/mpev.2001.0961

Hren, M. T., Sheldon, N. D., Grimes, S. T., Collinson, M. E., Hooker, J. J., Bugler, M., et al. (2013). Terrestrial cooling in Northern Europe during the Eocene-Oligocene Transition. *PNAS* 110, 7562–7567. doi:10.1073/pnas.1210930110

Hutchinson, D. K., Coxall, H. K., Lunt, D. L., Steinthorsdottir, M., de Boer, A. M., Baatsen, M., et al. (2021). The Eocene–Oligocene Transition: A review of marine and terrestrial proxy data, models and model–data comparisons. *Clim. Past.* 17, 269–315. doi:10.5194/cp-17-269-2021

Jin, H. Y. (2000). Middle Eocene mammals of Jeminay, Xinjiang. *Vert. Palasiat.* 38, 135–146.

Jones, K. E., Bielby, J., Cardillo, M., Fritz, S. A., O'Dell, J., Orme, D. L., et al. (2009). PanTHERIA: A species-level database of life history, ecology, and geography of extant and recently extinct mammals. *Ecology* 90, 2648. doi:10.1890/08-1494.1

Korth, W. W. (1984). Earliest Tertiary evolution and radiation of rodents in North America. *Bull. Carnegie Mus. Nat. Hist.* 24, 1–71. doi:10.5962/p.228603

Korth, W. W., and Emry, R. J. (1991). The skull of *Cerdormus* and a review of the Cedromurinae (Rodentia, Sciuridae). *J. Paleontol.* 65, 984–994. doi:10.1017/s0022336000033291

Korth, W. W. (1992). Fossil small mammals from the Harrison Formation (late Arikareean: Earliest Miocene), Cherry County, Nebraska. *Ann. Carnegie Mus.* 61, 69–131. doi:10.5962/p.215172

Korth, W. W. (2009). Mammals from the Blue Ash local fauna (late Oligocene), south Dakota. Rodentia, Part 3: Family Sciuridae. *Paludicola* 7, 47–60.

Korth, W. W. (1981). New Oligocene rodents from Western North America. *Ann. Carnegie Mus.* 50, 289–318. doi:10.5962/p.214493

Korth, W. W. (2014). Rodents (mammalia) from the Whitneyan (middle Oligocene) Cedar Pass Fauna of south Dakota. *Ann. Carnegie Mus.* 82, 373–398. doi:10.2992/007.082.0404

Korth, W. W. (1987). Sciurid rodents (mammalia) from the Chadronian and Orellan (Oligocene) of Nebraska. *J. Paleontol.* 61, 1247–1255. doi:10.1017/s0022336000029620

Korth, W. W. (1994). *The Tertiary Record of Rodents in North America*. New York: Springer Science+Business Media.

Legendre, S. (1989). Les communautés de mammifères du Paléogéne (eocéne supérieur et oligocéne) d'Europe occidentale: Structures, milieux et évolution. *Münch. Geowiss. Abh.* A16, 1–110.

Li, J. X., Yue, L. P., Roberts, A. P., Hirt, A. M., Pan, F., Guo, L., et al. (2018). Global cooling and enhanced Eocene Asian mid-latitude interior aridity. *Nat. Commun.* 9, 3026. doi:10.1038/s41467-018-05415-x

Li, Q., Xie, G. P., Takeuchi, G. T., Deng, T., Tseng, Z. J., Grohé, C., et al. (2014). Vertebrate fossils on the Roof of the World: Biostratigraphy and geochronology of highelevation Kunlun Pass Basin, northern Tibetan Plateau, and basin history as related to the Kunlun strike–slip fault. *Palaeogeogr. Palaeocl.* 411, 46–55. doi:10.1016/j.palaeo.2014.06.029

Linnaeus, C. (1758). *Systema naturae per regna tria naturae, secundum classes, ordines, genera, species, cum characteribus, differentiis, synonymis, locis*. Tenth edition. Stockholm: Laurentii Salvii.

Liu, Z. H., Pagani, M., Zinniker, D., DeConto, R., Huber, M., Brinkhuis, H., et al. (2009). Global cooling during the Eocene–Oligocene climate transition. *Science* 323, 1187–1190. doi:10.1126/science.1166368

Maridet, O., Daxner-Höck, G., Badamgarav, D., and Göhlich, U. B. (2014). New discoveries of sciurids (rodents, Mammalia) from the Valley of Lakes (Central Mongolia). *Ann. Naturhist. Mus. Wien Ser. A* 116, 271–291.

Matthew, W. D. (1903). The fauna of the Titanotherium Beds at Pipestone Springs, Montana. *Bull. Am. Mus. Nat. Hist.* 19, 197–226.

Matthew, W. D., and Mook, C. C. (1933). New fossil mammals from the Deep River beds of Montana. *Am. Mus. Novit.* 601, 1–7.

Matthew, W. D. (1910). On the osteology and relationships of *Paramys*, and the affinities of the Ischyromyidae. *Bull. Am. Nat. Hist.* 21, 21–26.

McKenna, M. C., and Bell, S. K. (1997). *Classification of Mammals above the Species Level*. New York: Columbia University Press.

Mein, P., and Ginsburg, L. (2002). Sur l'âge relatif des différents dépôts karstiques Miocènes de La Grive-Saint-Alban (Isère). *Mus. Hist. Nat. Lyon* 2, 7–47. doi:10.3406/mhnly.2002.1328

Meng, J., and McKenna, M. C. (1998). Faunal turnovers of Paleogene mammals from the Mongolian Plateau. *Nature* 394, 364–367. doi:10.1038/28603

Mercer, J. M., and Roth, V. L. (2003). The effects of Cenozoic global change on squirrel phylogeny. *Science* 299, 1568–1572. doi:10.1126/science.1079705

Miao, Y. F., Fang, X. M., Wu, F. L., Cai, M. T., Song, C. H., Meng, Q. Q., et al. (2013). Late Cenozoic continuous aridification in the Western Qaidam Basin: Evidence from sporopollen records. *Clim. Past.* 9, 1863–1877. doi:10.5194/cp-9-1863-2013

Miao, Y. F., Herrmann, M., Wu, F. L., Yan, X. L., and Yang, S. L. (2012). What controlled mid-late Miocene long-term aridification in central Asia? - global cooling or Tibetan Plateau uplift: A review. *Earth-Sci. Rev.* 112, 155–172. doi:10.1016/j.earscirev.2012.02.003

Minjin, B. (2004). An Oligocene sciurid from the Hsanda Gol Formation, Mongolia. *J. Vertebr. Paleontol.* 24, 753–756. doi:10.1671/0272-4634(2004)024[0753:aosfth]2.0.co;2

Montgelard, C., Forty, E., Aranl, V., and Matthee, C. A. (2008). Suprafamilial relationships among Rodentia and the phylogenetic effect of removing fast–evolving nucleotides in mitochondrial, exon and intron fragments. *BMC Evol. Biol.* 8, 321. doi:10.1186/1471-2148-8-321

Ni, X. J., Flynn, J. J., and Wyss, A. R. (2012). Imaging the inner ear in fossil mammals: High-resolution CT scanning and 3–D virtual reconstructions. *Palaeontol. Electron.* 15 (2.18A), 1–10. doi:10.26879/288

Osborn, H. E., and Matthew, W. D. (1909). Cenozoic mammal horizons of Western North America, with faunal lists of the Tertiary Mammalia of the West. *Bull. U.S. Geol. Surv.* 361, 1–138.

Oshida, T., Masuda, R., and Yoshida, M. C. (1996). Phylogenetic relationships among Japanese species of the family Sciuridae (Mammalia, Rodentia), inferred from nucleotide sequences of mitochondrial 12s ribosomal RNA genes. *Zool. Sci.* 13, 615–520. doi:10.2108/zsj.13.615

Pomel, A. N. (1853). *Catalogue méthodique et descriptif des vertébrés fossiles*. Paris: Baillière.

Pratt, A. E., and Morgan, G. S. (1989). New Sciuridae (Mammalia: Rodentia) from the early Miocene Thomas Farm local fauna, Florida. *J. Vertebr. Paleont.* 9, 89–100. doi:10.1080/02724634.1989.10011741

Prothero, D. R., and Emry, R. J. (1994). *The Terrestrial Eocene-Oligocene Transition*. New York: Columbia University Press.

Prothero, D. R., Ivany, L. C., and Nesbitt, E. A. (2003). *From Greenhouse to Icehouse: The Marine Eocene-Oligocene Transition*. New York: Columbia University Press.

Qiu, Z. D. (2019). "Family Sciuridae," in *Palaeoverterata Sinica Volum III Basal Synapsids and Mammals Fascicle 5 (1) (serial no. 18–1) Glires II: Rodentia I*. Editors C. K. Li and Z. D. Qiu (Beijing: Science Press), 70–160.

Qiu, Z. D., and Lin, Y. P. (1986). The Aragonian vertebrate fauna of Xiacaowan, Jiangsu - 5. Sciuridae (Rodentia, Mammalia). *Vert. Palasiat.* 24, 195–212.

Qiu, Z. D. (1996). *Middle Miocene Micromammalian Fauna from Tunggur, Nei Mongol*. Beijing: Science Press.

Qiu, Z. D. (2015). Revision and supplementary note on Miocene sciurid fauna of Sihong, China. *Vert. Palasiat.* 53, 219–237.

Qiu, Z. X., Deng, T., and Wang, B. Y. (2005). Early Pleistocene mammalian fauna from Longdan, Dongxiang, Gansu, China. *Palaeont. Sin. N. Ser. C* 27, 1–198.

Retallack, G. J., Orr, W. N., Prothero, D. R., Duncan, R. A., Kester, P. R., and Ambers, C. P. (2004). Eocene-Oligocene extinction and paleoclimatic change near Eugene, Oregon. *GSA Bull.* 116, 817–839. doi:10.1130/b25281.1

Roth, V. L., and Mercer, J. M. (2008). Differing rates of macroevlutionary diversification in arboreal squirrels. *Cur. Sci. India* 95, 857–861.

Simpson, G. G. (1945). The principles of classification and a classification of mammals. *Bull. Am. Mus. Nat. Hist.* 85, 1–350.

Stehlin, H. G. (1910). Remarques sur les faunules de Mammiféres des couches éocènes et oligocènes du Bassin de Paris. *Bull. Soc. Géol. Fr.* 9, 488–520.

Stehlin, H. G., and Schaub, S. (1951). Die Trigonodontie der simplicidentaten Nager. *Schweiz. paläont. abh.* 67, 1–385.

Steppan, S. J., Storz, B. L., and Hoffmann, R. S. (2004). Nuclear DNA phylogeny of the squirrels (Mammalia: Rodentia) and the evolution of arboreality from c-myc and RAG1. *Mol. Phylogenet. Evol.* 30, 703–719. doi:10.1016/s1055-7903(03)00204-5

Stidham, T. A., and Ni, X. J. (2014). Large anseriform (Aves: Anatidae: Rominvilliinae?) fossils from the late Eocene of Xinjiang, China. *Vert. Palasiat.* 52, 98–111.

Sun, J. M., Ni, X. J., Bi, S. D., Wu, W. Y., Ye, J., Meng, J., et al. (2014). Synchronous turnover of flora, fauna, and climate at the Eocene-Oligocene Boundary in Asia. *Sci. Rep.* 4, 7463. doi:10.1038/srep07463

Sun, J. M., and Windley, B. F. (2015). Onset of aridification by 34 Ma across the Eocene-Oligocene transition in central Asia. *Geology* 43, 1015–1018. doi:10.1130/g37165.1

Sun, X. J., and Wang, P. X. (2005). How old is the Asian monsoon system?—palaeobotanical records from China. *Palaeogeogr. Palaeocl.* 222, 181–222. doi:10.1016/j.palaeo.2005.03.005

Thorington, R. W., Jr. (1984). Flying squirrels are monophyletic. *Science* 225, 1048–1050. doi:10.1126/science.225.4666.1048

Thorington, R. W., Jr., and Heaney, L. R. (1981). Body proportions and gliding adaptations of flying squirrels (Petauristinae). *J. Mamm.* 62, 101–114. doi:10.2307/1380481

Thorington, R. W., Jr., and Hoffmann, R. S. (2005). "Family Sciuridae," in *Mammal species of the world. A taxonomic and geographic reference*. Editors D. E. Wilson and D. M Reeder. Third Edition Volume 2 (Baltimore: The Johns Hopkins University Press), 754–818.

Thorington, R. W., Jr., Koprowski, J. L., Steele, M. A., and Whatton, J. F. (2012). *Squirrels of the World*. Baltimore: The Johns Hopkins University Press.

Thorington, R. W., Jr., Pitassy, D., and Jansa, S. (2002). Phylogenies of flying squirrels (Pteromyinae). *J. Mamm. Evol.* 9, 99–135.

Tong, Y. S., and Li, Q. (2019). "Families Alagomyidae, Archetypomyidae, Ischyromyidae," in *Palaeoverterata Sinica Volum III Basal Synapsids and Mammals Fascicle 5 (1) (serial no. 18–1) Glires II: Rodentia I*. Editors C. K. Li and Z. D. Qiu (Beijing: Science Press), 20–42.

Vianey-Liaud, M. (1974). *Palaeosciurus goti* nov. sp., écureuil terrestre de l'Oligocène moyen du Quercy. Données nouvelles sur l'apparition des Sciuridés en Europe. *Ann. Paléont. (Vert.)* 60, 103–122.

Vianey-Liaud, M. (1985). "Possible evolutionary relationships among Eocene and lower Oligocene rodents of Asia, Europe and North America," in *Evolutionary relationships among rodents*. Editors W. P. Luckett and J. L. Hartenberger (New York: Plenum Press), 277–309.

Wang, B. Y. (2008). Additional rodent material from Houldjin Formation of Erenhot, Nei Mongol, China. *Vert. Palasiat.* 46, 21–30.

Wang, B. Y., and Dashzeveg, D. (2005). New Oligocene sciurids and aplodontids (Rodentia, Mammalia) from Mongolia. *Vert. Palasiat.* 43, 85–99.

Wang, B. Y., and Qiu, Z. X. (2003). Aepyosciurinae - a new subfamily of Sciuridae (Rodentia, Mammalia) from basal loess deposits at the northeastern border of Tibetan Plateau. *Chin. Sci. Bull.* 48, 691–695. doi:10.1007/bf03325657

Wang, B. Y., and Qiu, Z. X. (2004). Discovery of early Oligocene mammalian fossils from Danghe area, Gansu, China. *Vert. Palasiat.* 42, 130–143.

Wang, F. Y. (1984). Discovery of abundant early Tertiary plant fossils in Jeminay county, Xinjiang. *Xijiang Geol.* 2, 81–82.

Wang, P. X. (1984). "Progress in late Cenozoic palaeoclimatology of China: A brief review," in *The Evolution of the East Asian Environment*. Editor R. O. Whyte (Hongkong: Hong Kong University), Vol. 1.

Wang, X. M., Li, Q., Xie, G. P., Saylor, J. E., Tseng, Z. J., Takeuchi, G. T., et al. (2013). Mio–Pleistocene Zanda Basin biostratigraphy and geochronology, pre–ice age fauna, and mammalian evolution in Western Himalaya. *Palaeogeogr. Palaeoecl.* 374, 81–95. doi:10.1016/j.palaeo.2013.01.007

Welcomme, J.-L., Benammi, M., Crochet, J.-Y., Marivaux, L., Métais, G., Antoine, P.-O., et al. (2001). Himalayan forelands: Palaeontological evidence for Oligocene detrital deposits in the Bugti hills (balochistan, Pakistan). *Geol. Mag.* 138, 397–405. doi:10.1017/s0016756801005428

Wilson, R. W. (1960). Early Miocene rodents and insectivores from northeastern Colorado. *Univ. Kans. Paleont. Contrib. Vert.* 7, 1–92.

Wilson, R. W. (1949). On some White River fossil rodents. *Carnegie Inst. Wash. Publ.* 584, 27–50.

Wood, A. E., and Jepsen, G. L. (1937). The mammalian fauna of the White River Oligocene. Part II. Rodentia. *Trans. Am. Philos. Soc.* 28, 155–269. doi:10.2307/1005501

Wood, A. E. (1962). The early tertiary rodents of the family Paramyidae. *Am. Philos. Soc.* 52, 3–261. doi:10.2307/1005914

Wood, A. E. (1980). The Oligocene rodents of North America. *Am. Philos. Soc.* 70, 1–68. doi:10.2307/1006314

Zachos, J., Pagani, M., Sloan, L., Thomas, E., and Billups, K. (2001). Trends, rhythms, and aberrations in global climate 65 Ma to present. *Science* 292, 686–693. doi:10.1126/science.1059412

Ziegler, R., and Fahlbusch, V. (1986). Kleinsäuger-Faunen aus der basalen Oberen Süsswasser–Molasse Niederbayerns. *Zitteliana* 14, 3–58.

frontiers | Frontiers in Earth Science

TYPE Original Research
PUBLISHED 23 January 2023
DOI 10.3389/feart.2022.1018675

OPEN ACCESS

EDITED BY
Lucja A. Fostowicz-Frelik,
Institute of Paleobiology (PAN), Poland

REVIEWED BY
Olivier Maridet,
JURASSICA Museum, Switzerland
Lawrence John Flynn,
Harvard University, United States

*CORRESPONDENCE
Xijun Ni,
nixijun@ivpp.ac.cn
Qiang Li,
liqiang@ivpp.ac.cn

SPECIALTY SECTION
This article was submitted to Paleontology, a section of the journal Frontiers in Earth Science

RECEIVED 13 August 2022
ACCEPTED 25 November 2022
PUBLISHED 23 January 2023

CITATION
Ni X, Li Q, Deng T, Zhang L, Gong H, Qin C, Shi J, Shi F and Fu S (2023), New *Yuomys* rodents from southeastern Qinghai-Tibet Plateau indicate low elevation during the Middle Eocene. *Front. Earth Sci.* 10:1018675. doi: 10.3389/feart.2022.1018675

New *Yuomys* rodents from southeastern Qinghai-Tibet Plateau indicate low elevation during the Middle Eocene

Xijun Ni[1,2,3]*, Qiang Li[1,2,3]*, Tao Deng[1,2,3], Limin Zhang[1,2,3], Hao Gong[1,2], Chao Qin[1,2], Jingsong Shi[1], Fuqiao Shi[1] and Shubing Fu[1]

[1]Key Laboratory of Vertebrate Evolution and Human Origins, Institute of Vertebrate Paleontology and Paleoanthropology, Chinese Academy of Sciences, Beijing, China, [2]University of Chinese Academy of Sciences, Beijing, China, [3]CAS Center for Excellence in Life and Paleoenvironment, Beijing, China

Yuomys are medium-sized Hystricomorpha rodents. They are known for coming from areas of low elevation in China during the middle and late Eocene. Two new *Yuomys* were discovered from a locality near Xueshuo village in Litang County, Sichuan Province. The locality lies in the Gemusi pull-apart basin formed in the Litang Fault System (LTFS) in the Hengduan Mountains. The current average elevation is about 4200 m. One of the two new *Yuomys* is larger and shows clear lophodont and unilateral hypsodont morphology, similar to *Yuomys yunnanensis*, which was discovered as being from the early middle Eocene (Irdinmanhan, Asian Land Mammal Ages) in the Chake Basin of Jianshui County, Yunnan Province. The Chake Basin is one of the small pull-apart basins formed in the Xianshuihe-Xiaojiang Fault system (XSH-XJF). The other new *Yuomys* rodent is smaller, brachydont, and less lophodont than the larger new species. The small new *Yuomys* is smaller than all known *Yuomys* except *Yuomys huheboerhensis*, which is from the early middle Eocene Irdinmanhan of Inner Mongolia in Northern China. Given their narrow biochronological distribution and presumably preferred living environment, the occurrence of *Yuomys* in the pull-apart basins in LTFS and XSH-XJF suggests that the two deep fault systems probably started strike-slip movement by the early middle Eocene, about 49–45 million years ago. Well-studied middle Eocene mammalian faunas from Henan and Inner Mongolia include *Yuomys*, primates, and other low elevation forest mammals. We suggest that the two new *Yuomys* species reported here probably also lived in a similar low elevation forest environment.

KEYWORDS

***Yuomys*, Chuandian terrane, accommodation zone, strike-slip movement, plateau uplifting**

1 Introduction

Yuomys is a genus of rodents that existed in the middle and late Eocene in East Asia (Figure 1). Known species of *Yuomys* show a clear evolutionary tendency of developing lophodont and hypodont teeth and increasing body size. The evolutionary sequence of *Yuomys* clearly correlates with the biochronology sequence of Asia (Gong et al., 2021). Apart from the earliest species, *Yuomys huheboerhensis*, later *Yuomys* species are significantly large compared to contemporary rodents, such as ctenodactylids and myomorph rodents. *Y. huheboerhensis* is the oldest-known and the most primitive *Yuomys*. It was discovered from the early middle Eocene Irdin Manha Formation at the Huheboerhe locality in the Huheboerhe-Nuhetingboerhe area of the Erlian Basin of Inner Mongolia (Li and Meng, 2015). *Y. huheboerhensis* is only slightly larger than contemporary ctenodactylids and shows a tendency of developing lophodont teeth. *Yuomys yunnanensis* was discovered from the middle Eocene at the Chake locality near Jianshui County of Yunnan Province. Mammalian fauna correlation suggests that the Chake locality is also Irdinmanhan in age (Huang and Zhang, 1990), probably slightly younger than the fossil site of *Y. huheboerhensis*. *Yuomys weijingensis* was discovered in the Ulan Shireh area of Inner Mongolia. The locality was originally reported as late Eocene, but recent revision of the stratigraphic and mammalian fauna correlations suggest that *Y. weijingensis* should be middle Eocene Irdinmanhan in age (Li and Meng, 2015; Li, 2019; Gong et al., 2021). *Yuomys minggangensis* was discovered from the middle Eocene at the Tuanshan locality near the Xinji Village of Minggang Town, Xinyang City of Henan Province (Wang and Zhou, 1982). The age of the Tuanshan locality is probably also Irdinmanhan. The type species of *Yuomys*, *Yuomys cavioides*, came from the late middle Eocene Sharamurunian at the Rencun locality of Mianchi County, Henan Province (Li, 1975). *Yuomys cf. Y. cavioides* was present at the Ula Usu locality of Inner Mongolia (Li, 1975; Gong et al., 2021), which is Sharamurunian in age. *Yuomys* records of similar age are *Y. eleganes*, *Y. huangzhuangensis*, *Y. altunensis*, and *Y. magnus* from a locality near Dalishu village of Wucheng Town, Tongbai County of Henan Province (Wang, 1978), the Langtougou locality near Huangzhuang village of Qufu City of Shandong Province (Shi, 1989), the Altyn Tagh of Xinjiang Province (Wang, 2017), and the Erden Obo locality of Nomogeng, Siziwangqi County of Inner Mongolia (Li, 2019). The youngest known *Yuomys*, *Y. robustus*, was discovered from the late Eocene at a locality near the Bujiamiaozi village, Lingwu City of Ningxia Province. A specimen from the Zhanglizi Gou locality near Chengliu village of Jiyuan County, Henan Province was recently referred to *Y. robustus* (Gong et al., 2021).

Here we report two new species of *Yuomys* discovered from southeast Qinghai-Tibetan Plateau, where Paleogene mammalian fossils are very rare. Although the two new *Yuomys* species are represented by three specimens only, their morphology clearly distinguishes them from other *Yuomys* and fits in the evolutionary sequence of *Yuomys*. The discovery therefore provides solid evidence for biochronology correlation and paleoenvironmental reconstruction of Southeastern Qinghai-Tibet Plateau.

FIGURE 1
Locality of the Gemusi pull-apart basin and the distribution of *Yuomys*.

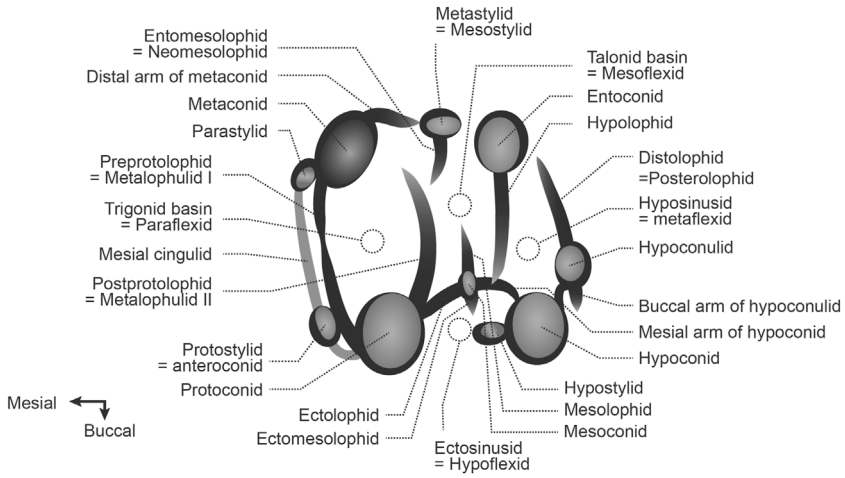

FIGURE 2
Dental terminology used for description and comparison.

2 Materials and methods

The *Yuomys* fossils reported here were discovered from the middle Eocene Gemusi Formation near Xueshuo Village of Litang County, Sichuan Province (Figure 1). The Gemusi Formation sedimentation was developed in the Gemusi pull-apart basin in the Litang Fault System (LTFS). The Gemusi Basin is about 150 km south of Litang city, near the headstream of the Shuiluo river, which is a branch of the Jinsha river. The average elevation of the Gemusi Basin is about 4200 m.

The Gemusi Formation is a set of brownish red-purplish fluvial and lacustrine sediments unconformably overlaying the black Triassic slates (Zong et al., 1996). The remaining thickness of the Gemusi Formation is over 300 m. The lower third of the Gemusi Formation includes conglomerates and coarse sandstones, imbedded with thin layers of mudstones. The middle and upper parts of the Gemusi Formation are dominated by mudstones and sandstone, imbedded with conglomerate layers. There is a thin layer of freshwater limestone in the middle part. There are two mammalian fossil layers. The lower fossil layer only includes some fossil fragments. The upper mammalian fossil layer is within a bed of siltstone enriched with calcareous nodules. The mammalian fossils from this layer include *Anthracokeryx litangensis Bothriodon* sp., *Sianodon* sp., *Caenolophus proficiens*, Brontotheriidae gen. & sp. indet., and the new *Yuomys* species reported here.

The dental morphology terminology used for description and comparison (Figure 2) was modified from Marivaux et al. (2019). Maps were generated at the Conservation Biology Institute Data Basin online mapping system (https://databasin.org/datasets/366a1bef53344c02bcd7d7611d5f61f7/).

3 Systematic paleontology

Class Mammalia Linnaeus, (1758). Order Rodentia Bowdich, (1821). Suborder Hystricomorpha Brandt. (1855). Infraorder Hystricognathi Tullberg, 1899. Family Yuomyidae Dawson et al. (1984). Genus Yuomys Li, 1975. *Yuomys dawai* nov. sp. Ni and Li. LSID urn:lsid:zoobank.org:act:7E3D50A6-A92E-4205-B7C2-A8AF0513A8F9. (Figure 3, Table 1).

Holotype—Specimen IVPP V 31,415, a left lower jaw fragment preserving dp4, m1, and m2.

Type locality—Locality GMS20201010LQ02 (29° 21′ 28.628″N, 100° 28′ 9.665″E), near Xueshuo village, Gemusi Basin, Litang County, Sichuan Province (Figure 1).

Referred specimen—The holotype only.

Age—Early middle Eocene, early Irdinmanhan of Asian Land Mammal Ages, about 49–45 Ma.

Etymology—The species name is dedicated to Dr. Jian'an Dawa, who is a doctor in the Community Hospital at the Xueshuo Village. Dr. Jian'an helped us in the field.

Diagnosis—Small *Yuomys*, brachydont, weakly lophodont. Dp4 mesial cingulid strong, preprotolophid, and postprotolophid enclosing trigonid basin; Dp4-m2 ectolophid oblique, joining the protoconid near buccal side, talonid basin and hyposinusid broad, mesoconid present, mesial arm of hypoconid long; dp4-m1 hypoconulid larger and more projecting than hypoconid; m1 mesolophid present.

Description—Only the holotype is available for description. The jaw preserves a part of the incisor, dp4, m1, and m2. The mental foramen is small and located at a point mesial to the dp4. The inferior masseter ridge is strong. It starts from the lateral side of the m1 and extends inferiorly and posteriorly, and entirely lateral to the incisor alveolar. The inferior masseter ridge extends

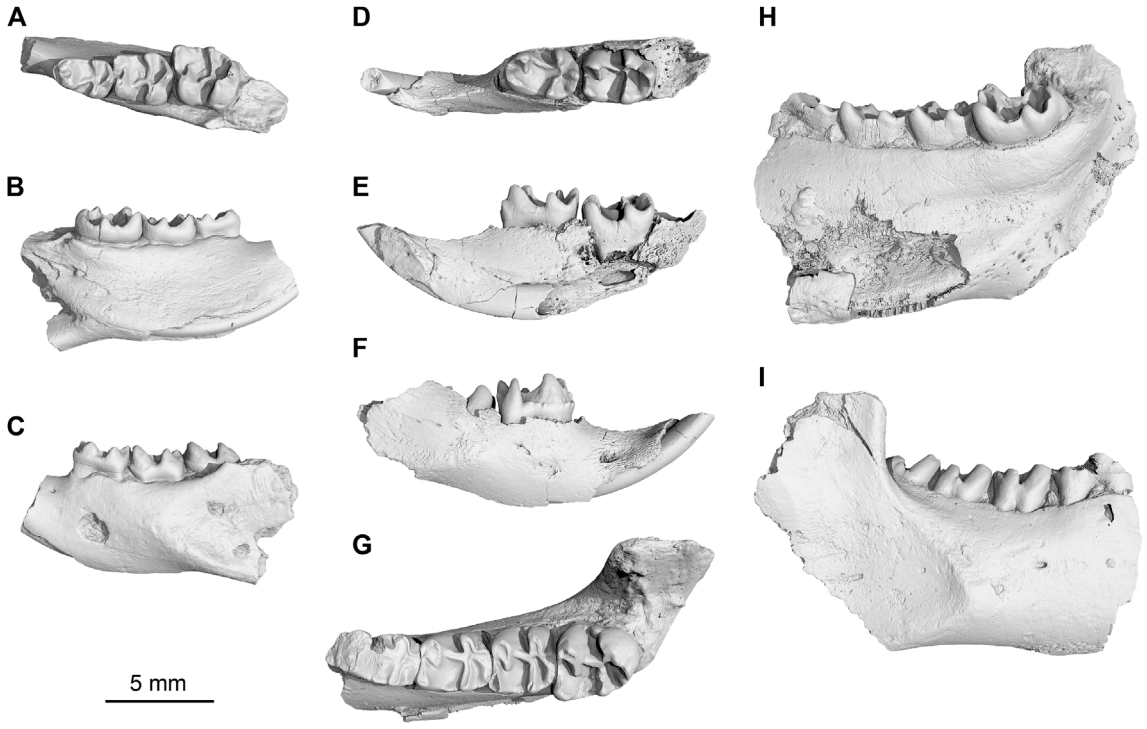

FIGURE 3
New *Yuomys* from the Gemusi pull-apart basin. **(A–C)**, *Yuomys dawai* sp. nov., IVPP V 31415, holotype, in occlusal, lingual, and buccal views; **(D–F)**, *Yuomys gemuensis* sp. nov., IVPP V 31417, in occlusal, lingual, and buccal views; **(G–I)**, *Y. gemuensis* sp. nov., IVPP V 31416, holotype, in occlusal, lingual, and buccal views.

TABLE 1 Measurements of *Yuomys* jaws discovered from the Gemusi Basin (in mm).

	IVPP V 31415			IVPP V 31416			IVPP V 31417		
	Length	Trigonid width	Talonid width	Length	Trigonid width	Talonid width	Length	Trigonid width	Talonid width
dp4	2.86	1.49	1.85	4.35	2.26	2.65	3.74	2.13	2.66
m1	2.99	2.19	2.50	3.46	3.36	3.61	3.43	3.21	3.43
m2	3.10	2.88	3.02	3.27	3.78	3.76			
m3				4.38	4.01	3.50			

to the angular process. Origin of the angular process distinctly buccal to the plane of the incisor alveolus is traditionally defined as hystricognathous jaw (Tullberg, 1899). The ventral side of the incisor has a weak longitudinal enamel stripe.

The buccal side of the check teeth is higher than the lingual size. The overall crown height is low. The dp4 is smaller than the m1 and m2. Its trigonid includes two main cusps, protoconid and metaconid. The two cusps are equal in size, but the metaconid is more mesially positioned. The preprotolophid is short. The buccal and lingual parts of the preprotolophid form a V-shaped notch. The postprotolophid connects the metaconid. The preprotolophid and postprotolophid enclose the trigonid basin. Mesial to the protoconid and metaconid, the mesial cingulid is strong. The dp4 talonid is wider than the trigonid. The talonid basin is broad. The hypoconid is mesial-distally compressed. The entoconid is smoothly fused with the hypolophid. The ectolophid is thin and oblique. It connects the protoconid near the buccal side. A small mesoconid is present in the middle of the ectolophid. The hypolophid connects the ectolophid at a position mesial to the hypoconid.

A short mesial arm of the hypoconid is present. The hypoconulid is larger than the hypoconid and strongly posterior projecting. The hyposinusid is large and deep. A fovea is present buccal and distal to the hypoconid-hypoconulid junction.

The m1 is similar to the dp4, but without mesial cingulid. The preprotolophid is high. The postprotolophid is short. It reaches the metaconid but does not close the trigonid basin completely. The talonid basin is even broader. A weak mesolophid is present. The hypoconulid is even more distally projecting than in the dp4. The hyposinusid almost as broad as the talonid basin.

The m2 is much larger than the m1. Its metaconid is higher and more mesially positioned than the protoconid. The preprotolophid is fused with the metaconid and is relatively higher and stronger than in the m1. The postprotolophid of the m2 is short and does not connect the metaconid. As a result, the distal side of the trigonid is open to the talonid. The talonid is slightly wider than the trigonid. The talonid basin is broad and shallow. The ectolophid is thin and oblique, meeting the protoconid near the buccal margin, as in the dp4 and m1. The mesoconid is weak but visible. There is no mesolophid in the talonid basin. The hypoconid is more mesial-distally compressed than in the dp4 and m1. The mesial arm of the hypoconid is long. The entoconid and hypolophid are fused into a curved ridge. The middle part of the hypolophid is swollen, forming a small cusp. The hypoconulid is smaller and lower than the hypoconid. The hyposinusid is as broad as that of the m1.

Comparison—*Yuomys huheboerhensis* is smaller than all other *Yuomys*. It is characterized by round and low cusps and a relatively square occlusal surface of lower molars. Different from *Y. dawai*, protoconid in *Y. huheboerhensis* has a stronger and higher but relatively shorter buccal part of the preprotolophid and a relatively shorter and weaker postprotolophid. This ridge runs towards the metaconid but does not join the latter cusp. The metaconid of *Y. huheboerhensis* is more mesial-distally compressed. Its buccal part is transformed into the lingual part of the preprotolophid. The buccal and lingual parts of preprotolophid are separated by a shallow notch. In *Y. huheboerhensis*, the lingual preprotolophid is much longer than the buccal preprotolophid. In *Y. dawai*, the metaconid is more conical, and the two parts of the preprotolophid are equally developed. The postprotolophid in *Y. dawai* runs more transversely and joins the base of the metaconid. *Y. huheboerhensis* lacks the mesial cingulid. The hypoconid in *Y. huheboerhensis* is more distal-lingually expanding. In the m1 of *Y. huheboerhensis*, the distal-lingual part of hypoconid is almost fused with the hypoconulid, which is more buccally positioned. There is a sulcus separating the distal-buccal parts of hypoconulid and hypoconid. In *Y. dawai*, the hypoconid is more conical and widely separated from the similarly conical hypoconulid. A longer ridge than that in *Y. huheboerhensis* connects the tips of hypoconid and hypoconulid. The hypoconulid in *Y. dawai* projects distally and is positioned near the middle line. The ectolophid in *Y. huheboerhensis* is short and straight, while it is long and oblique in *Y. dawai*. The mesoconid in *Y. huheboerhensis* is very weak, present as a small swelling on the ectolophid. In *Y. dawai*, the mesoconid is large. In both *Y. huheboerhensis* and *Y. dawai*, the entoconid and hypolophid are fused together. In *Y. huheboerhensis*, the hypolophid is low, and has a weaker connection at the mesial arm of the hypoconid. In *Y. dawai*, the hypolophid is higher and stronger, connecting the distal lingual part of the ectolophid. The talonid basin and ectosinusid buccal to the ectolophid are broader in *Y. dawai* than in *Y. huheboerhensis*.

Yuomys yunnanensis includes a jaw preserving the dp4-m2. The specimen is much larger and has higher crown and stronger cristids than *Y. dawai*. The dp4 of *Y. yunnanensis* has a parastylid and a weak protostylid, two small cusps mesial to the metaconid and protoconid, respectively, but lacks the mesial cingulid. The hypoconulid in *Y. yunnanensis* is less projecting and more buccally positioned than in *Y. dawai*. The buccal end of the hypolophid in *Y. yunnanensis* has a distal turn, which makes the lophid joining the distolophid at the junction between hypoconid and hypoconulid. As a result, the hyposinusid enclosed by the hypolophid and distolophid is much narrower than in *Y. dawai*. In *Y. dawai*, the hypolophid joins the ectolophid at a place mesial to the hypoconid. The m1-2 of *Y. yunnanensis* have squarer occlusal surfaces compared with those of *Y. dawai*. In *Y. yunnanensis*, the preprotolophid is proportionally much higher than that in *Y. dawai*. The m1 postprotolophid in *Y. yunnanensis* runs more distally, therefore the distal side of the trigonid is open. In *Y. dawai*, the m1 postprotolophid extends to the metaconid and closes the trigonid. The ectolophid in *Y. yunnanensis* extends to the tip of metaconid, completely separating the talonid basin and the ectosinusid. The mesolophid and mesoconid are absent. In *Y. dawai*, the ectolophid joins the middle part of the metaconid. The hypolophid in *Y. yunnanensis* joins the ectolophid near the hypoconid, while in *Y. dawai*, the junction is more mesially positioned. In *Y. yunnanensis*, the hyposinusid between the hypolophid and distolophid is narrower than in *Y. dawai*. The hypoconulid in *Y. dawai* is more projecting than in *Y. yunnanensis*.

The Irdinmanhan *Yuomys weijingensis* is probably of similar age to *Y. yunnanensis*. Unfortunately, the specimens of this species were all lost. Available figures and description of the species show that it is less lophodont and about the size of *Y. cavioides* but with more conical cusps.

Yuomys minggangensis includes a jaw fragment preserving the p4-m1. It is much larger than *Y. dawai*, has a squarer occlusal surface, and shows a strong unilateral hypsodonty. In *Y. minggangensis*, the buccal cusps (protoconid and hypoconid) are much larger than the lingual cusps (metaconid and entoconid). The preprotolophid is higher and forms a stronger ridge than in *Y. dawai*. The postprotolophid in *Y. minggangensis* is short and does not close the trigonid. The ectolophid is straighter and shorter than in *Y. dawai*, resulting

in a deeper and narrower ectosinusid. The talonid basin in *Y. minggangensis* is narrower than in *Y. dawai*. The mesoconid and mesolophid is absent in *Y. minggangensis*. The hypolophid is proportionally weaker and joins the joint point between ectolophid and hypoconid. The hypoconulid is less projecting, and the hyposinusid between the hypolophid and distolophid is narrower than in *Y. dawai*.

Yuomys eleganes is represented by a pair of lower jaws and some postcranial fragments. *Y. eleganes* is larger than *Y. dawai*. The occlusal surface of *Y. elegans* is squarer than in *Y. dawai*. Like in other *Yuomys*, the preprotolophid is higher and postprotolophid is shorter in *Y. eleganes* than in *Y. dawai*. The ectolophid in *Y. eleganes* is straighter and shorter. The mesoconid and mesolophid are absent. The talonid basin is narrower than in *Y. dawai*. Being similar to *Y. dawai*, the hypolophid joins the distal part of the ectolophid in *Y. eleganes*. The hypoconulid in *Y. elegans* is present as a swelling of the distolophid. The cusp is not separated from the hypoconid but present as a lingual extension of the hypoconid arm.

Yuomys cavioides is represented by a pair of almost complete lower jaws and two skull fragments preserving the complete upper dentation. *Y. cavioides* is much larger and has higher crown and stronger lophid than *Y. dawai*. In the m1-2 of *Y. cavioides*, the metaconid forms a high lophid and is fused with the buccal part of the preprotolophid. In *Y. dawai*, the metaconid is more conical. The buccal and lingual parts of the preprotolophid are weaker and separated by a notch. The postprotolophid in *Y. dawai* joins the metaconid. In *Y. cavioides*, the postprotolophid is present as a distal-lingual spur of the protoconid. The ectolophid is a high ridge connecting the tips of hypoconid and protoconid in *Y. cavioides*. The ectosinusid and talonid basin are all narrow and deep. No mesolophid and mesoconid are present. In *Y. dawai*, the ectolophid is low and does not extend to the tip of the protoconid. The ectosinusid and talonid basin are broad. A weak mesoconid and a weak mesolophid are present. The hypolophid in *Y. cavioides* is much higher and thicker than that in *Y. dawai*. The hyposinusid enclosed by hypolophid and distolophid is broader and deeper in *Y. dawai*.

Yuomys magnus is much larger than *Y. dawai*. The lower m2s of the two species are the available teeth for comparison. Both have a relatively long occlusal surface. *Y. magnus* has higher tooth crown and stronger lophids. Its hypolophid is stronger but does not connect the ectolophid or hypoconid. The hypoconulid of *Y. magnus* is more conical than in *Y. dawai*.

Yuomys robustus and *Yuomys huangzhuangensis* are known from upper teeth only. They are much larger than *Y. dawai* and have higher tooth crown than *Y. dawai* does.

Yuomys gemuensis nov. sp. Ni and Li. *LSID* urn:lsid:zoobank.org:act:8670E4D0-3DA8-4F67-A306-EA93CF785AD1. (Figure 3, Table 1).

Holotype—Specimen IVPP V 31416, a right lower jaw fragment preserving dp4 and m1-3.

Type locality—Locality GMS20201011SJS01 (29° 21′ 22.000″N, 100° 28′ 25.000″E), near Xueshuo village, Gemusi Basin, Litang County, Sichuan Province (Figure 1).

Referred specimen—IVPP V 31417, a right lower jaw fragment preserving incisor, dp4 and partially erupted m1. From Locality GMS20201011LQ02 (29° 20′ 43.955″N, 100° 28′ 35.899″E), near the Xueshuo Village, Gemusi Basin, Litang County, Sichuan Province (Figure 1).

Age—Early middle Eocene, early Irdinmanhan of Asian Land Mammal Ages, about 49–45 Ma.

Etymology—The specific epithet is from Gemusi, the name of a local lama temple, and the name of the Gemusi Basin.

Diagnosis—Brachydont; Dp4 present mesial and buccal cingulid, mesial metastylid large; Dp4-m2 present buccal arm of hypoconulid; hypolophid thin but well-developed, hypoconulid distally projecting and larger than hypoconid, distal buccal sulcus between hypoconid and hypoconulid deep; m1-3 ectolophid straight, attaching to protoconid distal wall, ectosinusid deep and narrow, hyposinusid broad.

Description—The holotype is a right lower jaw fragment. The preserved inferior masseter ridge root is strong and positioned buccal to the plane of the incisor. The ascending ramus of mandible is vertical and shields the posterior part of the m3. The specimen referred to is a jaw fragment preserving incisor, dp4, and m1. The diastema is thin and long. The mental foramen is mesial to the dp4 and near the incisor. The incisor is gently curved. The enamel is thin. There is a weak longitudinal enamel strip along the ventral side of the incisor. The dp4 is fully erupted but has no wear facet. The m1 is fully developed but still in eruption.

The cheek teeth are brachydont, and weakly lophodont. The buccal side of the cheek teeth is higher than the lingual side. The dp4 has an oval occlusal shape. Its trigonid is narrower than the talonid. The metaconid is buccal-lingually compressed. The tip of metaconid is higher and more mesially positioned than the protoconid. The distal arm of the metaconid is strong. The buccal and lingual parts of the preprotolophid is separated by a deep V-shaped notch. The postprotolophid is short and does not connect the metaconid, therefore the distal wall of the trigonid (postvallid) is open. The mesial cingulid is strong. It extends from the mesial side of the metaconid to the protoconid and becomes a weak buccal cingulid and ends at the mesial side of the hypoconid. A small parastylid is present at the lingual end of the mesial cingulid. There is also an incipient protostylid mesial to the protoconid. The talonid has a broad basin. Its lingual border has a low rim. The hypoconid is conical. Its mesial arm is very short. The entoconid is also conical, but its buccal side is fused into the hypolophid. The hypolophid buccally joins the distal arm of the hypoconid, instead of ectolophid. The ectolophid is thin and oblique. Its mesial part ends in the distobuccal side of the protoconid but does not extends to the

tip of the protoconid. The ectosinusid is deep and narrow. The hypoconulid is large and higher than the hypoconid. A strong and blunt buccal arm of hypoconulid is present. There is a deep and broad sulcus enclosed by the hypoconid, hypoconulid, and the buccal arm of the hypoconulid. The hyposinusid is broad.

The m1 has a rectangular occlusal shape. The trigonid and talonid are similar in width. The protoconid is robust and conical. The metaconid is mesial-distally compressed and fused with the preprotolophid. The postprotolophid is short and does not connect the metaconid. The talonid basin is broad. The hypoconid is mesial-distally compressed. Its mesial arm is very short. The entoconid is also mesial-distally compressed. It is fully fused with the hypolophid. The entoconid, hypolophid, and hypoconid form a transverse ridge. The ectolophid is straight. It connects the distal wall of the protoconid but does not extend to the protoconid tip. The ectosinusid between the protoconid and hypoconid is deep and narrow. The hypoconulid is much larger than the hypoconid. The buccal arm of the hypoconulid is strong. The sulcus buccal-distal to the joint of hypoconid and hypoconulid is relatively shallower and narrower than that of dp4. The m2 is smaller than the m1 and has a squarer occlusal shape than the m1. The cusp shape and ridge arrangement are similar to those of the m1. Because the tooth is relatively short, the talonid basin, ectosinusid, and hyposinusid of the m2 are all narrower than those of the m1. Between the metaconid and entoconid, the talonid basin border has a thicker rim and develops an incipient metastylid. The ectosinusid has a low buccal rim. There is an incipient hypostylid on the rim. The m3 is much larger than the m1 and m2. The m3 talonid is narrower than the trigonid, and the distal side of the tooth is rounded. Different from the m1 and m2, the protoconid and hypoconid of the m3 are more conical, and the ridges are thicker. The hypoconulid is less projecting and smaller than the hypoconid. There is a cusp-like swelling on the hypolophid. The metastylid and hypostylid are large.

Comparison—*Yuomys gemuensis* is more similar to *Y. yunnanensis* than to other *Yuomys* species. The dp4 of *Y. gemuensis* has a mesial cingulid and a buccal cingulid. The two cingulids are absent in *Y. yunnanensis*. The paratylid in *Y. gemuensis* is relatively smaller than that in *Y. yunnanensis*, and the protostylid is present as a nodule on the mesial cingulid. The hypoconid in *Y. yunnanensis* is more buccally expanded than in *Y. gemuensis*. The hypoconulid is less distally projecting. As a result, the distal valley enclosed by hypoconulid and hypolophid is narrower than in *Y. gemuensis*. A buccal arm rises from the buccal side of the hypoconulid in *Y. gemuensis*. The m1s of *Y. gemuensis* and *Y. yunnanensis* are similar in size and morphology. Slightly different from *Y. gemuensis*, the hypolophid in *Y. yunnanensis* is weaker, and the distal buccal sulcus between the hypoconid and hypoconulid is shallower. The m2 of *Y. yunnanensis* is proportionally larger than the m2 of *Y. gemuensis*. As in the m1, the m2 hypolophid in *Y. yunnanensis* is weaker and the distal buccal sulcus between the hypoconid and hypoconulid is shallower than in *Y. gemuensis*. The ectolophid extends to the tip of protoconid in *Y. yunnanensis*. In *Y. gemuensis*, the ectolophid does not extend to the tip of protoconid.

Yuomys huheboerhensis is much smaller and has more conical cusps than *Y. gemuensis*. The lingual and buccal preprotolophid of molars are separated by a notch in *Y. huheboerhensis*. In *Y. gemuensis*, the lingual and buccal preprotolophid are fused into a strong ridge connecting the protoconid and metaconid. As in *Y. gemuensis*, the ectolophid in *Y. huheboerhensis* does not extend to the tip of protoconid. A rudimentary mesoconid is present in some individuals in *Y. huheboerhensis*, but it is totally absent in *Y. gemuensis*. The talonid basin in *Y. huheboerhensis* is relatively broader than in *Y. gemuensis*. The hypolophid in *Y. huheboerhensis* is very weak. Its buccal end does not join the ectolophid, or has only a weak connection. Similar to *Y. gemuensis*, but different from most other *Yuomys*, the hypoconulid is more buccally positioned, and usually has a deep distal buccal notch separating it from the hypoconid in the m1-2. Different from *Y. gemuensis*, the m1-2 hypoconulid in *Y. huheboerhensis* barely projects above the hypoconid.

Yuomys minggangensis is much bigger than *Y. gemuensis* and shows stronger unilateral hyposodonty. The protoconid, metaconid, and hypoconid of *Y. minggangensis* are more conical and robust than those of *Y. gemuensis*. The entoconid and the hypolophid of *Y. minggangensis* are relatively weaker. The ectolophid in *Y. minggangensis* is short and straight, proportionally stronger than in *Y. gemuensis*. The hypoconulid of the m1 in *Y. minggangensis* is smaller than the hypoconid, whereas in *Y. gemuensis*, the hypoconulid is larger than hypoconid. The distal buccal side of the hypoconulid in *Y. minggangensis* lacks a buccal arm as in *Y. gemuensis*. In *Y. minggangensis*, the hyposinusid enclosed by the distolophid and hypolophid is also proportionally smaller.

Yuomys eleganes is of roughly the same size as *Y. gemuensis*. The cusps and ridges of both taxa are also equally developed. The m1-2 of *Y. eleganes* are deeply worn. Detailed morphology is not available for comparison. However, it is obvious that the hypolophid in *Y. eleganes* is more mesially positioned, and the talonid basin is narrower than in *Y. gemuensis*. The hypoconulid in *Y. eleganes* is probably fused with the hypoconid and present as an extension of the distal arm of hypoconid. No trace of sulcus is present between the hypoconid and hypoconulid. A small hypostylid in the ectosinusid mesial to the hypoconid is present in both taxa. The m3 of *Y. gemuensis* is of slightly bigger size. In both taxa, the preprotolophid is high, and the postprotolophid is a short spur. The m3 hypolophid connects the middle of the ectolophid in *Y. eleganes*, whereas the lophid joins the ectolophid near hypoconid in *Y. gemuensis*. As a result, the m3 talonid basin in *Y. eleganes* is narrower. There is a small metastylid mesial to the entoconids on the lingual edge of the talonid basin in *Y. eleganes*. This small cusp almost closes the lingual side of the

talonid basin. Similarly in *Y. gemuensis*, the lingual side of the talonid basis has a low and blunt rim, and the metastylid is also present. In the ectosinusid and mesial to the hypoconid, there is a small hypostylid in both taxa. The m3 hypoconulid in *Y. eleganes* is present as a swelling of the hypoconid distal lingual arm (distal lophid). There is no sulcus defining the border between hypoconid and hypoconulid, and probably no projection from the arm. In *Y. gemuensis*, the hypoconulid clearly projects above the distal lophid and is separated from the hypoconid by a shallow sulcus distal lingual to the junction between hypoconid and hypoconulid.

Yuomys cavioides is larger, more hypsodont and lophodont than *Y. gemuensis*. The postprotolophid is longer in *Y. cavioides* than in *Y. gemuensis*. The m3 postprotolophid in *Y. cavioides* is particularly longer, which reaches the lingual side of the hypolophid. The m1-3 ectolophids in *Y. cavioides* all extend to the tips of protoconid. The hypolophids are more mesially positioned and proportionally higher than in *Y. gemuensis*. The talonid basin and ectosinusid in *Y. cavioides* are narrower and deeper. The small hypostylid mesial to the hypoconid as that in *Y. gemuensis* is absent in *Y. cavioides*. A small metastylid mesial to the entoconid along the lingual tooth border of the m2-3 is present in *Y. cavioides* but is weaker in *Y. gemuensis*. The hypoconulid of the m1-2 is slightly smaller than hypoconid in *Y. cavioides*, whereas it is bigger than hypoconid in *Y. gemuensis*. The sulcus distal buccal to the junction between hypoconid and hypoconulid of the m1-2 in *Y. gemuensis* is deeper than that in *Y. cavioides*. The buccal ridge-like arm from hypoconulid is present in the m1-2 of *Y. gemuensis* but absent in *Y. cavioides*. The lingual extension of the distolophid is longer in *Y. gemuensis* than in *Y. cavioides*. The m3 hypoconulids and distolophids are equally developed in both taxa. Both have a shallow sulcus distal buccal to the junction between hypoconid and hypoconulid. This sulcus is absent in other *Yuomys*.

Yuomys magnus is larger than *Y. gemuensis*. The tooth crown of *Y. magnus* is higher than *Y. gemuensis*. The m2-3 ectolophid of *Y. magnus* is oblique and connects the protoconid near the buccal side. As a result, the m2-3 ectosinusid of *Y. magnus* is shallower and oblique. The m2 hypolophid of *Y. magnus* does not connect the ectolophid or hypoconid. The m3 hypolophid of *Y. magnus* has a weaker connection to the ectolophid than in *Y. gemuensis*. In *Y. gemuensis*, the m2 hypoconulid has a buccal arm that forms a transverse ridge from hypoconulid. The sulcus between this buccal arm and hypoconid is deep. In *Y. magnus*, the m2 hypoconid is conical and lacks a buccal extension.

Yuomys robustus is known from upper teeth only. It is much larger than *Y. gemuensis* and has higher tooth crown. *Yuomys huangzhuangensis* is also known from the upper teeth only. Its size matches that of *Y. gemuensis*. Relatively thicker ridges of *Y. huangzhuangensis* upper teeth suggest that the lower teeth of this species should also have thicker ridges than *Y. gemuensis*.

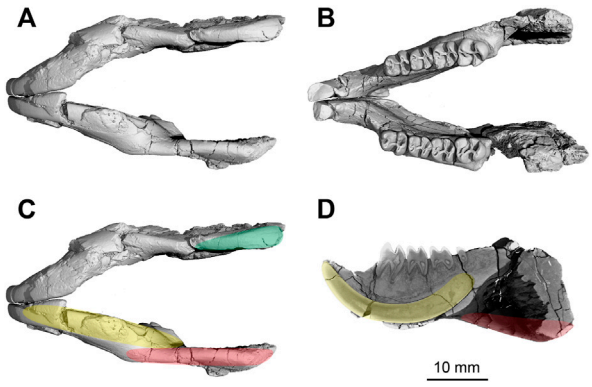

FIGURE 4
The low jaw of the type specimen of *Yuomys cavioides* (IVPP V 4796.1-2), showing the hystricognathous form. **(A)**, ventral view; **(B)**, occlusal view: **(C)**, yellow shadow indicating the plane of the incisive alveolus, red shadow indicating the plane of the angular process being distinctly lateral to the plane of the incisive alveolus, green shadow indicating expanded ventral edge of the angular process; **(D)**, virtual section of the right half mandible in medial view, yellow shadow indicting the posterior extension of the incisor, red shadow indicating the angular process.

4 Discussion

Huchon et al. (2000) defined "Ctenohystrica" as a suborder of Rodentia based on molecular evidence. Initially Ctenohystrica was defined as a crown-group that includes the least-inclusive clade of all extant family Ctenodactylidae and infraorder Hystricognathi. Marivaux et al. (2004) and Flynn et al. (2019) redefined Ctenohystrica as a more inclusive group that includes stem and extant Hystricognathi, stem and extant sciurognathous Ctenodactylidae, and all extant or extinct groups more closely related to them than to other sciurognathous rodents. Blanga-Kanfi et al. (2009) revised the rodent phylogeny based on the combined nucleotide datasets and supported the monophyly of Ctenohystrica. It is not difficult to see that the main connotation of Ctenohystrica has no difference with the traditional Hystricomorpha. Here we follow the systematic of Wilson and Reeder (2005) by using suborder Hystricomorpha. *Yuomys* are moderately diverse Eocene rodents. The taxonomy and distribution of *Yuomys* have been revised recently (Gong et al., 2021). Previously, *Yuomys* was considered as a rodent with a hystricomorphous skull but with a hystricognathous jaw. For this reason, *Yuomys* was traditionally assigned in the "trash bin" high level taxon Ctenodactyloidea. Our re-observation on the lower jaw of the type specimen of *Yuomys cavioides* revealed that this specimen is actually hystricognathous (Figure 4). In living hystricognaths, the origin of the angular process is distinctly lateral to the plane of the incisor alveolus. The inferior margin of the angular process is generally wide, and the reflexa part of lateral masseter passes around the ventral

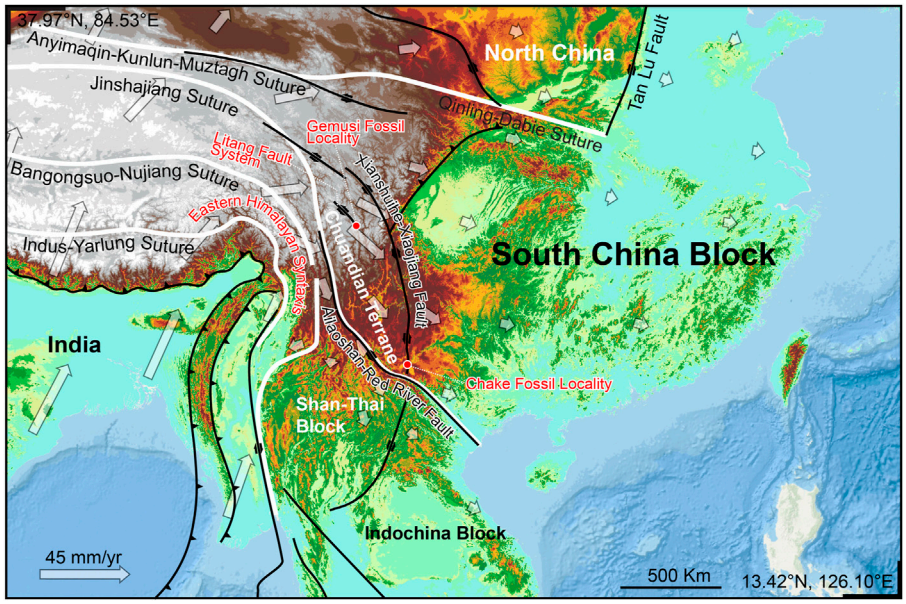

FIGURE 5
Chuandian Terrane and the major faults in the accommodation zone in the southeastern margin of Qinghai-Tibet Plateau. Hollow arrows indicating modern GPS velocity field (based on Wang and Shen 2020).

surface of the angular process to insert on the medial side of the angular process (Tullberg, 1899; Wood, 1985). The angular process of the type specimen of *Y. cavioides* is well preserved. The plane of angular process is clearly lateral to the plane of the incisive alveolus (Figure 4). The ventral edge of the angular process is widened (Figure 4) in a form generally present in living hystricognaths. We therefore categorized *Yuomys* and Yuomyidae as the infraorder Hystricognathi.

Yuomys dawai is much smaller with a lower tooth crown than other *Yuomys* species except *Yuomys huheboerhensis*. Compared to *Y. huheboerhensis*, *Y. dawai* shows more typical *Yuomys* features, suggesting that the sediments bearing *Y. dawai* is probably younger than that of *Y. huheboerhensis*, but it is still older than other *Yuomys*. *Yuomys gemuensis* and *Yuomys yunnanensis* from the Chake pull-apart basin closely resemble each other and both show similar development of tooth crown height and ridges. The similar evolutionary grade shared by these two species suggests that the fossil layers bearing the two *Yuomys* have the same mammalian age: early Irdinmanhan of Asian Land Mammal Age (about 49–45 Ma).

It has been demonstrated that about 1300–2500 km of the northward convergence between the Indian plate with the continent of Eurasia caused widespread crustal deformation, including mountain building, plate shortening, and plateau uplifting (Molnar and Stock, 2009; Copley et al., 2010; Cande and Stegman, 2011; van Hinsbergen et al., 2011; Tong et al., 2015; Yao et al., 2015; Ding et al., 2017; Wang and Shen, 2020). The most intriguing feature of this widespread crustal deformation is reflected by clockwise rotation of southeastern Qinghai-Tibet Plateau around the Eastern Himalayan Syntaxis (EHS) and lateral escape of crustal materials on the southeastern edge of the plateau relative to the rigid South China Block (Yin and Harrison, 2000; Tapponnier et al., 2001; Molnar and Stock, 2009; Copley et al., 2010; Cande and Stegman, 2011; van Hinsbergen et al., 2011; Tong et al., 2015). One theory is that the outward expansion along major strike-slip faults (such as Xianshuihe-Xiaojiang Fault, Litang Fault System, Three Rivers Faults, and Red River Fault) and clockwise strike-slip processes around EHS occur at the mantle scale (Tapponnier et al., 2001; Zhang et al., 2021). The development of the Cenozoic extensional intermountain basins in the southeast margin of Qinghai-Tibetan Plateau is kinematically linked with the strike-slip faults, and the sedimentation in these basins can provide important age constraints for the timing of fault development and orogenic processes (Li et al., 2015; Li et al., 2020).

The southeastern margin of Qinghai-Tibet Plateau was one of the most important accommodation zones during the India-Eurasia collision. The temporal and spatial evolution of the zone is tightly correlated with the crustal deformation and high topography evolution of Qinghai-Tibet Plateau (Figure 5). This accommodation zone comprises the Shan Thai Block (STB), Indochina Block (ICB), and Chuandian Terrane (CDT), which consists of fragments from the western part of South China Block (SCB) and the southern part of Songpan Ganzi fold belt (Wang et al., 1998; Wang et al., 2014; Tong et al., 2015). The CDT is separated from the relatively stable SCB in the north and northeast by the Xianshuihe-Xiaojiang Fault (XSH-XJF), and from the STB and ICB in the south and southwest by

the Ailao Shan-Red River Fault (ASRRF) (Wang et al., 1998; Tong et al., 2015; Li et al., 2017; Li et al., 2020).

The *Yuomys* fossils reported here were discovered from the Gemusi pull-apart basin, which was formed within the northwest striking LTFS. This fault system is located between the XSH-XJF to the north and ASRRF to the south. Its activity is controlled by the two latter faults (Chevalier et al., 2016). The *Yuomys* fossil from the Chake was discovered from a locality in the Chake pull-apart basin, which was formed within the southern end of the XSH-XJF. Similarities shared by the *Yuomys* from Gemusi and Chake suggest that they lived during the same geological epoch and similar adaptive environment, and consequently suggest that the Gemusi Basin and Chake Basin were formed roughly in the same period (about 49–45 Ma).

In a recent study, the mammalian fossil localities in the Gemusi Basin, which were reported in Zong et al. (1996), were wrongly pinned, and the fossil layer of Gemusi Formation was wrongly correlated to the upper part of the Relu Formation of the nearby Relu Basin (He et al., 2022). Our field tracing and previous stratigraphic correlations (Chen et al., 1983; Guo, 1986; Zong et al., 1996) indicate that the mammalian fossil layer of the Gemusi Formation should be correlated with the lower part of the Relu Formation (equivalent to the Changzong Formation in He et al., 2022), below the plant fossil strata of the Relu Formation. U-Pb dating of the zircons from the volcanic tuffs imbedded in the plant fossil layers of the Relu Formation showed an age of 42–40 Ma, and U-Pd dating of the zircons from the sandstone of the lower part of the Relu Formation indicated that the maximum depositional age is about 50 Ma (He et al., 2022). These dating results are consistent with our biochronological estimation.

Present-day CDT is characterized by clockwise rotation around EHS as revealed by GPS velocities (Figure 5, Zhang et al., 2004; Wang and Shen, 2020; Xu et al., 2022). A maximum shear strain rate of 40–60 nanostrain/yr is found along the XSH-XJF (Wang and Shen, 2020). The initiation timing of the strike-slip movement of XSH-XJF and ASRRF and the formation of the CDT is controversial. It was suggested that the CDT remained relatively stable and did not begin rotational extrusion movement before 17 Ma (Tong et al., 2015), while some other research suggested that the crustal deformation of the CDT began at ~ 35 Ma (Li et al., 2020). The *Yuomys* fossils from CDT constrain the timing of sedimentation within the Gemusi pull-apart basin and Chake pull-apart basin. Our paleontological evidence suggests that the initiation of CDT crustal movement could be earlier than 49 Ma.

The occurrence of *Yuomys* in CDT may suggest that the area had a lowland tropical environment during the middle Eocene. It is known that *Yuomys* occurred with small-sized stem anthropoid and tarsiiform primates, in, for example, the Mianchi-Yuanqu Basin in Henan Province and Erlian Basin in Inner Mongolia (Beard, 1998; Beard and Wang, 2004; Ni, 2010; Wang et al., 2018). Living and fossilized small primates are known to occur only in lowland tropical forest or jungle environments (Fleagle, 2013; Li and Ni, 2016; Ni et al., 2016). Plant fossils from the nearby Relu Formation indicate a lowland tropical environment (Chen et al., 1983; Guo, 1986; Su et al., 2009; He et al., 2022). It is therefore likely that the uplift of CDT and the strike-slip movement of XSH-XJF and ASRRF were not synchronous.

Data availability statement

The original contributions presented in the study are included in the article/supplementary material, further inquiries can be directed to the corresponding authors.

Author contributions

XN analyzed the data and wrote the manuscript. QL analyzed the data and edited the manuscript. TD analyzed the data. LZ, HG, and CQ CT-scanned the fossil. JS, FS, and SF collected data.

Funding

This project was supported by the Second Tibetan Plateau Scientific Expedition and Research Program (2019QZKK705), the National Natural Science Foundation of China (41988101, 41888101, 41625005), the Strategic Priority Research Program of Chinese Academy of Sciences (CAS XDB26030300, XDA20070203, XDA19050100).

Acknowledgments

We thank T. Stidham for comments and English-language editing. We thank Qian Li, Lawrence J. Flynn, and Olivier Maridet for comments and discussion.

Conflict of interest

The authors declare that the research was conducted in the absence of any commercial or financial relationships that could be construed as a potential conflict of interest.

Publisher's note

References

Beard, K. C. (1998). A new genus of tarsiidae (Mammalia: Primates) from the middle Eocene of shanxi Province, China, with notes on the historical biogeography of tarsiers. *Bull. Carnegie Mus. Nat. Hist.* 34, 260–277.

Beard, K. C., and Wang, J. (2004). The eosimiid primates (anthropoidea) of the heti formation, Yuanqu Basin, shanxi and henan provinces, people's republic of China. *J. Hum. Evol.* 46, 401–432. doi:10.1016/j.jhevol.2004.01.002

Blanga-Kanfi, S., Miranda, H., Penn, O., Pupko, T., Debry, R. W., and Huchon, D. (2009). Rodent phylogeny revised: Analysis of six nuclear genes from all major rodent clades. *BMC Evol. Biol.* 9, 71. doi:10.1186/1471-2148-9-71

Bowdich, T. E. (1821). *An analysis of the natural classifications of Mammalia, for the use of students and travellers*. Paris: J. Smith.

Brandt, J. F. (1855). Beiträge zur nähern Kenntniss der Säugethiere Russlands *St. Pétersbourg*. Saint Petersburg,Russia: De l'Imprimerie de l'Académie impériale des sciences.

Cande, S. C., and Stegman, D. R. (2011). Indian and African plate motions driven by the push force of the Réunion plume head. *Nature* 475, 47–52. doi:10.1038/nature10174

Chen, M., Kong, Z., and Chen, Y. (1983). On the discovery of palaeogene flora from the Western Sichuan Plateau and its significance in phytogeography. *Acta Bot. Sin.* 25, 482–491.

Chevalier, M.-L., Leloup, P. H., Replumaz, A., Pan, J., Liu, D., Li, H., et al. (2016). Tectonic-geomorphology of the Litang fault system, SE Tibetan Plateau, and implication for regional seismic hazard. *Tectonophysics* 682, 278–292. doi:10.1016/j.tecto.2016.05.039

Copley, A., Avouac, J.-P., and Royer, J.-Y. (2010). India-Asia collision and the Cenozoic slowdown of the Indian plate: Implications for the forces driving plate motions. *J. Geophys. Res.* 115, B03410. doi:10.1029/2009jb006634

Dawson, M. R., Li, C., and Qi, T. (1984). Eocene ctenodactyloid rodents (Mammalia) of eastern central Asia. *Carnegie Mus. Nat. Hist. Special Publ.* 9, 138–150.

Ding, L., Satybaev, M., Cai, F., Wang, H., Song, P., Ji, W.-Q., et al. (2017). Processes of initial collision and suturing between India and Asia. *Sci. China Earth Sci.* 60, 635–651. doi:10.1007/s11430-016-5244-x

Fleagle, J. G. (2013). *Primate adaptation and evolution*. Third Edition. New York: Academic Press.

Flynn, L. J., Jacobs, L. L., Kimura, Y., and Lindsay, E. H. (2019). Rodent suborders. *Foss. Impr.* 75, 292–298. doi:10.2478/if-2019-0018

Gong, H., Li, Q., and Ni, X. (2021). New species of Yuomys (Rodentia, ctenodactyloidea) from the upper Eocene of eastern Ningxia, China. *J. Vertebrate Paleontology* 41, e1938099. doi:10.1080/02724634.2021.1938099

Guo, S. (1986). "An Eocene flora from the Relu Formation in Litang county of sichuan and the history of Eucalyptus," in *The comprehensive scientific expedition to the qinghai-xizang plateau. Studies in qinghai-xizang (tibet) plateau. Special issue of hengduan mountains scientific expedition (II)*. Editor T. C. A. S. O. (Beijing: Beijing Science & Technology Press).

He, S., Ding, L., Xiong, Z., Spicer, R. A., Farnsworth, A., Valdes, P. J., et al. (2022). A distinctive Eocene Asian monsoon and modern biodiversity resulted from the rise of eastern Tibet. *Sci. Bull.* 67, 2245–2258. doi:10.1016/j.scib.2022.10.006

Huang, X., and Zhang, J. (1990). First record of early tertiary mammals from southern yunnan. *Vertebr. Palasiat.* 28, 296–303.

Huchon, D., Catzeflis, F. M., and Douzery, E. J. P. (2000). Variance of molecular datings, evolution of rodents and the phylogenetic affinities between Ctenodactylidae and Hystricognathi. *Proc. R. Soc. Lond. B* 267, 393–402. doi:10.1098/rspb.2000.1014

Li, C. (1975). *Yuomys*, a new ischyromyoid rodent genus from the upper Eocene of North China. *Vertebr. Palasiat.* 13, 58–70.

Li, Q. (2019). Eocene ctenodactyloid rodent assemblages and diversification from erden Obo, nei mongol, China. *Hist. Biol.* 31, 813–823. doi:10.1080/08912963.2017.1395422

Li, Q., and Meng, J. (2015). New ctenodactyloid rodents from the Erlian Basin, nei mongol, China, and the phylogenetic relationships of Eocene asian ctenodactyloids. *Am. Mus. Novitates* 3828, 1–20. doi:10.1206/3828.1

Li, Q., and Ni, X. (2016). An early Oligocene fossil demonstrates treeshrews are slowly evolving "living fossils". *Sci. Rep.* 5, 18627. doi:10.1038/srep18627

Li, S., Advokaat, E. L., Van Hinsbergen, D. J. J., Koymans, M., Deng, C., and Zhu, R. (2017). Paleomagnetic constraints on the Mesozoic-Cenozoic paleolatitudinal and rotational history of Indochina and South China: Review and updated kinematic reconstruction. *Earth-Science Rev.* 171, 58–77. doi:10.1016/j.earscirev.2017.05.007

Li, S., Deng, C., Dong, W., Sun, L., Liu, S., Qin, H., et al. (2015). Magnetostratigraphy of the Xiaolongtan Formation bearing Lufengpithecus keiyuanensis in Yunnan, southwestern China: Constraint on the initiation time of the southern segment of the Xianshuihe–Xiaojiang fault. *Tectonophysics* 655, 213–226. doi:10.1016/j.tecto.2015.06.002

Li, S., Su, T., Spicer, R. A., Xu, C., Sherlock, S., Halton, A., et al. (2020). Oligocene deformation of the chuandian Terrane in the SE margin of the Tibetan plateau related to the extrusion of Indochina. *Tectonics* 39, e2019TC005974. doi:10.1029/2019tc005974

Linnaeus, C. (1758). *Systema naturæ per regna tria naturæ, secundum classes, ordines, genera, species, cum characteribus, differentiis, synonymis, locis*. Washington, DC, USA: Biodiversity heritage library. Editio Decima, Holmiæ, (Impensis direct. Laurentii Salvii).

Marivaux, L., and Boivin, M. (2019). Emergence of hystricognathous rodents: Palaeogene fossil record, phylogeny, dental evolution and historical biogeography. *Zoological J. Linn. Soc.* 187, 929–964. doi:10.1093/zoolinnean/zlz048

Marivaux, L., Vianey-Liaud, M., and Jaeger, J.-J. (2004). High-level phylogeny of early tertiary rodents: Dental evidence. *Zoological J. Linn. Soc.* 142, 105–134. doi:10.1111/j.1096-3642.2004.00131.x

Molnar, P., and Stock, J. M. (2009). Slowing of India's convergence with Eurasia since 20 Ma and its implications for Tibetan mantle dynamics. *Tectonics* 28. doi:10.1029/2008tc002271

Ni, X., Li, Q., Li, L., and Beard, K. C. (2016). Oligocene primates from China reveal divergence between African and Asian primate evolution. *Science* 352, 673–677. doi:10.1126/science.aaf2107

Ni, X., Meng, J., Beard, K. C., Gebo, D. L., Wang, Y., and Li, C. (2010). A new tarkadectine primate from the Eocene of inner Mongolia, China: Phylogenetic and biogeographic implications. *Proc. R. Soc. B* 277, 247–256. doi:10.1098/rspb.2009.0173

Shi, R. (1989). Late Eocene mammalian fauna of Huangzhuang, Qufu, Shandong. *Vertebr. Palasiat.* 27, 87–102.

Su, T., Xing, Y., Yang, Q., and Zhou, Z. (2009). Reconstruction of mean annual temperature in Chinese Eocene paleofloras based on leaf margin analysis. *Acta Palaeontol. Sin.* 48, 65–72.

Tapponnier, P., Zhiqin, X., Roger, F., Meyer, B., Arnaud, N., Wittlinger, G., et al. (2001). Oblique stepwise rise and growth of the Tibet Plateau. *Science* 294, 1671–1677. doi:10.1126/science.105978

Tong, Y.-B., Yang, Z., Wang, H., Gao, L., An, C.-Z., Zhang, X.-D., et al. (2015). The Cenozoic rotational extrusion of the Chuan Dian Fragment: New paleomagnetic results from Paleogene red-beds on the southeastern edge of the Tibetan Plateau. *Tectonophysics* 658, 46–60. doi:10.1016/j.tecto.2015.07.007

Tullberg, T. (1899). Ueber das system der Nagethiere: Eine phylogenetische studie. *Nova Acta Regiae Soc. Sci. Ups.* 18, 1–514.

Van Hinsbergen, D. J. J., Kapp, P., Dupont-Nivet, G., Lippert, P. C., Decelles, P. G., and Torsvik, T. H. (2011). Restoration of cenozoic deformation in Asia and the size of greater India. *Tectonics* 30. doi:10.1029/2011tc002908

Wang, B. (2017). Discovery of *Yuomys* from altun Shan, Xinjiang, China. *Vertebr. Palasiat.* 55, 227–232.

Wang, B., and Zhou, S. (1982). Late Eocene mammals from pingchangguan basin, henan. *Vertebr. Palasiat.* 20, 203–215.

Wang, E., Burchfiel, B. C., Royden, L. H., Liangzhong, C., Jishen, C., Wenxin, L., et al. (1998). Late cenozoic xianshuihe-xiaojiang, Red River, and dali fault systems of southwestern sichuan and central yunnan, China. *Geol. Soc. Am.* 327. doi:10.1130/SPE327

Wang, E., Meng, K., Su, Z., Meng, Q., Chu, J. J., Chen, Z., et al. (2014). Block rotation: Tectonic response of the Sichuan basin to the southeastward growth of the Tibetan Plateau along the Xianshuihe-Xiaojiang fault. *Tectonics* 33, 686–718. doi:10.1002/2013tc003337

Wang, J. (1978). Fossil amynodontidae and ischyromyidae of tongbo, henan. *Vertebr. Palasiat.* 16, 22–29.

Wang, M., and Shen, Z.-K. (2020). Present-day crustal deformation of continental China derived from GPS and its tectonic implications. *J. Geophys. Res. Solid Earth* 125, e2019JB018774. doi:10.1029/2019jb018774

Wang, Y., Li, Q., Bai, B., Jin, X., Mao, F., and Meng, J. (2018). Paleogene integrative stratigraphy and timescale of China. *Sci. China Earth Sci.* 62, 287–309. doi:10.1007/s11430-018-9305-y

Wilson, D. E., and Reeder, D. M. (2005). "Mammal species of the world, literature cited," in *Mammal species of the world. A taxonomic and geographic reference*. Editor D. E. W. D. M. REEDER 3rd edition (Baltimore, MD, USA: Johns Hopkins University Press).

Wood, A. E. (1985). "The relationships, orgin and dispersal of the hystricognathous rodents," in *Evolutionary relationships among rodents. A multidisciplinary analysis*. Editors W. P. LUCKETT and J.-L. HARTENBERGER (New York: Springer Science+Business Media, LLC).

Xu, B.-B., Wang, Y., Zhang, Z.-Q., Yan, Y.-G., He, X.-H., Hao, M., et al. (2022). Slip distribution and block rotation of the Indo-South China region inferred from GNSS analyses. *J. Asian Earth Sci.* 233, 105206. doi:10.1016/j.jseaes.2022.105206

Yao, T., Wu, F., Ding, L., Sun, J., Zhu, L., Piao, S., et al. (2015). Multispherical interactions and their effects on the Tibetan plateau's Earth system: A review of the recent researches. *Natl. Sci. Rev.* 2, 468–488. doi:10.1093/nsr/nwv070

Yin, A., and Harrison, T. M. (2000). Geologic evolution of the himalayan-Tibetan orogen. *Annu. Rev. Earth Planet. Sci.* 28, 211–280. doi:10.1146/annurev.earth.28.1.211

Zhang, M., Guo, Z., Xu, S., Barry, P. H., Sano, Y., Zhang, L., et al. (2021). Linking deeply-sourced volatile emissions to plateau growth dynamics in southeastern Tibetan Plateau. *Nat. Commun.* 12, 4157. doi:10.1038/s41467-021-24415-y

Zhang, P. Z., Shen, Z., Wang, M., Gan, W., Bürgmann, R., Molnar, P., et al. (2004). Continuous deformation of the Tibetan Plateau from global positioning system data. *Geol.* 32, 809–812. doi:10.1130/g20554.1

Zong, G., Chen, W., Huang, X., and Xu, Q. (1996). *Cenozoic mammals and environment of hengduan mountains region*. Beijing: Ocean Press.

frontiers | Frontiers in Earth Science

TYPE Original Research
PUBLISHED 20 February 2023
DOI 10.3389/feart.2023.1127964

OPEN ACCESS

EDITED BY
Shuhai Xiao,
Virginia Tech, United States

REVIEWED BY
Xiaoming Wang,
Natural History Museum of Los Angeles County, United States
Yangfan Li,
Northwest University, China

*CORRESPONDENCE
Yuan-Qing Wang,
wangyuanqing@ivpp.ac.cn
Zhao-Qun Zhang,
zhangzhaoqun@ivpp.ac.cn

SPECIALTY SECTION
This article was submitted to Paleontology, a section of the journal Frontiers in Earth Science

RECEIVED 20 December 2022
ACCEPTED 08 February 2023
PUBLISHED 20 February 2023

CITATION
Wang B, Zhang Z-Q, Wang Y-Q, Li Q, Bai B, Liu Y, Mao F-Y, Wang H-B, Wang J, Gong Y-X, Dong L-P, Wang L-H, Ma H-D, Xu R-C and Wang X-Y (2023), Lithostratigraphy of a long, fossiliferous Oligocene sequence: Revisiting Saint Jacques, Nei Mongol, China.
Front. Earth Sci. 11:1127964.
doi: 10.3389/feart.2023.1127964

Lithostratigraphy of a long, fossiliferous Oligocene sequence: Revisiting Saint Jacques, Nei Mongol, China

Bian Wang[1,2], Zhao-Qun Zhang[1,2,3]*, Yuan-Qing Wang[1,2,3]*, Qian Li[1,2], Bin Bai[1,2], Yan Liu[1,2], Fang-Yuan Mao[1,2], Hai-Bing Wang[1,2], Jian Wang[1,3], Yan-Xin Gong[1,3], Li-Ping Dong[1,2], Li-Hua Wang[1,3], Hai-Dan Ma[1,3], Ran-Cheng Xu[1,3] and Xiao-Yang Wang[1,3]

[1]Key Laboratory of Vertebrate Evolution and Human Origins, Institute of Vertebrate Paleontology and Paleoanthropology, Chinese Academy of Sciences (CAS), Beijing, China, [2]CAS Center for Excellence in Life and Paleoenvironment, Beijing, China, [3]College of Earth and Planetary Sciences, University of Chinese Academy of Sciences, Beijing, China

For a hundred years the Saint Jacques area has been known to produce rich Oligocene vertebrate fossils, yet only a handful of previous studies have focused on this area. Since 2010, we have conducted 12 field expeditions to Saint Jacques, and here we report findings from our paleontological excavations and stratigraphical investigations. Twenty-two fossiliferous blocks across the area are recognized and a chronostratigraphic framework has been established to aid fossil collection. Fossil-mammal materials have been recovered in situ from 1635 localities and additionally from surface sediments. Fossiliferous blocks in the area are correlated by lithological similarity and lateral tracing. Lithologically, the area is mainly composed of reddish silty mudstone and muddy siltstone, with three distinctive layers of grayish white sandstone. The measured composite stratigraphic column spans 239 meters and are divided into 12 lithostratigraphic units. Contrary to previous knowledge that Saint Jacques contains two Oligocene mammalian assemblages, our preliminary biostratigraphic analysis of small mammals shows that the area documents successive faunal transition from the Eocene to possibly the early Miocene. The hyracodontid perissodactyl *Ardynia*, the ctenodactyloid rodent *Gobiomys*, and the basal Glires *Gomphos* from the bottom litho-units imply the presence of the Eocene–Oligocene boundary, while small mammal assemblage of the top units is similar to Miocene faunas in northern China and Mongolia. Thus, rock strata in Saint Jacques likely span the Eocene through the early Miocene, bracketing an entire Oligocene sequence within. In sum, our re-exploration of Saint Jacques has greatly expanded the chronostratigraphic and taxonomic coverage of the mammalian fossil collection from this area. This long, successive Oligocene sequence makes an important record for studying the Eocene–Oligocene Transition. Further study in this area will contribute to a range of paleontological and paleoenvironmental questions.

KEYWORDS

Nei Mongol, lithostratigaphy, Saint Jacques, Eocene-Oligocene boundary, Oligocene-Miocene boundary, mammals

Introduction

The Oligocene epoch is a transitional time period marked by the most striking climate change in the Cenozoic from greenhouse to icehouse conditions, mainly evidenced by marine records (Zachos et al., 2001; Coxall et al., 2005; Eldrett et al., 2009; Westerhold et al., 2020) but less terrestrial records (Dupont-Nivet et al., 2007; Hren et al., 2013). This change in global climate is likely associated with the profound shifts observed in continental faunal and floral compositions (e.g., Zhang et al., 2012; Sun et al., 2014). The continental interior of Asia has been a focal region for studying faunal turnovers across the Eocene–Oligocene boundary (e.g., Meng and McKenna, 1998; Kraatz and Geisler, 2010). To better understand the response of land mammals to significant global and regional climatic changes, long sequences of terrestrial sediments with successive fossil records and precise stratigraphic calibration are pivotal.

Saint Jacques is one of the classic Oligocene fossil sites of Asia. Sitting on the right bank of the Yellow River near the town of Balagong, Hanggin Banner, Ordos City, Nei Mongol Autonomous Region, China, the namesake of the fossiliferous area is in fact a small town across the Yellow River in Dengkou County, Bayannur City (Figures 1A,B). Although known for its rich vertebrate fossils for nearly a century, detailed accounts on the lithology of the Saint Jacques area are still lacking, hindering finer divisions of the depositional sequence and fossil assemblages.

Geological setting

Located in the northwestern margin of the Ordos block, the study area is bounded by the Jilantai Basin to the west, Hetao Basin to the north, and Yinchuan Basin to the south. Cenozoic strata are well exposed in the gullies along the Yellow River, from Balagong area in the north to Qianlishan area in the south (Wang, 1987). Our preliminary exploration in the region finds no exposure of Cenozoic strata superimposed with Mesozoic strata. In the Qianlishan area, the Cenozoic strata overlie the Cambrian strata by faults. The earliest Cenozoic strata in this area is possibly Early–Middle Eocene, as evidenced by our findings of *Gomphos* fossil from Saint Jacques. Late Eocene to Oligocene strata are superimposed by Neogene strata. Quaternary terrace sediments of the Yellow River cover most of the highland. Major faults in the Saint Jacques area cut through the Eocene, Oligocene, and Neogene strata, revealing that tectonic movements were active during late Cenozoic period, as studied by Shi et al. (2020) in their review of the neotectonics around the Ordos block.

History of research

Vertebrate fossils were first discovered in the Saint Jacques area by French paleontologists Pierre Teilhard de Chardin and Emile Licent while exploring along the Yellow River in 1923 (Teilhard de Chardin and Licent, 1924a, 1924b). They initially considered the site Pliocene in age, but soon revised it to the Oligocene based on the occurrence of *Paraceratherium* (Teilhard de Chardin and Licent, 1924c). Later, the mammalian fossils from Saint Jacques were reported in detail by Teilhard de Chardin, (1926). In the decades to follow, this area was rarely investigated except for a short visit by the Sino-Soviet Paleontological Expedition in 1959 (Chow and Rozhdestvensky, 1960). In 1977 and 1978, more extensive explorations by the Institute of Vertebrate Paleontology and Paleoanthropology (IVPP) were carried out, revealing a greater exposure of fossiliferous area than previously recognized (Wang, 1987). However, further work on its geology was hampered by its complicated structure. Wang (1987) noted that "it [was] difficult to define a formal lithostratigraphic unit based on beds exposed in Saint-Jacques area" (p.45). Based on similarity in lithology and assemblage of mammal fossils, the beds in Saint Jacques were thought to be equivalent to the lower member of the Wulanbulage Formation in Qianlishan district (Wang, 1987). Further investigation on the mammal fossil have led subsequent authors to recognize two local faunas from different horizons at Saint Jacques, one from early Oligocene and the other possibly late Oligocene (Wang, 1987; Wang and Emry, 1991; Wang and Qiu, 2003). The faunas in Saint Jacques are primarily composed of small mammals, especially ctenodactyloid rodents, although several species of ungulates and carnivores are also present (Meng and McKenna, 1998; Wang and Qiu, 2003).

For over a decade now, a new team of IVPP researchers have been conducting field explorations back in the Saint Jacques area and have collected abundant fossil-mammal materials from different blocks and stratigraphic levels. New specimens of the carnivore *Palaeogale sectoria*, the hyracodontid *Ardynia*, and the lagomorph *Ordolagus* have been recently reported (Wang and Zhang, 2015; Bai et al., 2018; Angelone and Zhang, 2021), and studies on other groups are still underway.

In this study, we present the first detailed description of the lithology of the Saint-Jacques depositional sequence, along with a preliminary list of identified small mammals based on discoveries accumulated over 12 field seasons. Stratigraphical correlation of sections across the area provides a means for age comparison between fossils collected from different fault blocks. Our fine lithological divisions of this long sequence, coupled with abundant fossil material from extensive field surveys, allow for an analysis of faunal succession with improved temporal resolution. Although Saint Jacques deposits have long been considered to be exclusively Oligocene, we show that the area has well exposed sections with rich fossils that document successive faunal turnover from the Eocene to the Miocene, bracketing the entire Oligocene sequence within.

Methods

We carried out annual field expeditions to Saint Jacques in 2010 through 2022, with a gap year in 2016. Major faults in the area have previously hampered precise lithostratigraphical and biostratigraphical correlation in the past. Therefore, for the convenience of stratigraphical investigations and to avoid mixing faunal compositions across the faulted area, we divided the area into 22 fossiliferous blocks. Each block contains geographically and stratigraphically continuous exposure of beds bounded either by major faults or by topographic features. Blocks are divided into varied numbers of stratigraphic layers. Divisions are based on

10.3389/feart.2023.1127964

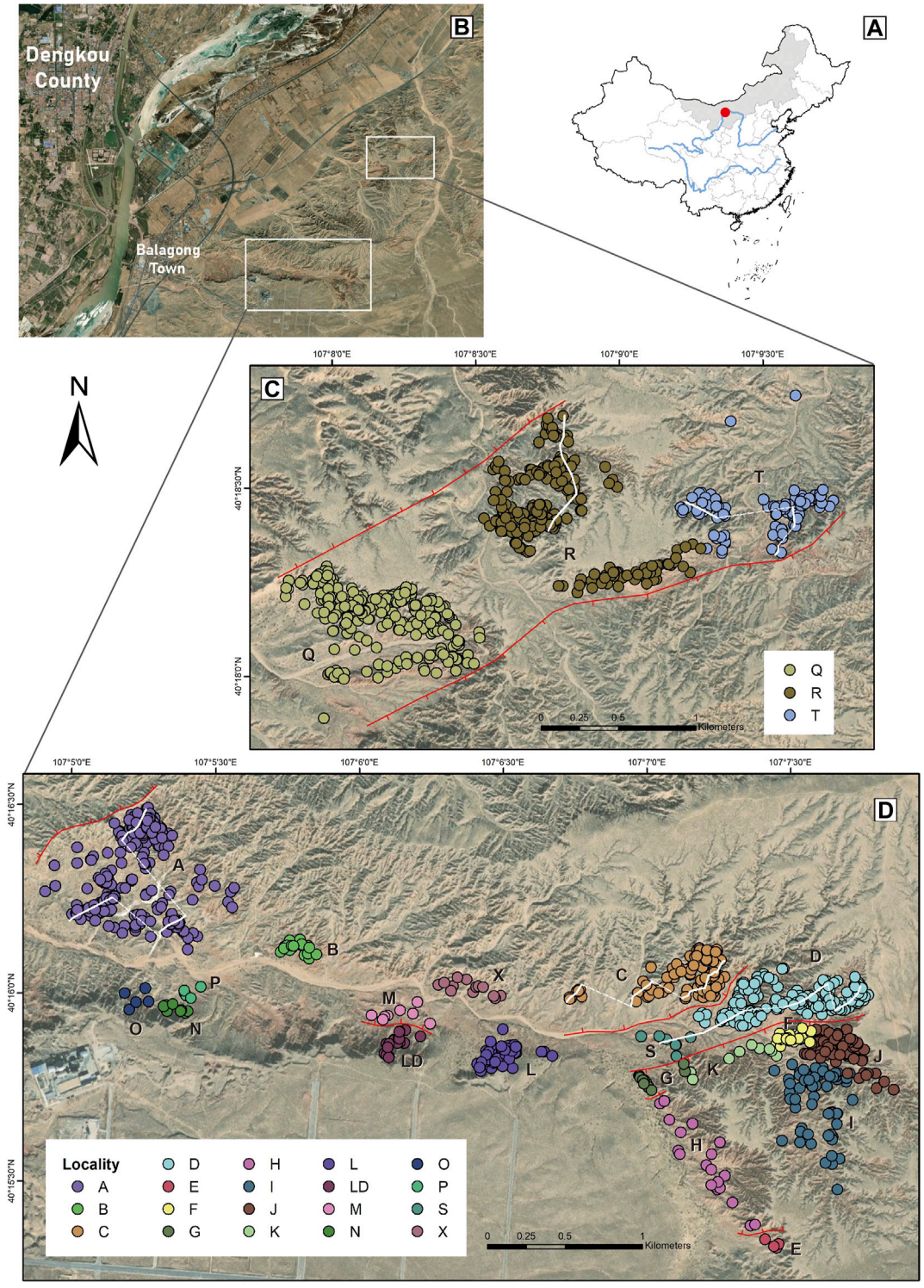

FIGURE 1
Location of Saint Jacques and its fossil localities. **(A)** Map of China, showing the location of Saint Jacques (red circle) in Nei Mongol (gray area). **(B)** The Saint Jacques fossiliferous area is near the town of Balagong, across the Yellow River from Dengkou County. Fossil localities are densely distributed in **(C)** Sanshenggongbei and **(D)** Langhaogou. White lines in **(C)** and **(D)**: measured stratigraphic sections. Red lines: faults.

changes in particle size and sediment color, and they are ordered from bottom to top. For example, the strata exposed in block A are divided into eight layers, referred to as A1 (bottom) through A8 (top). We recorded fossil occurrences by their stratigraphic layers in their respective blocks, then we correlated facies across blocks by similarity in lithology.

TABLE 1 Stratigraphic levels of selected small mammals identified from Saint Jacques.

	Taxon	Eocene			Oligocene							Miocene	
		L1 S1 LD1	L2 S2 LD2	D1 Q1 T1	R2 Q2 H1 D3 T2+3	R3 Q3 J2 D4 T4	A3 R4 Q4 J5 D5 T5	A4 D6 Q5+6+7 R5+6+7	A5 C5 Q8 R8	A6 C6 R9	A7 C7 R10	C8+9	C10
Erinaceidae	*Amphechinus*								√			√	
	Palaeoscaptor				√	√	√	√	√		√		
Changlelestidae	*Zaraalestes*			√	√	√	√						
Ochotonidae	*Sinolagomys*												√
	Sinolagomys ulunguensis										√	√	
	Sinolagomys cf. *major*										√	√	
	Sinolagomys cf. *kansuensis*										√	√	
	Sinolagomys cf. *pachygnathus*										√	√	
	Sinolagomys pachygnathus										√		
	Sinolagomys major										√		
	Sinolagomys kansuensis									√	√	√	
	cf. *Sinolagomys*								√				
	cf. *Desmatolagus*							√	√				
	Desmatolagus cf. *pusillus*							√	√				
	Desmatolagus pusillus						√	√	√				
	Desmatolagus gobiensis				√	√	√	√					
	Desmatolagus cf. *vetustus*				√	√	√						
	Desmatolagus vetustus				√	√							
	Desmatolagus cf. *gobiensis*			√	√	√	√	√	√				
	Desmatolagus	√	√	√	√	√	√	√	√	√	√		
Leporidae	*Ordolagus teilhardi*						√		√				

(Continued on following page)

10.3389/feart.2023.1127964

TABLE 1 (*Continued*) Stratigraphic levels of selected small mammals identified from Saint Jacques.

	Taxon	Eocene			Oligocene							Miocene	
		L1 S1 LD1	L2 S2 LD2	D1 Q1 T1	R2 Q2 H1 D3 T2+3	R3 Q3 J2 D4 T4	A3 R4 Q4 J5 D5 T5	A4 D6 Q5+6+7 R5+6+7	A5 C5 Q8 R8	A6 C6 R9	A7 C7 R10	C8+9	C10
	Ordolagus			√	√	√	√	√	√				
	Leporidae indet.		√	√	√	√	√	√	√				
Cricetidae	*Ayakozomys*												√
	Tachyoryctoides										√	√	
	Tachyoryctoides (small)									√			
	Tachyoryctoides kokonorensis									√			
	Eucricetodon youngi										√		
	Eucricetodon jilantaiensis							√	√				
	Eucricetodon asiaticus							√	√				
	Eucricetodon				√	√	√	√	√		√		
	Cricetops dormitor				√	√	√	√					
	Cricetops minor				√								
	Selenomys mimicus				√	√	√						
Ctenodactylidae	*Prodistylomys*												√
	Yindirtemys suni										√		
	Yindirtemys cf. *deflexus*									√			
	Yindirtemys deflexus								√				
	Yindirtemys grangeri								√		√		
	Yindirtemys cf. *grangeri*								√				
	Yindirtemys							√	√	√	√		
	Bounomys ulantatalensis								√				
	Bounomys cf. *ulantatalensis*							√	√				
	Bounomys bohlini						√						

(Continued on following page)

10.3389/feart.2023.1127964

TABLE 1 (*Continued*) Stratigraphic levels of selected small mammals identified from Saint Jacques.

	Taxon	Eocene			Oligocene							Miocene	
		L1 S1 LD1	L2 S2 LD2	D1 Q1 T1	R2 Q2 H1 D3 T2+3	R3 Q3 J2 D4 T4	A3 R4 Q4 J5 D5 T5	A4 D6 Q5+6+7 R5+6+7	A5 C5 Q8 R8	A6 C6 R9	A7 C7 R10	C8+9	C10
	Bounomys cf. *bohlini*					√	√						
	Tataromys sigmodon							√	√				
	Tataromys plicidens							√	√				
	Tataromys						√	√	√				
	Tataromys minor					√	√	√	√				
	Tataromys cf. *minor*			√	√	√	√	√	√				
	Karakoromys			√	√	√	√						
	Karakoromys decessus			√	√	√	√						
	Karakoromys cf. *decessus*		√	√	√	√	√						
Aplodontidae	*Promeniscomys*							√					
Cylindrodontidae	*Anomoemys*					√	√	√	√				
	Anomoemys lohiculus					√	√	√					
	Ardynomys			√	√								
Tsaganomyidae	*Tsaganomys altaicus*						√	√	√				
	Tsaganomys				√	√	√	√	√		√		
	Cyclomylus				√	√	√	√					
	Cyclomylus lohensis				√	√		√					
Dipodidae	*Heosminthus*				√								
	Parasminthus				√	√	√	√	√				
	cf. *Parasminthus*		√	√	√	√							
	Allosminthus		√	√	√	√	√						
Gobiomyidae	*Gobiomys*		√										

10.3389/feart.2023.1127964

10.3389/feart.2023.1127964

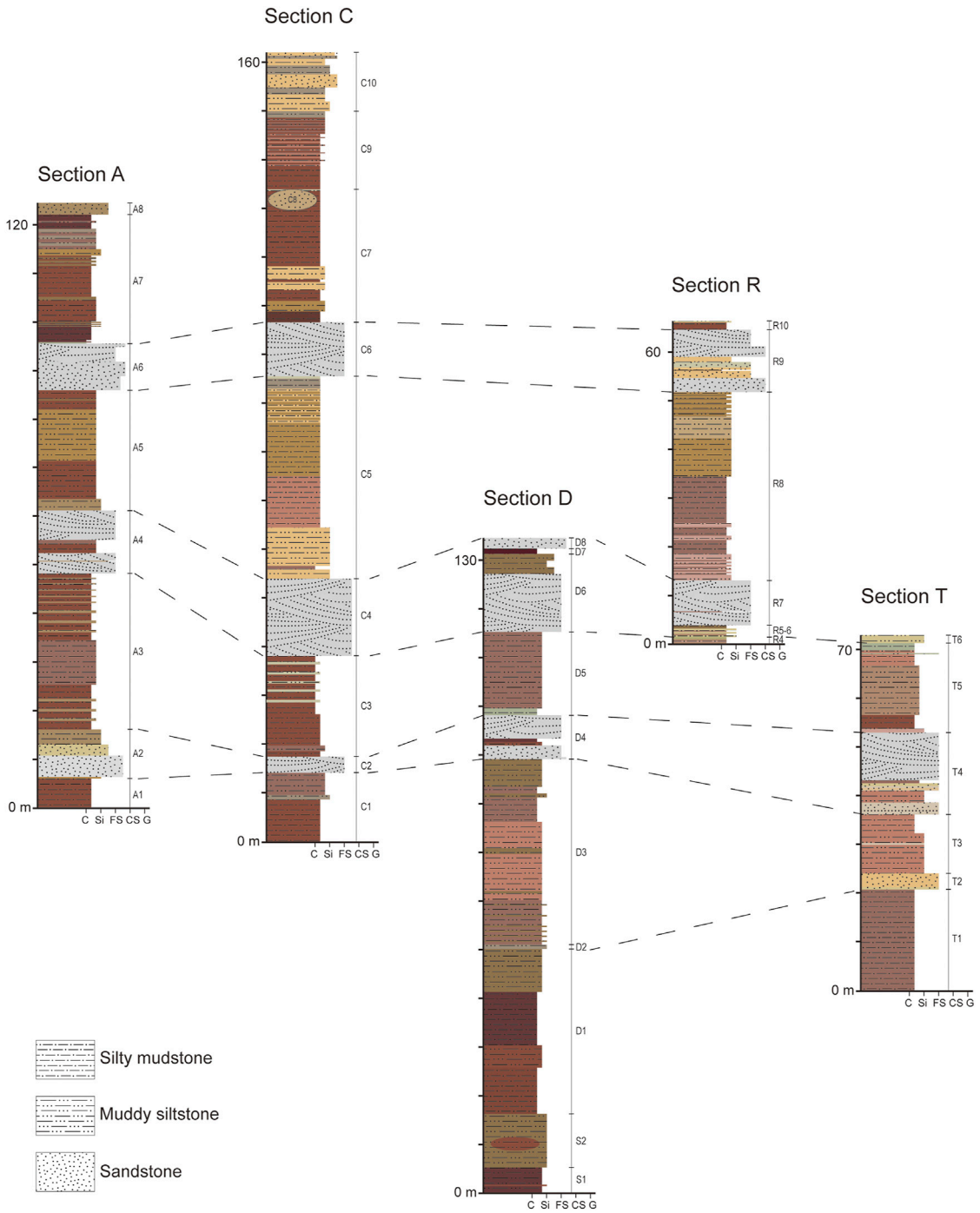

FIGURE 2
Stratigraphic columns of five measured sections at Saint Jacques, showing the correlation of units in different sections. Grain-size scale: C = clay; Si = silt; FS = fine sand; CS = coarse sand; G = gravel.

Fossil collection started in 2011. Two collection methods are used: *in situ* collecting and surface collecting. When fossils are found *in situ*, we record the coordinates and elevation of the location and consider it a fossil locality. A locality is typically an area of a few meters across or less. Each locality is tied to a block and a stratigraphic level. Fossils that have been washed out from the place of burial and transported for a short distance were also collected from the surface. In these cases, we can usually still determine the lithological layer that the fossils are from, even though we cannot pinpoint an exact location. During each field season, we sorted through our findings daily and made field catalogue. Further identification and research were conducted after returning from the field. In order to minimize preservation bias, we made efforts to collect more thoroughly from blocks and layers in which fossils were not as abundant.

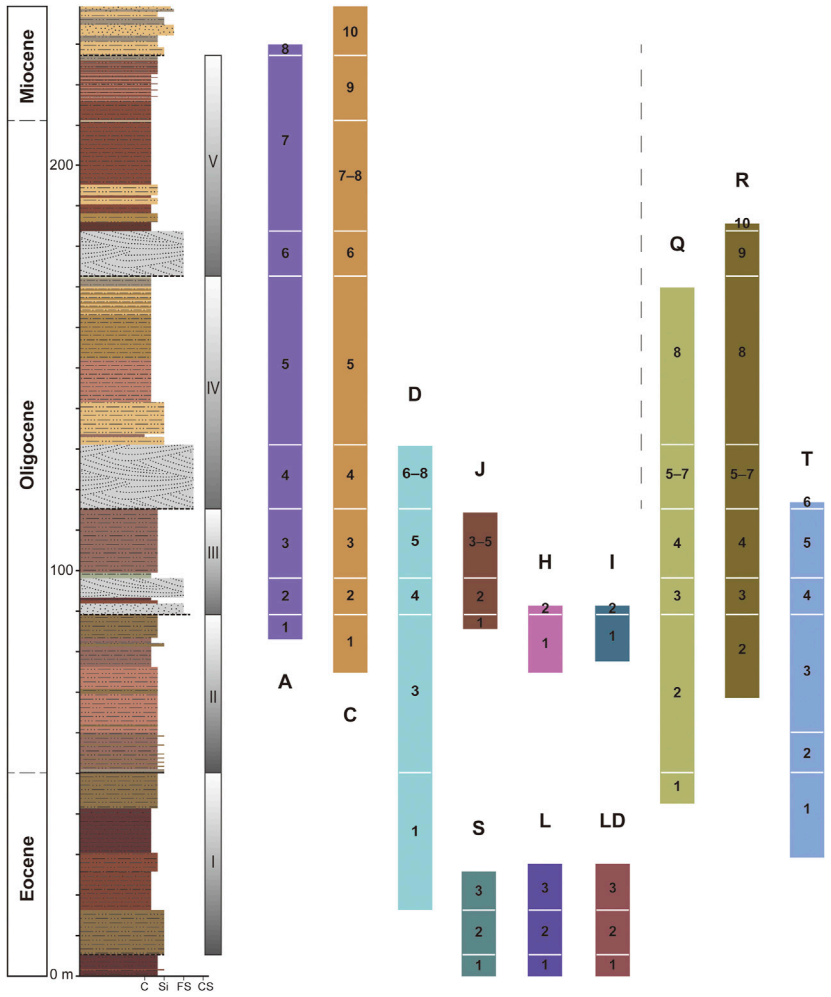

FIGURE 3
Composite stratigraphic profile for Saint Jacques (left column) and lithostratigraphic correlation of the main fossiliferous blocks (colored bars). Thicknesses of litho-units in individual blocks are not to scale. Color scheme of blocks matches legend in Figure 1. Grain-size scale: C = clay; Si = silt; FS = fine sand; CS = coarse sand.

We measured five stratigraphic sections using a Brunton compass, a tape measure, and Jacob's staff. Rock strata in Saint Jacques gently dip north-northeast at 5–20°. Because the dip of the beds is generally low, we measured sections primarily with a tape measure and then corrected for dip. Where the exposure is suitable, we used Jacob's staff to measure the thicknesses of beds directly. The measured sections combined encompass nearly the entire stratigraphic sequence exposed in Saint Jacques. Three of the five measured sections are in Langhaogou, the E-W trending gully along which previous discoveries were made. The other two sections are located in what we refer to as Sanshenggongbei, approximately 4 km to the northeast of Langhaogou, a fossiliferous area that we newly discovered. The measured sections span about 100 m in elevation, close to the total topographic relief in Langhaogou. We mapped the locations of stratigraphic sections using a GPS device and described lithologies in detail as we measured sections. We recognized correlations of measured and unmeasured sections on the basis of the lateral and vertical relationships of facies sharing similar lithological properties and fossil evidence.

Results

Across the 22 fossiliferous blocks in Saint Jacques, we have documented 1635 fossil localities (Figure 1). The Sanshenggongbei area is divided into blocks Q, R, and T, which all have densely packed localities (Figure 1C). The other 19 blocks are distributed in Langhaogou, where more faults are present. Here, blocks A, C, D, J, and I have the most number of localities. Older strata in Langhaogou are generally in more southerly located blocks.

Lithostratigraphic correlation and classification

The five measured lithostratigraphic sequences are in blocks A, C, S–D, R, and T (Figure 2). Blocks S and D are stratigraphically continuous, only separated by a gully, and S3 partially overlaps with the lower part of D1. Fossiliferous layers are continuously numbered, except in two cases. D2 is a band of light colored

FIGURE 4
Outcrop photographs of selected measured sections.

siltstone sandwiched by reddish beds below and above. Vertebrate fossils are rare in D2; this layer is primarily used to separate D3 from D1, thereby achieving a higher stratigraphic resolution. The other exception is C8, a large lens of channel sandstone that cuts into the upper part of C7. Blocks A and C are largely comparable in lithology, only block C is thicker and includes more strata at the top. A5 and C5 have a distinctive brownish yellow color that differentiates this layer from strata below and above. This color is also observed in R8 in northern Saint Jacques. A7 and C7 are characterized by multiple bands of reddish mudstone (Figure 4). Additional fossiliferous areas that have been correlated to the measured sections similarity in lithology and fossil composition include blocks H, I, J, L, LD, and Q (Figure 3). Block E, representing the lower-most strata in this area, produced some remains of *Gomphos* but can not be correlated with any other blocks, and it is here excluded from the composite profile. Altogether, 12 lithostratigraphic units are recognized in ascending order:

Litho-unit 1 (S1, L1, LD1): Dark red muddy siltstone. The sedimentary structure is uniform with no visible lamination. This unit is rich in turtle fossils, while mammalian fossils are scarce. No underlying strata are exposed in block S or block L.

Litho-unit 2 (S2, L2, LD2): Brownish yellow fine sandstone interbedded with variably thick lenses of siltstone mixed with dark red muddy pebbles, carbonate nodules, and coarse sand. Cross bedding and lamination are developed in this unit. This unit includes the earliest occurrences of Leporidae, Ctenodactylidae, and Dipodidae in the sequence and the only occurrence of *Gobiomys*.

Litho-unit 3 (D1, S3, T1, L3, Q1): Thick layer of brownish red muddy siltstone to dark red silty mudstone. The color becomes lighter upwards with increasing amount of muddy siltstone. Massive, with no visible lamination. Fossils are sporadically discovered without any particularly rich locality. *Karakoromys decessus* and *Ordolagus* first occur in this unit.

Litho-unit 4 (A1, C1, D3, T2+3, R2, Q2, J1, H1, I1): The basal part of this unit is represented by thin layers of light brown siltstone with lamination; the upper part is composed of massive, structureless lighter brownish red muddy siltstone and darker brownish red silty mudstone. This unit contains well-preserved small mammal fossils, including relatively complete skulls and jaws. Species richness is markedly higher than in the underlying unit. *Cricetops*, *Selenomys*, *Cyclomylus* and other taxa begin to appear in the sequence.

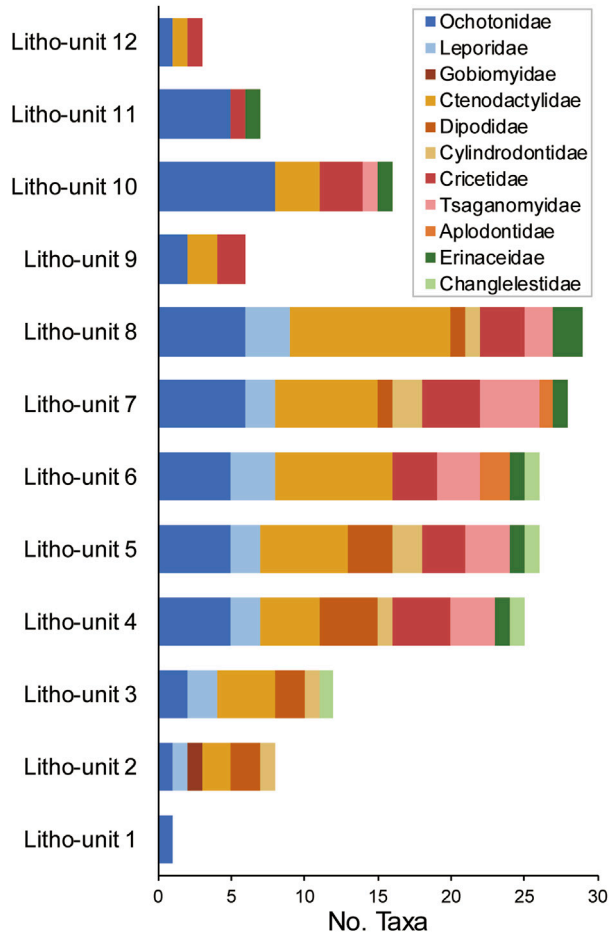

FIGURE 5
Number of small-mammal taxa in different lithostratigraphic units. Lagomorph families are in blue colors, rodent families in warm colors, and insectivore families in green colors.

Litho-unit 5 (A2, C2, D4, T4, R3, Q3, J2, H2, I2): Grayish white fine-to medium-grained sandstone with large-scale cross bedding, interbedded with lenses of coarser-grained sands with carbonate nodules or muddy pebbles. Vertebrate fossils are rich, including fish, frog, salamander, turtles, birds, and mammals. The mammalian fauna is similar to that of litho-unit 4.

Litho-unit 6 (A3, C3, D5, R4, T5, Q4, J3+4+5): Pale brownish red muddy siltstone or silty mudstone. Massive and structureless. Fossils are sporadically distributed. In block Q, a large lens of siltstone and fine sandstone is observed within the Q4; the lens is pinched off eastwards. *Desmatolagus*, *Tataromys*, and *Karakoromys* are abundant.

Litho-unit 7 (A4, C4, D6+7+8, R5+6+7, T6, Q5+6+7): Grayish white fine-to medium-grained sandstone with large-scale cross bedding. The reddish silty mudstone bed in between the sandstone varies in thickness from 0 to 2–3 m in different blocks. Fossils are rich in the sandstone. *Karakoromys* disappears from this unit.

Litho-unit 8 (A5, C5, Q8, R8): Thick layer of yellowish brown muddy siltstone and silty mudstone, massive and structureless, with manganese nodules. Small mammals are sporadically distributed in this unit. *Sinolagomys* first appear from the upper part of this unit.

Litho-unit 9 (A6, C6, R9): Grayish white fine-to coarse-grained sandstone with large-scale cross bedding. Large mammalian fossils are rich, including skulls and postcranial of giant rhinos. *Tachyoryctoides* are first documented from this unit.

Litho-unit 10 (A7, C7+8, R10): Massive brownish red silty mudstone interbedded with bands of reddish mudstone. C8 is composed of fine or coarse sandstone, pinched off westwards, thickening eastwards, and punctuated by a fault on the west side. Fossils of *Sinolagomys* and large-sized *Yindirtemys* are abundant in this unit.

Litho-unit 11 (C9): Alternating light brownish red muddy siltstone and dark brown silty mudstone. *Sinolagomys* remains abundant while *Yindirtemys* disappears in this unit.

Litho-unit 12 (C10): Pale orange fine-grained sandstone, with light brown muddy siltstone in the upper part. Small-sized *Sinolagomys*, *Prodistylomys*, and some insectivores are documented in this unit.

We created a composite stratigraphic profile of Saint Jacques using measurements from blocks S, D, and C, which combined encompass the longest temporal and lithostratigraphic records (Figure 4). The composite section spans 239 m. Particle size of the sediments is generally small. Aside from the three layers of fine- to medium-grained sandstone, the sequence is mainly composed of reddish silty mudstone and muddy siltstone. Rock color is generally darker towards the bottom and lighter towards the top. Section S through the bottom of section D (litho-units 1–3) is marked by dark red silty mudstone and moderate brown muddy siltstone. Several layers of pale orange yellow muddy siltstone appear in the upper half of the sequence.

Small mammals in stratigraphic context

Fossil mammals are collected from litho-unit 1 through litho-unit 11. With a preliminary examination of the small mammals from these units, we have identified 65 taxa belonging in eleven families of small mammals, including seven families of rodents (Aplodontidae, Ctenodactylidae, Cricetidae, Cylindrodontidae, Dipodidae, Gobiomyidae, Tsaganomyidae), two families of lagomorphs (Leporidae and Ochotonidae), and two families of insectivores (Changlelestidae and Erinaceidae) (Table 1). Additionally, the basal Glires *Gomphos* has been found in block E, putting it to stratigraphically below litho-unit 1.

Taxonomic richness of small mammals increases progressively from litho-unit 1 to litho-unit 8 and then sharply declines in higher units (Figure 5). The greatest increase occurs between litho-units 3 and 4. This pattern is a result of a step increase in the number of ochotonid taxa as well as the appearance of cricetids, tsaganomyids, and erinaceids in litho-unit 4. Ctenodactylid richness increases relatively steadily across these units. Among the rodents, the aplodontids appear the latest in the sequences and have the shortest duration—they are only found in litho-units 6 and 7. An abrupt drop in taxonomic richness is observed in litho-unit 9. The abundance of relatively complete large-mammal fossils in this unit suggests that flow velocity was high and not ideal for the deposition of small-mammal material. Therefore, the decline in the richness of small mammals may reflect, at least in part, the condition of preservation rather than a true ecological signal.

Faunal turnover appears to be gradual across the sequence (Table 1). Even though the taxonomic richness remains relatively stable during the deposition of litho-unit 4 through litho-unit 8, the small-mammal fauna was not static. Rather, a stepwise transition in the taxonomic composition is documented, especially for the ochotonids, ctenodactylids, and cricetids.

Discussion

Our re-exploration of the Saint Jacques area has revealed developed terrestrial sediments with rich fossils. The significance of this work is several fold. First, we have recovered fossils from a larger area at Saint Jacques than previously known. In addition to the localities in Langhaogou (roughly equivalent to the former Saint Jacques site), we discovered a fossiliferous area to the northeast that was unknown before. These areas have been intensively surveyed over 12 field seasons, as shown by the high density of new fossil localities (Figure 1). Our continuous field expeditions have yielded thousands of pieces of fossil-mammal material, all tied to specific stratigraphic units. Comparing to the existing fauna lists of Saint Jacques (e.g., Meng and McKenna, 1998; Wang and Qiu, 2003), a number of taxa are recorded for the first time, including *Sinolagomys ulunguensis*, *S. pachygnathus*, *Yindirtemys suni*, *Yindirtemys grangeri*, *Gobiomys*, *Tachyoryctoides kokonorensis*, *Eucricetodon jilantaiensis*, *Cyclomylus lohiculus*, *Allosminthus*, *Parasminthus*, *Prodistylomys*, and *Ayakozomys*. Our thorough investigation of the field area thus reveals a fuller picture of the mammalian assemblages of Saint Jacques.

Second, we conducted the first detailed study on the lithological subdivision of Saint Jacques strata. This provided a lithological context for the fossiliferous sequence and allowed for the correlation of facies across blocks. The establishment of this chronostratigraphic framework formed the basis for documenting and understanding the deposition of fossil materials, with improved temporal resolution. We recognize 12 lithostratigraphic units in Saint Jacques, and mammalian fossils have been collected from all of them (Table 1; Figure 5). Additional material (i.e., *Gomphos*) has been found in even older strata (block E) in the area. This fine division of stratigraphic units allows for analyses of faunal transition in smaller time bins and with reduced errors introduced by time averaging.

Third, a preliminary examination of the rich small-mammal materials (especially rodents and lagomorphs) reveals that faunal assemblages in Saint Jacques show successive evolutionary stages. Most taxa occur in stratigraphically continuous litho-units (Table 1), documenting the pattern of faunal succession. No prominent hiatus in the depositional sequence has been observed. This record, therefore, provides an excellent opportunity for further studying the faunal composition of continental Asia from the late Eocene through the Oligocene. Wasiljeff et al. (2020) recently provided better age constraint on the Ulantatal sequence in Nei Mongol and demonstrated that major faunal turnover preceded (instead of precisely at) the Eocene–Oligocene (E–O) boundary. Research on the magnetostratigraphy of the Saint Jacques sequence is still underway. A deeper look into the timing and pattern of faunal transition in Saint Jacques will help elucidate the potential complexity in terrestrial faunal responses to broad-scale changes in climate and environment.

Prior to our revisit of Saint Jacques in 2010, the common understanding of its paleontology was that the area contained two local faunas, one of early Oligocene age and the other late Oligocene (e.g., Wang and Qiu, 2003). In contrast, our work now suggests that the sedimentary strata in Saint Jacques likely span the Eocene through the early Miocene, bracketing a long, successive Oligocene sequence within. Bai et al. (2018) reported *A. praecox* from L2 (litho-unit 2), correlating this unit to the Ergilian Asian Land Mammal Age (latest Eocene). In line with this result, we have identified *Gobiomys* in L2 (litho-unit 2). This rodent genus is known exclusively from the Eocene of Nei Mongol (Wang, 2001; Li et al., 2022). The presence of *Ardynia praecox* and *Gobiomys* shows that the lower Saint Jacques sequence extends into the Eocene. Another taxon that sheds light on the E–O boundary is *Ardynomys*, a primitive cylindrodontids previously known from the late Eocene of Nei Mongol (Wang and Wang, 1991; Wang and Meng, 2009; Gomes Rodrigues et al., 2014; Wasiljeff et al., 2020; Wasiljeff and Zhang, 2022), the late Eocene to the early Oligocene of Mongolia (Dashzeveg, 1996; Daxner-Höck et al., 2017), and the late Eocene of North America (Wood, 1970; 1974; Korth, 1992). In Saint Jacques, *Ardynomys* occurs in litho-units 3 and 4. Considering the occurrence of other Oligocene taxa (e.g., *Desmatolagus gobiensis*, *Eucricetodon*, *Cricetops*, *Selenomys mimicus*, *Tsaganomys*) in litho-unit 4, the epoch boundary is most likely within litho-unit 3 at Saint Jacques. Taxa in the top layers at Saint Jacques show similarity with late Oligocene to early Miocene faunas in northern China and Mongolia. For example, *T. kokonorensis*, *Sinolagomys pachygnathus*, *Eucricetodon youngi*, and *Y. suni* are representatives of the Xiejian faunas of China, considered to be the early Miocene in age (Li and Qiu, 1980; Qiu and Qiu, 1995; Qiu et al., 2001; Wang and Qiu, 2012; Qiu et al., 2013). In Saint Jacques, these species occur in litho-units 10 and 11. *T. kokonorensis* (litho-unit 10), *Y. suni* (litho-unit 11), *Prodistylomys* (litho-unit 12), and *Ayakozomys* (litho-unit 12) occur in the Valley of Lakes, Mongolia during the latest Oligocene to the early Miocene (Daxner-Höck et al., 2015; 2017; Harzhauser et al., 2017).

To conclude, our re-investigation of Saint Jacques has greatly expanded the chronostratigraphic and taxonomic coverage of the mammalian fossil collection from this area. Our preliminary biostratigraphic analysis of small mammals shows that the area preserves faunal succession from the late Eocene to the early Miocene, making it an important record for studying mammalian faunal turnovers during both the Eocene–Oligocene and the Oligocene–Miocene transitions.

Data availability statement

The original contributions presented in the study are included in the article/Supplementary Material, further inquiries can be directed to the corresponding authors.

Author contributions

Data synthesis and manuscript preparation: BW, Z-QZ, and Y-QW. All authors participated in field work and data collection.

Funding

Field work was supported by the Strategic Priority Research Program of Chinese Academy of Sciences (XDB26000000), the National Natural Science Foundation of China (41472003), and the Special Fund for Fossil Excavation and Preparation of the Chinese Academy of Sciences.

Acknowledgments

We are grateful to many individuals for their field assistance over the years: Wei Zhou, Shi-Jie Li, Qi Li, Yong-Xing Wang, Yong-Fu Wang, Xin-Yue Zhang, Ping Wang, and others. We would also like to thank the reviewers for their constructive feedback on the manuscript.

Conflict of interest

The authors declare that the research was conducted in the absence of any commercial or financial relationships that could be construed as a potential conflict of interest.

Publisher's note

All claims expressed in this article are solely those of the authors and do not necessarily represent those of their affiliated organizations, or those of the publisher, the editors and the reviewers. Any product that may be evaluated in this article, or claim that may be made by its manufacturer, is not guaranteed or endorsed by the publisher.

References

Angelone, C., and Zhang, Z.-Q. (2021). Climate change and evolution of early lagomorphs (Mammalia): A study perspective based on new materials of *Ordolagus* from Nei Mongol (northern China). *Vert. PalAsiat.* 59, 138–168.

Bai, B., Wang, Y.-Q., and Zhang, Z.-Q. (2018). The late Eocene hyracodontid perissodactyl *Ardynia* from Saint Jacques, Inner Mongolia, China and its implications for the potential Eocene–Oligocene boundary. *Palaeoworld* 27, 247–257. doi:10.1016/j.palwor.2017.09.001

Chow, M. C., and Rozhdestvensky, A. K. (1960). Exploration in Inner Mongolia — A preliminary account of the 1959 field work of the Sino-Soviet paleontological expedition (SSPE). *Vert. PalAsiat.* 4, 1–10.

Coxall, H. K., Wilson, P. A., Palike, H., Lear, C. H., and Backman, J. (2005). Rapid stepwise onset of Antarctic glaciation and deeper calcite compensation in the Pacific Ocean. *Nature* 433, 53–57. doi:10.1038/nature03135

Dashzeveg, D. (1996). A new *Ardynomys* (Rodentia, Cylindrodontidae) from the Eocene of the eastern Gobi desert, Mongolia. *Palaeovertebrata* 25, 339–348.

Daxner-Höck, G., Badamgarav, D., Barsbold, R., Bayarmaa, B., Erbajeva, M., Göhlich, U. B., et al. (2017). Oligocene stratigraphy across the Eocene and Miocene boundaries in the Valley of Lakes (Mongolia). *Palaeobio. Palaeoenv.* 97, 111–218. doi:10.1007/s12549-016-0257-9

Daxner-Höck, G., Badamgarav, D., and Maridet, O. (2015). Evolution of Tachyoryctoidinae (Rodentia, Mammalia): Evidences of the Oligocene and early Miocene of Mongolia. *Ann. Naturhist. Mus. Wien, Ser. A* 117, 161–195.

Dupont-Nivet, G., Krijgsman, W., Langereis, C., Abels, H. A., Dai, S., and Fang, X. (2007). Tibetan plateau aridification linked to global cooling at the Eocene–Oligocene transition. *Nature* 445, 635–638. doi:10.1038/nature05516

Eldrett, J., Greenwood, D., Harding, I., and Huber, M. (2009). Increased seasonality through the Eocene to Oligocene transition in northern high latitudes. *Nature* 459, 969–973. doi:10.1038/nature08069

Gomes Rodrigues, H., Marivaux, L., and Vianey-Liaud, M. (2014). Rodent paleocommunities from the Oligocene of Ulantatal (Inner Mongolia, China). *Palaeovertebrata* 38 (1–11), e3. doi:10.18563/pv.38.1.e3

Harzhauser, M., Daxner-Höck, G., Erbajeva, M. A., López-Guerrero, M., Maridet, O., Oliver, A., et al. (2017). Oligocene and early Miocene mammal biostratigraphy of the Valley of Lakes in Mongolia. *Palaeobio. Palaeoenv.* 97, 219–231. doi:10.1007/s12549-016-0264-x

Hren, M. T., Sheldon, N. D., Grimes, S. T., Collinson, M. E., Hooker, J. J., Bugler, M., et al. (2013). Terrestrial cooling in northern Europe during the Eocene–Oligocene transition. *Proc. Natl. Acad. Sci. U.S.A.* 110, 7562–7567. doi:10.1073/pnas.1210930110

Korth, W. W. (1992). Cylindrodonts (Cylindrodontidae, Rodentia) and a new genus of eomyid, *Paranamatomys*, (Eomyidae, Rodentia) from the Chadronian of Sioux County, Nebraska. *Trans. Neb. Acad. Sci.* 19, 75–82.

Kraatz, B. P., and Geisler, J. H. (2010). Eocene–Oligocene transition in Central Asia and its effects on mammalian evolution. *Geology* 38, 111–114. doi:10.1130/g30619.1

Li, C.-K., and Qiu, Z.-D. (1980). Early Miocene mammalian fossils of Xining basin, Qinghai. *Vert. PalAsiat.* 18, 198–214.

Li, Q., Li, Q., Xu, R., and Wang, Y. (2022). Rodent faunas, their paleogeographic pattern, and responses to climate changes from the early Eocene to the early Oligocene in Asia. *Front. Ecol. Evol.* 10, 955779. doi:10.3389/fevo.2022.955779

Lopatin, A. V. (2004). Early Miocene small mammals from the North Aral Region (Kazakhstan) with special reference to their biostratigraphic significance. *Paleontol. J.* 38, S217–S323.

Meng, J., and McKenna, M. (1998). Faunal turnovers of palaeogene mammals from the Mongolian plateau. *Nature* 394, 364–367. doi:10.1038/28603

Qiu, Z.-X., and Qiu, Z.-D. (1995). Chronological sequence and subdivision of Chinese Neogene mammalian faunas. *Palaeogeogr. Palaeoclimatol. Palaeoecol.* 116, 41–70. doi:10.1016/0031-0182(94)00095-p

Qiu, Z.-X., Qiu, Z.-D., Deng, T., Li, C.-K., Zhang, Z.-Q., Wang, B.-Y., et al. (2013). "Neogene land mammal stages/ages of China: Toward the goal to establish an Asian land mammal stage/age scheme," in *Fossil Mammals of Asia: Neogene Biostratigraphy and Chronology*, eds. X.-M. Wang, L. J. Flynn, and M. Fortelius (New York: Columbia University Press), 29–90.

Qiu, Z., Wang, B., Qiu, Z., Heller, F., Yue, L., Xie, G., et al. (2001). Land-mammal geochronology and magnetostratigraphy of mid-Tertiary deposits in the Lanzhou basin, Gansu Province, China. *Eclogae. Geol. Helv.* 94, 373–385.

Shi, W., Dong, S. W., and Hu, J. M. (2020). Neotectonics around the Ordos block, north China: A review and new insights. *Earth Sci. Rev.* 200, 102969. doi:10.1016/j.earscirev.2019.102969

Sun, J., Ni, X., Bi, S., Wu, W., Ye, J., Meng, J., et al. (2014). Synchronous turnover of flora, fauna, and climate at the Eocene–Oligocene boundary in Asia. *Sci. Rep.* 4, 7463. doi:10.1038/srep07463

Teilhard de Chardin, P. (1926). Description de mammifères Tertiaires de Chine et de Mongolie. *Ann. Paleontol.* 15, 1–52.

Teilhard de Chardin, P., and Licent, E. (1924a). On the geology of the northern, Western and southern borders of the Ordos, China. *Geol. Bull. China* 3, 37–44. doi:10.1111/j.1755-6724.1924.mp3001004.x

Teilhard de Chardin, P., and Licent, E. (1924b). Observations géologiques sur la bordure occidentale et méridional de l'Ordos. *Bull. Soc. Géol. Fr. Ser. 4.* 24, 29–91.

Teilhard de Chardin, P., and Licent, E. (1924c). Observations complémentaires sur la géologiques de l'Ordos. *Bull. Soc. Géol. Fr. Ser. 4.* 24, 462–464.

Wang, B.-Y. (1987). Discovery of Aplodontidae (Rodentia, Mammalia) from middle Oligocene of Nei Mongol, China. *Vert. PalAsiat.* 25, 32–45.

Wang, B.-Y., and Emry, R. J. (1991). Eomyidae (Rodentia: Mammalia) from the Oligocene of Nei Mongol, China. *J. Vert. Paleontol.* 11, 370–377. doi:10.1080/02724634.1991.10011404

Wang, B.-Y. (2001). Eocene ctenodactyloids (Rodentia, Mammalia) from Nei Mongol, China. *Vert. PalAsiat.* 39, 98–114.

Wang, B.-Y., and Meng, J. (2009). *Ardynomys* (Cylindrodontidae, Rodentia) from Nei Mongol, China. *Vert. PalAsiat.* 47, 240–244.

Wang, B.-Y., and Qiu, Z.-X. (2003). Note on early Oligocene ursids (Carnivora, Mammalia) from Saint Jacques, Nei Mongol, China. *Bull. Am. Mus. Nat. Hist.* 279, 116–124.

Wang, B.-Y., and Qiu, Z.-X. (2012). *Tachyoryctoides* (Muroidea, Rodentia) fossils from early Miocene of Lanzhou basin, Gansu Province, China. *Swiss J. Palaeontol.* 131, 107–126. doi:10.1007/s13358-011-0038-z

Wang, B.-Y., and Wang, P.-Y. (1991). Discovery of early medial Oligocene mammalian fauna from Kekeamu, Alxa left banner, Nei Mongol. *Vert. PalAsiat.* 29, 64–71.

Wang, J., and Zhang, Z.-Q. (2015). Phylogenetic analysis on *Palaeogale* (Palaeogalidae, Carnivora) based on specimens from Oligocene strata of Saint-Jacques, Nei Mongol. *Vert. PalAsiat.* 53, 310–334.

Wasiljeff, J., Kaakinen, A., Salminen, J. M., and Zhang, Z.-Q. (2020). Magnetostratigraphic constraints on the fossiliferous Ulantatal sequence in Inner Mongolia, China: Implications for Asian aridification and faunal turnover before the Eocene–Oligocene boundary. *Earth Planet. Sci. Lett.* 535, 116125. doi:10.1016/j.epsl.2020.116125

Wasiljeff, J., and Zhang, Z.-Q. (2022). Stratigraphical significance of Ulantatal sequence (Nei Mongol, China) in refining the latest Eocene and Oligocene terrestrial regional stages. *Vert. PalAsiat.* 60, 42–53.

Westerhold, T., Marwan, N., Drury, A. J., Liebrand, D., Agnini, C., Anagnostou, E., et al. (2020). An astronomically dated record of Earth's climate and its predictability over the last 66 million years. *Science* 369, 1383–1387. doi:10.1126/science.aba6853

Wood, A. E. (1974). Early Tertiary vertebrate faunas Vieja group trans-pecos, Texas: Rodentia. *Tex. Mem. Mus. Bull.* 21, 1–112.

Wood, A. E. (1970). The early Oligocene rodent *Ardynomys* (family Cylindrodontidae) from Mongolia and Montana. *Am. Mus. Novit.* 2418, 1–18.

Zachos, J., Pagani, M., Sloan, L., Thomas, E., and Billups, K. (2001). Trends, rhythms, and aberrations in global climate 65 Ma to present. *Science* 292, 686–693. doi:10.1126/science.1059412

Zhang, R., Kravchinsky, V. A., and Yue, L. (2012). Link between global cooling and mammalian transformation across the Eocene–Oligocene boundary in the continental interior of Asia. *Int. J. Earth Sci.* 101, 2193–2200. doi:10.1007/s00531-012-0776-1

Zhang, Z.-Q., Liu, Y., Wang, L.-H., Kaakinen, A., Wang, J., Mao, F.-Y., et al. (2016). Lithostratigraphic context of Oligocene mammalian faunas from Ulantatal, Nei Mongol, China. *C. R. Palevol.* 15, 903–910. doi:10.1016/j.crpv.2015.05.012

frontiers | Frontiers in Ecology and Evolution

TYPE Original Research
PUBLISHED 27 February 2023
DOI 10.3389/fevo.2023.1076819

OPEN ACCESS

EDITED BY
Grégoire Métais,
Centre National de la Recherche Scientifique, France

REVIEWED BY
Yuan-Qing Wang,
Institute of Vertebrate Paleontology and Paleoanthropology (CAS), China
Louis De Bonis,
University of Poitiers, France

*CORRESPONDENCE
Alexander Averianov
✉ dzharakuduk@mail.ru
Jian-Hua Jin
✉ lssjjh@mail.sysu.edu.cn

SPECIALTY SECTION
This article was submitted to Paleontology, a section of the journal Frontiers in Ecology and Evolution

RECEIVED 22 October 2022
ACCEPTED 06 February 2023
PUBLISHED 27 February 2023

CITATION
Averianov A, Obraztsova E, Danilov I and Jin J-H (2023) A new hypercarnivorous hyaenodont from the Eocene of South China. *Front. Ecol. Evol.* 11:1076819. doi: 10.3389/fevo.2023.1076819

A new hypercarnivorous hyaenodont from the Eocene of South China

Alexander Averianov[1,2]*, Ekaterina Obraztsova[2], Igor Danilov[1,2] and Jian-Hua Jin[1]*

[1]State Key Laboratory of Biocontrol and Guangdong Provincial Key Laboratory of Plant Resources, School of Life Sciences, Sun Yat-sen University, Guangzhou, China, [2]Zoological Institute of the Russian Academy of Sciences, St. Petersburg, Russia

A new hyaenodont *Maocyon peregrinus*, gen. et sp. nov., is described based on a partial skull and associated mandible from the upper Eocene Youganwo Formation at Maoming locality in Guangdong Province, China. It shows certain similarities with the Hyainailouroidea in the skull structure, including anteroposteriorly extended jugal/squamosal suture, presence of a preglenoid crest, a lateral expansion of the squamosal posterior to the zygomatic arch, a transversally expanded mastoid process, a nuchal crest that does not extend laterally to mastoid process, and large occipital condyles. The phylogenetic analysis clusters the new taxon with *Oriensperodon dahkoensis* from the late middle Eocene of China and Myanmar and places this clade within the Hyainailouridae in a polytomy with the Apternodontinae and the Hyainailourinae.

KEYWORDS

Mammalia, Hyaenodonta, Hyainailouroidea, Eocene, Asia

Introduction

Hyaenodonta is an extinct group of placental carnivorous mammals that flourished mostly in the Paleogene of Africa, North America, Europe, and Asia. The oldest hyaenodonts are known from the Paleocene of Africa (Gheerbrant, 1995; Solé et al., 2009) and Asia (Meng et al., 1998). Hyaenodonts included a number of small-sized mesocarnivorous animals, as well as larger hypercarnivorous taxa with specialized sectorial dentition. According to the recent phylogenetic analyses, the hypercarnivory was evolved independently in two (Polly, 1996), or three lineages of hyaenodonts (Rana et al., 2015; Borths et al., 2016; Borths and Seiffert, 2017). These three lineages are Hyaenodontinae, Teratodontinae, and Hyainailourinae. The sister taxa Hyainailourinae and Apterodontinae form the clade Hyainailouridae and the latter with its sister taxon Teratodontinae form the clade Hyainailouroidea (Borths et al., 2016; Borths and Seiffert, 2017). The Hyainailourinae were most diverse in Africa where about a dozen of taxa are currently recognized (von Stromer, 1926; Savage, 1965, 1973; Holroyd, 1999; Morlo et al., 2007; Rasmussen and Gutiérrez, 2009; Morales and Pickford, 2017; Borths and Stevens, 2019). Four genera are known in Europe (Lange-Badré, 1979; Ginsburg, 1980; Solé et al., 2015). Two genera of the Hyainailourinae each known from North America and Asia, are *Hemipsalodon* and *Oriensperodon*, respectively (Mellett, 1969; Egi et al., 2007).

The oldest hyainailourid is *Oriensperodon* from the middle Eocene of South China and Myanmar, known from mandible and maxilla fragments and dentition (Chow, 1975; Egi et al., 2007). The genus *Oriensperodon*, originally referred to the Hyainailouridae (Egi et al., 2007), was once considered as a member of the Hyaenodontinae (Lewis and Morlo, 2010; Solé et al.,

2014). Removal of *Oriensptero*don from the Hyainailouridae leaves no counterarguments about the African origin of that clade (Solé et al., 2014, 2015). However, the more recent phylogenetic analyses placed *Oriensptero*don as the most basal member of the Hyainailourinae (Borths et al., 2016; Borths and Seiffert, 2017; Borths and Stevens, 2017, 2019). Here we describe a new hyaenodont taxon, closely related to *Oriensptero*don, based on a partial skull from the late Eocene of South China (Figure 1).

Materials and methods

Dental terminology and measurements follow Borths and Seiffert (2017).

We calculated the body mass of the new taxon as based on the equation $Log10(P) = [3.5104 \times Log10((\Sigma M)/3)] - 2.6469$ provided by Solé et al. (2021), where P is the estimated body mass (in grams) and ΣM the sum of the length of the three lower molars (in mm). The length of the lower molars (m1-3) in SYSU-M-5 is equal to 48.5 mm (Table 1; the unknown m1 length was estimated as 11.7 mm based on its alveolus). The body mass of this specimen calculated using this equation is 39.43 kg. The body mass of *Oriensptero*don *dahkoensis* is estimated as 89.73 kg based on the same equation (m1-3 length is 61.3 mm; Egi et al., 2007).

For the phylogenetic analysis we used the data matrix presented by Solé et al. (2021). The matrix includes 107 taxa and 156 characters. *Maocyon peregrinus* gen. et sp. nov. can be coded by 53 of these characters (34.0%): 30(1); 31(2); 32(1); 33(2); 34(2); 35(1); 36(1); 37(1); 38(0); 39(1); 40(1); 41(2); 42(1); 43(0); 44(2); 45(2); 46(2); 48(2); 49(2); 50(0); 51(1); 52(1); 53(0); 54(1); 55(1); 56(1); 57(1); 58(1); 59(0); 60(1); 61(1); 62(0); 63(1); 64(1); 65(1); 86(0); 87(2); 88(0); 99(1); 101(2); 107(1); 109(0); 110(2); 114(1); 115(1); 117(0); 118(1); 125(0); 126(1); 127(1); 128(1); 129(0); and 130(1). The characters 41, 42, 46, 48, 49, 50, 51, 52, 53, 54, 55, 87, 101, and 110 were treated as ordered. Phylogenetic analysis was performed using the Bayesian "tip-dating" phylogenetic methods first applied to Hyaenodonta by Borths et al. (2016). We run the analysis in MrBayes 3.2 program (Ronquist et al., 2012) using the MrBayes formatted nexus files with all analytical parameters provided by Solé et al. (2021). This nexus file is included in the Supplementary materials.

Results

Class Mammalia (Linnaeus, 1758)
Infraclass Eutheria (Gill, 1872)
Superoder Ferae (Linnaeus, 1758)
Order Hyaenodonta (Van Valen, 1967)
Superfamily Hyainailouroidea (Pilgrim, 1932)
Family Hyainailouridae (Pilgrim, 1932). Genus Maocyon, gen. Nov.

Type species

Maocyon peregrinus sp. nov.
urn:lsid:zoobank.org:act:66BEBEAA-87C6-49C4-92C2-41DA70748FB4.

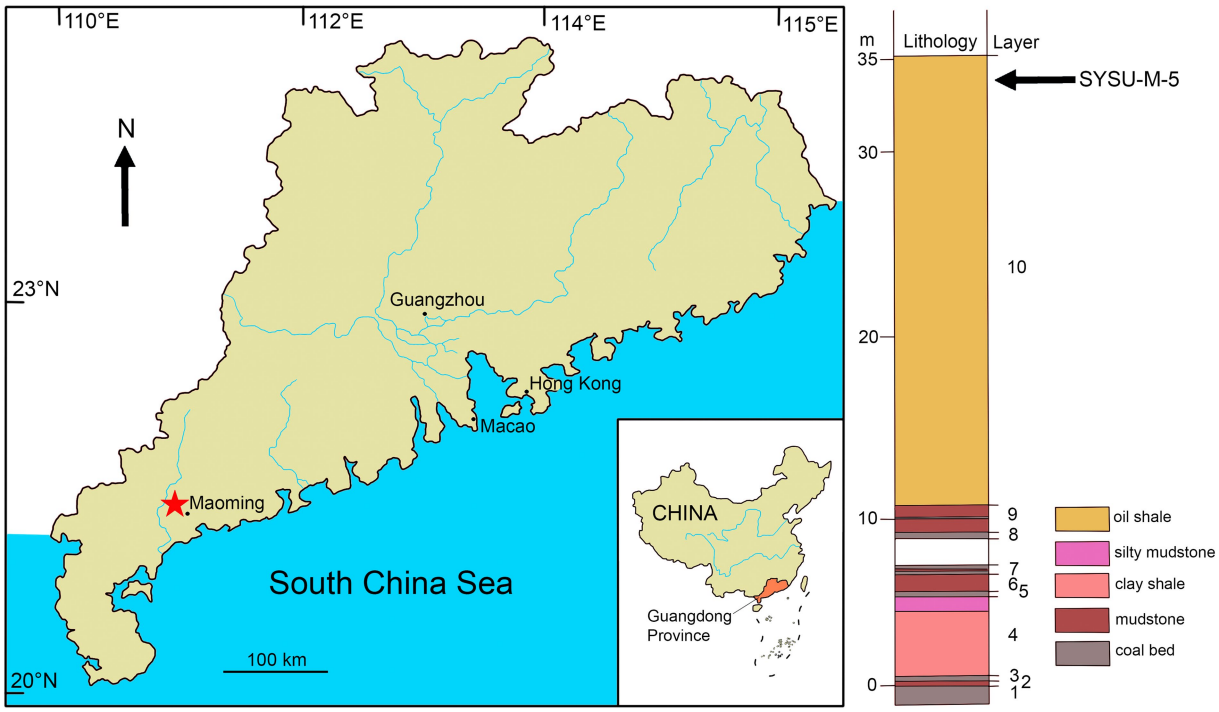

FIGURE 1
Geographic position of Maoming locality designated by star on the map of Guangdong Province, China (left) and stratigraphic position of SYSU-M-5, holotype of *Maocyon peregrinus*, gen. et sp. nov., indicated by arrow on the stratigraphic column of the Youganwo Formation (right).

TABLE 1 Dental measurements of SYSU-M-5, the holotype of *Maocyon peregrinus*, gen. et sp. nov.

Measurement	Left	Right
M2 metastyle mesiodistal length	7.8	8.8
M3 mesiodistal length	13.3	13.7
M3 labilingual width	20.5	19.8
M3 metastyle mesiodistal length	1.9	-
m1 talonid mesiodistal length	6.3	-
m1 talonid labiolingual width	6.5	-
m2 mesiodistal length	16.9	-
m2 trigonid mesiodistal length	11.1	-
m2 talonid mesiodistal length	5.8	7.0
m2 trigonid labiolingual width	10.5	10.2
m2 talonid labiolingual width	8.6	8.4
m3 mesiodistal length	19.9	-
m3 trigonid mesiodistal length	12.7	12.0
m3 talonid mesiodistal length	7.2	-
m3 trigonid labiolingual width	12.8	12.9
m3 talonid labiolingual width	7.9	-

Diagnosis

As for the type and only species.

Etymology

From Maoming City and *Cyon* (Noun, masculine), Latinized form of Greek κύων, a dog.

Maocyon peregrinus sp. nov.

Holotype

SYSU-M-5, a partial skull with associated mandible.

Repository

SYSU-M, Mammal fossil collection from the Maoming Basin in the School of Life Sciences, Sun Yatsen University, Guangzhou, China.

Type locality and horizon

The oil shale quarry (21°42' N, 110°53′ E) located near Maoming City, Maoming Basin, Guangdong Province, China; Youganwo Formation, upper Eocene.

Diagnosis

Referred to the Hyainailouroidea by anteroposteriorly extended suture of the jugal/squamosal, presence of a preglenoid crest, a lateral expansion of the squamosal posterior to the zygomatic arch, a transversally expanded mastoid process, a nuchal crest that does not extend laterally to mastoid process, and large occipital condyles (diagnostic characters are after Solé et al. (2015)). Differs from all Hyainailouroidea except *Oriensperodon* by retention of a rudimentary (ridge-like) metaconid on lower molars. Differs from *Oriensperodon* (Chow, 1975; Egi et al., 2007) by more rudimentary metaconid on m3 and dorsoventrally shallower mandibular body.

Etymology

From Latin *peregrīnus* (Adjective, masculine), foreign, alien, or exotic, an allusion to the Asiatic provenance of this taxon belonging to the predominantly Afro-European clade.

Description

SYSU-M-5 represents the posterior portion of the skull associated with posterior parts of the left and right dentaries (Figures 2–6). The ventral part of the orbit and zygoma are preserved on the right side (Figures 2, 3, 5) while only posterior part of the zygoma is present on the left side (Figures 2–4). The left dentary is missing anterior to m1 (Figure 4) and the right dentary is broken at the p4 (Figure 5). The palate and anterior part of the basicranium is unprepared and obscured by the attached dentaries (Figure 3). The skull is slightly distorted dorsoventrally. The specimen belongs to an aged individual with heavily worn dentition and obliterated sutures between the skull bones.

The skull has an anterioposteriorly elongated basicranial and ethmoidal regions, as in oldest hyainailourines such as *Pterodon* and *Kerberos* (Solé et al., 2015). The whole length of the skull could be around 30 cm based on proportions of *Kerberos langebadreae* (Solé et al., 2015). The narrowest part of the braincase is distinctly posterior to the missing postorbital process (Figure 2), as is typical for the Hyainailouridae (Solé et al., 2015).

Only posterior part of maxilla is preserved. The left maxilla fragment with M2-3 was separated from the skull during preparation (Figure 7). On the right maxilla, also preserving M2-3, there is the zygomatic process of the maxilla connecting with the jugal (Figure 5), but the maxillary-jugal suture is not discernable. The ventral border of orbit is horizontal.

The zygomatic arch is dorsoventrally high, increasing in height posteriorly (Figure 5). A minute postorbital process is present along the dorsal margin of the zygoma at the jugal-squamosal junction. Thus the orbit is largely open at least ventrally (the dorsal border of the orbit is not preserved). The jugal-squamosal suture is anteroposteriorly extended between the postorbital process and the preglenoid process (Figure 5), as in other hyainailourides (Solé et al., 2015).

On the lateral side of the braincase the fronto-parietal suture is not discernable. The early obliteration of the fronto-parietal suture is a typical feature for the Hyainailouridae (Solé et al., 2015). On the parietal, the sagittal crest is high, approximately 20 mm in its maximum height, which is about one third of the skull height in this part (Figures 2, 5). The maximum height of the sagittal crest is opposite the paroccipital apophysis where the parietals are ventrally depressed. The dorsal profile of the sagittal crest is somewhat convex.

10.3389/fevo.2023.1076819

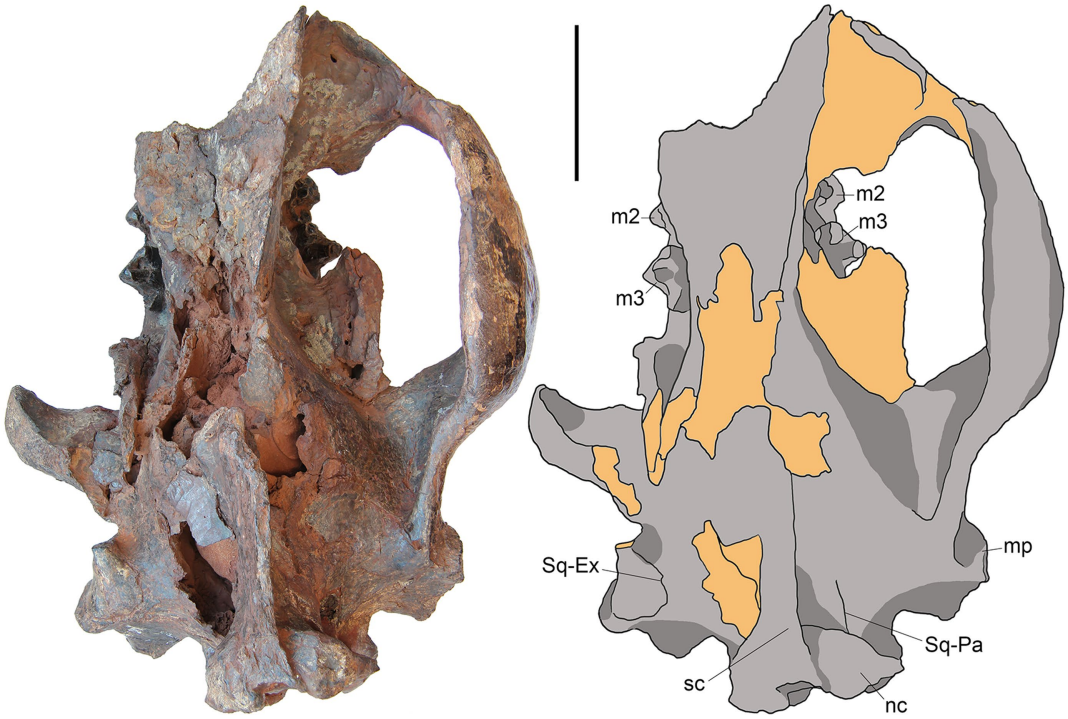

FIGURE 2
M. peregrinus, gen. et sp. nov., SYSU-M-5, holotype, a partial skull with associated mandibles in dorsal view (photograph and explanatory drawing). Youganwo Formation, upper Eocene, Maoming locality, Guangdong Province, China. mp, mastoid process; nc, nuchal crest; sc, sagittal crest; Sq-Ex, squamosal-exoccipital suture; Sq-Pa, squamosal-parietal suture. On this and following figures, the broken area and matrix are designated by the yellow color. Scale bar equals 5cm.

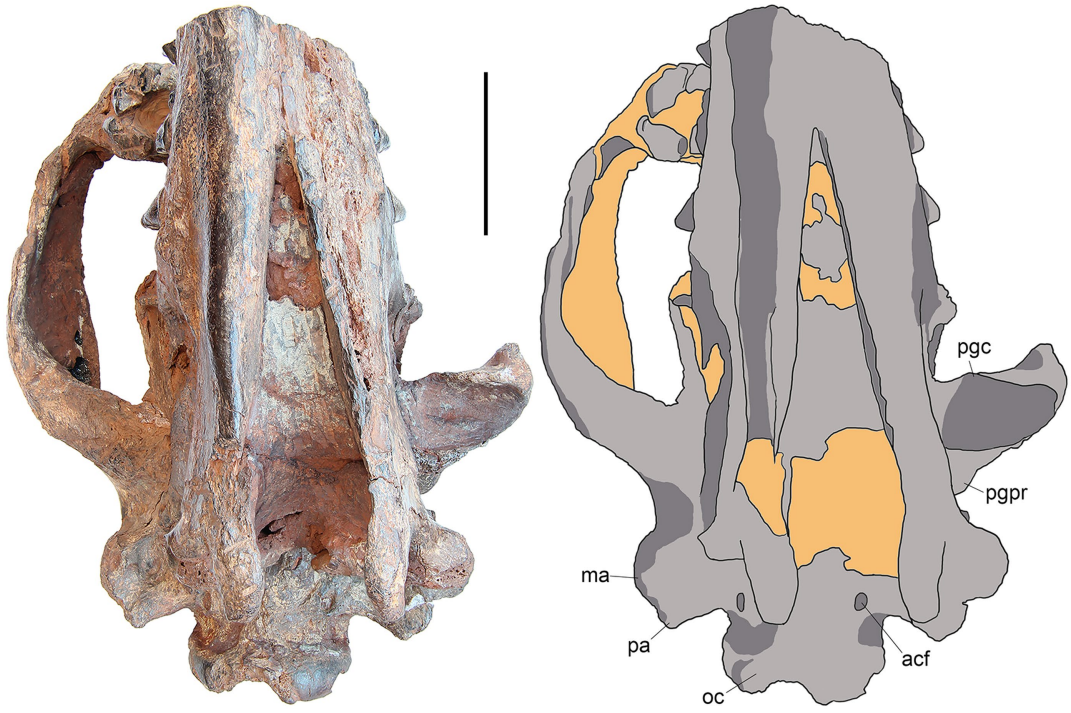

FIGURE 3
M. peregrinus, gen. et sp. nov., SYSU-M-5, holotype, a partial skull with associated mandibles in ventral view (photograph and explanatory drawing). Youganwo Formation, upper Eocene, Maoming locality, Guangdong Province, China. acf, anterior condyloid foramen; ma, mastoid apophysis; oc, occipital condyle; pa, paroccipital apophysis; pgc, preglenoid crest; pgpr, postglenoid process. Scale bar equals 5cm.

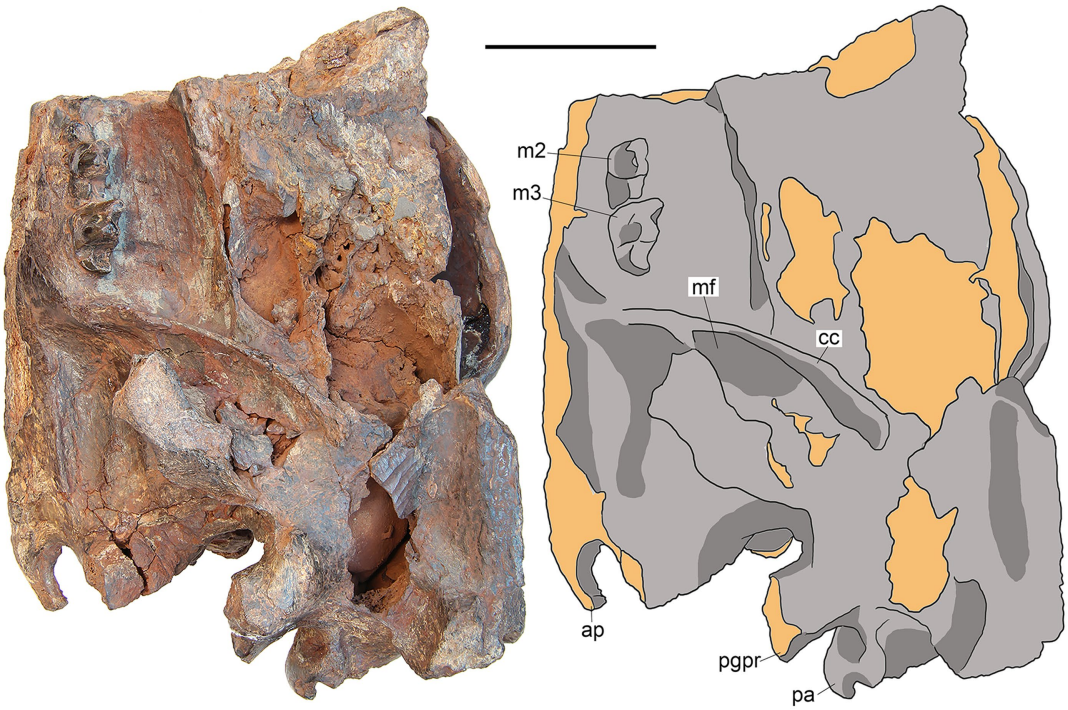

FIGURE 4
M. peregrinus, gen. et sp. nov., SYSU-M-5, holotype, a partial skull with associated mandibles in left lateral view (photograph and explanatory drawing). Youganwo Formation, upper Eocene, Maoming locality, Guangdong Province, China. ap, angular process; cc, coronoid crest; mf, masseteric fossa; pa, paroccipital apophysis; pgpr, postglenoid process. Scale bar equals 5cm.

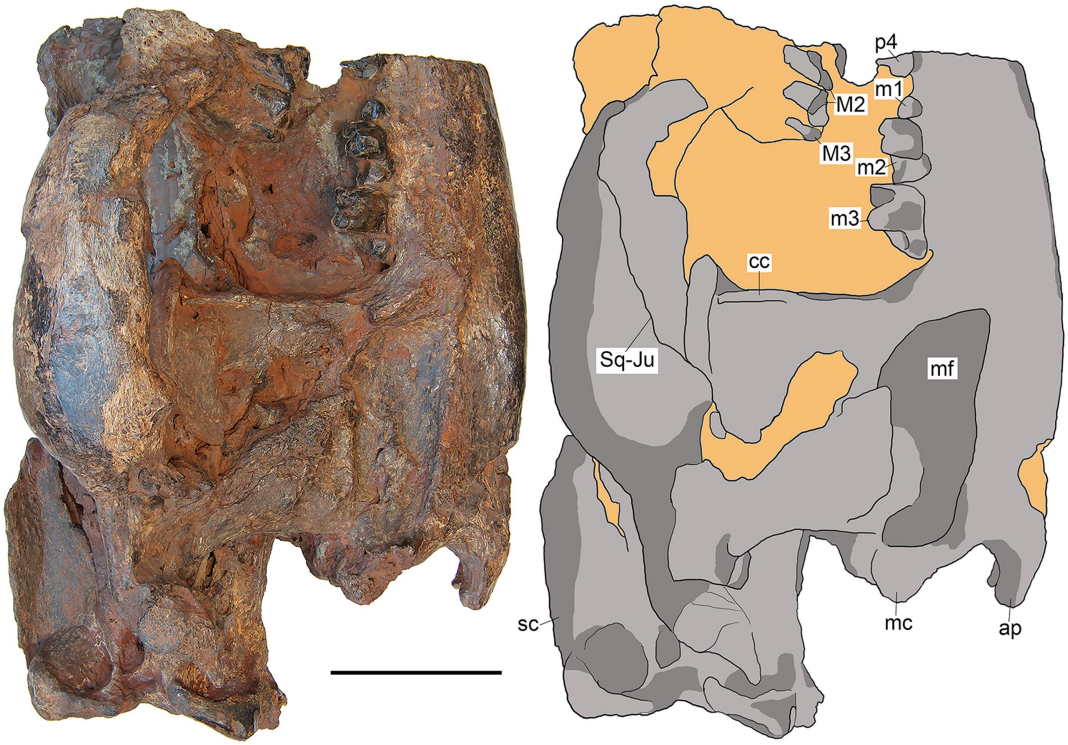

FIGURE 5
M. peregrinus, gen. et sp. nov., SYSU-M-5, holotype, a partial skull with associated mandibles in right lateral view (photograph and explanatory drawing). Youganwo Formation, upper Eocene, Maoming locality, Guangdong Province, China. ap, angular process; cc, coronoid crest; mc, mandibular condyle; mf, masseteric fossa; sc, sagittal crest; Sq-Ju, squamosal-jugal suture. Scale bar equals 5cm.

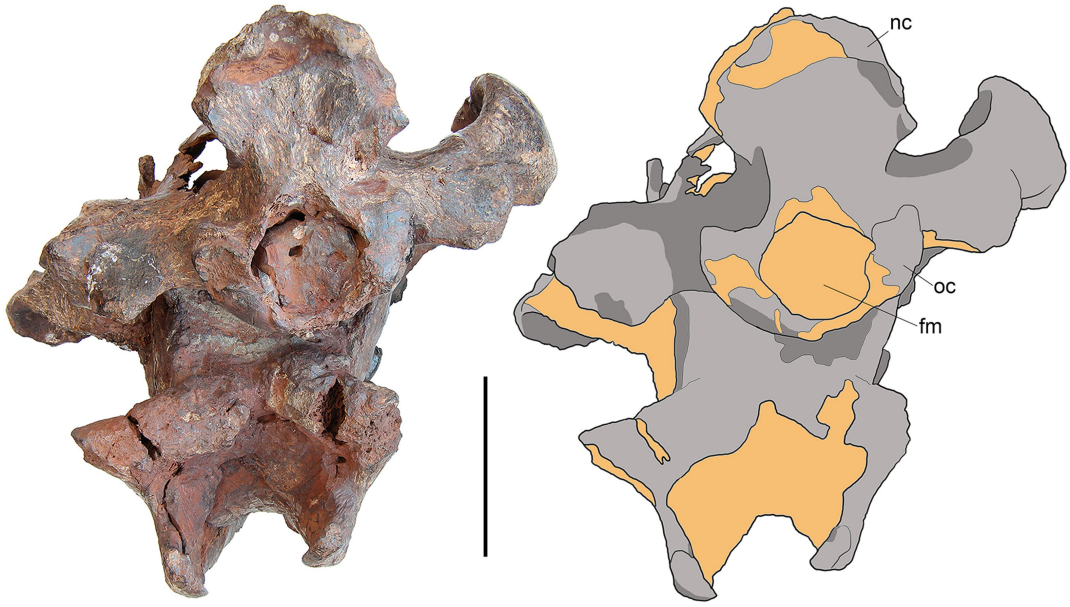

FIGURE 6
M. peregrinus, gen. et sp. nov., SYSU-M-5, holotype, a partial skull with associated mandibles in posterior view (photograph and explanatory drawing). Youganwo Formation, upper Eocene, Maoming locality, Guangdong Province, China. fm, foramen magnum; oc, occipital condyle; nc, nuchal crest. Scale bar equals 5cm.

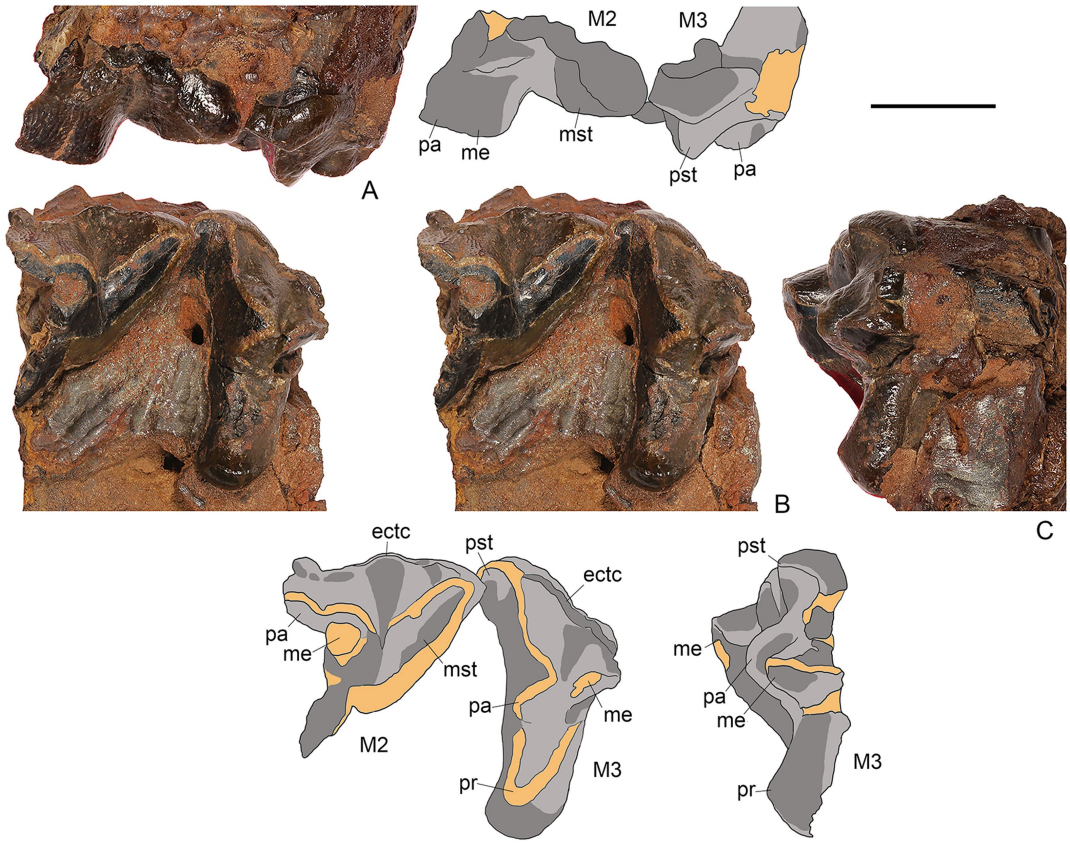

FIGURE 7
M. peregrinus, gen. et sp. nov., SYSU-M-5, holotype, left maxilla with M2-3, in labial **(A)**, occlusal [**(B)** stereopair], and posterior **(C)** views (photographs and explanatory drawings). Youganwo Formation, upper Eocene, Maoming locality, Guangdong Province, China. ectc, ectocingulum; me, metacone; mst, metastyle; pa, paracone; pr, protocone; pst, parastyle. Scale bar equals 1cm.

The squamosal forms the mandibular glenoid with pre- and postglenoid processes (Figures 2, 3). The preglenoid process is in the form of a distinct crest along the anterior border of the mandibular glenoid (Figure 3), as in other Hyainailouridae (Solé et al., 2015). The mediolateral width of the glenoid fossa is more than twice greater than its anteroposterior length. The postglenoid process, better preserved on the left side (Figures 3, 4), deepens ventrally in medial direction. Its distalmost part is missing and the preserved portion shows no curvature in anterior direction. As preserved, the preglenoid process is dorsoventrally higher than the postglenoid process. The lateral margin of the squamosal between the postglenoid and mastoid processes is everted dorsally and medially. Posterior to the zygomatic arch the squamosal is mediolaterally expanded, reaching close to the sagittal crest (Figure 2). The latter condition is characteristic for the Hyainailouridae (Solé et al., 2015). The mastoid process is extensive, with the squamosal-exoccipital suture clearly visible on the dorsal side (Figure 2). The knob-like mastoid apophysis is projecting laterally (Figure 3), a typical character of the Hyainailouridae (Solé et al., 2015). A thin plate-like paroccipital apophysis is posterolaterally directed (Figures 3, 4).

On the occiput, the nuchal crests are short and do not reach the mastoid processes (Figures 2, 6), as typical for the Hyainailouridae (Solé et al., 2015). The nuchal crests converge ventrally and terminate above the occipital condyles. The supraoccipital forming the posterior surface of the nuchal crest is depressed dorsal to the foramen magnum. The large occipital condyles are lateral and ventral to the foramen magnum (Figure 6). This condition is characteristic for the Hyainailouridae (Solé et al., 2015). The ventral margin of the foramen magnum is indented anteriorly.

On the ventral side of the basicranium, the anterior condyloid foramen (=anterior opening of the hypoglossal canal) is placed at the base of the paroccipital apophysis (Figure 3).

Only M2-3 are preserved from the upper dentition; they are better preserved on the left side, where, however, M2 is anteriorly incomplete (Figure 7). On M2, the paracone and metacone are fused into an amphicone. Both cusps are separated by a shallow groove on the labial side. The metacone is ovoid in cross-section, slightly compressed labiolingually. The metastyle is long and blade-like, directed distolabially. It is distinctly longer than the postmetacrista and separated from the latter by the carnassial notch. The ectoflexus of M2 is shallow. The occlusal surface of the paracone and the metacone are heavily worn. The M3 has a long parastylar region and the preparacrista. The metacone is large, only slightly smaller than the paracone. The trigon is transversely long and mesiodistally short. The protocone apex is worn. There are faint lingual and distal cingula. All mesial side of M3 is heavily worn, with a distinct groove in the parastylar region. Both M2 and M3 have a rather strong ectocingulum.

The preserved part of the mandibular body tapers anteriorly, with the minimal height at p4 (Figure 5). The ventral margin of the mandibular body is straight. The coronoid process is an extensive thin plate with the anterior margin nearly perpendicular to the alveolar plane (Figure 5). The posterior margin of the coronoid process is distinctly convex. The mandibular condyle is massive, with the cylindrical and mediolaterally elongate articular surface. It is positioned above the alveolar plane (Figure 4). The angular process is small and hook-like, with the distal end directed posterodorsally (Figures 4, 5). There is no concavity along the ventral margin of the mandibular ramus anterior to the angular process, as in other Hyainailouridae (Solé et al., 2015). The masseteric fossa is deep, delimited anteriorly by a sharp coronoid crest and ventrally by the condyloid crest (Figures 4, 5). The anterior angle of the masseteric fossa is well posterior to m3.

Only posterior part of the right p4 is preserved (Figures 8C,D). This tooth was distinctly larger than m1. The talonid is damaged and it is not clear how large was its hypoconid. Only talonids of m1 are preserved from both sides (Figure 8). However, judging from it and the mesial alveolus size, it is clear that m1 was the smallest lower molar. m3 is the largest lower molar. The paraconid is about twice lower than the protoconid. The metaconid is ridge-like on m2-3. The talonid is simple, single-cusped, but distinctly basined, at least on m3. The talonid of m3 is proportionally shorter mesiodistally compared with m2. At least on m3 there is a distinct vertical keel along the mesiolabial side of the paraconid. There is a distinct labial cingulid on m2-3.

Measurements

For dental measurements, see Table 1.

Comparison

The comparison with *Oriienspterodon dahkoensis* from the late middle Eocene of China and Myanmar (Egi et al., 2007) is limited to the dentary and lower dentition (M2-3 are unknown). Maocyon differs from Oriienspterodon by smaller size, shallower mandibular body, and more reduced metaconid on lower molars.

Kerberos langebadreae from the Bartonian of France is known from a complete skull and postcranial skeleton (Solé et al., 2015). The new taxon differs from *Kerberos* by deeper mandibular body, vertical coronoid process of dentary, more pronounced ectocingulum and larger protocone on upper molars, more separate paracone and metacone on M2, a well developed metacone on M3, and a larger talonid on lower molars.

Maocyon differs from *Pterodon dasyuroides* from the Priabonian of Western Europe (Lange-Badré, 1979) by anteroposteriorly shorter occiput, lack of occipital crest, separate paracone and metacone on M2-3, much larger M3, presence of metaconid on lower molars, and larger talonid on m2-3.

The gigantic *Hemipsalodon grandis* from the late Eocene – early Oligocene of North America (Mellett, 1969) is similar with *Maocyon* by having separate paracone and metacone and pronounced ectocingulum on upper molars, and large M3. It different by its much larger size, deeper mandibular body, reduced talonid and lack of metaconid on lower molars.

Discussion

The "all compat" (majority rule plus compatible groups) consensus tree produced by tip-dating Bayesian analysis (Figure 9; see Supplementary information for the complete tree) is identical

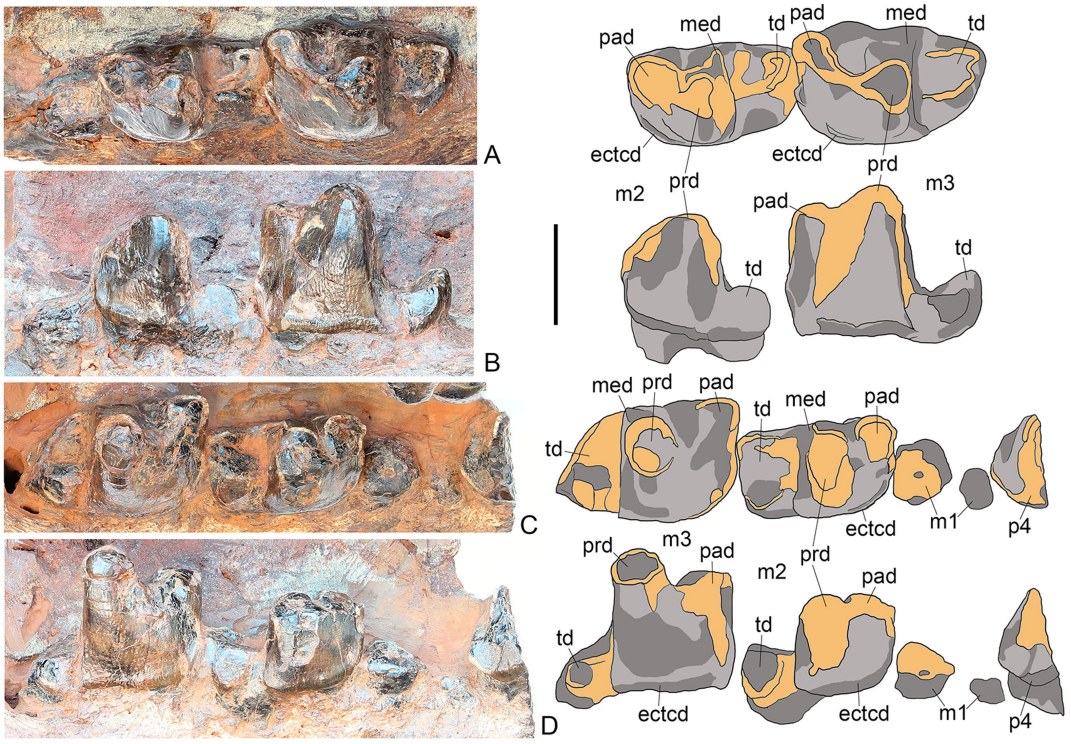

FIGURE 8
M. peregrinus, gen. et sp. nov., SYSU-M-5, holotype, lower dentition (photographs and explanatory drawings). Youganwo Formation, upper Eocene, Maoming locality, Guangdong Province, China. A, B, left m2-3, in occlusal **(A)** and labial **(B)** views. **(C,D)**, right p4, m1-3, in occlusal **(C)** and labial **(D)** views. ectcd, ectocingulid; med, metaconid, pad, paraconid; prd, protoconid; td, talonid. Scale bar equals 1cm.

to the tree obtained by Solé et al. (2021) in the interrelationships of the taxa outside the Hyainailouroidea but differs in number of details within this group. The position of *Furodon crocheti* and *Paratritemnodon indicus* is more resolved; both taxa are referred to the Teratodontinae which has the same branch support (PP = 29%). *Koholia atlasense* and *Tritemnodon agilis* do not form a clade. *Oriensperodon dahkoensis* is not the basalmost member of the Hyainailourinae, but placed in a polytomy with Hyainailourinae and Apterodontinae. *M. peregrinus* is found as a sister taxon to *Oriensperodon dahkoensis*. Compared with the cladogram obtained by Solé et al. (2021), our analysis reveals a better branch support for the Hyainailouroidea (PP = 55 versus 39%), Hyainailouridae (PP = 35 versus 30%), and Hyainailourinae (PP = 51 versus 26%).

The previously known members of the Hyainailouridae are large creodonts with the body mass 46–98 kg (Solé et al., 2015). The estimated body mass of *M. peregrinus* (39 kg) is distinctly smaller. It is less than half that of its older sister taxon *Oriensperodon dahkoensis* (90 kg). According to Carbone et al. (2007), carnivores larger than 20 kg generally hunt prey greater than or equal to their own body mass.

Most taxa of the Hyainailouroidea were distributed in Africa, with few species known from Europe, East Asia, India, and North America (Figure 9). *Oriensperodon* and *Maocyon* are the only East Asian taxa referred to the Hyainailouridae (Figure 9). *Oriensperodon* is currently the oldest known member of that clade (late middle Eocene). The Bayesian "tip-dating" phylogenetic methods estimates the origin of the clade *Oriensperodon* + *Maocyon* as 43.68 Ma. However, estimation of the time of divergence of the Hyainailourinae is slightly older (44.35 Ma). This advocates for the origin of the Hyainailourinae in Africa and dispersal of the ancestors of the *Oriensperodon-Maocyon* clade from Africa, as was previously suggested (Borths and Stevens, 2019).

Oriensperodon dahkoensis is known by fragmentary specimens from three late middle Eocene localities: Rencun Member of the Heti Formation, Henan Province, central China; upper part of the Lumeiyi Formation, Yunnan Province, southern China; and upper part of the Pondaung Formation, Myanmar (Chow, 1975; Egi et al., 2007; Peigné et al., 2007). The age of the Youganwo Formation, producing *M. peregrinus*, is likely basal late Eocene (Averianov et al., 2019). A somewhat more derived nature of *Maocyon* compared with *Oriensperodon*, expressed by more reduced metaconid on lower molars, is consistent with its younger geological age.

The upper Eocene Youganwo Formation at Maoming locality produces abundant remains of predominantly aquatic or semiaquatic vertebrates (Table 2). Among mammals, the remains of groups that preferred mesic habitats, like amynodontid perissodactyls and anthracotheriid artiodactyls, are most common. The carnivorous mammals are extremely rare in this locality, being known previously only from a single specimen of the nimravid *Maofelis cantonensis* (Averianov et al., 2016). The holotype of the

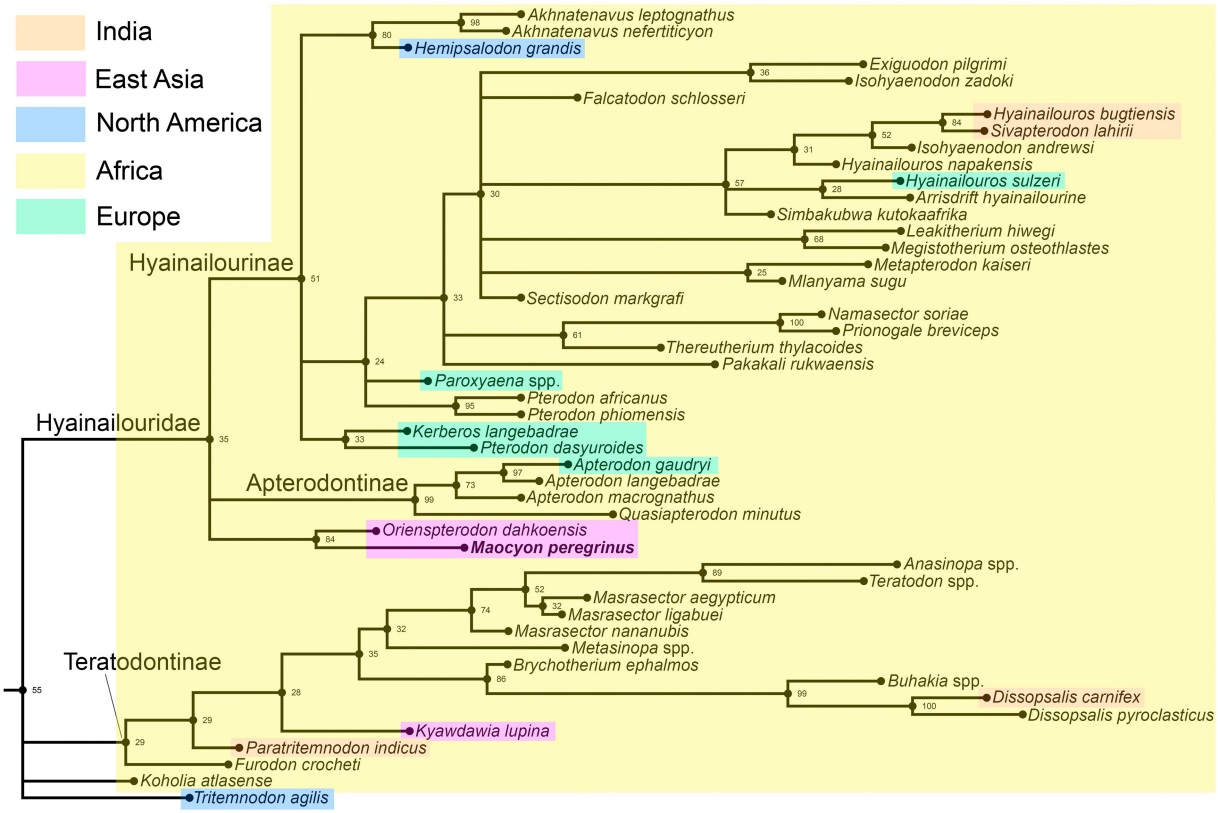

FIGURE 9
Segment of the "all compat" (majority rule plus compatible groups) consensus tree produced by tip-dating Bayesian analysis showing interrelationships within the Hyainailouroidea (see Supplementary material for the complete tree). Posterior probability (PP) shown at the relevant node.

TABLE 2 List of the vertebrates from the upper Eocene Youganwo Formation at Maoming locality, Guangdong Province, China.

Family	Species	References
Cyprinidae	*Eoprocypris maomingensis* (Liu, 1957) [=*Cyprinus maomingensis* Liu, 1957 in Liu, 1957]	Liu (1957) and Chen et al. (2015)
Adocidae	*Adocus inexpectatus* (Danilov et al., 2013)	Danilov et al. (2013)
Carettochelyidae	*Anosteira maomingensis* (Chow and Liu, 1955)	Chow and Liu (1955), Tong et al. (2010) and Danilov et al. (2017)
Geoemydidae	*Isometremys lacuna* (Chow and Yeh, 1962)	Chow and Yeh (1962) and Claude et al. (2012)
Geoemydidae	*Guandongemys pingi* (Claude et al., 2012)	Claude et al. (2012)
Trionychidae	*Trionyx impressus* (Yeh, 1963)	Yeh (1963)
Crocodyloidea	*Maomingosuchus petrolica* (Yeh, 1958) [=*Tomistoma petrolica* Yeh, 1958 in Yeh, 1958; Li, 1975]	Yeh (1958), Li (1975) and Shan et al. (2017)
Alligatoroidea	*Dongnanosuchus hsui* (Shan et al., 2021) [=Alligatoridae indet. in Skutschas et al., 2014]	Skutschas et al. (2014) and Shan et al. (2021)
Nimravidae	*Maofelis cantonensis* (Averianov et al., 2016)	Averianov et al. (2016)
Amynodontidae	*Cadurcodon maomingensis* (Averianov et al., 2017)	Averianov et al. (2017)
Brontotheriidae	*Maobrontops paganus* (Averianov et al., 2018)	Averianov et al. (2018)
Anthracotheriidae	*Anthracokeryx naduongensis* (Ducrocq et al., 2015) [=*Lunania cf. L. youngi* Chow, 1957 in Wang et al., 2007]	Wang et al. (2007) and Averianov et al. (2019)

creodont *M. peregrinus* described in this paper is only the second specimen of carnivorous mammals from this fauna.

Data availability statement

The new taxon described in this paper (*Maocyon peregrinus*) has been registered on ZooBank: https://zoobank.org/, 66BEBEAA-87C6-49C4-92C2-41DA70748FB4.

Author contributions

AA designed the research, performed phylogenetic analysis, wrote the paper, and prepared illustrations and Tables 1, 2. EO cleaned the specimen from matrix. ID prepared photographs, read and approved manuscript. J-HJ conceived and acquired funding, read and approved manuscript. All authors contributed to the article and approved the submitted version.

Funding

This work was supported by the National Natural Science Foundation of China (nos. 41820104002 and 42111530024). The work of AA was supported by the Zoological Institute, Russian Academy of Sciences (project 122031100282-2).

Acknowledgments

We thank Floréal Solé and two reviewers for reading the text and comments.

Conflict of interest

The authors declare that the research was conducted in the absence of any commercial or financial relationships that could be construed as a potential conflict of interest.

Publisher's note

Supplementary material

The Supplementary material for this article can be found online at: https://www.frontiersin.org/articles/10.3389/fevo.2023.1076819/full#supplementary-material

References

Averianov, A. O., Danilov, I. G., Chen, W., and Jin, J. (2018). A new brontothere from the Eocene of South China. *Acta Palaeontol. Pol.* 63, 189–196. doi: 10.4202/app.00431.2017

Averianov, A. O., Danilov, I. G., Jin, J., and Wang, Y. (2017). A new amynodontid from the Eocene of South China and phylogeny of Amynodontidae (Perissodactyla: Rhinocerotoidea). *J. Syst. Palaeont.* 15, 927–945. doi: 10.1080/14772019.2016.1256914

Averianov, A. O., Obraztsova, E. M., Danilov, I. G., and Jin, J. (2019). Anthracotheriid artiodactyl Anthracokeryx and an upper Eocene age for the Youganwo formation of southern China. *Hist. Biol.* 31, 1–8. doi: 10.1080/08912963.2017.1421639

Averianov, A. O., Obraztsova, E. M., Danilov, I. G., Skutschas, P. P., and Jin, J. (2016). First nimravid skull from Asia. *Sci. Rep.* 6:25812. doi: 10.1038/srep25812

Borths, M. R., Holroyd, P. A., and Seiffert, E. R. (2016). Hyainailourine and teratodontine cranial material from the late Eocene of Egypt and the application of parsimony and Bayesian methods to the phylogeny and biogeography of Hyaenodonta (Placentalia, Mammalia). *PeerJ.* 4:e2639. doi: 10.7717/peerj.2639

Borths, M. R., and Seiffert, E. R. (2017). Craniodental and humeral morphology of a new species of Masrasector (Teratodontinae, Hyaenodonta, Placentalia) from the late Eocene of Egypt and locomotor diversity in hyaenodonts. *PLoS One* 12:e0173527. doi: 10.1371/journal.pone.0173527

Borths, M. R., and Stevens, N. J. (2017). The first hyaenodont from the late Oligocene Nsungwe formation of Tanzania: Paleoecological insights into the Paleogene-Neogene carnivore transition. *PLoS One* 12:e0185301. doi: 10.1371/journal.pone.0185301

Borths, M. R., and Stevens, N. J. (2019). *Simbakubwa kutokaafrika*, gen. Et sp. nov. (Hyainailourinae, Hyaenodonta, 'Creodonta,' Mammalia), a gigantic carnivore from the earliest Miocene of Kenya. *J. Vert. Paleont.* 39:e1570222. doi: 10.1080/02724634.2019.1570222

Carbone, C., Teacher, A., and Rowcliffe, J. M. (2007). The costs of carnivory. *PLoS Biol.* 5:e22. doi: 10.1371/journal.pbio.0050022

Chen, G. J., Chang, M.-M., and Liu, H. Z. (2015). Revision of *Cyprinus maomingensis* Liu, 1957 and the first discovery of Procypris-like cyprinid (Teleostei, Pisces) from the late Eocene of South China. *Sci. China Earth Sci.* 58, 1123–1132. doi: 10.1007/s11430-015-5085-7

Chow, M.-C. (1957). On some Eocene and Oligocene mammals from Kwangsi and Yunnan. *Vertebr. PalAsiatica* 1, 201–214.

Chow, M.-C. (1975). Some carnivores from the Eocene of China. *Vertebr. PalAsiatica* 13, 165–168.

Chow, M.-C., and Liu, C.-L. (1955). A new anosterine turtle from Maoming, Kwangtung. *Acta Palaeont. Sin.* 3, 275–282.

Chow, M.-C., and Yeh, H.-K. (1962). A new emydid from Eocene of Maoming, Kwangtung. *Vertebr. PalAsiatica* 6, 225–229.

Claude, J., Zhang, J.-Y., Li, J.-J., Mo, J.-Y., Kuang, X.-W., and Tong, H. (2012). Geoemydid turtles from the late Eocene Maoming Basin, Southern China. *Bull. Soc. Géol. France* 183, 641–651. doi: 10.2113/gssgfbull.183.6.641

Danilov, I. G., Obraztsova, E. M., Chen, W., and Jin, J. (2017). The cranial morphology of *Anosteira maomingensis* (Testudines, pan-Carettochelys) and the evolution of pan-carettochelyid turtles. *J. Vert. Paleont.* 37:e1335735. doi: 10.1080/02724634.2017.1335735

Danilov, I. G., Syromyatnikova, E. V., Skutschas, P. P., Kodrul, T. T., and Jin, J. (2013). The first 'true' *Adocus* (Testudines, Adocidae) from the Paleogene of Asia. *J. Vert. Paleont.* 33, 1071–1080. doi: 10.1080/02724634.2013.768254

Ducrocq, S., Benammi, M., Chavasseau, O., Chaimanee, Y., Suraprasit, K., Pha, D. P., et al. (2015). New anthracotheres (Cetartiodactyla, Mammalia) from the Paleogene of northeastern Vietnam: biochronological implications. *J. Vert. Paleontol.* 35:e929139. doi: 10.1080/02724634.2014.929139

Egi, N., Tsubamoto, T., and Takai, F. (2007). Systematic status of Asian "*Pterodon*" and early evolution of hyaenaelurine hyaenodontid creodonts. *J. Paleontol.* 81, 770–778. doi: 10.1666/pleo0022-3360(2007)081[0770:SSOAPA]2.0.CO;2

Gheerbrant, E. (1995). Les mammifères paléocenes du Bassin d'Ouarzazate (Maroc). III. Adapisoriculidae et autres mammifères (Carnivora, ?Creodonta, Condylarthra, ?Ungulata et incertae sedis). *Palaeontogr. Abt. A* 237, 39–132. doi: 10.1127/pala/237/1995/39

Gill, T. (1872). Arrangement of the families of mammals. With analytical tables. *Smiths. Misc. Coll.* 11, 1–98.

Ginsburg, L. (1980). *Hyainailouros sulzeri*, mammifère créodonte du Miocène d'Europe. *Ann. de Paléont. (Vert.)* 66, 19–73.

Holroyd, P. A. (1999). New Pterodontinae (Creodonta: Hyaenodontidae) from the late Eocene-early Oligocene Jebel Qatrani formation, Fayum Province. *Egypt. PaleoBios.* 19, 1–18.

Lange-Badré, B. (1979). Les Créodontes (Mammalia) d'Europe occidentale de l'Éocéne supérieur à l'Oligocéne supérieur. *Mém. Mus. Nat. D'hist. Nat. Sér. C.* 42, 1–249.

Lewis, M. E., and Morlo, M. (2010). "Creodonta" in *Cenozoic mammals of Africa*. eds. L. Werdelin and W. J. Sanders (Berkeley, Los Angeles, London: University of California Press), 543–560.

Li, J. L. (1975). A new material on *Tomistoma petrolica* of Maoming, Kwantung. *Vertebr. PalAsiatica* 13, 190–191.

Linnaeus, C. (1758). *Systema naturae per regna tria naturae, secundum classes, ordines, genera, species, cum characteribus, differentiis, synonymis, locis Regnum Animale*, vol. *1. Editio decima, reformata* ed (Stockholm: Laurentius Salvius)

Liu, H.-T. (1957). A new fossil cyprinid fish from Maoming, Kwangtung. *Vertebr. PalAsiatica* 1, 151–153.

Mellett, J. S. (1969). A skull of *Hemipsalodon* (Mammalia, Deltatheridia) from the Clarno formation of Oregon. *Am. Mus. Novitates.* 2387, 1–19.

Meng, J., Zhai, R., and Wyss, A. R. (1998). The late Paleocene Bayan Ulan fauna of Inner Mongolia, China. *Bull. Carnegie Mus. Nat. Hist.* 34, 148–185.

Morales, J., and Pickford, M. (2017). New hyaenodonts (ferae, Mammalia) from the early Miocene of Napak (Uganda), koru (Kenya) and Grillental (Namibia). *Foss. Imprint.* 73, 332–359. doi: 10.2478/if-2017-0019

Morlo, M., Miller, E. R., and El-Barkooky, A. N. (2007). Creodonta and Carnivora from Wadi Moghra, Egypt. *J. Vert. Paleont.* 27, 145–159. doi: 10.1671/0272-4634(2007)27[145:CACFWM]2.0.CO;2

Peigné, S., Morlo, M., Chaimanee, Y., Ducrocq, S., Tun, S. T., and Jaeger, J.-J. (2007). New discoveries of hyaenodontids (Creodonta, Mammalia) from the Pondaung formation, middle Eocene, Myanmar – paleobiogeographic implications. *Geodiversitas.* 29, 441–458.

Pilgrim, G. E. (1932). The fossil Carnivora of India. *Palaeont. Indica.* 18, 1–232.

Polly, D. P. (1996). The skeleton of *Gazinocyon vulpeculus* gen. Et comb. nov. and the cladistic relationships of Hyaenodontidae (Eutheria, Mammalia). *J. Vert. Paleont.* 16, 303–319. doi: 10.1080/02724634.1996.10011318

Rana, R. S., Kumar, K., Zack, S. P., Solé, F., Rose, K. D., Missiaen, P., et al. (2015). Craniodental and postcranial morphology of *Indohyaenodon raoi* from the early eocene of India, and its implications for ecology, phylogeny, and biogeography of hyaenodontid mammals. *J. Vert. Paleont.* 35:e965308. doi: 10.1080/02724634.2015.965308

Rasmussen, D. T., and Gutiérrez, M. (2009). A mammalian fauna from the late Oligocene of northwestern Kenya. *Palaeontogr. Abt. A* 288, 1–52. doi: 10.1127/pala/288/2009/1

Ronquist, F., Teslenko, M., Van Der Mark, P., Ayres, D. L., Darling, A., Höhn, A. S., et al. (2012). MrBayes 3.2: efficient Bayesian phylogenetic inference and model choice across a large model space. *Syst. Biol.* 61, 539–542. doi: 10.1093/sysbio/sys029

Savage, R. J. G. (1965). Fossil mammals of Africa: 19. The Miocene Carnivora of East Africa. *Bull. Br. Mus. (Nat. Hist.) Geol.* 10, 242–316.

Savage, R. J. G. (1973). *Megistotherium*, gigantic hyaenodont from Miocene of Gebel Zelten, Libya. *Bull. Br. Mus. (Nat. Hist.) Geol.* 22, 484–511.

Shan, H.-Y., Wu, X.-C., Cheng, Y.-N., and Sato, T. (2017). Maomingosuchus petrolica, a restudy of 'Tomistoma' *petrolica* Yeh, 1958. *Palaeoworld* 26, 672–690. doi: 10.1016/j.palwor.2017.03.006

Shan, H.-Y., Wu, X.-C., Sato, T., Cheng, Y.-N., and Rufolo, S. (2021). A new alligatoroid (Eusuchia, Crocodylia) from the Eocene of China and its implications for the relationships of Orientalosuchina. *J. Paleontol.* 95, 1321–1339. doi: 10.1017/jpa.2021.69

Skutschas, P. P., Danilov, I. G., Kodrul, T. T., and Jin, J. (2014). The first discovery of an alligatorid (Crocodylia, Alligatoroidea, Alligatoridae) in the Eocene of China. *J. Vert. Paleont.* 32, 471–476. doi: 10.1080/02724634.2013.809725

Solé, F., Amson, E., Borths, M. R., Vidalenc, D., Morlo, M., and Bastl, K. (2015). A new large hyainailourine from the Bartonian of Europe and its bearings on the evolution and ecology of massive hyaenodonts (Mammalia). *PLoS One* 10:e0135698. doi: 10.1371/journal.pone.0135698

Solé, F., Gheerbrant, E., Amaghzaz, M., and Bouya, B. (2009). Further evidence of the African antiquity of hyaenodontid ("Creodonta", Mammalia) evolution. *Zool. J. Linnean Soc.* 156, 827–846. doi: 10.1111/j.1096-3642.2008.00501.x

Solé, F., Lhuillier, J., Adacid, M., Bensalahd, M., Mahboubi, M., and Tabuce, R. (2014). The hyaenodontids from the Gour Lazib area (?Early Eocene, Algeria): implications concerning the systematics and the origin of the Hyainailourinae. *J. Syst. Palaeont.* 12, 303–322. doi: 10.1080/14772019.2013.795196

Solé, F., Morlo, M., Schaal, T., and Lehmann, T. (2021). New hyaenodonts (Mammalia) from the late Ypresian locality of Prémontré (France) support a radiation of the hyaenodonts in Europe already at the end of the early Eocene. *Geobios* 66-67, 119–141. doi: 10.1016/j.geobios.2021.02.004

Tong, H., Zhang, J.-Y., and Li, J.-J. (2010). *Anosteira maomingensis* (Testudines: Carettochelyidae) from the late Eocene of Maoming, Guangdong, southern China: new material and re-description. *Neues Jahrb. Geol. Palaontol. Abh.* 256, 279–290. doi: 10.1127/0077-7749/2010/0053

Van Valen, L. M. (1967). New Paleocene insectivores and insectivore classification. *Bull. Am. Mus. Nat. Hist.* 135, 217–284.

von Stromer, E. (1926). *Reste Land-und Süsswasser-Bewohnender Wirbeltiere aus den Diamantfeldern Die Diamantenwuste Südwest-Afrikas. Vol. 2* (Berlin: E. Kaiser), 107–153.

Wang, Y.-Y., Zhang, Z.-H., and Jin, J. (2007). Discovery of Eocene fossil mammal from Maoming Basin, Guangdong. *Acta Sci. Nat. Univ. Sunyatseni.* 46, 131–133.

Yeh, H.-K. (1958). A new crocodile from Maoming, Kwangtung. *Vertebr. PalAsiatica* 2, 237–242.

Yeh, H.-K. (1963). Fossil turtles of China. *Palaeont. Sin. N. Serv. C.* 18, 1–112.

frontiers | Frontiers in Earth Science

TYPE Original Research
PUBLISHED 02 March 2023
DOI 10.3389/feart.2023.1137891

OPEN ACCESS

EDITED BY
Lucja A. Fostowicz-Frelik,
Institute of Paleobiology, Polish Academy of Sciences, Poland

REVIEWED BY
Mieczyslaw Wolsan,
Museum and Institute of Zoology, Polish Academy of Sciences, Poland
Xiaoming Wang,
Natural History Museum of Los Angeles County, United States

*CORRESPONDENCE
Bin Bai,
baibin@ivpp.ac.cn
Yuan-Qing Wang,
wangyuanqing@ivpp.ac.cn

SPECIALTY SECTION
This article was submitted to Paleontology, a section of the journal Frontiers in Earth Science

RECEIVED 05 January 2023
ACCEPTED 10 February 2023
PUBLISHED 02 March 2023

CITATION
Zhang X-Y, Bai B and Wang Y-Q (2023), Bear or bear-dog? An enigmatic arctoid carnivoran from the late Eocene of Asia. *Front. Earth Sci.* 11:1137891. doi: 10.3389/feart.2023.1137891

Bear or bear-dog? An enigmatic arctoid carnivoran from the late Eocene of Asia

Xin-Yue Zhang[1,2], Bin Bai[1]* and Yuan-Qing Wang[1,2]*

[1]Key Laboratory of Vertebrate Evolution and Human Origins of Chinese Academy of Sciences, Institute of Vertebrate Paleontology and Paleoanthropology, Chinese Academy of Sciences, Beijing, China, [2]College of Earth and Planetary Sciences, University of Chinese Academy of Sciences, Beijing, China

Records of Paleogene arctoids are scarce in Asia, but there are abundant records in Europe and North America. In this study, we report a new arctoid taxon, *Lonchocyon qiui* gen. et sp. nov., from the late Eocene Baron Sog Formation of the Erlian Basin, Inner Mongolia, China. This is the first report of a relatively complete, large arctoid taxon from the Erlian Basin. The new taxon is characterized by its overall large size; a deep mandible with a marginal process and a rudimentary premasseteric fossa; and much-reduced premolars, including p4, sectorial carnassial m1 with basined talonid, and unreduced m2-3. *Lonchocyon* exhibits a combination of morphologies present in both amphicyonids and the early ursid hemicyonines. The mandibular force profiles suggest that *Lonchocyon* could have delivered powerful canine bites while subduing prey, like large felids do today, and it may have occupied a specialized ecological niche as a predator consuming both soft flesh and hard objects.

KEYWORDS

Erlian Basin, late Eocene, Amphicyonidae, Hemicyoninae, arctoid, mandibular force profile

1 Introduction

Amphicyonidae is a diverse extinct family of Carnivora, with their oldest fossil records in the middle Eocene and their youngest in the late Miocene. Amphicyonidae have been considered as close relatives of Ursidae (Hunt, 1998a; Wang et al., 2005; Rose, 2006). Fossil records of amphicyonids are relatively scarce in Asia compared to the abundant materials from Europe and North America, and most known Asian amphicyonids are from the Miocene, taking *Gobicyon* (Jiangzuo et al., 2019), *Amphicyon*, and *Cynelos* (Jiangzuo et al., 2018) for instance. The only two unequivocal Paleogene amphicyonids are *Guangxicyon* from the middle Eocene Nadu Formation and Amphicyonidae gen. et sp. indet. from the late Eocene Ergilin Dzo Formation (Zhai et al., 2003; Egi et al., 2009). The early ursid group Hemicyoninae is known to have existed from the early Oligocene to the Miocene of Eurasia and is considered as an ancestor of the ursid group Ursinae (Hunt, 1998b; Rose, 2006; Bonis, 2013). Only a few Paleogene ursids have been reported in Asia, including *Cephalogale* sp. from the early Oligocene of Saint Jacques and ?*Cephalogale* sp. from the early Oligocene Hsanda Gol Formation (Wang and Qiu, 2003; Wang et al., 2005).

The Erlian Basin in Inner Mongolia has nearly continuous fossiliferous sedimentary deposits from the late Paleocene to the Oligocene and has been explored extensively and investigated since the third Central Asiatic Expedition (CAE) of the American Museum of

Natural History in the early 20th century (Wang et al., 2012; Bai et al., 2018). Based on the nearly continuous Paleogene deposits and their abundance of mammalian fossils, the Eocene mammalian faunas of the Erlian Basin form the basis of the Eocene Asian Land Mammal Ages (ALMA) (Wang et al., 2007; Wang et al., 2019). A number of carnivorous or scavenging mesonychids and creodonts have been reported from the Erlian Basin (Matthew and Granger, 1925a; Matthew and Granger, 1925b; Szalay and Gould, 1966). However, reports of Carnivora from the Erlian Basin are rarer. Apart from a left m1 of *Miacis invictus* from the Irdin Manha Formation (Matthew and Granger, 1925a) and a left p4 of Miacidae indet. from the Ulan Shireh Formation (Ye, 1983), there are only a few mentions of carnivorans in the fossil faunal lists without further description, such as Carnivora gen. et sp. indet. from the Arshanto Formation (Russell and Zhai, 1987) and cf. "*Cynodictis*" from the Ulan Shireh Formation (Manning, pers. comm. 1977 cited in an article by Russell and Zhai (1987)). In this study, we report a new genus and species of arctoids from the late Eocene Baron Sog Formation of the Erlian Basin (Figure 1). This new material is not only the first arctoid collected from the Erlian Basin but is also one of the earliest arctoid records from Eurasia.

2 Materials and methods

This fossil specimen (IVPP V 28616, Institute of Vertebrate Paleontology and Paleoanthropology, Chinese Academy of Sciences, Beijing) is composed of a left mandible with the canine, p4, m1, root of p3, and alveoli of i1-3, p1-2, and m2-3 (Figures 2, 3). The specimen was collected at the base of the Baron Sog Formation at Haerhada, Baiyin Obo Sumu in the Erlian Basin, Inner Mongolia, China (Wang et al., 2012; Bai et al., 2018) (Figure 1A). The formation was named after the Baron Sog Lamasery and can be easily traced along the northern escarpment of the Baron Sog Mesa (Berkey et al., 1929; Wang et al., 2012). The sediments of the late Eocene Baron Sog Formation are dominated by grayish-white sandstone (Figures 1B, C), bearing *Embolotherium andrewsi* and *Zaisanamynodon brosovi* from the Baron Sog Mesa, where the Baron Sog Formation was named (Wang, 2003; Wang et al., 2012; Bai et al., 2018). The Ulan Gochu Formation, underlying the Baron Sog Formation, is dominated by red silty clay and once yielded *Amynodontopsis parvidens* and *Embolotherium grangeri* at the Baron Sog Mesa (Wang et al., 2012; Bai et al., 2018). *Ardynomys olsoni* was also reported from the Ulan Gochu Formation, 4 miles north of the Baron Sog Lamasery (Wang and Meng, 2009). The Shara Murun Formation, which is overlain by the Ulan Gochu Formation and dominated by gray sandstone and sandy clays with varied colors, produced *Sharamynodon mongoliensis*, *Rhinotitan* sp., *Pachytitan ajax*, and *Titanodectes minor* at the Baron Sog Mesa (Bai et al., 2018). The top of the section is capped by Quaternary sediments that commonly form a weathering layer and cover the upper (most) part of the underlying Baron Sog Formation at the slope in some places (Figure 1B). Some new materials of perissodactyls and artiodactyls have been unearthed from the Baron Sog Formation at Haerhada in our recent fieldwork and are under preparation or study.

We adopt the widely accepted phylogenetic hypothesis that Amphicyonidae consists of five subfamilies, Haplocyoninae, Temnocyoninae, Daphoeninae, Thaumastocyoninae, and Amphicyoninae (Hunt, 1998a; Morales et al., 2019), and belongs to Arctoidea (e.g., Jiangzuo et al., 2018; Morales et al., 2021a), which also comprises Ursidae, Pinnipedia, and Musteloidea; Cephalogalini

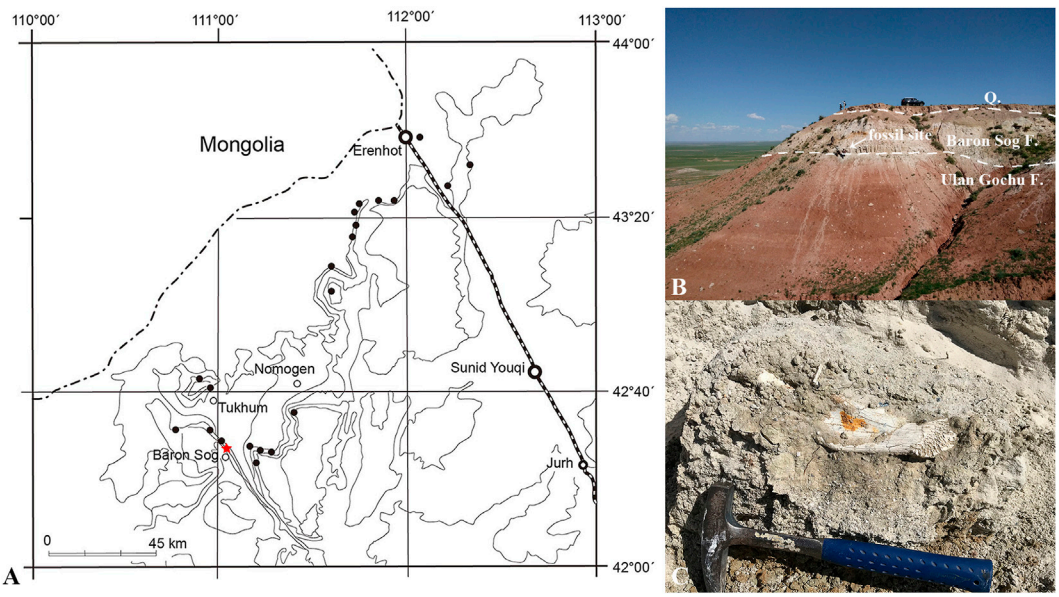

FIGURE 1
Locality bearing *Lonchocyon qiui* gen. et sp. nov. (IVPP V 28616) from the late Eocene of the Baron Sog Formation, Erlian Basin, Inner Mongolia, China. **(A)** Topographic map showing the fossil localities in the Erlian Basin with Haerhada marked by a red star, modified from Wang et al. (2012). **(B)** Outcrop of the fossil site showing the Baron Sog Formation and underlying Ulan Gochu Formation; **(C)** the lower jaw of IVPP V 28616 *in situ*.

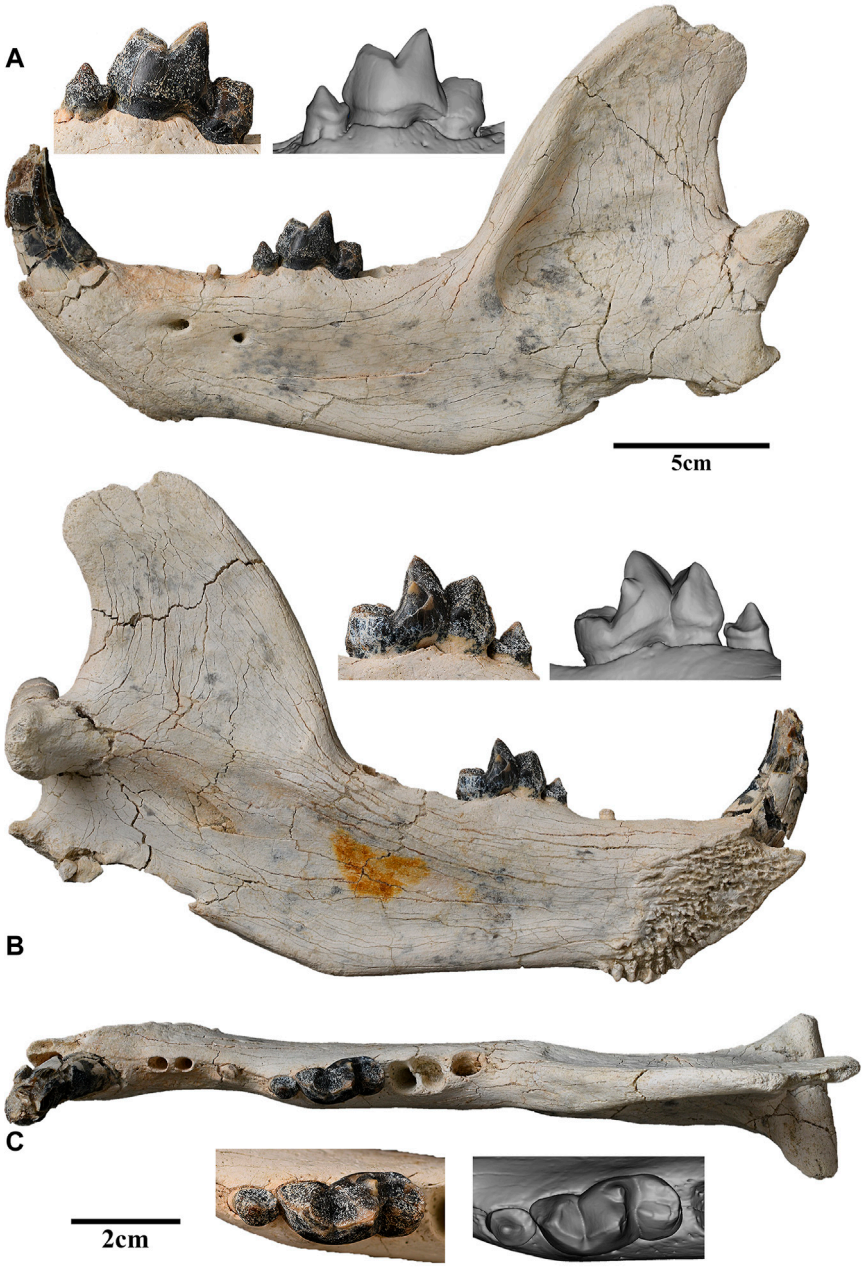

FIGURE 2
Left lower jaw of *Lonchocyon qiui* gen. et sp. nov. with c, p4, and m1 (IVPP V 28616): **(A)** lateral view; **(B)** lingual view; and **(C)** occlusal view. Scale bar equals 5 cm for the lower jaw and 2 cm for the teeth.

and Phoberocyonini belong to Hemicyoninae, and the latter is a subfamily of Ursidae (Bonis, 2013).

The methods of dental and mandibular measurements follow Peigné and Heizmann (2003), Yang et al. (2005), and Xia et al. (2005) (Tables 1, 2). The specimen was CT scanned using the GE phoenix v|tome|x m 300/180 KV housed at the Key Laboratory of Vertebrate Evolution and Human Origins of the Institute of Vertebrate Paleontology and Paleoanthropology, Chinese Academy of Sciences, with a beam energy of 150 kV and flux of 130 μA. The CT data are available in the MorphoSource: https://www.morphosource.org/concern/media/000495496. This published work and the nomenclatural acts it contains have been registered in ZooBank: https://zoobank.org/References/878ad9f1-66de-41be-9384-db339a130560.

We use the beam theory to study the mandibular force profiles of the new specimen. This method is improved and explained in detail by Therrien (2005) in order to estimate the dorsoventral and labiolingual buttress of the mandibles in carnivorans and to reconstruct their feeding behaviors. The data from the new holotype specimens, *Ysengrinia tolosana* (IVPP FV 0086) and

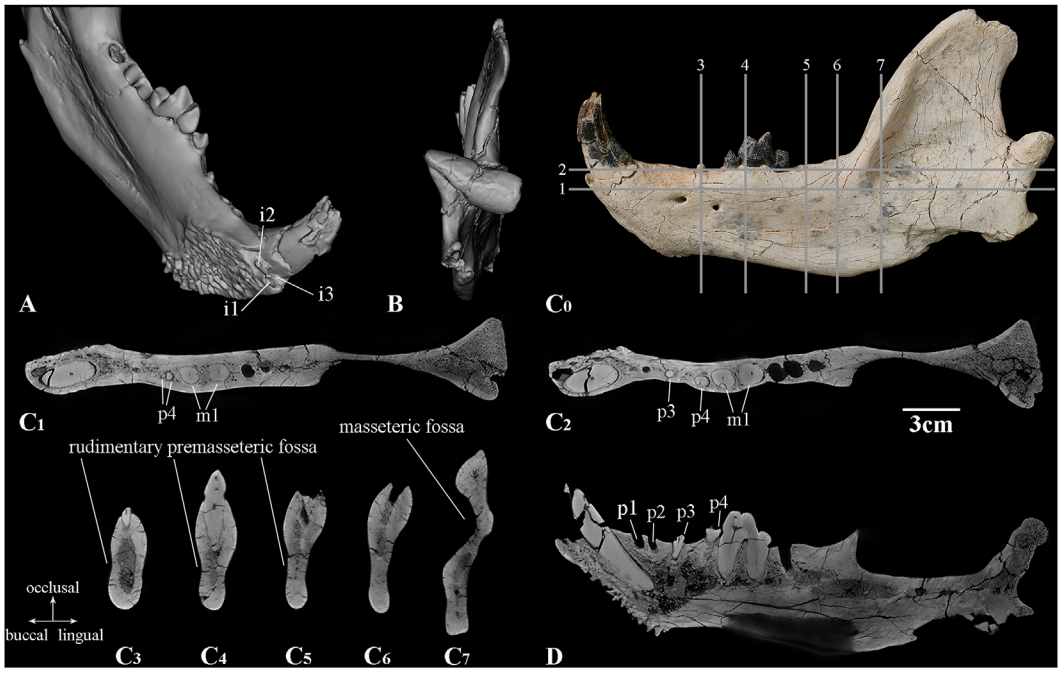

FIGURE 3
CT images of the left lower jaw of *Lonchocyon qiui* gen. et sp. nov. (IVPP V 28616): **(A)** dorsolingual view showing the incisors alveoli; **(B)** posterior view; **(C_0)** lateral view of the lower jaw with the lines showing the positions of horizontal sections in **(C_1, C_2)**; cross sections in **(C_3–C_7)**; and **(D)** sagittal section of the lower jaw. Scale bar equals 3 cm for the CT sections.

TABLE 1 Measurements of the lower teeth of *L. qiui* gen. et sp. nov. (IVPP V 28616) (mm). Abbreviations: L, length; W, width; H, height; TLi, trigonid lingual length; TW, talonid width; *, measured from alveoli or root.

Measurement	Lc	Wc	Hc	*Lp1	*Wp1	*Lp2	*Wp2	*Lp3
Value (mm)	24.86	13.75	24.43	5.89	4.73	5.14	4.53	5.57
Measurement	*Wp3	Lp4	Wp4	Hp4	Lm1	Wm1	Hm1	TLim1
Value (mm)	4.62	8.45	7.03	8.27	27.28	12.86	17.16	19.41
Measurement	TWm1	*Lm2	*Wm2	*Lm3	*Wm3	Lp1-p4	Lm1-m3	Lp1-m3
Value (mm)	11.82	17.27	10.16	8.48	6.49	49.29	56.36	101.23

TABLE 2 Measurements of the mandible of *L. qiui* gen. et sp. nov. (IVPP V 28616) (mm). Abbreviations: HVR, height of the vertical ramus (from the apex of the coronoid to the most ventral point of the angular process); MHVR, middle height of the vertical ramus (from the deepest point of the mandibular notch to the most ventral point of the angular process); LM, length of the mandible; MAT, moment arm of the temporalis muscle; Cm3, distance between the condyle and the posterior margin of m3; DMm3, depth of the mandible on the posterior margin of m3; WMm3, width of the mandible on the posterior margin of m3.

Measurement	HVR	MHVR	LM	MAT	Cm3	DMm3	WMm3
Value (mm)	127.39	57.52	247.46	87.55	104.26	66.04	20.09

Ursus arctos (IVPP OV 2103), are from first-hand measurements, and other comparative data are derived from Therrien (2005) (*Panthera leo*, *Crocuta crocuta*, and *Canis lupus*), Hunt (2011) (*Temnocyon macrogenys*, *Delotrochanter oryktes*, and *Borocyon robustum*), and Morales et al. (2021a) (*Ammitocyon kainos* and *Magericyon anceps*).

3 Systematic paleontology

Order—Carnivora Bowdich, 1821
Infraorder—Arctoidea Flower, 1869
Lonchocyon gen. nov.
Type species—*Lonchocyon qiui* gen. et sp. nov.

Included species—Only the type species.

Etymology— "*Lonch*" is the Greek term for "spear", indicating its spear-like paraconid of the lower carnassial; "*cyon*" is the Greek word for dog.

Diagnosis—As for the type and only species.

Lonchocyon qiui gen. et sp. nov.

Holotype—IVPP V 28616, a nearly complete left mandible with the canine, p4, m1, root of p3, and alveoli of i1-3, p1-2, and m2-3.

Etymology—Named in honor of Professor Zhan-Xiang Qiu for his great contributions to our knowledge of carnivoran evolution and systematics.

Type locality and horizon—Haerhada, Baiyin Obo Sumu, Siziwang Qi (Banner), Inner Mongolia, China; Baron Sog Formation; the late Eocene.

Diagnosis—Differs from amphicyonids and early ursids by the combination of a large size with a deep mandible, extremely reduced premolars including p4, sectorial lower carnassial (m1) with a spear-like paraconid, a cristid extending from the apex the paraconid to the carnassial notch, a basined talonid, and unreduced molars posterior to the carnassial.

3.1 Description

The left mandible is overall well-preserved with only slight breakage near the incisor region, the dorsal border of the coronoid process, and the angular process. The mandibular symphysis is rough with interdigitating rugosities, which are anteroposteriorly aligned in the dorsal half and more radial on the more rugose posteroventral part. The posterodorsal corner of the symphysis is relatively smooth compared to the remaining dorsal part. The greatest anteroposterior length of the symphysis is ~63 mm, and the greatest dorsoventral height is ~46 mm. The long axis of the symphysis forms an angle of ~45° with the alveolar border, measuring ~72 mm of its length. The posterior margin of the symphysis is at the anteroposterior level of p3.

The horizontal ramus is very deep dorsoventrally, gradually becoming deeper from p1 to m3, then its ventral border rises into a small, distinct, and medially projecting marginal process, which is for the insertion of the digastric muscle. There are two mandibular foramina: the larger anterior foramen is ventral to the diastema between p2 and p3 and positioned at the dorsoventral level near the dorsal one-third of the mandibular height, and the smaller posterior foramen is ventral to the anterior border of p4 and slightly ventral to the anterior foramen. There is a rudimentary shallow premasseteric fossa anterior to the marginal process and likely extending ventral to m1 (Figure 3C). The masseteric fossa is deep and extensive for the insertion of the middle and deep layers of the masseter muscle, and its anterior part does not reach the level of m3.

The coronoid crest is inclined posteriorly and broadens in its distal half. The mandibular notch is wide and shallow, gently curved from the coronoid process to the condyloid process. The coronoid process is high and broad, overhanging the anterior border of the condyloid process. The condyloid process, positioned level with the apex of the m1 protoconid, is very robust and composed of two parts with the long axis inclined slightly medially (Figure 3B). The lateral half of the condyloid process is roughly conical, bluntly pointed laterally, and buttressed ventrally with the articular facet facing more dorsally than posteriorly. However, its medial half is semi-cylindrical with a truncated medial border that is buttressed anteriorly and with the articular facet facing posteriorly and extended to the ventral side. The articular facets of the condyloid process are convex dorsoventrally and divided by a distinct synovial fossa on the dorsal side. Although the angular process is incomplete, it is projected posteriorly and separated from the marginal process by a wide, shallow indentation. A rough, narrow triangular depression is present along the lateral side of the indentation. The margin of the mandibular foramen is partially cracked, and it is positioned slightly ventral to the condyloid process.

The incisors are not present, but three alveoli are preserved. These incisor alveoli indicate that i1-i2 are much smaller than i3, and the i1 alveolus is compressed strongly lateromedially (Figure 3A). The root of i2 is slightly smaller than that of i1, and it also is situated posteriorly and slightly labially. Therefore, i2 and i1 are aligned nearly longitudinally rather than transversely. The root of i3 is placed mostly labial to that of i1, is roughly triangular in outline, and is prominently larger than i1 and i2. The canine is large, robust, laterally compressed, and nearly erect with an oval outline in cross section, as in many arctoids. The apex of the canine is broken but was likely recurved distally.

The postcanine diastema between the canine and the most anterior alveolus is 9.73 mm in length. Posterior to the postcanine diastema, two closely placed with a 2.28 mm diastema and anteriorly inclined alveoli are interpreted as deriving from a single-rooted p1 and p2 rather than a double-rooted p2 with p1 absent (Figure 3D). Judging from the coalesced double-rooted p4 and the single-rooted p3, it is unlikely that the two alveoli belong to a double-rooted p2 with p1 absent and would contrast with the common characteristics of most carnivorans that premolars are enlarged posteriorly.

p3 has only one broken root preserved, which is separated from p2 and p4 by two diastemas with 8.29 mm and 9.84 mm length, respectively. p4 is complete and much reduced with two nearly coalesced roots (Figures 3C$_1$, C$_2$). The main cuspid of p4 is pointed and sharp with a flat lingual surface and a convex buccal surface. Both the anterior and posterior crests of p4 are straight and distinct, and the former is anterolingually extended, while the latter is posteriorly directed. A cingulid-like basin is present along the lingual and posterior sides of the crown with a swollen shelf on the posterior side. There is no accessory cuspid or cingulid cuspid on p4.

m1 is very large with a high trigonid. The paraconid is spear-like and composed of three facets, which are bordered by three ridges descending from the apex of the paraconid: an anterior cristid is slanted posteriorly and extends slightly lingually down to the base of the crown; a shorter lingual cristid descends to the notch between the paraconid and protoconid on the lingual side; and third, the posterior cristid forms the anterior half of the carnassial blade. The paraconid is composed of a buccal convex face and anterolingual and posterolingual flat facets. The protoconid is the highest cuspid of m1 but is smaller than the paraconid in a buccal view. The preprotocristid extends anterobuccally and forms the posterior half of the carnassial blade. A slightly worn facet is present along the buccal edge of the blade. The notch between the two cristids of the carnassial blade forms a near-right angle in the buccal view. Another blunt, indistinct ridge descends anterolingually from the

protoconid to the notch between the paraconid and protoconid on the lingual side, forming a deep V-shaped notch with the lingual cristid of the paraconid. Therefore, a flat anterior face is present between the two cristids of the protoconid. The paraconid and the protoconid are separated by a distinct groove on the occlusal and lingual sides. The enamel of the lingual surface of the metaconid is partially broken. The much smaller metaconid is about half the height of the protoconid (but nearly as high as the paraconid), positioned posterolingually to the protoconid, and does not surpass the protoconid posteriorly in buccal view. The posterior surface of the trigonid is nearly vertical or slightly anteriorly slanted. The talonid is short, but not very low, and slightly narrower than the trigonid. The buccal surface of the talonid is lingually inclined, while the lingual surface of the talonid is vertical. The hypoconid crest is slightly anterolingually extended and lies in the middle of the talonid. The entoconid crest is slightly lower than the hypoconid crest, and the two crests join on the posterior side. Therefore, the talonid forms a loop on the occlusal surface. The boundary between the trigonid and talonid is demarcated by a distinct groove, which is continuous on the occlusal and buccal surfaces. There is no cingulid on m1.

The alveolus of m2 is relatively large and composed of two equal-sized portions, indicating m2 is double-rooted and not reduced. The alveolus of m2 is oriented slightly obliquely rather than perpendicularly to the long axis of the crown. The alveolus of m3 is much smaller than that of m2 and oval in outline, indicating m3 is single rooted. Furthermore, the size of the molars becomes smaller posteriorly from m1 to m3. The long axis of the molar series is slightly anterobuccally extended, whereas that of the premolar series is slightly anterolingually directed. Therefore, the angle between the two axes is about 160°.

3.2 Comparison and discussion

The most conspicuous characteristics of the late Eocene *Lonchocyon* are the spaced, highly reduced premolars with single-rooted p1-3, and the two fused roots of p4. Among the five subfamilies of Amphicyonidae (i.e., Haplocyoninae, Temnocyoninae, Daphoeninae, Thaumastocyoninae, and Amphicyoninae), Haplocyoninae and Temnocyoninae share a synapomorphy of developed premolars as sister groups (Hunt, 2011), and the North American endemic Daphoeninae has unreduced premolars. By contrast, both Thaumastocyoninae and Amphicyoninae tend to reduce the premolars, but the earliest members of these two subfamilies from the Paleogene still retain the primitive unreduced premolars, unlike the new specimen. For instance, the earliest thaumastocyonine *Ysengrinia tolosana* from MP 30 and the amphicyonine *Cynodictis* from the late Eocene have a well-developed p4 with a posterior accessory cuspid and a p3 with two roots, while *Cynodictis* has a much smaller size than *Y. tolosana* and the new specimen (Kuss, 1965; Bonis, 1978; Heizmann and Kordikova, 2000; Solé et al., 2021). The amphicyonine *Pseudocynopsis* and *Cynelos* from Quercy, France, have reduced, spaced premolars, but p2-4 retains two separate roots (Ginsburg, 1965; 1966; Kuss, 1965). The presence of a single root of p3 has been reported in the Late Miocene amphicyonine *Magericyon*. However, the latter lacks dp1/p1-p2 and has a double-rooted p4 (Peigné et al., 2008). Ursidae also exhibits a trend toward reduced premolars. However, only Pliocene and extant *Ursus* could have a single root in p1-3, which is even sometimes absent. Hemicyoninae and early members of Ursinae *Ballusia* and *Ursavus* have reduced, simple premolars, but p2-3 is double-rooted and p4 is relatively large (Qiu et al., 1985; Ginsburg and Morales, 1998; Qiu et al., 2014).

The p4 of *Lonchocyon* is characterized by its rather small size with two fused roots and a small posterior shelf, as well as the lack of a posterior accessory cuspid. The length ratio of p4 to m1 is 0.31 in *Lonchocyon* (Figure 4A), which is less than the ratio in *Magericyon* (0.38, 0.42), while the ratios in other genera of amphicyonines (0.44–0.67) and thaumastocyoninae (0.48–0.71) are usually much greater (Solé et al., 2022). The ratio of p4 to m1 length in the ursine *Ballusia* and *Ursavus* ranges from 0.44 to 0.61 (Qiu et al., 2014), and the ratio in *Ursus minimus* ranges from 0.45 to 0.59 (Baryshnikov and Lavrov, 2013). The p4 of *Lonchocyon* has no posterior accessory cuspid, which is in contrast to the Amphicynodontidae, hemicyonine Cephalogalini, *Phoberocyon*, and most Amphicyonidae with a distinct posterior accessory cuspid on p4 (Hunt, 1998b; Ginsburg and Morales, 1998). However, the posterior accessory cuspid on p4 also is reduced or even absent in some amphicyonids, such as *Guangxicyon* (Zhai et al., 2003), the amphicyonine *Magericyon* (Peigné et al., 2008), and the Pseudarctini, which comprises *Pseudarctos*, *Ictiocyon*, and *Dehmicyon* (Morales et al., 2021b). p4 has lost the posterior accessory cuspid in some derived Ursidae, including *Hemicyon*, *Zaragocyon*, *Plithocyon*, and Ursinae (Ginsburg and Morales, 1995; Ginsburg and Morales, 1998; Hunt, 1998b).

The m1 of *Lonchocyon* is characterized by its larger size (length = 27.28 mm) compared to contemporaneous Amphicyonidae and Hemicyoninae and by its large, spear-like paraconid (Figure 4B). The m1 paraconid of *Lonchocyon* is composed of three faces bordered by a slanted, anterior cristid, a lingual cristid, and a posterior cristid. The lingual cristid is present in some mustelids like extant *Gulo gulo*. By contrast, the lingual cristid is absent and the lingual surface of the paraconid is somewhat swollen in the compared Paleogene Amphicyonidae and hemicyonine Cephalogalini (Hunt, 1998a; Bonis, 2013). In addition, a faint, blunt ridge descends from the anterolingual surface of the protoconid on m1 of *Lonchocyon*, forming a triangular anterior surface of the protoconid with the preprotocristid. A similar anterior surface of the protoconid on m1 seems only present in the Oligocene Cephalogalini *Adelpharctos*, according to Bonis (1971). The metaconid of m1 is moderately reduced, nearly as high as the paraconid, and not retracted, relative to the protoconid in *Lonchocyon*, which is similar to the development of the m1 metaconid in early amphicyonine *Cynodictis palmidens* (Bonis, 1978), *Pseudocyonopsis* (Kuss, 1965), haplocyonine *Haplocyon dombroskyi* (Bonis, 1966), and thaumastocyonine *Y. tolosana* (Kuss, 1965). By contrast, the m1 metaconid is either relatively large in the daphoenine *Daphoenus*, *Brachyrhynchocyon* (Loomis, 1931; Scott and Jepsen, 1936), and haplocyonine *Parhaplocyon* (Bonis, 1966) or more reduced or even absent in the daphoenine *Daphoenictis* (Hunt, 1974), derived temnocyonines (Hunt, 2011), haplocyonine *Haplocyon crucians*, *Haplocyonides* (Hürzeler, 1940; Bonis, 1966), some derived amphicyonines like *Magericyon* (Peigné et al., 2008),

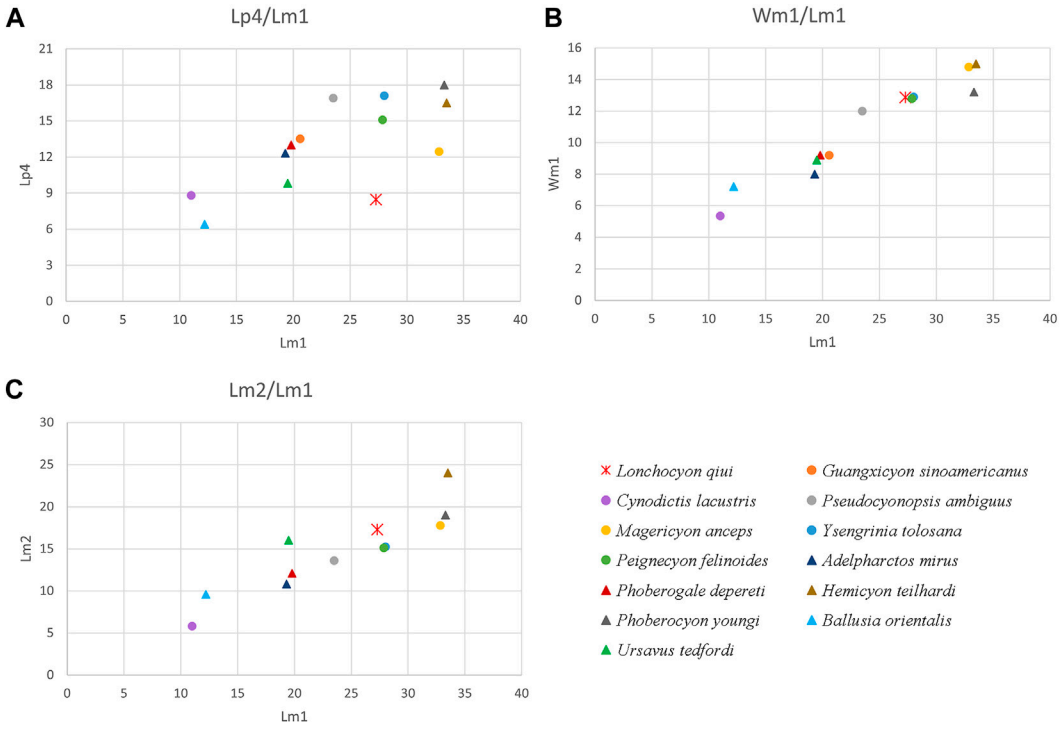

FIGURE 4
Scatter diagram of dental proportions in *L. qiui* gen. et sp. nov. (IVPP V 28616) and other compared arctoids: **(A)** length of p4 versus m1; **(B)** width versus length of m1; **(C)** length of m2 versus m1.

and derived thaumastocyoninae (Morales et al., 2019; Morales et al., 2021a). The hemicyonine ursids are characterized usually by a retracted metaconid relative to the protoconid on m1, which is different from Amphicyonidae, Amphicynodontidae, and *Lonchocyon*. However, the m1 metaconid is not retracted in the hemicyonine cephalogalini *Filholictis* (Cirot and Bonis, 1992; Bonis, 2013). On the other hand, the m1 metaconid is slightly retracted in the haplocyonine *Parhaplocyon* (Bonis, 1966) and strongly retracted (but sometimes lost) in *Gobicyon* (Jiangzuo et al., 2019). The talonid of m1 in *Lonchocyon* is more similar to early ursids than to amphicyonids in being nearly as wide as the trigonid and forming a shallow basin with the almost equally developed hypoconid crest and entoconid crest joining posteriorly. By contrast, the m1 talonid is usually slightly narrower than the trigonid (sometimes wider; for instance, in *Crassidia* (Heizmann and Kordikova, 2000)) hypoconid (crest) dominates the talonid with a low entoconid (crest), and the talonid opens posteriorly in amphicyonids (Kuss, 1965; Hunt, 1998a; 2011; Morales et al., 2021b). However, the hemicyonine Cephalogalini differs from *Lonchocyon* by having a continuous lingual ridge of the talonid gently joining the metaconid without any notch and displaying a relatively wider basin of the talonid with a more buccally placed hypoconid crest (Bonis, 2013).

The ratio of m2 length to m1 length is 0.63 in *Lonchocyon* (Figure 4C), similar to the ratios in early thaumastocyonine Ysengrini (*Crassidia* and *Ysengrinia*) (0.58–0.62) but greater than the more derived Thaumastocyonini (0.37–0.54) (Solé et al., 2022). Furthermore, the talonid of m2 is shorter and narrower than the trigonid in the earliest thaumastocyonine *Y. tolosana* from the late Oligocene, but the talonid alveolus is slightly wider than the trigonid alveolus in *Lonchocyon*. Among the three tribes in Amphicyoninae, the ratio of m2 length to m1 length in *Lonchocyon* is close to those of Amphicyonini (0.63-0.71), *Pseudocyon* (0.6, 0.64), and Pseudarctini *Dehmicyon schlosseria* (0.59), greater than that of the Magericyonini *Magericyon* (0.45, 0.54) and lesser than that of the Pseudarctini *Ictiocyon* (0.72) and *Pseudarctos* (0.71) (Morales et al., 2021b; Solé et al., 2022). The early amphicyonine *Pseudocyonopsis* from the Oligocene to early Miocene has a similar ratio between m2 length to m1 length (0.59, 0.61) to *Lonchocyon* (Kuss, 1965). Among the Hemicyoninae, the ratio of m2 to m1 length in the Cephalogalini is the variable between 0.51 and 0.71 (Bonis, 2013), and the ratios of the early *Hemicyon*, *H. gargan*, and *Zaragocyon* (0.58–0.61) are similar to that of *Lonchocyon* (Ginsburg and Morales, 1995; Ginsburg and Morales, 1998).

The lower jaw of *Lonchocyon* is very large, with a deep horizontal ramus and a distinct marginal process, which are distinguished from relatively slender mandibles without marginal processes in early Amphicyonidae and Hemicyoninae (Scott and Jepsen, 1936; Ginsburg, 1966; Bonis, 2013). Few caniform taxa have a marginal process, except for *Ursus*, *Ailuropoda* (Davis, 1964), and some fossil ursids like *Ursavus tedfordi* (Qiu et al., 2009). The marginal process is the main insertion site for the digastric muscle in *Ursus* and *Ailuropoda* (Davis, 1964). This feature may not have many phylogenetic implications with the currently limited sample, but it does suggest that *Lonchocyon* likely had powerful digastric muscles, as in *Ursus* and *Ailuropoda*. In addition, the mandible

TABLE 3 Dorsoventral mandibular force (logZx/L) values of *L. qiui* and compared carnivorans along the mandible.

	post m3	m2/m3	m1/m2	p4/m1	p3/p4	Canine
Lonchocyon qiui	−0.08	−0.17	−0.35	−0.44	−0.57	−0.38
Ysengrinia tolosana	−0.16	−0.22	−0.28	−0.45	−0.58	−0.37
Temnocyon macrogenys	−0.19	−0.26	−0.46	−0.65	−0.80	−0.58
Borocyon robustum	−0.07	−0.21	−0.31	−0.54	−0.67	−0.55
Delotrochanter oryktes	−0.28	−0.34	−0.49	−0.73	−0.85	−0.55
Magericyon anceps		−0.92	−1.00	−1.27	−1.40	−0.60
Ammitocyon kainos		−0.99	−1.17	−1.13	−1.38	−0.78
Canis lupus	−0.47	−0.55	−0.64	−0.77	−0.97	−0.92
Ursus arctos	−0.03	−0.31	−0.55	−0.54	−0.48	−0.22
Panthera leo			−0.29	−0.47	−0.64	−0.38
Crocuta crocuta			−0.23	−0.45	−0.67	−0.61

TABLE 4 Labiolingual mandibular force (logZy/L) values of *L. qiui* and compared carnivorans along the mandible.

	post m3	m2/m3	m1/m2	p4/m1	p3/p4	Canine
Lonchocyon qiui	−0.60	−0.65	−0.77	−0.86	−0.99	−0.32
Ysengrinia tolosana	−0.60	−0.65	−0.67	−0.85	−0.98	−0.41
Temnocyon macrogenys	−0.83	−0.89	−1.05	−1.07	−1.30	−0.69
Borocyon robustum	−0.59	−0.67	−0.71	−0.93	−1.02	−0.63
Delotrochanter oryktes	−0.94	−0.94	−1.00	−1.16	−1.34	−0.71
Magericyon anceps		−0.41	−0.51	−0.79	−0.92	−0.52
Ammitocyon kainos		−0.32	−0.47	−0.58	−0.76	−0.22
Canis lupus	−0.98	−1.05	−1.07	−1.09	−1.26	−0.88
Ursus arctos	−0.50	−0.66	−0.97	−0.99	−0.83	−0.28
Panthera leo			−0.64	−0.80	−0.93	−0.48
Crocuta crocuta			−0.76	−0.83	−0.96	−0.69

of *Lonchocyon* has a shallow depression along the posterior ventral border of the horizontal ramus on the lateral surface, possibly suggesting a rudimentary premasseteric fossa (Figure 3C), which is more distinct in derived hemicyonines, some derived amphicyonids like *Gobicyon* and *Ammitocyon*, and some ursines (Frick, 1926; Hunt, 1998b; Jiangzuo et al., 2019; Morales et al., 2021a).

There are only two unequivocal amphicyonids with supporting detailed descriptions from the Eocene of Asia. One is a small indeterminate amphicyonid with a right M2 (for the second upper molar, rather than lower molar) (length: 6.35 mm; width: 8.5 mm) found in the Upper Eocene Ergilin Dzo Formation of Mongolia (Egi et al., 2009). Few comparisons can be made with our new specimen because of the lack of lower dentitions. However, the amphicyonid from the Ergilin Dzo Formation is much smaller than the specimen IVPP V 28616. Another is *Guangxicyon sinoamericanus*, an aberrant, short-jawed amphicyonid from the middle Eocene Nadu Formation of the Bose Basin, Guangxi Province, southern China (Zhai et al., 2003; Wang et al., 2019 for timescale). *Lonchocyon* differs from *Guangxicyon* in having a larger size (*Guangxicyon* m1 length and width are 20.6 mm and 9.2 mm, respectively), a deeper mandible, a single-rooted p3, a much-reduced p4, an m1 with more trenchant trigonid and a shallow-basined talonid, and a double-rooted m2. However, *Guangxicyon* is also very aberrant among amphicyonids in terms of its early development of brachygnathy with a single-rooted p2 and m2 instead of losing p1-3 or m2-3.

Only a few Cephalogalini have been discovered, with scarce materials in Paleogene Asia. A left M2 (the second upper molar) of *Cephalogale* sp. (IVPP V 12429) from the early Oligocene of Saint Jacques (Wang and Qiu, 2003) and a left ramal fragment with m2 of ?*Cephalogale* sp. (MAE SG.97.5396) from the early Oligocene Hsanda Gol Formation (Wang et al., 2005) are the only reported Asian Paleogene Cephalogalini. Our specimen can make few comparisons with them due

TABLE 5 Relative mandibular force (Zx/Zy) values of *L. qiui* and compared carnivorans along the mandible.

	post m3	m2/m3	m1/m2	p4/m1	p3/p4	Canine
Lonchocyon qiui	3.29	2.98	2.65	2.50	2.65	0.88
Ysengrinia tolosana	2.79	2.73	2.46	2.62	2.53	1.11
Temnocyon macrogenys	4.35	4.05	3.73	2.66	3.23	1.30
Borocyon robustum	3.33	2.88	2.56	2.41	2.23	1.20
Delotrochanter oryktes	4.51	4.01	3.24	2.67	3.13	1.46
Magericyon anceps		0.31	0.33	0.33	0.33	0.83
Ammitocyon kainos		0.21	0.20	0.28	0.24	0.27
Canis lupus	3.23	3.10	2.67	2.12	1.94	0.90
Ursus arctos	2.91	2.21	2.64	2.76	2.19	1.15
Panthera leo			2.28	2.11	1.94	1.25
Crocuta crocuta			3.43	2.37	1.93	1.20

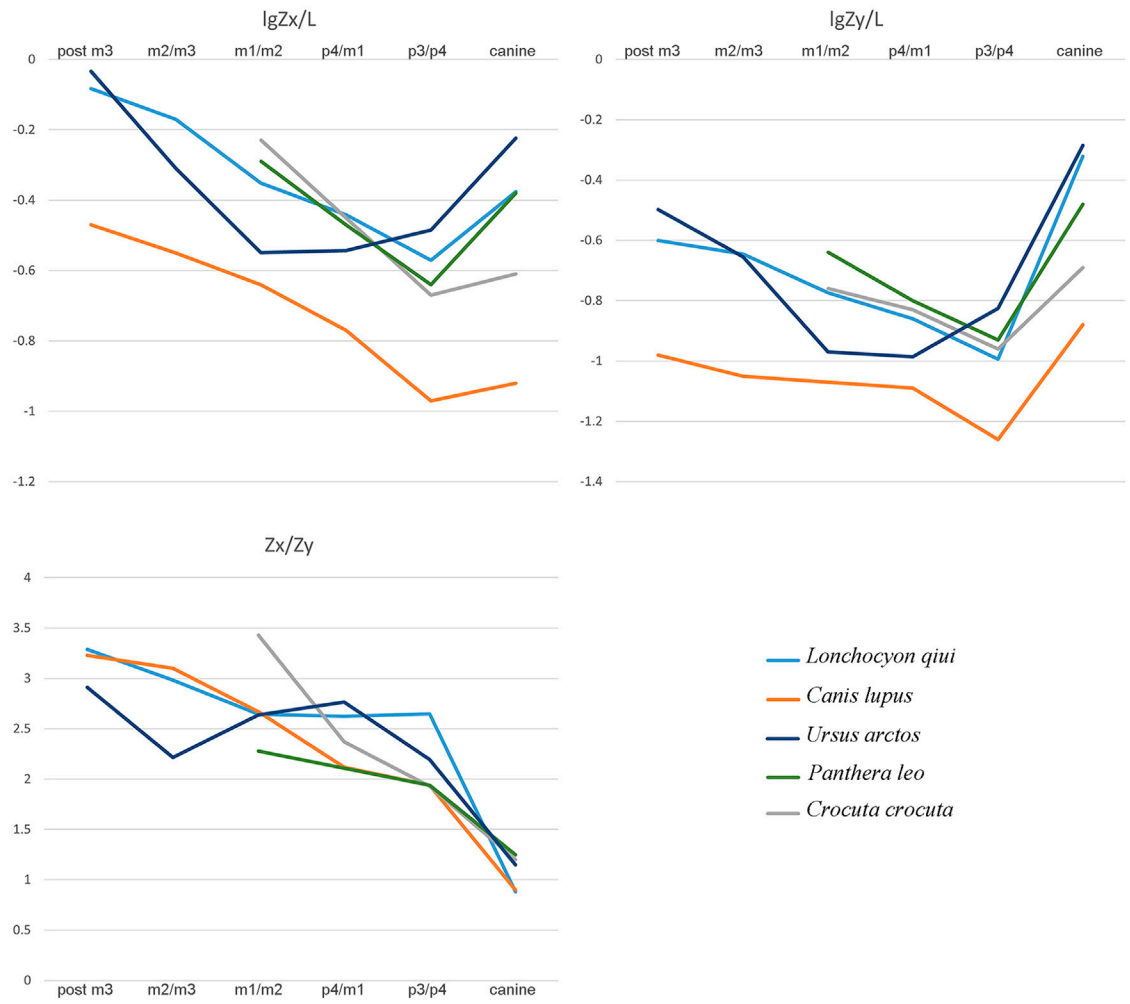

FIGURE 5
Comparison of mandibular force profiles among *L. qiui*, *C. lupus*, *U. arctos*, *P. leo*, and *C. crocuta*.

to the lack of comparable materials, although the former is evidently larger than these *Cephalogale*.

In summary, *Lonchocyon* is unique due to its relatively large size, highly reduced premolars separated by diastemas, and spear-like paraconid on m1 compared to other Paleogene arctoids. The carnassial tooth and lower jaw show a combination of both Amphicyonidae and Hemicyoninae traits, with the trigonid having a reduced metaconid that is not retracted, which is similar to the former and having a shallowly basined talonid of m1 and a rudimentary premasseteric fossa, which are probably allied with both Amphicyonidae and Hemicyoninae. There is no doubt that *Lonchocyon* represents an early offshoot of Arctoidea, but its phylogenetic relationships among amphicyonids or early ursids remain unclarified since the discovery of additional complete material is pending.

4 Paleobiology

The robust canine, the sectorial trigonid of m1, and the deep mandible of *Lonchocyon* suggest its hypercarnivorous adaptations. This trend in adaptation evolved independently many times among all subfamilies of the Amphicyonidae, such as the *Borocyon* of Daphoencyoninae, *Haplocyonoides* of Haplocyoninae, some *Temnocyon* species of Temnocyoninae, the Magericyonini of Amphicyoninae, and all genera of Thaumastocyoninae (Hunt, 2011; Morales et al., 2019; Morales et al., 2021b). The shallow talonid basin of m1 indicates the presence of a plesiomorphic pattern in *Lonchocyon*, but other hypercarnivorous amphicyonids have hypoconid-dominant talonids. The hypercarnivorous trend also evolved in the *Phoberocyon–Plithocyon* clade of Hemicyoninae, or Phoberocyonini, which is distinguished from other hemicyonines by well-developed carnassials (P4 and m1) (Ginsburg and Morales, 1995). Inferred from the alveoli, the m2 of *Lonchocyon* is unreduced, which is a plesiomorphic trait, and different from Magericyonini and Thaumastocyoninae with their reduced m2, while the m2 of hypercarnivorous hemicyonines are also unreduced. The function of m2 is mainly crushing in carnivorans. Hypercarnivores tend to develop the shearing rather than crushing functions of their dentitions, at the same time, they often have a reduced m2. Additionally, all premolars are highly reduced including p4 in *Lonchocyon*, but many hypercarnivorous arctoids have a functional p4 without much reduction, except the Magericyonini of Amphicyoninae. The Magericyonini, consisting of *Magericyon* and possibly *Pseudocyon*, have reduced p4 as in *Lonchocyon*. The similarity between the reduced p4 of *Lonchocyon* and Magericyonini could be the result of parallel evolution, considering the younger *Pseudocyon* distributed from MN4 to MN7 and *Magericyon* distributed from MN9 to MN10. In conclusion, the hypercarnivorous adaptations of *Lonchocyon* are plesiomorphic and aberrant.

In order to investigate the paleobiology of *Lonchocyon* in a quantitative way, we use beam theory (Therrien, 2005) to study the mandibular force profiles of the new specimen. Some carnivorans with a similar mandibular length to that of *Lonchocyon* were selected and include the extinct amphicyonids *Y. tolosana*, *Temnocyon macrogenys*, *B. robustum*, *D. oryktes*, *M. anceps*, and *A. kainos* and the extant carnivorans *C. lupus*, *U. arctos*, *P. leo*, and *Crocuta crocuta*. We compared the dorsoventral mandibular force profiles (Zx/L), the labiolingual mandibular force profiles (Zy/L), and the relative mandibular force (Zx/Zy) of these carnivorans (Tables 3, 4, 5; Figure 5) to assess the mandibular function of *Lonchocyon*. Generally, a large Zx/L value indicates the ability to withstand high dorsoventral stresses, and a large Zy/L indicates high labiolingual and torsional stresses (Therrien, 2005).

The dorsoventral mandibular force profiles (Zx/L) of *Lonchocyon* exhibit similar tendencies to canids and other amphicyonids (Table 3). The Zx/L values of *Lonchocyon* are similar to *Y. tolosana* and *P. leo* and are higher than most other amphicyonids compared at the same loci. The Zx/L values of the canine are higher than other taxa except *Y. tolosana* and *U. arctos*, reaching nearly the same value as *P. leo*, which suggests that the new taxon could deliver powerful canine bites to subdue prey as large felids do, rather than the rapid and shallow bites delivered by canids, which always hunt in packs. The Zx/L value after canine rises gradually along the horizontal ramus, which is similar to other carnivorans except *U. arctos,* with a decline from p3/p4 to m1/m2.

The labiolingual mandibular force profiles (Zy/L) of *Lonchocyon* also exhibit similarities with canids and other amphicyonids and are lower than the Zx/L values at the same loci (Table 4), as in most carnivorans, except for the value of the canine larger than Zx/L. The Zy/L values of *Lonchocyon* (except the canine) are similar to those of *Y. tolosana*, *B. robustum*, *P. leo*, and *C. crocuta*, lower than those of *A. kainos* and *M. anceps* and higher than those of other amphicyonids. The Zy/L value of the canine even surpasses *P. leo* and is lower than those of *A. kainos* and *U. arctos*. The extremely large value suggests that the new taxon could withstand huge labiolingual and torsional stresses while restraining prey with its powerful canine bites. The Zy/L values also rise steadily along the horizontal ramus posterior to the canine, similar to other carnivorans, except *U. arctos*.

In terms of the relative mandibular force (Zx/Zy) (Table 5), *Lonchocyon* exhibits a distinct difference with other caniforms which is its near plateau from p3/p4 to m1/m2, corresponding to its sectorial carnassial tooth and reduced premolars that the former is mainly used to slice meat with little need for withstanding extra buccolingual or torsional stresses. From the m1/2 boundary to the posterior side of m3, the Zx/Zy values exhibit a steep slope, indicating that the molars posterior to the carnassial possess the ability to crack hard objects as extant canids can, which needs to suffer more buccolingual stresses. In addition, the Zx/Zy value of *Lonchocyon* is lower than those in other amphicyonids except *Y. tolosana* and *B. robustum*.

According to the aforementioned analyses, *Lonchocyon* possesses a robust mandibular symphysis that would have facilitated the delivery of powerful canine bites while subduing the prey. After the probably functionless premolars and the meat-slicing carnassial, the posterior molars may have had the ability to crush certain hard materials. Specifically, *Lonchocyon* has a dentition with a combination of both shearing and crushing functions and likely occupied a special ecological niche as a predator consuming both flesh and hard objects. Considering its size, the new taxon likely fed primarily on prey animals of the same size or even larger than itself, as large felids are able to do

today. It was also likely to have been a solitary hunter, different from extant canids, which have a pack-hunting lifestyle (Therrien, 2005).

5 Conclusion

Lonchocyon represents a specialized carnivoran from the late Eocene of Asia. The new specimen is the first arctoid discovered in the Erlian Basin and the first late Eocene arctoid from northern China. This large, deep-jaw arctoid has reduced premolars, a sectorial m1 with a cristid from the paraconid to the carnassial notch on the lingual side, an unretracted metaconid, a shallowly basined talonid, and unreduced m2-3. *Lonchocyon* shows a combination of morphologies present in both amphicyonids and the early ursid hemicyonines and represents an early offshoot of amphicyonids or hemicyonines in Asia. Furthermore, the analyses of the mandibular force profile indicate that *Lonchocyon* has primary hypercarnivorous characteristics with powerful canine bite, a sectorial carnassial tooth for slicing, and posterior molars that are able to process hard objects.

Data availability statement

The original contributions presented in the study are included in the article/supplementary material; further inquiries can be directed to the corresponding authors.

Author contributions

X-YZ wrote the manuscript, analyzed the data, and prepared the figures; BB and Y-QW designed the research and improved and edited the manuscript.

Funding

This study was financially supported by grants from the Strategic Priority Research Program of the Chinese Academy of Sciences (XDB26000000) and the National Natural Science Foundation of China (42272011, 41572021, and 41672014).

Acknowledgments

The authors would like to thank Qian Li, Ran-Cheng Xu, Xiao-Yang Wang, Wei Zhou, Shi-Jie Li, Fu-Qiao Shi, Yan Li, Yong-Xing Wang, Yong-Fu Wang, and Qi Li for their assistance in the fieldwork; Zhan-Xiang Qiu, Zhao-Qun Zhang, Qi-Gao Jiangzuo, and Dan Lu for their helpful discussions; Zhan-Xiang Qiu for providing some important references; Shi-Jie Li for preparation of the specimen; Wei Gao for photography; and Ye-Mao Hou for CT scanning assistance. The authors are grateful to Thomas Stidham for his assistance with the English editing of an early draft of the manuscript.

Conflict of interest

The authors declare that the research was conducted in the absence of any commercial or financial relationships that could be construed as a potential conflict of interest.

Publisher's note

References

Bai, B., Wang, Y. Q., Li, Q., Wang, H. B., Mao, F. Y., Gong, Y. X., et al. (2018). Biostratigraphy and diversity of Paleogene perissodactyls from the Erlian Basin of inner Mongolia, China. *Am. Mus. Novit.* 3914, 1–60. doi:10.1206/3914.1

Baryshnikov, G. F., and Lavrov, A. V. (2013). Pliocene bear *Ursus minimus* Devèze de Chabriol et Bouillet, 1827 (Carnivora, Ursidae) in Russia and Kazakhstan. *Russ. J. Theriol.* 12, 107–118. doi:10.15298/rusjtheriol.12.2.07

Berkey, C. P., Granger, W., and Morris, F. K. (1929). Additional new formations in the later sediments of Mongolia. *Am. Mus. Novit.* 385, 1–12.

Bonis, L. D. (1966). Sur l'évolution du genre *Haplocyon* Schlosser (Carnivora). *Bull. Soc. Géol. Fr.* S7-VIII, 114–117. doi:10.2113/gssgfbull.S7-VIII.1.114

Bonis, L. de. (1971). Deux nouveaux carnassiers des Phosphorites du Quercy. *Ann. Paléontol.* 57, 117–127.

Bonis, L. D. (1978). La poche à phosphate de Ste-Neboule (Lot) et sa faune de vertébrés du Ludien supérieur. 12. – fissipèdes (Carnivores). *Palaeovertebrata* 8, 301–311.

Bonis, L. D. (2013). Ursidae (mammalia, Carnivora) from the late Oligocene of the "phosphorites du Quercy" (France) and a reappraisal of the genus *Cephalogale* geoffroy, 1862. *Geodiversitas* 35, 787–814. doi:10.5252/g2013n4a4

Cirot, E., and Bonis, L. de. (1992). Révision du genre *Amphicynodon*, carnivore de l'Oligocène. *Palaeontogr. Abt. A* 220, 103–130.

Davis, D. D. (1964). The giant panda: A morphological study of evolutionary mechanisms. *Field. (Zool. Mem.)* 3, 1–339.

Egi, N., Tsubamoto, T., and Tsogtbaatar, K. (2009). New amphicyonid (mammalia: Carnivora) from the upper Eocene Ergilin Dzo Formation, Mongolia. *Paleontol. Res.* 13, 245–249. doi:10.2517/1342-8144-13.3.245

Frick, C. (1926). The Hemicyoninae and an American tertiary bear. *Bull. Am. Mus. Nat. Hist.* 56, 1–119.

Ginsburg, L. (1965). L'"*Amphycion" ambiguus* des Phosphorites du Quercy. *Bull. Mus. Natl. Hist. Nat.* 37, 724–730.

Ginsburg, L. (1966). Les Amphicyons des Phosphorites du Quercy. *Ann. Paléontol.* 52, 23–64.

Ginsburg, L., and Morales, J. (1998). Les Hemicyoninae (Ursidae, Carnivora, Mammalia) et les formes apparentées du Miocène inférieur et moyen d'Europe occidentale. *Ann. Paléontol.* 84, 71–123. doi:10.1016/S0753-3969(98)80003-7

Ginsburg, L., and Morales, J. (1995). *Zaragocyon daamsi* n. gen. sp. nov., Ursidae primitif du Miocène inférieur d'Espagne. *Cr. Acad. Sci. Série 2. Sci. Terre Planèt.* 321, 811–815.

Heizmann, E. P. J., and Kordikova, E. G. (2000). Zur systematischen Stellung von "*Amphicyon" intermedius* H. v. Meyer, 1849 (Carnivora, Amphicyonidae). *Carolinea* 58, 69–82.

Hunt, R. M., Jr. (1998a). "Amphicyonidae," in *Tertiary mammals of north America*. Editors C. Janis, K. Scott, and L. Jacobs (London: Cambridge University Press), 196–227.

Hunt, R. M., Jr. (1974). *Daphoenictis*, a cat-like carnivore (mammalia, Amphicyonidae) from Oligocene of north America. *J. Paleontol.* 48, 1030–1047.

Hunt, R. M., Jr. (2011). Evolution of large carnivores during the mid-cenozoic of north America: The temnocyonine radiation (mammalia, Amphicyonidae). *Bull. Am. Mus. Nat. Hist.* 358, 1–153. doi:10.1206/358.1

Hunt, R. M., Jr. (1998b). "Ursidae," in *Tertiary mammals of north America*. Editors C. Janis, K. Scott, and L. Jacobs (London: Cambridge University Press), 174–195.

Hürzeler, J. (1940). *Haplocyonoides* nov. gen., ein aberranter Canide aus dem Aquitanien des Hesslers (Mainzer Becken). *Eclogae Geol. Helv.* 33, 224–229.

Jiangzuo, Q. G., Li, C. X., Zhang, X. X., Wang, S. Q., Ye, J., and Li, Y. (2018). Diversity of Amphicyonidae (Carnivora, mammalia) in the middle Miocene halamagai formation in ulungur river area, xinjiang, northwestern China. *Hist. Biol.* 32, 187–202. doi:10.1080/08912963.2018.1477142

Jiangzuo, Q. G., Wang, S. Q., Li, C., Sun, D. H., Zhang, X. X., and O'Regan, H. (2019). New material of *Gobicyon* (Carnivora, Amphicyonidae, Haplocyoninae) from northern China and a review of aktaucyonini evolution. *Pap. Palaeontol.* 7, 307–327. doi:10.1002/spp2.1283

Kuss, S. E. (1965). Revision der europäischen Amphicyoninae (Canidae, Carnivora, Mammalia) ausschließlich der voroberstampischen Formen. *Sitz. Heid. Akad. Wiss.* 1, 1–168.

Loomis, F. B. (1931). A new Oligocene dog. *Am. J. Sci.* s5-22, 100–102. doi:10.2475/ajs.s5-22.128.100

Matthew, W. D., and Granger, W. (1925a). New mammals from the Irdin Manha Eocene of Mongolia. *Am. Mus. Novit.* 198, 1–10.

Matthew, W. D., and Granger, W. (1925b). New mammals from the shara Murun Eocene of Mongolia. *Am. Mus. Novit.* 196, 1–12.

Morales, J., Abella, J., Sanisidro, O., and Valenciano, A. (2021a). *Ammitocyon kainos* gen. et sp. nov., a chimerical amphicyonid (Mammalia, Carnivora) from the late Miocene carnivore traps of Cerro de los Batallones (Madrid, Spain). *J. Syst. Palaeontol.* 19, 393–415. doi:10.1080/14772019.2021.1910868

Morales, J., Fejfar, O., Heizmann, E., Wagner, J., and Abella, J. (2019). A new Thaumastocyoninae (Amphicyonidae, Carnivora) from the early Miocene of tuchořice, the Czech republic. *Foss. Impr.* 75, 397–411. doi:10.2478/if-2019-0025

Morales, J., Fejfar, O., Heizmann, E., Wagner, J., Valenciano Vaquero, A., and Abella, J. (2021b). The Amphicyoninae (Amphicyonidae, Carnivora, mammalia) of the early Miocene from tuchořice, the Czech republic. *Foss. Impr.* 77, 126–144. doi:10.37520/fi.2021.011

Peigné, S., and Heizmann, E. P. (2003). The Amphicyonidae (mammalia: Carnivora from ulm-westtangente (MN2, early Miocene), baden-württemberg, Germany-systematics and ecomorphology. *Stuttg. Beitr. Nat. Ser. B. Geol. Paläontol.* 54, 21–35.

Peigné, S., Salesa, M. J., Antón, M., and Morales, J. (2008). A new amphicyonine (Carnivora: Amphicyonidae) from the upper Miocene of batallones-1, madrid, Spain. *Palaeontology* 51, 943–965. doi:10.1111/j.1475-4983.2008.00788.x

Qiu, Z. X., Deng, T., and Wang, B. Y. (2014). A late Miocene *Ursavus* skull from guanghe, gansu, China. *Vert. Palasiat* 52, 1–9.

Qiu, Z. X., Deng, T., and Wang, B. Y. (2009). First bear material from dongxiang, gansu ---Addition to the longdan mammalian fauna (2). *Vert. Palasiat.* 47, 245–264.

Qiu, Z. X., Yan, D. F., and Jia, H. (1985). Dentition of the *Ursavus* skeleton from shanwang, shandong province. *Vert. Palasiat.* 23, 264–275.

Rose, K. D. (2006). *The Beginning of the age of mammals*. Baltimore: The John Hopkins University Press.

Russell, D. E., and Zhai, R. J. (1987). The Paleogene of Asia: Mammals and stratigraphy. *Mem. Mus. Natl. Hist. Nat. Série C. Sci. Terre* 52, 1–488.

Scott, W. B., and Jepsen, G. L. (1936). The mammalian fauna of the white river Oligocene: Part I. Insectivora and Carnivora. *Trans. Am. Philos. Soc.* 28, 1–153. doi:10.2307/1005507

Solé, F., Fischer, V., Denayer, J., Speijer, R., Fournier, M., Le Verger, K., et al. (2021). The upper Eocene-Oligocene carnivorous mammals from the Quercy Phosphorites (France) housed in Belgian collections. *Geol. Belg.* 24, 1–16. doi:10.20341/gb.2020.006

Solé, F., Lesport, J. F., Heitz, A., and Mennecart, B. (2022). A new gigantic carnivore (Carnivora, Amphicyonidae) from the late middle Miocene of France. *PeerJ* 10, e13457. doi:10.7717/peerj.13457

Szalay, F. S., and Gould, S. J. (1966). Asiatic mesonychidae (mammalia, condylarthra). *Bull. Am. Mus. Nat. Hist.* 132, 129–173.

Therrien, F. (2005). Mandibular force profiles of extant carnivorans and implications for the feeding behaviour of extinct predators. *J. Zool.* 267, 249–270. doi:10.1017/S0952836905007430

Wang, B. Y., and Meng, J. (2009). *Ardynomys* (cylindrontidae, rodentia) from nei mongol, China. *Vert. Palasiat.* 47, 240–244.

Wang, B. Y. (2003). Oligocene rodents from the nomogen (= nom khong) area of nei mongol, China, and comments on related stratigraphy. *Vert. Palasiat.* 41, 211–219.

Wang, B. Y., and Qiu, Z. X. (2003). Notes on early Oligocene ursids (Carnivora, mammalia) from Saint Jacques, nei mongol, China. *Bull. Am. Mus. Nat. Hist.* 22, 116–124. doi:10.1206/0003-0090(2003)279<0116:C>2.0.CO;2

Wang, X. M., McKenna, M. C., and Dashzeveg, D. (2005). *Amphicticeps* and *amphicynodon* (Arctoidea, Carnivora) from Hsanda Gol Formation, Central Mongolia and and phylogeny of basal arctoids with comments on zoogeography. *Am. Mus. Novit.* 3483, 1–57. doi:10.1206/0003-0082(2005)483[0001:AAAACF]2.0.CO;2

Wang, Y. Q., Li, Q., Bai, B., Jin, X., Mao, F. Y., and Meng, J. (2019). Paleogene integrative stratigraphy and timescale of China. *Sci. China Earth Sci.* 62, 287–309. doi:10.1007/s11430-018-9305-y

Wang, Y. Q., Meng, J., and Jin, X. (2012). Comments on Paleogene localities and stratigraphy in the Erlian Basin, nei mongol, China. *Vert. Palasiat.* 50, 181–203.

Wang, Y. Q., Meng, J., Ni, X. J., and Li, C. K. (2007). Major events of Paleogene mammal radiation in China. *Geol. J.* 42, 415–430. doi:10.1002/gj.1083

Xia, L., Yang, Q. S., Feng, Z. J., Quan, G. Q., and Ma, Y. (2005). A guide to the measurement of mammal skull Ⅱ: Perissodactyla, Artiodactyla and Carnivora. *Chin. J. Zool.* 40, 67–73. doi:10.13859/j.cjz.2005.06.012

Yang, Q. S., Xia, L., Ma, Y., Feng, Z. J., and Quan, Q. G. (2005). A guide to the measurement of mammal skull Ⅰ:Basic measurement. *Chin. J. Zool.* 40, 50–56. doi:10.13859/j.cjz.2005.03.011

Ye, J. (1983). Mammalian fauna from the late Eocene of ulan Shireh area, inner Mongolia. *Vert. Palasiat.* 21, 109–118.

Zhai, R. J., Ciochon, R. L., Tong, Y. S., Savage, D. E., Morlo, M., Holroyd, P. A., et al. (2003). An aberrant amphicyonid mammal from the latest Eocene of the Bose Basin, Guangxi, China. *Acta palaeont. Pol.* 48, 293–300.

frontiers | Frontiers in Earth Science

TYPE Original Research
PUBLISHED 14 March 2023
DOI 10.3389/feart.2023.1117911

OPEN ACCESS

EDITED BY
Lucja A. Fostowicz-Frelik,
Polish Academy of Sciences, Poland

REVIEWED BY
Grégoire Métais,
Centre National de la Recherche Scientifique (CNRS), France
Takehisa Tsubamoto,
Ehime University, Japan

*CORRESPONDENCE
Bin Bai,
baibin@ivpp.ac.cn

SPECIALTY SECTION
This article was submitted to Paleontology, a section of the journal Frontiers in Earth Science

RECEIVED 07 December 2022
ACCEPTED 27 February 2023
PUBLISHED 14 March 2023

CITATION
Bai B, Wang Y-Q, Theodor JM and Meng J (2023), Small artiodactyls with tapir-like teeth from the middle Eocene of the Erlian Basin, Inner Mongolia, China. *Front. Earth Sci.* 11:1117911. doi: 10.3389/feart.2023.1117911

Small artiodactyls with tapir-like teeth from the middle Eocene of the Erlian Basin, Inner Mongolia, China

Bin Bai[1]*, Yuan-Qing Wang[1,2], Jessica M. Theodor[3] and Jin Meng[1,4,5]

[1]Key Laboratory of Vertebrate Evolution and Human Origins of Chinese Academy of Sciences, Institute of Vertebrate Paleontology and Paleoanthropology, Chinese Academy of Sciences, Beijing, China, [2]College of Earth and Planetary Sciences, University of Chinese Academy of Sciences, Beijing, China, [3]Department of Biological Sciences, University of Calgary, Calgary, AB, Canada, [4]Division of Paleontology, American Museum of Natural History, New York, NY, United States, [5]Earth and Environmental Sciences, Graduate Center, City University of New York, New York, NY, United States

Artiodactyls diversified during the Eocene and Oligocene in North America and Europe after their first Holarctic appearance at the beginning of the Eocene. However, the relationships among early artiodactyls, European endemic forms, and later derived suiforms, tylopods, and ruminants remain unclear. Early artiodactyls are relatively rare in Asia compared to those known from North America and Europe; thus, investigation of Eocene artiodactyls from Asia is important to resolve these issues. Here we report two new genera and three new species of small early artiodactyls from middle Eocene deposits of the Erlian Basin, Inner Mongolia, China. The new materials represent a morphologically gradational series from Asian Land Mammal Ages Irdinmanhan to Sharamurunian, characterized by a trend towards bilophodonty in the lower molars. Morphologic and phylogenetic analyses suggest that these new taxa have a close relationship with the enigmatic European *Tapirulus*, which currently consists of five species that range from the middle Eocene to the early Oligocene. The close relationship between the Erlian specimens and *Tapirulus* suggests possible faunal exchanges between Europe and Asia during the middle Eocene, a view that has been supported by other mammalian groups across the two continents. The evolution of bilophodonty in Tapirulidae and Raoellidae is probably attributable to convergence.

KEYWORDS

Erlian Basin, Eocene Artiodactyla, Tapirulidae, Homacodontidae, Tethys Sea

1 Introduction

The first appearance of Artiodactyla, Perissodactyla, and Primates in the fossil record marks the Paleocene-Eocene transition when modern mammal orders appeared as archaic groups declined. Asian Paleogene artiodactyls are relatively rare compared to North American and European faunas, and Asian artiodactyls are mostly reported from the Southeast Asia and Indo-Pakistani subcontinent (Theodor et al., 2007). The late middle Eocene Pondaung fauna of Myanmar and the Late Eocene Krabi fauna of Thailand preserve a relatively diverse artiodactyl assemblage, including dichobunids (Métais et al., 2007; Ducrocq et al., 2022), diacodexeids (Ducrocq et al., 2016), anthracotheres (Ducrocq et al., 2001),

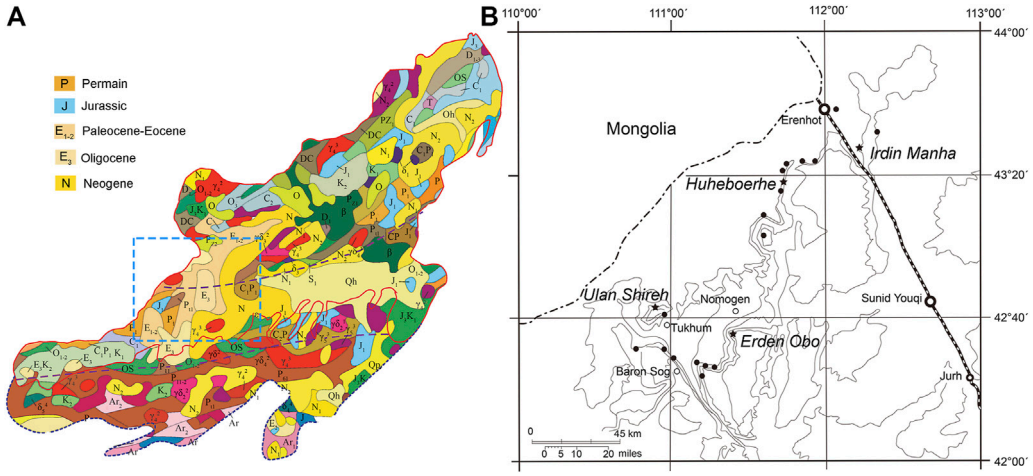

FIGURE 1
Geological map and fossil localities of the Erlian Basin. **(A)** geological map of the Erlian Basin (modified from Zhang et al., 2019, Fig. 3, with permission from S. Fu); **(B)** Paleogene fossil localities in the Erlian Basin with solid stars indicating the localities where new artiodactyl fossils were unearthed (modified from Bai et al., 2018, Fig. 1).

ruminants (Métais et al., 2000; Métais et al., 2001; Métais, 2006; Ducrocq et al., 2020), and some indeterminate groups (Tsubamoto et al., 2013). Early and middle Eocene artiodactyls from Indo-Pakistan include diacodexeids, dichobunids, and endemic raoellids (Theodor et al., 2007; Thewissen et al., 2020). A few diacodexeids, dichobunids, helohyids, and controversial raoellids are known from the middle Eocene of Andarak 2, Kyrgyzstan (Averianov, 1996), Chakpaktas Svita of Kazakhstan (Gabunia, 1971; Gabunia, 1973), and Khaichin-Ula II of Mongolia (Vislobokova, 2004a; Vislobokova, 2004b; Vislobokova, 2004008; Orliac and Ducrocq, 2012). The Eocene mammal faunas from China are dominated by diverse perissodactyls (Bai et al., 2020), however, artiodactyls from the middle Eocene Shanghuang fissure-fillings of Jiangsu Province are more diverse and abundant than in contemporary Chinese faunas. *Elaschitotherium*, the homacodontid *Limeryx*, diacodexeids such as *Jiangsudon*, and indeterminate suoids have been reported from Shanghuang fissures (Métais et al., 2004; Métais et al., 2005; Métais et al., 2008; Orliac and Ducrocq, 2012).

The Erlian Basin is located in the south of the Mongolia Plateau and at the junction between the North China Block and the Siberian Plate (Zhang et al., 2019; Fu et al., 2021). The continental Mesozoic and Cenozoic sediments are widely distributed in the Erlian Basin, including the nearly continuous Paleogene deposits bearing abundant mammalian fossils (Figure 1), which form the basis of the Eocene Asian Land Mammal Ages (Wang et al., 2012; Wang et al., 2019). Artiodactyl fossils have been reported from the Erlian Basin since the Central Asiatic Expedition (CAE) by the American Museum of Natural History in the 1920s, including *Gobiohyus*, *Erlianhyus*, and an achaenodont from the Irdin Manha Formation (Matthew and Granger, 1925a; Coombs and Coombs, 1977; Li and Li, 2021), *Archaeomeryx* from the Shara Murun Formation (Matthew and Granger, 1925b; Vislobokova, 2002), *Entelodon* from the Houldjin and upper Naogangdai formations (Matthew and Granger, 1923; Jiang, 1983; Lucas and Emry, 1996; Wang et al., 2009), and *Brachyhyops* from the "Ulan Gochu Formation" at Twin Oboes (Wang and Qiu, 2002). We report new artiodactyl material with lophodont-like teeth from the middle Eocene of the Erlian Basin, Inner Mongolia, the first small, basal artiodactyls from the Erlian Basin since the CAE expedition. This material shows striking similarities with the enigmatic European *Tapirulus*, supporting faunal exchange between Europe and Asia during the early middle Eocene. In addition, we discuss the unusual evolution of bilophodonty in artiodactyls.

2 Materials and methods

Several isolated teeth, fragmentary low jaws, and a calcaneus were recovered from the Irdin Manhan Formation at Irdin Manha and Huhoboerhe, a right lower jaw with p4–m3 from the upper part of the "Basal White" at Erden Obo (Urtyn Obo), and a left lower jaw with m2–3 from the base of the Shara Murun Formation at Ula Usu (Figure 1). A left lower jaw with m1 talonid, m2–3, and a left astragalus are probably from the Ulan Shireh Formation at North Mesa, but their specific horizon and locality remain uncertain.

Phylogenetic analyses were conducted using the parsimony Traditional Search method in TNT 1.5 (Goloboff et al., 2008; Goloboff and Catalano, 2016). The data matrix used in the analyses, modified from the data of Métais et al. (2004), contained a total of 31 taxa and 34 dental characters. All characters were equally weighted, and four characters (3, 7, 8, 13) were ordered. The heuristic search algorithm was used with 1,000 replications of random stepwise addition and tree-bisection-reconnection (TBR) branch swapping. Then the Traditional Search was again conducted on trees from RAM because some replications overflowed. Branches were collapsed when their minimum length was equal to zero.

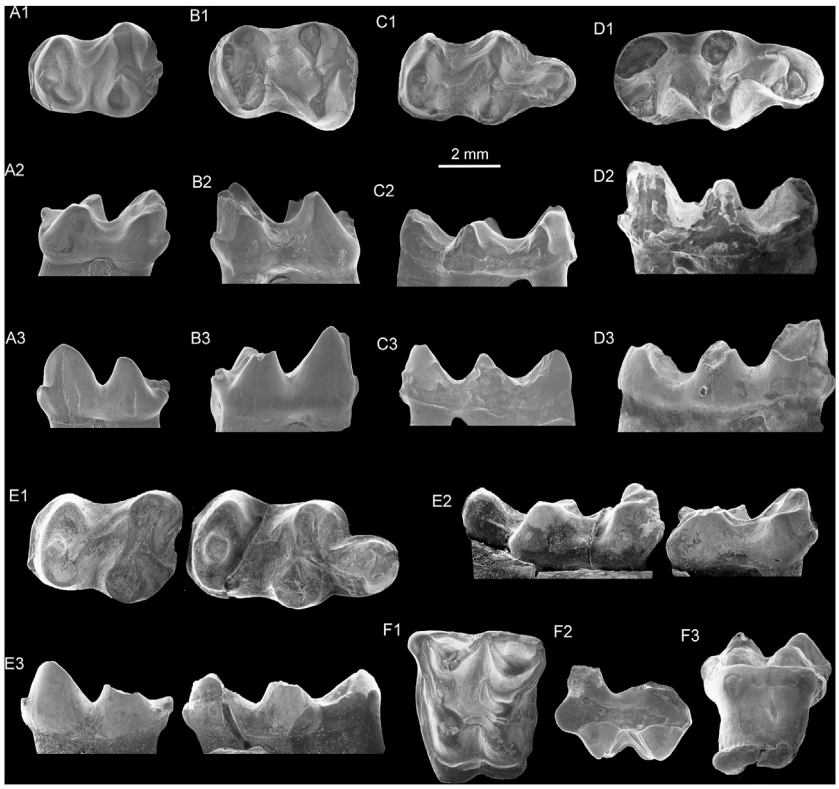

FIGURE 2
Lower molars of *Obotherium parvum* gen. et sp. nov. **(A–E)** and the upper molar of ? *Obotherium parvum* **(F)**. **(A)** right m1/2 (holotype, IVPP V 31726); **(B)** left m1/2 (V 31727.1); **(C)** right m3 (V 31727.2); **(D)** left m3 (V 31728.1); **(E)** right m2–3 (V 31729); **(F)** left M1/2 (IVPP V 31730): **(A1–F1)**, occlusal view; **(A2–F2)**, buccal view; **(A3–F3)**, lingual view.

3 Systematic paleontology

Order ARTIODACTYLA Owen, 1848
Family TAPIRULIDAE Cope, 1879
Type genus—*Tapirulus* Gervais, 1850
Included genera—type genus, *Obotherium* gen. nov., and *Tapiruloides* gen. nov.

Diagnosis—Small artiodactyls with a flat, narrow, elongated skull with reduced mastoid and relatively longer preorbital portion, without preorbital fossa; relatively wide but short brain; neopallium only slightly differentiated; dentition bilophodont in derived forms; lower molars with a transversely extended posthypocristid, a more or less complete hypolophid, an elongated, well-developed hypoconulid on m1–2, and m3 hypoconulid enlarged into a third lobe; premolars, canine, and incisors in continuous series without diastema (modified from Sudre, 1978; Erfurt and Métais, 2007).

Age and distribution—Middle Eocene to early Oligocene of Europe and Middle Eocene of Asia.

Obotherium gen. nov.
Type species—*Obotherium parvum* sp. nov.
Etymology—Obo, a pile of rocks with wood often found on the top of mesas for Heaven-worship ceremonies; Latin, *-therium*, beast.
Included species—Type and *Obotherium tongi* sp. nov.

Diagnosis—Lower molars with anteroposteriorly compressed trigonid, talonid wider than trigonid, entoconid slightly more anteriorly placed to hypoconid, and cristid obliqua extended to the point buccal to the midpoint of the protocristid; p3 trenchant, p4 with well-developed metaconid and distinct paraconid.
Differential diagnosis—Differs from *Tapirulus* by an entoconid more anteriorly placed to the hypoconid on the lower molars, and premolars less elongated. Differs from *Tapiruloides* by an anteriorly slanted trigonid, a less complete hypolophid, a distinct cristid obliqua on the lower molars, and a less sharp hypoconulid on m3.
Age and distribution—Middle Eocene of Asia.

Obotherium parvum sp. nov.
(Figures 2A–E; Table 1)
Holotype—IVPP V 31726, a right m1/2 (Figure 2A).
Etymology—Latin, *parvus*, little; in allusion to its small size.
Type locality and horizon—Irdin Manha Formation, Irdin Manha, Erlian Basin (field no. 11107). Irdinmanhan ALMA.
Paratype—IVPP V 31727.1–.2 (Figures 2B, C), a left m1/2 and a right m3 (field no. 11377); IVPP V 31728.1 (Figure 2D), a fragmentary lower jaw with a left m3 (field no. 11155). All from Irdin Manha Formation at Irdin Manha.

TABLE 1 Measurements of the lower molars of *Obotherium* and *Tapiruloides* (in mm) (*: approximate value).

		m1/2 L	m1/2 AW	m1/2 PW	m3 L	m3 AW	m3 PW
Obotherium parvum	V 31726 (holotype)	4.30	2.52	3.10			
	V 31727.1–.2	4.50	3.12	3.55	5.65	2.80	3.00
	V 31728.1				6.21	2.95	3.10
	V 31729	4.80	3.11	3.68	6.90	3.50	3.60
Obotherium aff. *O. tongi*	V 31732.1	4.82	3.15	3.50	5.91	3.10	3.30
	V 31733				5.80	2.95	3.10
	V 31734				5.90	2.98	3.12
Obotherium sp. 1	V 31735	4.30	2.50	2.89			
Obotherium sp. 2	V 31736	4.60	2.61	3.00			
Tapiruloides usuensis	V 31737 (holotype)	5.60	3.30*	3.81	6.52	3.22	3.21

Referred specimen—IVPP V 31729 (Figure 2E), a right lower jaw with m2–3, Irdin Manha Formation at Huheboerhe (field no. HIL082–1).

Differential diagnosis—Differs from *Obotherium tongi* by a less anteroposteriorly compressed trigonid with a reduced paraconid, a less complete hypolophid composed of postentocristid and posthypocristid, a bifurcated posthypocristid with one branch descending to hypoconulid on m1-2, a less posteriorly extended hypoconulid on m1-2, and a prehypoconulid cristid of m3 joining the posthypocristid.

3.1 Description

Four fragmentary lower jaws, each bearing a single molar, and a right lower jaw with m2–3 are referred to *Obotherium parvum*. The hypoconulid on IVPP V 31726, the protoconid and entoconid on V 31727.1, and nearly all tips of the cuspids show partial breakage, except the hypoconid on V 31728.1.

The trigonid of m1/2 is anteroposteriorly compressed with the metaconid lingual to the protoconid. The protoconid and hypoconid are lower than the metaconid and entoconid, respectively. The protocristid is more heavily worn on the posterior wall than the paracristid on the holotype. The paracristid is slightly notched with an indistinct paraconid on the holotype or a small one anterobuccally placed to the protoconid on the paratype. The talonid is considerably wider, longer, and slightly lower than the trigonid. The hypoconid is more buccally placed than the protoconid, extending a cristid obliqua anterolingually to the base and slightly buccal to the midpoint of the protocristid. The entoconid is slightly more anteriorly placed than the hypoconid. The hypolophid of the preultimate molar is somewhat interrupted at the conjunction of posthypocristid and postentocristid, and the postentocristid is transversely extended. The posthypocristid is nearly transversely extended and diverges into two ridges near its lingual extremity: one descends posteriorly to the hypoconulid, and another short one is anterolingually extended, joining the postentocristid. Although the hypoconulid is partially broken on both V 31726 and V 31727.1, it is a low cuspid rising from a distinct postcingulid, slightly lingually placed to the median of the posterior border, and does not expand posteriorly. The precingulid is relatively weaker than the postcingulid, while the buccal and lingual cingulids are absent.

The m3 is similar to m1/2 in morphology but differs from the latter in having a talonid slightly wider than the trigonid, an entoconid nearly lingually placed to the hypoconid, and the hypoconulid enlarged into a third lobe. The transverse posthypocristid slightly posteriorly descends to the median between the hypoconid and entoconid, where it joins the distinct prehypoconulid cristid. The hypoconulid lobe is relatively long and high. A ridge along the lingual border of the hypoconulid lobe is distinct on V 31728.1, weak on V 31727.2, and nearly absent on V 31729. The buccal cingulid at the base of the hypoconulid lobe is weak or absent. A weak precingulid is present as in m1/2.

3.2 Comparisons

With Homacodontidae—Among early artiodactyls, *Obotherium* is more similar to the mainly Homacodontidae and Dichobunidae; however, both are considered to be paraphyletic. The early Eocene *Hexacodus* from the North American Wasatchian was initially only known from two lower jaws representing two species, *H. pelodes* and *H. uintensis* (Gazin, 1952). Gazin (1962) assigned several upper cheek teeth and a lower jaw to *Hexacodus* cf. *H. pelodes*. The genus *Hexacodus* is probably paraphyletic (Gazin, 1962; Stucky, 1998). *Obotherium parvum* is similar to *Hexacodus pelodes* in having: 1) an anteroposteriorly compressed trigonid on the lower molars with the paraconid closely appressed to the metaconid; 2) the metaconid lingual to the protoconid; 3) the talonid wider than the trigonid on m1-2; and 4) the posthypocristid transversely extended with its lingual end sending a weak spur posteriorly to the hypoconulid. The lower molars of *Hexacodus pelodes* differ from those of *Obotherium parvum* in having the cristid obliqua more lingually extended to the midpoint of the protocristid, the isolated entoconid lingual to the hypoconid without the postentocristid (m2 likely with a short postentocristid on USNM 19215),

hypoconulid more lingually placed, distinct buccal cingulids, and m3 hypoconulid much smaller.

The early-middle Eocene homacodontids from the North American Bridgerian are represented by small *Microsus* and relatively larger *Homacodon* (Stucky, 1998), similar to *Obotherium parvum* in having above characters 1–3. *Microsus* resembles *Obotherium parvum* in having a transversely extended posthypocristid on the lower molars and the postentocristid of m2 joining posthypocristid (Sinclair, 1914, fig. 22–23). *Microsus* sp. (USNM 364914 and other USNM specimens) has a hypolophid that connects hypoconid and entoconid, and a strongly developed prehypoconulid cristid intersecting the posthypocristid at a 90° angle (Stucky, 1998); the relatively complete hypolophid in *Microsus* sp. is similar to *Obotherium parvum*. The lower molars of *Homacodon* have bunodont lingual cuspids and buno-selenodont buccal cuspids with posthypocristid posterolingually directed to the hypoconulid (Sinclair, 1914), unlike the transversely extended posthypocristid in *Obotherium*, *Hexacodus*, and *Microsus*. However, the hypoconulid of m1-2 in *Homacodon* is nearly medially placed on the postcingulid as in *Obotherium parvum*.

The North American Uintan homacodontids, including *Bunomeryx*, *Hylomeryx*, *Pentacemylus*, *Mytonomeryx*, and *Mesomeryx*, are separated from other homacodontids as a family Bunomerycidae by Gentry and Hooker (1988). The relationship between Uintan homacodontids and later artiodactyls is controversial in that some genera are probably closely related to Tylopoda, while others are close to Ruminantia (Stucky, 1998; Norris, 1999). The lower molars of Uintan homacodontids differ from *Obotherium parvum* in their preselenodont condition: paracristid deeply but narrowly notched (Gentry and Hooker, 1988), cristid obliqua more lingually extended, and hypoconid selenodont with posthypocristid usually posterolingually extended to the lingually placed hypoconulid (Gazin, 1955). *Mesomeryx* is as small as *Microsus cuspidatus* and is known from the upper teeth (Peterson, 1919; Gazin, 1955). The lower molars of *Bunomeryx* differ from those of other Uintan homacodontids in that the posthypocristid is more transversely extended and descends posteriorly at an angle to behind the entoconid (Stucky, 1998), and a weak cristid present on the buccal surface of the entoconid on m1-2 as in *Obotherium parvum*. However, the hypoconulid of m1-2 in *Obotherium parvum* is more medially placed. *Hylomeryx* comprises two species *H. annectens* and *H. quadricuspis* (Peterson, 1919; Gazin, 1955). The lower cheek teeth of *H. quadricuspis* (CM 2346) are heavily worn and crescentic, but the conditions in *H. annectens* are confusing. The holotype of *H. annectens* (CM 2335) has a transversely extended hypolophid more distinct than a weak posthypocristid on m1-2 (Peterson, 1919, Pl. 36, Fig. 6), whereas the paratype of *H. annectens* (CM 2944) has a distinct crescentic hypoconid with the distinct posthypocristid posterolingually extended on m1-3 (Peterson, 1919, Fig. 10). In general, *Obotherium parvum* is similar to Uintan homacondontids in having a small size, enlarged hypoconulid lobe on m3, and crescentic hypoconid on the lower molars. However, *Obotherium parvum* shows some more basal characters on the lower molars: a complete or shallowly notched paracristid, a more distinct paraconid, and the talonid considerably wider than the trigonid.

Limeryx and *Asiohomacodon* from Asia were provisionally assigned to Homacodontidae or Homacodontinae (Tsubamoto et al., 2003; Métais et al., 2005; Theodor et al., 2007), and they show bunoselenodont or fully selenodont teeth which differ from *Obotherium parvum*.

With Dichobunidae—Dichobunidae is composed of four subfamilies: Dichobuninae, Eurodexeinae, Lantianiinae, and Hyperdichobuninae (Theodor et al., 2007). Dichobuninae is restricted to Europe from the early Eocene to the late Oligocene, and is generally more bunodont than *Obotherium parvum* (Theodor et al., 2007). Oligocene dichobunines *Synaphodus* and *Metriotherium* with selenodont dentition are considerably larger than *Obotherium parvum*, although a lophid-like cristid joins the hypoconid and entoconid on the lower molars in *Metriotherium* (Lavocat, 1951; Theodor et al., 2007). The lower molars of Eocene dichobunines differ from those of *Obotherium parvum* by larger size, more bunodont teeth, and smaller and shorter hypoconulid on m3. *Messelobunodon* is further distinguished by an isolated paraconid on the lower molars, and *Neufferia* is characterized by the hypoconid and entoconid divided by a deep valley without hypoconulid (Franzen, 1981; Franzen, 1994; Theodor et al., 2007). *Dichobune* is comprised of five species ranging from the middle Eocene to the early Oligocene (Theodor et al., 2007). *Dichobune* differs from *Obotherium parvum* by the rounded, more or less isolated metaconid and entoconid, crescentic protoconid and hypoconid, a weak ridge between the hypoconid and the entoconid (in *Dichobune jehenni* and *D. leporinum*), and the hypoconulid distinct or absent (in *D. leporinum*) (Stehlin, 1906; Sudre, 1978; Brunet and Sudre, 1980; Hooker and Weidmann, 2000).

Eurodexeinae comprises four genera (*Eygalayodon*, *Lutzia*, *Eurodexis*, and *Parahexacodus*) and ranges from the late early Eocene to early middle Eocene (MP10 to MP13 or 14) in Europe (Erfurt and Sudre, 1996; Theodor et al., 2007). This group is similar to North American basal homacodontids and *O. parvum* in having a small size, anteroposteriorly compressed trigonid with reduced paraconid on the lower molars, and the posthypocristid transversely extended joining the postentocristid if present (Sudre and Erfurt, 1996). However, these are probably a result of similar ecological adaptation, and eurodexeines are rooted in the European stock of *Diacodexis* (Sudre and Erfurt, 1996; Theodor et al., 2007). Lower molars of Eurodexeinae differ from those of *Obotherium parvum* in having trigonid much higher than the talonid, talonid lingually enclosed by the preentocristid (in *Eurodexis*, *Parahexacodus*, and *Eygalayodon*), entoconid lingual or posterior to the hypoconid, posthypocristid not bifurcated, and m3 hypoconulid relatively small but stout (Sudre and Erfurt, 1996; Theodor et al., 2007).

The middle-late Eocene Hyperdichobuninae is comprised of *Hyperdichobune* and *Mouillacitherium*, and represents a poorly known miniature, primitive group (Gentry and Hooker, 1988; Hooker and Weidmann, 2000; Theodor et al., 2007). *Hyperdichobune* comprises five species known from MP13 to MP 19 (Theodor et al., 2007), and four species of the genus were initially assigned to *Dichobune* (Stehlin, 1906; 1910). The lower molars of *Hyperdichobune* show some similarities with those of *Obotherium parvum* in having a talonid wider than trigonid (in *H. langi*), entoconid slightly more anteriorly placed to the hypoconid (in *H. langi* and *H. nobilis*), a connection between the hypoconid and

entoconid on m2 (in *H. nobilis*), and enlarged hypoconulid lobe on m3 (Stehlin, 1906; 1910; Sudre, 1972). The lower molars of *Hyperdichobune* mainly differ from those of *Obotherium parvum* in having an isolated, rounded entoconid, relatively weak crescentic hypoconid with posthypocristid directly joining the hypoconulid (Stehlin, 1906; 1910; Sudre, 1972). *Mouillacitherium* comprises three species that form a lineage from *M. cartieri via M. schlosseri* to *M. elegans*, and ranges from MP14 to MP18 (Sudre, 1978; Theodor et al., 2007). The lower molars of *Mouillacitherium* mainly differ from those of *Obotherium parvum* in having acute metaconid and entoconid, crescentic protoconid and hypoconid, and distinct preentocristid and postmetacristid, although there is a tendency to form a connection between the hypoconid and entoconid in *Mouillacitherium* (Stehlin, 1906; Stehlin, 1910; Sudre, 1978).

Lantianiinae is restricted to the middle Eocene of Asia, comprising *Lantianius, Eolantianius*, and *Elaschitotherium* (Métais et al., 2004; Theodor et al., 2007). *Elaschitotherium* is known from the middle Eocene Shanghuang fissure-filling of Jiangsu, China (Métais et al., 2004; Métais et al., 2008). The lower molars of *Elaschitotherium* are similar to those of *Obotherium parvum* in having an anteroposteriorly compressed trigonid on m2-3, the talonid wider than the trigonid, the entoconid slightly anterior to the hypoconid, a transversely extended posthypocristid, and a cristid obliqua more buccally extended. The lower molars of *Elaschitotherium* differ from those of *Obotherium parvum* in having a conical, isolated entoconid, a slightly transversely compressed metaconid, an incipient preentocristid (in *E. crepaturus*), more lingually placed hypoconulid on m1-2, and a relatively smaller m3 hypoconulid. The m1 of *Elaschitotherium qii* (IVPP V 12759.47) varies in possessing a complete hypolophid as in *Obotherium parvum* (Métais et al., 2004, Fig. 2G), but the former has a deeply notched hypolophid to which the prehypoconulid cristid is directly oriented.

Eolantianius russelli known from the middle Eocene Andarak 2, Kyrgyzstan is represented by DP4 and upper molars (Averianov, 1996; Averianov and Godinot, 2005), showing a striking resemblance to *Elaschitotherium qii* (Métais et al., 2004). An isolated m2 and m3, tentatively assigned to ? *Eolantianius russelli* by Averianov (1996), are very similar to those of *Obotherium parvum* in a smaller size, a reduced paraconid, a talonid wider than the trigonid, a more buccally directed cristid obliqua, entoconid anterior to hypoconid, nearly complete hypolophid, transversely extended posthypocristid, a large, medially placed hypoconulid joining the posthypocristid by a cristid, and an enlarged hypoconulid lobe on m3. However, m2-3 of ?*Eolantianius russelli* differs from *Obotherium parvum* by a less compressed trigonid. Absent the upper molar of ? *Obotherium parvum* described below, we might have assigned the lower dentition from the Erlian Basin to ? *Eolantianius;* however, it is uncertain whether m2-3 of ? *Eolantianius russelli* was unearthed from the same horizon as the upper molars from Andarak II (Russell and Zhai, 1987). It seems likely that the lower molars assigned to ? *Eolantianius russelli* represent a different taxon from the uppers of *Eolantianius russelli*, and should be transferred to *Obotherium*.

With *Tapirulus*—*Tapirulus* is a European artiodactyl known from the middle Eocene to the early Oligocene (Erfurt and Métais, 2007), *Tapirulus* currently consists of five species that succeed each other in a chronocline and is characterized by its bilophodont tooth pattern (Stehlin, 1910; Sudre, 1978; Hooker and Weidmann, 2000; Erfurt and Métais, 2007). Its phylogenetic position is controversial, and the genus has been included in Dacrytheriinae (or Dacrytheriidae) (Viret, 1961; Sudre, 1978; McKenna and Bell, 1997), a tylopod *incertae sedis* (Hooker and Weidmann, 2000), or Choeropotamidae (Hooker and Thomas, 2001; Erfurt and Métais, 2007). *Tapirulus majori* (MP13) and *T. depereti* (MP 14) are fragmentary, but the lower molars are strikingly similar to *Obotherium parvum,* having an anteroposteriorly compressed trigonid with a reduced paraconid, an incomplete transverse ridge between the hypoconid and entoconid, a posthypocristid descending a cristid to a relatively distinct hypoconulid, and the talonid slightly wider than the trigonid (Stehlin, 1910). However, the hypoconulid is more posteriorly extended in *Tapirulus majori*, *T. depereti* than in *Obotherium parvum*, and the former two species have the entoconid nearly lingual to the hypoconid (Stehlin, 1910, Pl. 19, fig. 24, 30). These two characters are consistent with later species of *Obotherium* described below. The lower molars of *Tapirulus schlosseria* from MP 16 have a second ridge rising from the hypoconulid to the hypolophid (Stehlin, 1910, p. 1075), somewhat reminiscent of those of *Obotherium parvum*. Late middle Eocene–early Oligocene *Tapirulus perrierensis* and *T. hyracinus* are characterized by more bilophodont teeth (Stehlin, 1910; Sudre, 1978), nearly identical to the new material of a left lower jaw with m2-3 (IVPP V 31737) from Ula Usu described below.

Obotherium parvum is more similar to *Tapirulus majori* and *T. depereti* than to any other early artiodactyls, suggesting a close relationship. Both *Obotherium* and *Tapirulus* likely descended from early North American homacodontids. The new species is assigned to a new genus *Obotherium* rather than to *Tapirulus*, because the differences between the new species and the type species of *Tapirulus* (T. *hyracinus*) warrant generic distinction; it is possible that *Tapirulus majori* and *T. depereti* differ from other species of *Tapirulus* at the generic level (Stehlin, 1910) and are more reasonably included in *Obotherium*.

? *Obotherium parvum*

Material—IVPP V 31730, a left M1 (Figure 2F).

Locality and horizon—Irdin Manha Formation, Irdin Manha escarpment (field no. 13054), Erlian Basin.

3.3 Description

The M1 is quadrate in outline and brachydont (Length: 4.40 mm; Anterior Width: 4.90 mm; Posterior Width: 4.65 mm). The ectoloph is W-shaped with a buccally flexed centrocrista. The preparacrista extends from the paracone to the posterobuccal side of the parastyle. The parastyle is distinct and anteriorly projected, while the mesostyle is weak and represented by a bulge from the cingulum. The metastyle is absent. The metacone is slightly larger and more lingually appressed than the paracone. The buccal surfaces of the paracone and metacone are nearly flat, and a faint rib is present on the metacone. The protocone is at the level of the paracone without a postprotocrista. The paraconule is small, indistinct, and closer to the protocone than to paracone. The protoloph, composed of preprotocrista and preparaconule crista, is complete and joins the

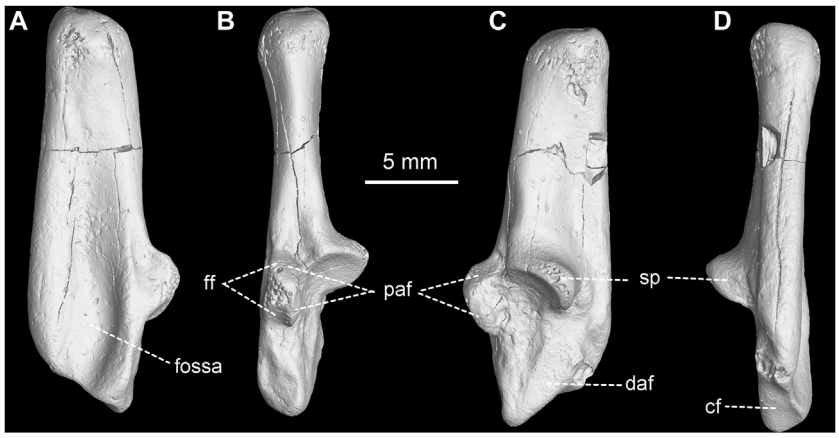

FIGURE 3
Right calcaneus of Tapirulidae gen. et sp. indet. (IVPP V 31728.2). **(A)** lateral view; **(B)** anterior view; **(C)** medial view; **(D)** posterior view. Abbreviation: *cf*, cuboid facet; *daf*, distal astragalar facet; *ff*, fibular facet; *paf*, proximal astragalar facet; *sp*, sustentacular process.

parastyle. The hypocone is large and conical, slightly more lingually placed than the protocone, and more anteriorly situated than the metacone. A well-developed prehypocrista extends anterobuccally from the hypocone to the middle valley, then curves towards the protocone for a short distance before joining the apex of the protocone, enclosing the lingual opening of the middle valley. The metaconule is crescentic and separated from the hypocone by a narrow groove. The premetaconule crista extends from the metaconule to the anterolingual base of the metacone; the postmetaconule crista is longer and joins the postmetacrista at the base. The cingula are complete and continuous around the anterior, lingual, and posterior bases of the crown with the lingual one relatively stronger. Worn facets are present along the postcingulum, the buccal half of the precingulum, and the middle of the lingual cingulum. The buccal cingulum is complete and weak.

3.4 Comparisons

The morphology of this isolated upper molar shows some similarities with Uintan homacodontids, including a quadrate outline of the crown, selenodont, a W-shaped ectoloph, a well-developed hypocone on M1 and/or M2 (except *Mesomeryx* and *Pentacemylus*), and a selenodont metaconule (Gazin, 1955). The reduced paraconule and weak mesostyle in IVPP V 31730 are more similar to *Hylomeryx* than to other Uintan homacodontids, but *Hylomeryx* has a more bunodont paracone and metacone on the upper molars (Peterson, 1919; Gazin, 1955). The upper molars of Wasatchian and Bridgerian *Hexacodus* cf. *H. pelodes*, *Microsus*, and *Homacodon* are distinguished from V 31730 by more bunodont dentition, straight centrocrista, and relatively large paraconule (Gazin, 1955; Gazin, 1962; West, 1984). V 31730 is unique in having a prehypocrista towards the protocone and partially enclosing the talon lingually; similarly, the incipient hypocone rising from the cingulum on M2 of *Hexacodus* cf. *H. pelodes* also extends a slight crest toward the protocone (Gazin, 1962).

The combination of W-shaped ectoloph, well-developed hypocone, a quadrate outline of the crown, and lack of postprotocrista toward the metaconule in V 31730 is distinguishable from Dichobunidae (Erfurt and Métais, 2007; Theodor et al., 2007). *Dichobune*, with quadrate outline and distinct hypocone on the upper molars, also differs from V 31730 in having the protoloph descending towards the anterior cingulum before reaching the anterobuccal corner of the crown (Sudre, 1978). Although the upper molars of Lantianiinae are clearly different from V 31730, *Eolantianius* is more similar to V 31730 in having a subquadrate outline of the crown, distinct parastyle, and a faint paraconule without a postparaconule crista than *Elaschitotherium* (Averianov, 1996; Métais et al., 2004). However, these similarities are more probably attributable to parallel evolution rather than a close phylogenetic relationship, considering the bunodont paracone and metacone and straight ectoloph in *Eolantianius*.

The upper molars of *Tapirulus majori*, *T. depereti*, and *T. schlosseri* from MP13 to MP16 are rare and mostly known from isolated teeth, however, *Tapirulus perrierensis* and *T. hyracinus* from late Eocene to the early Oligocene are known from complete maxilla and skull (Stehlin, 1910; Sudre, 1978; Erfurt and Métais, 2007). *Tapirulus majori* and *T. depereti* resemble V 31730 in having a distinct parastyle, relatively weak paraconule on the upper molars, and crescentic metaconule. *Tapirulus depereti* is similar to V 31730 in having a W-shaped ectoloph on the upper molars, while the centrocrista of the upper molar is nearly straight or slightly buccally flexed in *T. majori* (Stehlin, 1910). *Tapirulus schlosseri*, *T. perrierensis* and *T. hyracinus* possess W-shaped ectoloph on the upper molars, but they are distinguished by the advanced bilophodont dentition with compressed, transversely extended protoloph and metaloph (Stehlin, 1910). The most conspicuous difference between V 31730 and the middle Eocene *Tapirulus* is the lack of hypocone on the known upper molars in *Tapirulus*. However, the upper molars of the middle Eocene *Tapirulus* are fragmentary and only known from M2 or M3, and it is possible that M1 possesses a distinct hypocone as in V 31730 since the hypocone can be very

FIGURE 4
Right lower jaw of *Obotherium tongi* gen. et sp. nov. with p3-m3 and alveoli of canine, p1, and root of p2 (IVPP V 31731). **(A)** occlusal view; **(B)** buccal view; **(C)** lingual view.

variable on different molars. The M1 hypocone is well-developed but absent or highly reduced on M2–3 in *Bunomeryx*, while it is present on M1–2 but absent on M3 in *Homacodon*, *Microsus*, *Hylomeryx*, and *Mytonomeryx* (Gazin, 1955; Theodor et al., 2007).

The specimen V 31730 was also discovered from the Irdin Manha Formation at Irdin Manha as the holotype and paratype of *Obotherium parvum*. They both have a similar evolutionary level with the Uintan homacodontids and strikingly resemble *Tapirulus*, indicating V 31730 probably represents the upper molar of *Obotherium parvum*. However, pending the discovery of more material of the upper cheek teeth of this small artiodactyl, we tentatively assigned the specimen to *Obotherium parvum* with a question mark.

Gen. et sp. indet.

Material—IVPP V 31728.2 (Figure 3), a left calcaneus from the Irdin Manha Formation at Irdin Manha (field no. 11155).

3.5 Description

The calcaneus is discovered from the same pit as V 32728.1, a left lower jaw with m3 of *Obotherium parvum*, so it may belong to *O. parvum* considering their comparable small size. The calcaneus (IVPP V 31728.2) is strongly lateromedially compressed (Figure 3). The lateral surface of the calcaneus has a moderately deep fossa on the distal two-thirds length presumably for the attachment of the calcaneofibular ligaments. The fibular facet on the ectal process is proximodistally convex with the long axis parallel to that of the calcaneus. However, its proximal half is confluent with astragalar facet and seems very narrow. The proximal astragalar facet is composed of two parts: one on the medial side of the distal half of the fibular facet, and the other occupies the proximal surface of the ectal process. A shallow fossa is present proximal to the ectal process. There is a flat, triangular distal astragalar facet on the medial side of the calcaneus. The sustentacular process is weakly medially projected with a rounded, concave facet, which is oriented more distally than anteriorly. The sustentacular facet is continuous with the medial surface of the ectal process. Distally, the cuboid facet is narrow, flat, and distoposteriorly directed.

Calcaneus Measurements (mm): Length=21.80; Proximal width=3.93; Minimum width of shaft=2.47; Width at sustentaculum=5.40; Distal width=2.72; Dorsoplantar depth of tuber=4.93; Depth at ectal process=8.07; Depth at distal end=6.14.

3.6 Comparisons

This calcaneus is compared with *Diacodexis* and *Bunophorus* (Guthrie, 1968; Kumar et al., 2010). This calcaneus differs from

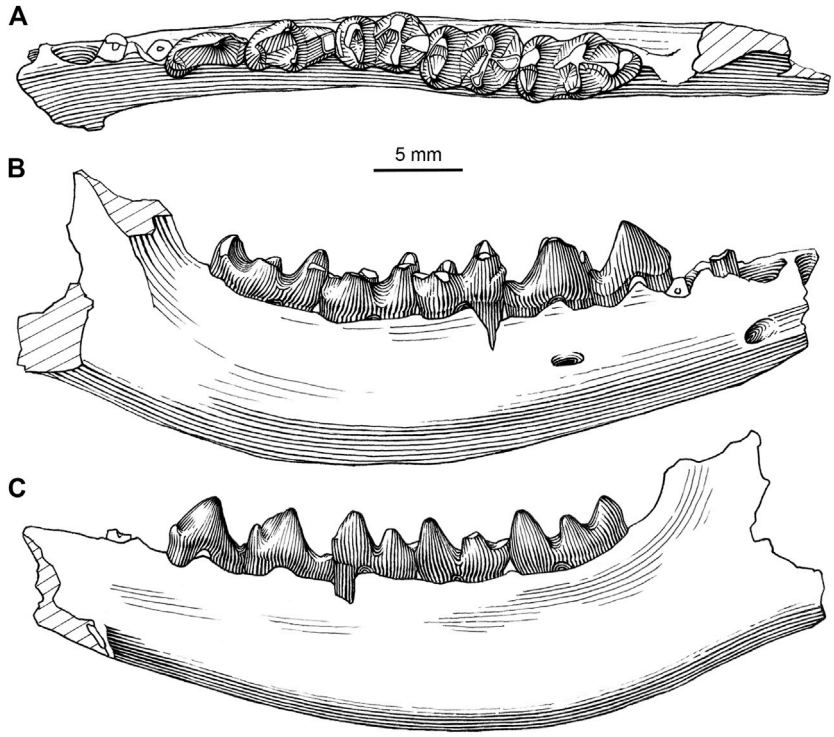

FIGURE 5
Line drawing of the right lower jaw of *Obotherium tongi* gen. et sp. nov. with p3-m3 and alveoli of canine, p1, and root of p2 (IVPP V 31731). **(A)** occlusal view; **(B)** buccal view; **(C)** lingual view.

Diacodexis and *Bunophorus* by a relatively longer calcaneal tuber, a less medially projected sustentaculum, nearly confluent astragalar and fibular facets on the proximal half of the ectal process (Guthrie, 1968; Kumar et al., 2010). The calcaneus of *Diacodexis* has a relatively deeper fossa on the lateral side and a more distinct peroneal process than IVPP V 31728.2 (Kumar et al., 2010).

Obotherium tongi sp. nov.
(Figures 4, 5; Table 2)

Holotype—IVPP V 31731, a nearly complete right lower jaw with p3-m3.

Etymology—Named in honor of Prof. Yong-Sheng Tong for his contribution to the Paleogene mammals from China.

Differential diagnosis—Differs from *Obotherium parvum* by a more anteroposteriorly compressed trigonid without a paraconid, a more complete hypolophid with a long prehypoconulid cristid joining the middle of the hypolophid on m1-2 or directed to the lingual side of the hypoconid on m3, and a more posteriorly extended hypoconulid on m1-2.

Type locality and horizon—the upper part of the "Basal White" layer at Erden Obo (field no. 10227), Erlian Basin. Irdinmanhan ALMA.

3.7 Description

The horizontal mandibular ramus is slender and relatively shallow with a convex ventral border. The depth of the horizontal ramus is nearly consistent and becomes slightly shallower anteriorly. Two mental foramina are preserved: The anterior one is rounded, below p1, while the posterior one is elongated and below p4. The posterior border of the symphysis is at about the level of the anterior border of the p2.

The lower canine and the cheek teeth are closely spaced without diastema. The partial canine alveolus is preserved and nearly vertical, indicating canine is larger than p1. The alveolus of p1 is a relatively large anteroposteriorly elongated oval. The p2 preserves two roots with the posterior one situated anterobuccal rather than anterior to the p3 paraconid. The crown of p3 is laterally compressed and composed of a main, sharp cuspid. Two cristids descend from the main cuspid: a short, slightly convex anterior one descends to a faint paraconid, while a long, slightly concave one terminates in a low, distinct hypoconid. The cingulid is absent on p3.

The trigonid of p4 is wider, longer, and higher than the talonid. The metaconid is as large as the protoconid, lingually and slightly posteriorly situated to the latter. The protocristid, the widest portion of the crown, is moderately notched. The paracristid is distinct, nearly anteriorly extended from the protoconid. The paraconid is prominent and medially placed, separated from the paracristid by a relatively deep notch. The talonid tapers posteriorly and its posterolingual part is broken. The buccally placed hypoconid seems more distinct than that of p3. The feeble cristid obliqua ascends from the hypoconid to the point below the notch of the protocristid.

The lower molars are slightly worn, increasing in size posteriorly. Trigonid of m1 is strongly anteroposteriorly

TABLE 2 Comparative measurements of *Obotherium tongi* and other related taxa. (in mm) (*: approximate value; #: measured from the plate).

	Obotherium tongi	*Tapirulus perrierensis*	*Tapirulus hyracinus*	*Hexacodus pelodes*	*Microsus cuspidatus*	*Homacodon vagans*
	V 31731	Sudre (1978)		Gazin (1952)	West (1984)	
p1 L	2.50*					
p W	1.30*					
p2 L	3.80*		7			
p2 W	1.50*		2.5			
p3 L	4.72	6	7.2			
p3 W	1.80	2	2.8			
p4 L	5.00	5	6.5	4.5	4.15	5.23
AW/PW	2.85/2.10	2.5	3–3.6	2.8	2.35/2.78	2.77
m1 L	5.21	5–5.3	6–6.6	4.2	4.28	5.25
AW/PW	3.00/3.30	2.8–3	3.1–4.4	3.0	2.5/2.78	3.48/3.88
m2 L	5.43	5.5	6.2–7.1	4.4	4.3	5.40
AW/PW	3.41/3.78	3.2	3.6–4.2	3.7	2.9/3.2	4.0/4.27
m3 L	6.80	6.3–7.5	6.5–7.4	4.75#	5.05	6.77
AW/PW	3.41/3.40	2.8–3	3.2–4.1	2.63#/2.75#	3.03/2.95	4.0/3.7
p1–4 L	15.78		27.1#			
m1–3 L	16.66		21.5#			

compressed with the metaconid lingual to the protoconid. The protoconid and hypoconid are lower than the metaconid and entoconid, respectively. Both protocristid and paracristid are moderately notched and join the apex of the metaconid. The paracristid forms an angled arch anteriorly, while the protocristid is nearly transversely extended. The paraconid is absent. The talonid is considerably wider, longer, and slightly lower than the trigonid. The hypoconid is more buccally placed than the protoconid, extending a cristid obliqua anterolingually to the half height of the protocristid and to the midpoint (or slightly buccal to the notch) of the protocristid. A worn facet is present on the anterobuccal side of the hypoconid. The entoconid is more anteriorly placed than the hypoconid. The hypolophid is complete, widely notched, and slightly anterolingually oblique. The medially placed hypoconulid is well-developed but heavily worn, joining the midpoint of the hypolophid by a long prehypoconulid cristid. The hypoconulid forms a relatively large third lobe with a somewhat pointed posterior border. A narrow worn facet is present along the posterobuccal border of the hypoconulid. The precingulid is distinct, while the cingulids are absent on other sides of the crown.

The m2 is morphologically similar to m1, but the metaconid and entoconid are slightly more anteriorly placed relative to their opposite cuspids than in m1. Furthermore, the hypoconulid joins the hypolophid slightly buccal to the midpoint, and the posterior border of the crown is more rounded. The m1 is placed slightly buccal to the m2, and the hypoconulid of m1 is situated anterior to the protoconid of m2. The morphology of m3 differs from that of m1-2, having a paracristid interrupted at the notch, a talonid slightly wider than the trigonid, a weaker hypolophid with a more isolated entoconid and a bunodont hypoconid, and the entoconid nearly lingual to the hypoconid. The hypoconulid of m3 expands into a large lobe with a prehypoconulid cristid joining the posterolingual side of the hypoconid.

3.8 Comparisons

The lower molars of *Obotherium tongi* share the following characters with *O. parvum*: an anteroposteriorly compressed trigonid, a well-developed hypolophid, an entoconid slightly anteriorly situated to the hypoconid, a distinct, nearly medial-placed hypoconulid on m1-2, a talonid wider than a trigonid on m1-2, a cristid obliqua extending slightly buccal to the midpoint of the protocristid, and a large hypoconulid lobe on m3. The lower molars of *Obotherium tongi* are more advanced than those of *O. parvum* in having a more compressed trigonid without a paraconid, a more complete hypolophid with a long prehypoconulid cristid joining the middle of the hypolophid on m1-2 or directed to the lingual side of the hypoconid on m3, and a more posteriorly extended hypoconulid on m1-2. *Obotherium parvum* and *O. tongi* are clearly closely related, and the latter provides morphologic information about *Obotherium* unknown in *O. parvum*.

The lower jaw of *Obotherium tongi* is characterized by the convex ventral border and concave alveolar border, more similar to the arctocyonid *Chriacus* than to *Diacodexis* (Rose, 1996). The

horizontal ramus of the lower jaw in *Diacodexis* is slender and shallow with a nearly straight ventral border, and becomes slightly shallower forwards (Boivin et al., 2018). A fragmentary lower jaw of *Diacodexis indicus* (GU 1622) with a convex ventral border and consistent height between m3 and m1 is unlike other specimens of the same species (Kumar et al. (2010), the differences attributed to sexual dimorphism. Short diastemata are usually present among the teeth from the canine to p3 in *Diacodexis* (Kumar et al., 2010; Boivin et al., 2018), while the premolars and canine of *Obotherium tongi* are closely spaced without diastemata. The shallow lower jaw of *Homacodon* has a less convex ventral border and nearly straight alveolar border compared to *Obotherium tongi* (West, 1984), while lower jaws of other homacodontids, such as *Hylomeryx*, *Mytonomeryx*, and *Pentacemylus*, have a deeper horizontal ramus that shallows anteriorly with nearly straight ventral and alveolar borders (Peterson, 1919; Gazin, 1955). Lower premolars and canine are closely spaced without diastemata in *Homacodon,* the paratype of *Hylomeryx annectens* (CM 2944), and in *Obotherium tongi* (Peterson, 1919; West, 1984). Diastemata are variably present among lower premolars and canine in *Bunomeryx elegans*, *Mytonomeryx*, and *Pentacemylus* (Peterson, 1919; Gazin, 1955). Similarly, the lower jaws of dichobunines (i.e., *Dichobune leporine*), hyperdichobunines (i.e., *Mouillacitherium elegans*), and eurodexeines (i.e., *Eurodexis ceciliensis*, *Parahexacodus germanicus*) can be distinguished from *Obotherium tongi* by the straight or slightly convex ventral border, a straight alveolar border, and diastemata variably present among premolars and canine (Sudre, 1978; Erfurt and Sudre, 1996).

Relatively complete lower jaws of *Tapirulus* are only known from *T. schlosseri* and *T. hyracinus* (Stehlin, 1910). They differ from *Obotherium tongi* in having a straight ventral border and alveolar border, and horizonal ramus becoming shallower forwards. The canine and the premolars are also spaced closely together in *T. schlosseri* (Stehlin, 1910, fig. 216), while short diastemata are present among premolars in *T. hyracinus* (Stehlin, 1910, fig. 217).

The well-developed metaconid on p4 in *Obotherium tongi* is similar to Uintan homacondontids, while the metaconid is absent or incipient in *Hexacodus* and *Homacodon*, and relatively smaller in *Microsus* (Sinclair, 1914; Gazin, 1955). The p4 of dichobunids usually also has a distinct metaconid as in *Obotherium tongi* (Theodor et al., 2007). The p4 of *Tapirulus* (excluding *T. majori,* whose p4 is not preserved) has a distinct metaconid, but p3 of *T. schlosseri*, *T. perrierensis*, and *T. hyracinus* have a much more distinct paraconid and a well-developed cuspid posterior to the protoconid (Stehlin, 1910; Sudre, 1978). The premolar series is elongated and relatively longer than the molar series in later *Tapirulus*, such as *T. schlosseri* and *perrierensis* (Table 2), whereas the premolar series is slightly shorter than the molar series in *O. tongi*.

The convex ventral border and alveolar border of the lower jaw in *Obotherium tongi* are different from those of early artiodactyls, but show some similarities with the arctocyonid *Chriacus* and ruminant *Archaeomeryx* (Vislobokova, 2002). The closely spaced premolars and canine, and distinct metaconid on p4 in *Tapirulus* also support a close phylogenetic relationship with *Obotherium*.

Obotherium aff. *O. tongi*
(Figure 6; Table 1)

Material—IVPP V 31732.1–2 (Figures 6A, D), a left lower jaw with m1 talonid and m2–3, and a left astragalus, the Ulan Shireh Formation, North Mesa; IVPP V 31733 (Figure 6B), a right lower jaw with m3, the Irdin Manha Formation, Huheboerhe (field no. 13069); IVPP V 31734 (Figure 6C), a left lower jaw with m3, the Irdin Manha Formation, Huheboerhe (field no. HIL 174).

3.9 Description

The lower molars of V 31732.1 from Ulan Shireh are similar to those of *O. tongi* in morphology, but the former has a smaller size, a more erect trigonid, a more complete hypolophid, a more reduced hypoconulid on m1–2 with a weak prehypoconulid cristid, a more pointed hypoconulid on m2, and the prehypoconulid cristid of m2-3 joining the midpoint of the hypolophid as in m1. The ventral border of the horizontal ramus is nearly straight. The lower jaw with m1-3 shows some more derived characters than that of *O. tongi*, but due to the lack of more complete material and information about dental variation in *O. tongi*, we tentatively assign the lower jaw to *Obotherium* aff. *O. tongi* instead of a new species of *Obotherium*.

Two lower jaws with left and right m3 from the Irdin Manha Formation at Huheboerhe are assigned to *Obotherium* aff. *O. tongi*. They are similar to V 31732.1 in having a small size, a more complete hypolophid, a prehypoconulid cristid joining the midpoint of the hypolophid, and the hypoconulid lobe relatively small.

A left astragalus (IVPP V 31732.2) is presumed, being found close by IVPP V 31732.1, and represents the same species (Figure 6D). The proximal and distal trochleae are somewhat laterally inclined, and not aligned. The long axis of the proximal trochlea is oriented laterally about 9° (trochlear angle) relative to that of the entire bone, while the long axis of the distal trochlea is oriented medially at the angle of 15°. The proximal trochlea is deep and asymmetrical with the lateral part wider than the medial one. The medial and lateral edges of the trochlear are relatively sharp and roughly equal in height. A relatively wide fossa with a deep pit is present distal to the proximal trochlea for the anterior process of the tibia. The medial surface of the proximal trochlea is nearly vertical with an indistinct shallow fossa on its distal half. A relatively distinct medial process is present posterior to the medial surface of the proximal trochlea. The neck of the astragalus is short but prominent, and is demarcated by a lateral notch. The distal trochlea is divided by a distinct ridge into a wide, shallowly-grooved medial surface for the navicular and a narrow, lateral facet for the cuboid. Proximal to the distal trochlea there is a shallow fossa for the navicular stop. Both the navicular and cuboid facets extend to the posterior side at the same extent, but the cuboid facet tapers towards the posterior side. On the posterior side, the sustentacular facet is convex proximodistally, flat laterally, and elongated rectangular in outline with the long axis parallel to that of the entire bone. The notch between the sustentacular facet and the distal trochlea is relatively shallow. The medial border of the sustentacular facet is limited by an indistinct ridge, which is laterodistally oriented joining the lateral border of the cuboid facet. Lateral to the ridge is a narrow facet which is possibly for the medial sustentacular facet of the calcaneus.

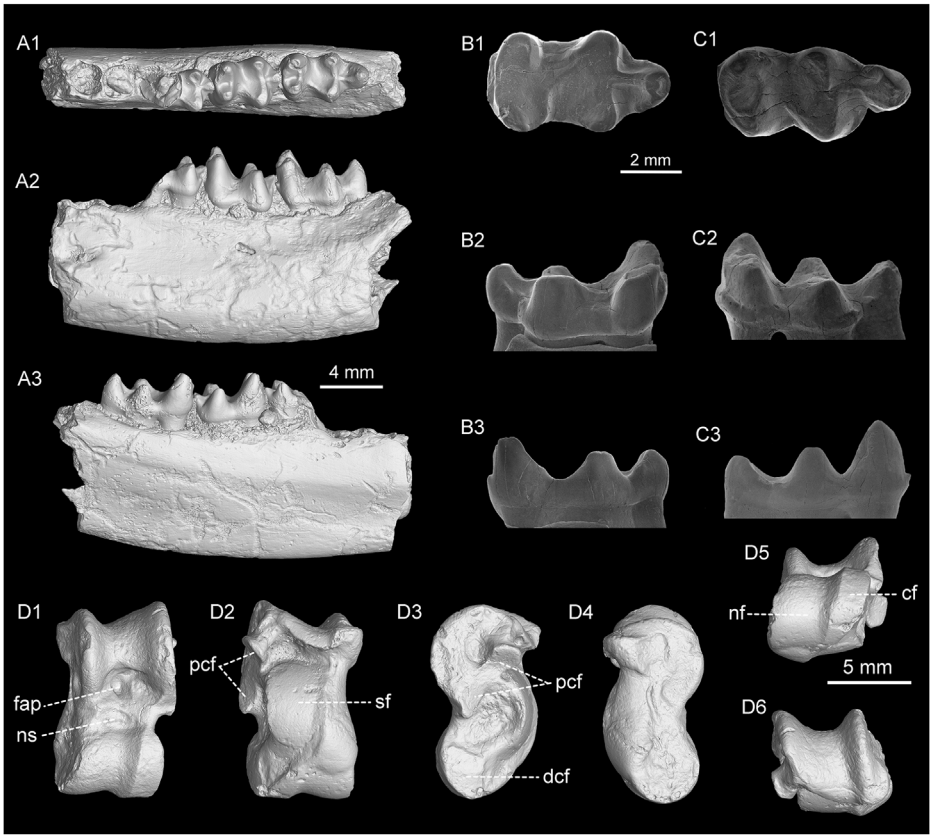

FIGURE 6
Lower jaw, astragalus, and isolated m3 of *Obotherium* aff. *O. tongi* . **(A)** left lower jaw with m1 talonid and m2-3 (IVPP V 31732.1); **(B)** right m3 (IVPP V 31733); **(C)** left m3 (V 31734): **(A1–C1)**, occlusal view; **(A2–C2)**, buccal view; **(A3–C3)**, lingual view; **(D)** left astragalus (IVPP V 31732.2) in **(D1)** anterior; **(D2)** posterior; **(D3)** lateral; **(D4)** medial; **(D5)** distal; and **(D6)** proximal views. Abbreviations: *cf*, cuboid facet; *dcf*, distal calcaneal facet; *fap*, fossa for anterior process of tibia; *nf*, navicular facet; *ns*, fossa serving as a navicular stop; *pcf*, proximal calcaneal facet; *sf*, sustentacular facet.

Medial to this ridge there is a slightly inflated surface, which becomes wider distally, for the plantar calcaneonavicular ligament. The proximal calcaneal facet on the lateral side of the astragalus is narrow, elongated, and concave, facing more laterally than posteriorly. The astragalar sulcus is relatively distinct on the posterior side, separating the sustentacular facet from the proximal calcaneal facet. On the lateral side, there is a wide and relatively shallow fossa between the two facets. A small, shallow fossa on the lateral surface of the proximal trochlea is present above the proximal calcaneal facet. The distal calcaneal facet is relatively large, fan-shaped, and flat.

Astragalar Measurements (IVPP V 31732.2, in mm): Length=11.87; Trochlear width=5.79; Distal width=5.53; Navicular width=4.02.

3.10 Comparisons

Vislobokova (2004a) erected a new species *Chorlakkia valerii* for a left lower jaw with m2–3 from the middle Eocene of Khaichin-Ula II, Mongolia. As noted by Vislobokova (2004a), *Chorlakkia valerii* is distinguished from the type species *Chorlakkia hassani* by the absence of twinned entoconid and hypoconulid on the lower molars (Gingerich et al., 1979), and by possession of other advanced characters, such as relatively elongated crowns of m2 and m3, a wider talonid compared to the trigonid, a more anterior position of the entoconid, and a narrower hypoconulid of m3. We suggest *Chorlakkia valerii* is better assigned to *Obotherium* based on an anteroposteriorly compressed trigonid, a talonid wider than the trigonid, an entoconid more anteriorly placed to the hypoconid, a cristid obliqua extending buccally to the midpoint of the protocristid, a well-developed hypoconulid in medial position, a transversely extended posthypocristid, and a possibly weak hypolophid according to the plate 9 of Vislobokova (2004a). The combination of a posthypocristid transversely extending to the midpoint of the crown on m3, a relatively small hypoconulid on m3, an erect trigonid and the lack of the paraconid in *Obotherium valerii* (='*Chorlakkia*' *valerii*) indicate it is more similar to *O. tongi* than to *O. parvum*.

The astragali of *Diacodexis*, *Eurodexis*, and *Elaschitotherium* are compared with that of *Obotherium* (Guthrie, 1968; West, 1984; Martinez and Sudre, 1995; Sudre and Erfurt, 1996; Métais et al., 2004; Kumar et al., 2010). The astragalus of *Obotherium* generally resembles *Diacodexis* and *Eurodexis* in having a distal trochlea medially deflected to the proximal trochlea, a distinct ridge separating the navicular and cuboid facets on the distal trochlea, and a well-developed facet for the plantar calcaneonavicular ligament. The astragalus of *Obotherium* is

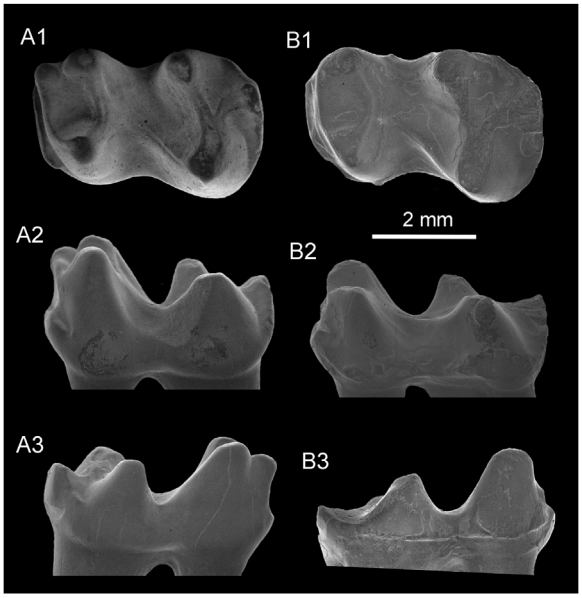

FIGURE 7
The lower molars of *Obotherium* sp.1 **(A)** and *Obotherium* sp. 2 **(B)**. **(A)** left m1/2 (IVPP V 31735); **(B)** left m1/2 (V 31736): **(A1–B1)**, occlusal view; **(A2–B2)**, buccal view; **(A3–B3)**, lingual view.

more similar to *Diacodexis indicus* than to *Eurodexis* and North American *Diacodexis* in having a deep fossa for the anterior process of tibia, and the navicular and cuboid facet equally extended towards the posterior side (Schaeffer, 1947; Martinez and Sudre, 1995; Sudre and Erfurt, 1996; Kumar et al., 2010). The astragalus of *Elaschitotherium*, which resembles that of *Eurodexis*, is distinguished from *Obotherium* by a shallow fossa for the anterior process of the tibia, a less distinct ridge separating the navicular and cuboid facets, navicular facet more posteriorly extended than the cuboid facet, and two separated proximal calcaneal facets (Métais et al., 2004).

Obotherium sp. 1
(Figure 7A; Table 1)

Material—IVPP V 31735, a left m1/2 from the Irdin Manha Formation at Huheboerhe (field no. 13088).

3.11 Description

The left m1/2 differs from both *Obotherium tongi* and *O. parvum* in having a relatively longer trigonid with a more distinct and separate paraconid. The complete hypolophid and distinct hypoconulid with a long prehypoconulid cristid are similar to those of *O. tongi*.

Obotherium sp. 2
(Figure 7B; Table 1)
Material—IVPP V 31736, a left m1/2 from the Irdin Manha Formation at Irdin Manha (field no. 11377).

3.12 Description

The m1/2 is similar to *Obotherium tongi* in having an anteroposteriorly compressed trigonid, a complete hypolophid, and a posteriorly pointed hypoconulid with a long prehypoconulid cristid. But the prehypoconulid cristid is more oriented to the hypoconid in IVPP V 31736 than in *O. tongi*. The m1/2 probably represents a variation of *O. tongi*.

Tapiruloides gen. nov.
Type species—*Tapiruloides usuensis* gen. et sp. nov.
Etymology—Greek, *-oides*, like; in allusion to its similarities with *Tapirulus*.
Included species—type species only.
Diagnosis—Lower molars nearly bilophodont; trigonid highly anteroposteriorly compressed without a paraconid, talonid wider than trigonid with entoconid more anteriorly placed than hypoconid, complete hypolophid slightly notched, cristid obliqua almost absent, prehypoconulid cristid joining the midpoint of the hypolophid in a high position, and hypoconulid of m3 high and beak-like.
Differential diagnosis—Differs from *Tapirulus* and *Obotherium* by almost absent cristid obliqua on the lower molars and a beak-like hypoconulid on m3; further differs from *Tapirulus* by a slightly more anteriorly placed entoconid to the hypoconid on the lower molars.
Age and Distribution—Sharamurunian (middle Eocene) of the Erlian Basin, Inner Mongolia, China.

Tapiruloides usuensis gen. et sp. nov.
(Figure 8; Table 1)
Holotype—IVPP V 31737, a left lower jaw with m2-3.
Etymology—In reference to the locality of the holotype "Ula Usu", meaning "the well of mountain water" in Mongolian.
Diagnosis—as for the genus.
Locality and horizon—the base of the Shara Murun Formation, Ula Usu (field no. 10013), Erlian Basin.

3.13 Description

The horizontal ramus below m2–3 is shallow and slightly convex. The preserved anteroventral portion of the masseteric fossa is relatively deep.

The metaconid, entoconid, and hypoconulid of m2 are partially broken. The m2 is bilophodont. The trigonid is strongly anteroposteriorly compressed without a paraconid. The high paracristid and protocristid connect the protoconid and metaconid anteriorly and posteriorly, respectively. The protocristid is slightly deeper notched. The talonid is longer and wider than the trigonid. The hypolophid, which is composed of transverse posthypocristid and postentocristid, is high and nearly complete with a shallow notch between the junction. The entoconid is slightly more anteriorly placed than the hypoconid. A small, oval-shaped worn facet is obliquely aligned at the base of the talonid between the protocristid and hypolophid, representing the vestige of the cristid obliqua. Although the hypoconulid is partially broken, it is relatively large and posteriorly extended. The anterior extremity of the

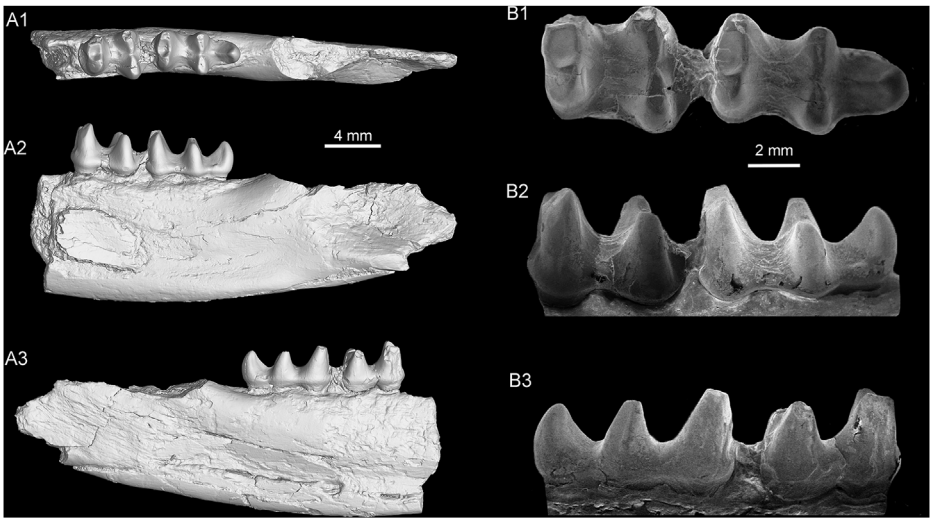

FIGURE 8
Left lower jaw of *Tapiruloides usuensis* gen. et sp. nov. with m2-3 (IVPP V 31737). **(A1–B1)** occlusal view; **(A2–B2)**, buccal view; **(A3–B3)**, lingual view.

prehypoconulid cristid joins the hypolophid in a high position that is slightly below the notch of the latter. A weak but distinct precingulid is present.

The m3 is similar to m2 in morphology, but the former has a talonid slightly wider than the trigonid, and the entoconid is nearly lingually placed to the hypoconid. Furthermore, the hypoconulid of m3 is expanded into a third lobe, and the apex of the hypoconulid is beak-like, as high as the hypoconid. The prehypoconulid cristid is sharp and straight, descending from the hypoconulid to the posterior side of the hypolophid, where a weak ridge rises again to a relatively high position below the notch of the hypolophid. The prehypoconulid cristid divides the hypoconulid lobe into two equal-sized, steep lingual and buccal surfaces. A tiny cingulid is present at the base of the buccal side of the hypoconulid lobe.

3.14 Comparisons

The species probably derived from *Obotherium* based on the following synapomorphies on m2–3: Anteroposteriorly compressed trigonid, talonid wider than the trigonid, a slightly anteriorly placed entoconid to the hypoconid, and a well-developed hypoconulid. The m2-3 of V 31737 shows some more derived characters than *Obotherium* in having a more complete hypolophid, nearly vertical trigonid, and a nearly absent cristid obliqua. On the other hand, V 31737 strikingly resembles *Tapirulus perrierensis* and *T. hyracinus* in having bilophodont dentitions (Stehlin, 1910; Sudre, 1978), but differs from the latter two species by a talonid wider than the trigonid, a relatively short talonid on m2, and a nearly absent cristid obliqua. The assignment of the specimen to a new genus rather than to *Tapirulus* is based not only on the morphologic differences but also on the observation that V 31737 is probably more closely related to *Obotherium* than to *Tapirulus*.

4 Discussion

4.1 Phylogenetic position of *Obotherium* and *Tapiruloides*

In order to investigate the phylogenetic position of *Obotherium* within early artiodactyls, a cladistic analysis was conducted based on the morphological data matrix modified from Métais et al. (2004). The data matrix of Métais et al. (2004), comprising 26 dental characters and 26 taxa, includes early artiodactyl groups from Eurasia and North America, such as Homacodontidae and Lantianiinae. Five taxa (*Obotherium parvum*, *O. tongi*, *Tapiruloides usuensis*, *Tapirulus majori*, and *T. hyracinus*) and eight characters were added to the Métais et al. (2004) matrix, with modifications of four original character states (character 14–16, 18). The character states of the upper molar in *Obotherium parvum* were based on the specimen IVPP V 31730 assigned to ? *O. parvum*, and the character states of the lower molar in *Eolantianus* were changed to the question marks due to doubtful association with upper teeth. The modified data matrix is comprised of 31 taxa with three outgroups and 34 dental characters (Supplementary Material). The cladistic analyses result in 124 MPTs, each with 163 steps. Both a strict consensus tree (CI = 0.343, RI = 0.626) and a 50% majority-rule consensus tree (CI = 0.277, RI = 0.490) were constructed (Figure 9).

Although many polytomies are present in the topology of the strict consensus tree (Figure 9A), several clades are supported. *Obotherium*, *Tapiruloides*, and *Tapirulus* form a polytomous clade, which is nested in a polytomy with homacodontids, *Dichobune*, *Cuisitherium*, and a 'ruminant' clade. This polytomy group forms a sister group to *Hyperdichobune*-Lantianiinae, and Lantianiinae is composed of *Eolantianus* as a sister group to a *Lantianus-Elaschitotherium* clade. *Eurodexis*, *Pakibune*, *Chorlakkia*, and *Diacodexis* are polytomous basal groups. The *Obotherium-Tapirulus-Tapiruloides* clade is supported by seven unambiguous

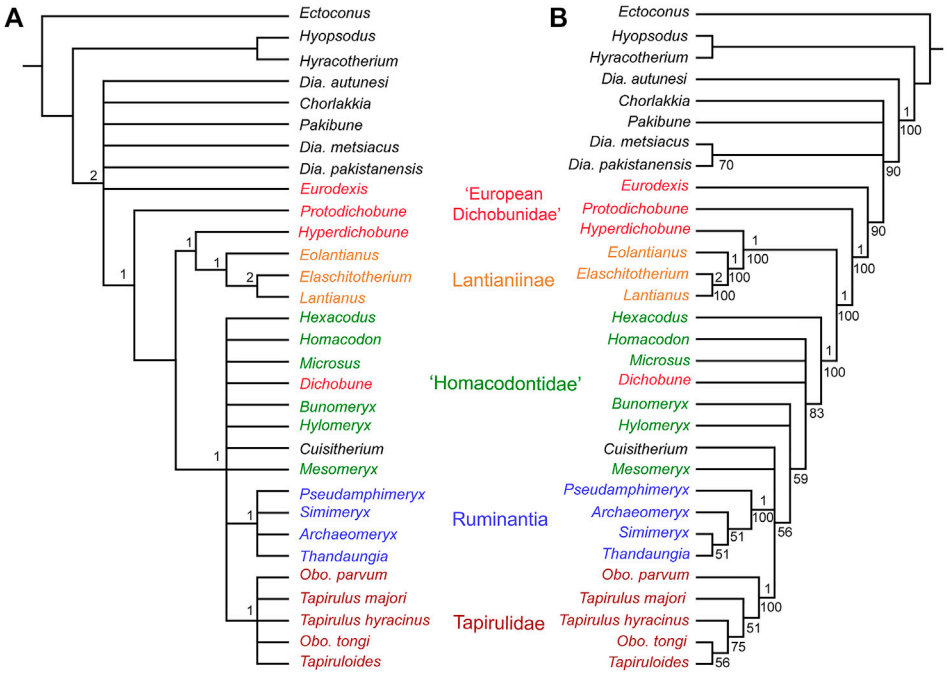

FIGURE 9
Strict consensus **(A)** and 50% majority-rule consensus **(B)** trees of the 124 MPTs in the phylogenetic analyses of the early artiodactyls with a focus on Tapirulidae. Values above the branches are Bremer Support at the nodes, and below the branches are the percentage of 50% majority-rule consensus trees.

synapomorphies: developed premetaconule cristae on the upper molars (8:1→2), continuous lingual cingulum (12:1→0), absent buccal cingulids on the lower molars (14:1→2), well-developed p4 metaconid (25:1→2), strong p4 paraconid (26:1→2), transversely extended posthypocristid (32:1→2), and a long m1-2 hypoconulid (33:0→1). Thus, the enigmatic European *Tapirulus* is not a choeropotamid, a tylopod, an anoplotheriid, or a dacrytheriid (Hooker and Thomas, 2001; Erfurt and Métais, 2007), but is closely related to *Obotherium* and *Tapiruloides* from Asia. The Tapirulidae were probably descended from a North American basal homacodontid, such as *Hexacodus* from the middle and late Wasatchian. Although Métais et al. (2004) noticed striking resemblances between primitive European hyperdichobunines and Asian lantianiines, they attributed the similarities to convergence. However, our topology shows the two subfamilies from a sister group, supported by well-developed parastyles on the upper molars (13:1→2).

The 50% majority-rule consensus tree partially resolves some of these polytomies (Figure 9B). *Tapiruloides* and *Obotherium tongi* are sister taxa, and *Tapirulus hyracinus*, *Tapirulus majori*, and *Obotherium parvum* are successive sister taxa to the *Tapiruloides-Obotherium tongi* clade. The result implies that *Obotherium parvum* is the most basal taxon within the clade, and both *Obotherium* and *Tapirulus* are paraphyletic. Paraphyly of *Obotherium* could be attributed to the lack of upper dentition in *Tapiruloides* and *Obotherium tongi*. *Pseudamphimeryx* is included within Ruminantia as a sister group to *Archaeomeryx* and *Simimeryx-Thandaungia* clade. Ruminantia is supported by gradual increase in size from M1 to M2 (1:1→3), buccal cingulum absent on the upper molars (4:1→0), postprotocrista and metaconule connection present (6:0→1), and postcingulid weak (24:1→0). The European endemic Amphimerycidae including *Amphimeryx* and *Pseudamphimeryx* was considered to be more closely related to xiphodontids or dacrytheriids than to ruminants, although a fused cubonavicular is present in *Amphimeryx collatarsus* (Erfurt and Métais, 2007). Similarly, Amphimerycidae is a sister group to *Archaeomeryx* within European bunoselenodont families (Luccisano et al., 2020), suggesting it is allied with ruminants (Simpson, 1945; McKenna and Bell, 1997). *Cuisitherium* is controversial, having been assigned to Dacrytheriidae (Sudre et al., 1983), Choeropotamidae (Hooker and Thomas, 2001; Erfurt and Métais, 2007), or Haplobunodontidae (Luccisano et al., 2020). Our analyses indicate that *Cuisitherium* is probably allied with ruminants and tapirulids. Homacodontidae is not monophyletic, and *Hexacodus* represents the most basal taxon consistent with its primitive characters and early Eocene age. It is interesting that *Dichobune* is more closely related to homacodontids than to other European endemic artiodactyls, consistent with the topology of basal artiodactyls by Luccisano et al. (2020). *Protodichobune* and *Eurodexis* are successive sister groups to Lantianiinae-Hyperdichobuninae and Homacodontidae-*Dichobune-Cuisitherium*-Ruminantia-Tapirulidae clade. *Diacodexis* is not monophyletic, and *D. antunesi* is a sister group to other early artiodactyls in this analysis; but *Diacodexis* is monophyletic in the Luccisano et al. (2020)

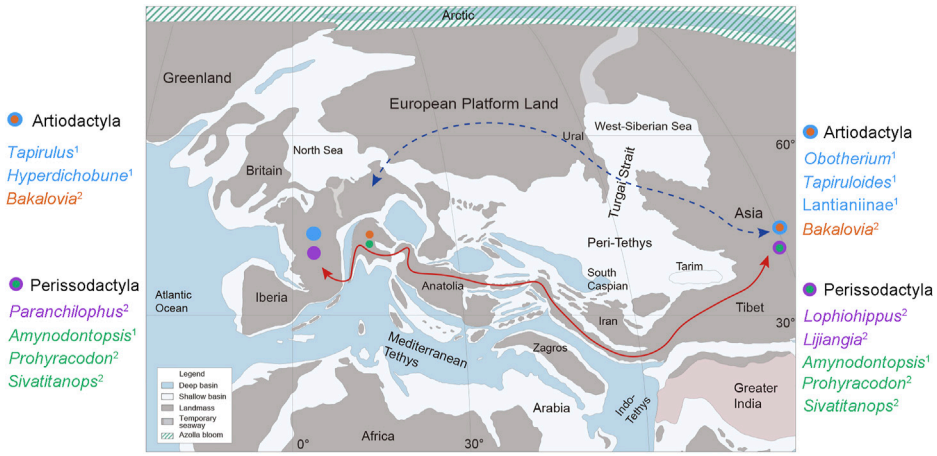

FIGURE 10
Paleogeography of Tethys region during the middle Eocene and probable dispersal routines between Asian and European mammal groups. The superscript numbers 1 and 2 indicate the early middle Eocene and late middle Eocene taxa, respectively. (The paleogeographic map was modified from Palcu and Krijgsman, 2022, fig. 8, with permission from W. Krijgsman).

phylogeny. *Pakibune* and *Chorlakkia* are unresolved basal groups of early artiodactyls.

4.2 Palaeobiogeography

Europe was connected with North America and Asia during the early Eocene (McKenna, 1975; 1983; Krause and Maas, 1990); however, after the Early Eocene, Europe, mainly composed of archipelagos, was isolated from Asia and North America until the Oligocene. The European mammalian faunas from the middle through late Eocene are mostly endemic. By contrast, immigration of mammals was frequent between Asia and North America *via* the Bering land bridge during the middle and late Eocene (Woodburne, 2004), and Eocene mammals from Asia show more or less similarity with those from North America, but share few taxa with Europe.

Erfurt and Métais (2007) noted that the Geiseltalian/Robiacian transition (MP13/14) is characterized by the sudden appearance of several selenodont artiodactyls in Europe, however, the origin of these endemic selenodont artiodactyls remains obscure. Heissig (1993) proposed a close relationship between anoplotheriids and North American oreodonts based on astragalar morphology, and they may have dispersed from eastern Europe "Fennosarmatian Platform", which was separated from western Europe during the middle and late Eocene by broad seaways from the North Sea Basin to the Black Sea. The European endemic Mixtotheriidae, Cainotheriidae, Anoplotheriidae, and Xiphodontidae have been included in Tylopoda (Gentry and Hooker, 1988; Theodor et al., 2005), and their first appearances are at MP13 or MP14 (Erfurt and Métais, 2007). Amphimerycidae has long been included in Ruminantia (McKenna and Bell, 1997; Theodor et al., 2005), but their similarities are attributed to convergence (Métais et al., 2004). Erfurt and Métais (2007) suggest these endemic artiodactyls are of autochthonous origin from unknown European dichobunoids. However, our analyses show *Obotherium* and *Tapiruloides* are closely related to *Tapirulus*, and *Obotherium parvum* is the most basal taxon in the clade and probably gave rise to European *Tapirulus*. Morphological similarities between Irdinmanhan *Obotherium* and *T. majori*, *T. depereti* from MP13 and MP14 suggest a biogeographic connection between Asia and Europe during the early middle Eocene. Thus, some endemic European artiodactyls are probably of allochthonous origin from Asia as exemplified by *Obotherium* and *Tapirulus*. In addition, the earliest *Hyperdichobune* from MP13 and Asian Lantianiinae are also closely related, supporting a connection between Europe and Asia during the early middle Eocene. Dispersal routes between Europe and Asia during the middle-late Eocene are across the Turgai Strait or more likely along the Tethyan shore as evidenced by shared perissodactyls and other mammal groups (Figure 10) (Böhme et al., 2013; Missiaen and Gingerich, 2014; Bai, 2017; Palcu and Krijgsman, 2022). The Balkanatolia mammalian fauna from the Balkans to the Caucasus is characterized by an endemic phase during the Ypresian and Lutetian, and an invasive phase from Asian taxa during the Bartonian-Priabonian (Licht et al., 2022). Although many Asian ungulates and rodents first appeared during the late middle Eocene (Bartonian) in Balkanatolia, the first appearance of Asian-derived *Amynodontopsis* aff. *bodei* (Tissier et al., 2018; Licht et al., 2022) and western Europe derived *Galatiadelphys* (Métais et al., 2018) from the upper Lutetian suggests that a possible southern route emerged and facilitated the dispersal during the early middle Eocene.

The nearly contemporary North American artiodactyl assemblage is characterized by the first appearance of agriochoerids, oromerycids, and protoceratids in the middle Uintan (Ui2), and the first appearance of hypertragulids, leptomerycids, and anthracotheriids in the late Uintan (Ui3) (Janis et al., 1998; Erfurt and Métais, 2007). These new forms may be derived North American homacodontids (Stucky, 1998) or immigrants from Asia (Vislobokova, 1998; Métais and Vislobokova, 2007). The latter hypothesis needs further investigation and fieldwork on Eocene artiodactyls from Asia. The Irdinmanhan ALMA, which is

usually correlated with the Uintan NALMA (Bai et al., 2017; Speijer et al., 2020; Bai et al., 2021), could be at least correlated to European MP13-14 based on the similarities between *Obotherium* and early *Tapirulus*.

4.3 Evolution of bilophodont teeth in artiodactyls

The teeth of artiodactyls are divided into bunodont and selenodont types, as well as the intermediate bunoselenodont. Both selenodonty in ruminants and bilophodonty in tapirulids probably derived from the bunoselenodont early homacodontid *Hexacodus*. From the Irdinmanhan *Obotherium* to Sharamurunian *Tapiruloides*, the main changes in the lower molars lie in the reduction of the paraconid and cristid obliqua, a more complete hypolophid, and elongated hypoconulid on m1-2. The relatively long prehypoconulid cristid in *Obotherium tongi* is likely derived from a posterolingually extended branch of the bifurcated posthypocristid in *O. parvum*. The prehypoconulid cristid joins the point buccal to the midpoint of the hypolophid on m1-2 in *Obotherium parvum*, but it nearly joins the midpoint of hypolophid in *O. tongi* and *Tapiruloides*. Bilophodont teeth are completely formed in *Tapiruloides*, but the trigonid still retains a narrow redundant basin. Similarly, the lower molars of *Tapirulus hyracinus* and *T. perrierensis* are essentially bilophodont with a reduced cristid obliqua and a narrow trigonid basin (Sudre, 1978). The evolution of bilophodont upper molars in *Tapirulus* lies in the compression and elevation of the protoloph and crescentic metaconule, reduction of the paraconule, and strongly buccally deflected centrocrista (Sudre, 1978). Stehlin (1910) suggested that the "posterior loph" joining the lingual side of the metacone on the upper molars in *Tapirulus schlosseri* developed from a median crista (endometacristule) between the crescentic metaconule in *T. depereti*, so the "metaloph" in later *Tapirulus* is not homologous with the premetaconule crista as in most artiodactyls. More complete material of the upper molars of early *Tapirulus* is required to verify this explanation.

Raoellidae is an endemic artiodactyl group known from the early to middle Eocene deposits in the Indo-Pakistani subcontinent, characterized by bilophodont upper molars (Thewissen et al., 1987; Theodor et al., 2007; Singh Rana et al., 2021). Orliac and Ducrocq (2012) assigned m3 and p4, originally included in indeterminate Suiodea (Métais et al., 2008), from the Shanghuang fissure of China to raoellid ?*Khirtharia* cf. *major*. The bilophodont upper molars of Raoellidae are characterized by weak or small paraconules, and posterior crest contacting the base of the middle of the metacone (Thewissen et al., 1987); thus, Thewissen et al. (1987) suggest that Raoellidae may be related to *Tapirulus*. But the upper molars of Raoellidae have a more or less straight centrocrista in contrast to the W-shaped ectoloph in derived *Tapirulus*. It is controversial whether the posterolingual cusp on the upper molars in Raoellidae is a metaconule or hypocone (Theodor et al., 2007; Thewissen et al., 2020). The lower molars of Raoellidae have a distinct cristid obliqua, and lack the hypoconulids on m1-2 (Thewissen et al., 1987), while those of *Tapirulus* usually have reduced or absent cristid obliqua and well-developed hypoconulids on m1-2 (Sudre, 1978). The similar bilophodont upper molars in Raoellidae and *Tapirulus* is therefore attributed to the convergence. Raoellidae has recently been considered to be the sister to Cetacea (Thewissen et al., 2007; Cooper et al., 2012; Thewissen et al., 2020), and distantly related to *Tapirulus*.

Some listriodontine and schizochoerine suids from the Neogene also developed bilophodont molars, such as the listriodontines *Listriodon*, *Lopholistriodon* and schizochoerines *Yunnanochoerus*, *Schizochoerus* from the Miocene of Eurasia and Africa with lophodont molars, which were derived from bunolophodont groups with accessory cusps (van der Made and Han, 1994; van der Made, 1996; van der Made, 1997; Pickford and Morales, 2003; Harris and Liu, 2007). The multiple appearances of bilophodont teeth in different lineages of artiodactyls are attributed to the convergence and are convergent on the bilophodont teeth in Tapiridae.

Data availability statement

The datasets presented in this study can be found in online repositories. The names of the repository/repositories and accession number(s) can be found in the article/Supplementary Material. The data matrix was deposited in Morphobank (Project 4563).

Author contributions

All authors contributed to the initial discussions. BB, Y-QW, and JM designed the research. BB wrote the manuscript and analyzed data; Y-QW, JT, and JM improved and edited the manuscript; BB prepared the figures; BB and Y-QW collected data.

Funding

Funding was provided by grants from the Strategic Priority Research Program of the Chinese Academy of Sciences (XDB26000000), the National Natural Science Foundation of China (42272011 and 41672014), Frick Funds from the Division of Paleontology, American Museum of Natural History, and a Discovery Grant from the Natural Sciences and Engineering Research Council of Canada.

Acknowledgments

We are grateful to Qian Li, Xun Jin, Fang-Yuan Mao, Hai-Bing Wang, Wei Zhou, Shi-Jie Li, Qi Li, Cheng-Kai Sun, Yong-Xing Wang, Yong-Fu Wang, Xiao-Yang Wang, Ran-Cheng Xu, Hai Xing, Xin-Yue Zhang (all IVPP), K. Christopher Beard (University of Kansas, Lawrence, United States), and Daniel L. Gebo (Northern Illinois University, DeKalb, United States) for assistance in the field; Xun Jin and Wei Gao (both IVPP) for photography; Ye-Mao Hou (IVPP) for μ-CT scanning; Yong Xu for the drawing of Figure 5; Zhao-Qun Zhang, Ban-Yue Wang, Xi-Jun Ni, Jie Ye, Zhan-Xiang Qiu, and Su-Kuan Hou (all IVPP) for helpful discussion. We thank O. Maridet, P. Li, M. Scheuplein, and D. Mertmann for providing

important references; A. Henrici and A. McAfee (both Carnegie Museum of Natural History) for taking photos of *Hylomeryx annectens* (CM 2335); S. Fu and W. Krijgsman for the permission of usage of geological map in Figure 1 and paleogeographic map in Figure 9, respectively.

Conflict of interest

The authors declare that the research was conducted in the absence of any commercial or financial relationships that could be construed as a potential conflict of interest.

The handling editor LFF declared a past co-authorship with the author JM.

Publisher's note

Supplementary material

The Supplementary Material for this article can be found online at: https://www.frontiersin.org/articles/10.3389/feart.2023.1117911/full#supplementary-material

References

Averianov, A. O. (1996). Artiodactyla from the early Eocene of Kyrgyzstan. *Palaeovertebrata* 25, 359–369.

Averianov, A. O., and Godinot, M. (2005). Ceratomorphs (mammalia, Perissodactyla) from the early Eocene Andarak 2 locality in Kyrgyzstan. *Geodiversitas* 27, 221–237.

Bai, B. (2017). Eocene pachynolophinae (Perissodactyla, palaeotheriidae) from China, and their palaeobiogeographical implications. *Palaeontology* 60, 837–852. doi:10.1111/pala.12319

Bai, B., Meng, J., Janis, C. M., Zhang, Z. Q., and Wang, Y. Q. (2020). Perissodactyl diversities and responses to climate changes as reflected by dental homogeneity during the Cenozoic in Asia. *Ecol. Evol.* 10, 6333–6355. doi:10.1002/ece3.6363

Bai, B., Wang, Y.-Q., Zhang, X.-Y., and Meng, J. (2021). A new species of the "condylarth" *Hyopsodus* from the middle Eocene of the Erlian Basin, Inner Mongolia, China, and its biostratigraphic implications. *Acta Palaeontol. Pol.* 66, 767–777. doi:10.4202/app.00908.2021

Bai, B., Wang, Y. Q., Li, Q., Wang, H. B., Mao, F. Y., Gong, Y. X., et al. (2018). Biostratigraphy and diversity of Paleogene perissodactyls from the Erlian Basin of Inner Mongolia, China. *Am. Mus. Novit.* 3914, 1–60. doi:10.1206/3914.1

Bai, B., Wang, Y. Q., Mao, F. Y., and Meng, J. (2017). New material of Eocene helaletidae (Perissodactyla, tapiroidea) from the Irdin Manha Formation of the Erlian Basin, inner Mongolia, China and comments on related localities of the Huheboerhe area. *Am. Mus. Novit.* 3878, 1–44. doi:10.1206/3878.1

Böhme, M., Aigstorfer, M., Antoine, P.-O., Appel, E., Havlik, P., Métais, G., et al. (2013). Na duong (northern vietnam) – An exceptional window intoEocene ecosystems from south-east Asia. *Zitteliana* A53, 120–167.

Boivin, M., Orliac, M. J., Antunes, M. T., Godinot, M., Laurent, Y., Marandat, B., et al. (2018). New material of *Diacodexis* (mammalia, artiodactyla) from the early Eocene of southern Europe. *Geobios* 51, 285–306. doi:10.1016/j.geobios.2018.06.003

Brunet, M., and Sudre, J. (1980). Deux nouveaux dichobunides (Artiodactyla, Mammalia) de l'Oligocene inferieur d'Europe. *Proc. Koninklijke Nederl. Akademie van Wetenschappen (B)* 83, 121–143.

Coombs, M. C., and Coombs, W. P. (1977). Dentition of *Gobiohyus* and a reevaluation of the helohyidae (artiodactyla). *J. Mammal.* 58, 291–308. doi:10.2307/1379328

Cooper, L. N., Thewissen, J. G. M., Bajpai, S., and Tiwari, B. N. (2012). Postcranial morphology and locomotion of the Eocene raoellid indohyus (artiodactyla: Mammalia). *Hist. Biol.* 24, 1–32. doi:10.1080/08912963.2011.624184

Ducrocq, S., Soe, A. N., Aung, A. K., Benammi, M., Bo, B., Chaimanee, Y., et al. (2001). A new anthracotheriid artiodactyl from Myanmar, and the relative ages of the Eocene anthropoid primate-bearing localities of Thailand (Krabi) and Myanmar (Pondaung). *J. Vertebrate Paleontology* 20, 755–760. doi:10.1671/0272-4634(2000)020[0755:ANAAFM]2.0.CO;2

Ducrocq, S., Soe, A. N., Chavasseau, O., Sein, C., Chaimanee, Y., Lazzari, V., et al. (2020). New basal ruminants from the Eocene of the pondaung formation, Myanmar. *J. Vertebrate Paleontology* 39, e1722682. doi:10.1080/02724634.2019.1722682

Ducrocq, S., Soe, A. N., Sein, C., Chaimanee, Y., Chavasseau, O., and Jaeger, J.-J. (2022). *Neochorlakkia myaingensis* n. gen., n. sp., a new Dichobunidae (Mammalia, Cetartiodactyla) from the middle Eocene Pondaung Formation, Myanmar. *Comptes Rendus Palevol* 21, 115–122. doi:10.5852/cr-palevol2022v21a4

Ducrocq, S., Soe, A. N., Sein, C., Lazzari, V., Chaimanee, Y., Valentin, X., et al. (2016). First record of a diacodexeid artiodactyl in the middle Eocene Pondaung Formation (Myanmar). *Palaeontol. Z.* 90, 611–618. doi:10.1007/s12542-016-0283-y

Erfurt, J., and Métais, G. (2007). "Endemic European Paleogene artiodactyls," in *The evolution of artiodactyls*. Editors D. R. Prothero and S. E. Foss (Baltimore: John Hopkins University Press), 59–84.

Erfurt, J., and Sudre, J. (1996). Eurodexeinae, eine neue unterfamilie der Artiodactyla (Mammalia) aus dem unter-und mitteleozän europas. *Palaeovertebrata* 25, 371–390.

Franzen, J. L. (1981). Das erste Skelett eines Dichobuniden (Mammalia, Artiodactyla), geborgen aus mitteleozänen Ölschiefem der "Grube MesseI" bei Darmstadt (Deutschland, S-Hessen). *Senckellb. Lethaea* 61, 299–353.

Franzen, J. L. (1994). Neue Säugerfunde aus dem Eozän des Eckfelder Maares bei Manderscheid (Eifel). *Mainz. Naturwiss. Arch. Beih.* 16, 177–187.

Fu, S., Liu, Z., Ge, J., Tian, N., Yin, K., Wang, X., et al. (2021). Tectono-sedimentary analysis of the lower cretaceous succession in the sags of the ondor sum uplift, southern Erlian Basin, NE China. *Mar. Petroleum Geol.* 124, 104851. doi:10.1016/j.marpetgeo.2020.104851

Gabunia, L. K. (1971). On a new representative of condylarths (condylarthra) from the Eocene of zaisan depression. *Bull. Acad. Sci. Georgian SSR* 61, 233–235.

Gabunia, L. K. (1973). On the presence of the diacodexinae in the Eocene of Asia. *Bull. Acad. Sci. Georgian SSR* 71, 741–744.

Gazin, C. L. (1962). A further study of the lower Eocene mammalian faunas of southwestern Wyoming. *Smithson. Misc. Collect.* 144, 1–98.

Gazin, C. L. (1955). A review of the upper Eocene artiodactyla of North America. *Smithson. Misc. Collect.* 128, 1–96.

Gazin, C. L. (1952). The lower Eocene Knight Formation of Western Wyoming and its mammalian faunas. *Smithson. Misc. Collect.* 117, 1–82.

Gentry, A., and Hooker, J. (1988). "The phylogeny of the Artiodactyla," in *The phylogeny of the tetrapods*. Editor M. J. Benton (Oxford: Clarendon Press), 235–272.

Gingerich, P., Russell, D. E., Sigogneau-Russell, D., and Hartenberger, J. (1979). "*Chorlakkia hassani*, A new middle Eocene dichobunid (mammalia, artiodactyla) from the kuldana formation of kohat (Pakistan)," in *Contributions from the Museum of Paleontology* (Ann Arbor, Michigan: University of Michigan), 25, 117–124.

Goloboff, P. A., and Catalano, S. A. (2016). TNT version 1.5, including a full implementation of phylogenetic morphometrics. *Cladistics* 32, 221–238. doi:10.1111/cla.12160

Goloboff, P. A., Farris, J. S., and Nixon, K. C. (2008). TNT, a free program for phylogenetic analysis. *Cladistics* 24, 774–786. doi:10.1111/J.1096-0031.2008.00217.X

Guthrie, D. A. (1968). The tarsus of Early Eocene artiodactyls. *J. Mammal.* 49, 297–302. doi:10.2307/1377987

Harris, J. M., and Liu, L. P. (2007). "Superfamily suoidea," in *The evolution of artiodactyls*. Editors D. R. Prothero and S. E. Foss (Baltimore: The Johns Hopkins University Press), 130–150.

Heissig, K. (1993). The astragalus in anoplotheres and oreodonts, phylogenetical and paleogeographical implications. *Kaupia* 3, 173–178.

Hooker, J. J., and Thomas, K. M. (2001). A new species of *amphirhagatherium* (Choeropotamidae, artiodactyla, mammalia) from the late Eocene headon hill formation of southern england and phylogeny of endemic European 'anthracotherioids'. *Palaeontology* 44, 827–853. doi:10.1111/1475-4983.00203

Hooker, J. J., and Weidmann, M. (2000). The Eocene mammal faunas of Mormont, Switzerland: Systematic revision and resolution of dating problems. *Schweiz. Palaeontol. Abh.* 120, 1–143.

Janis, C., Effinger, J., Harrison, J., Honey, J., Kron, D., Lander, B., et al. (1998). "Artiodactyla," in *Evolution of tertiary mammals of North America*. Editors C. M. Janis, K. M. Scott, and L. L. Jacobs (Cambridge: Cambridge University Press), 337–357.

Jiang, H.-X. (1983). Division of the Paleogene in the Erlian Basin of inner Mongolia. *Geol. Inn. Mogolia* 2, 18–36.

Krause, D. W., and Maas, M. C. (1990). "The biogeographic origins of late Paleocene-early Eocene mammalian immigrants to the Western Interior of North America," in *Dawn of the age of mammals in the northern part of the rocky mountain interior*. Editors T. M. Bown and K. D. Rose North America (Boulder, Colorado: Geological Society of America Special Paper), 71–105.

Kumar, K., Rose, K. D., Rana, R. S., Singh, L., Smith, T., and Sahni, A. (2010). Early Eocene artiodactyls (mammalia) from Western India. *J. Vertebrate Paleontology* 30, 1245–1274. doi:10.1080/02724634.2010.483605

Lavocat, R. (1951). *Révision de la faune des mammifères oligocènes d'Auvergne et du Velay*. Paris: Science Avenir Editions.

Li, Q., and Li, Q. (2021). A new middle Eocene bunodont artiodactyl from the Erlian Basin (nei mongol, China). *Hist. Biol.* 34, 1941–1949. doi:10.1080/08912963.2021.1989679

Licht, A., Métais, G., Coster, P., İbilioğlu, D., Ocakoğlu, F., Westerweel, J., et al. (2022). Balkanatolia: The insular mammalian biogeographic province that partly paved the way to the Grande Coupure. *Earth-Science Rev.* 226, 103929. doi:10.1016/j.earscirev.2022.103929

Lucas, S. G., and Emry, R. J. (1996). Late Eocene entelodonts (mammalia: Artiodactyla) from inner Mongolia, China. *Proc. Biol. Soc. Wash.* 109, 397–405.

Luccisano, V., Sudre, J., and Lihoreau, F. (2020). Revision of the Eocene artiodactyls (mammalia, placentalia) from aumelas and saint-martin-de-londres (montpellier limestones, hérault, France) questions the early European artiodactyl radiation. *J. Syst. Palaeontol.* 18, 1631–1656. doi:10.1080/14772019.2020.1799253

Martinez, J. N., and Sudre, J. (1995). The astragalus of Paleogene artiodactyls–comparative morphology, variability and prediction of body-mass. *Lethaia* 28, 197–209. doi:10.1111/j.1502-3931.1995.tb01423.x

Matthew, W. D., and Granger, W. (1925a). New mammals from the Irdin Manha Eocene of Mongolia. *Am. Mus. Novit.* 198, 1–10.

Matthew, W. D., and Granger, W. (1925b). New mammals from the Shara Murun Eocene of Mongolia. *Am. Mus. Novit.* 196, 1–12.

Matthew, W. D., and Granger, W. (1923). *The fauna of the Houldjin gravels*. New York: American Museum of Natural History, 1–6.

McKenna, M. C., and Bell, S. K. (1997). *Classification of mammals above the species level*. New York: Columbia University Press.

McKenna, M. C. (1975). Fossil mammals and early Eocene north-atlantic land continuity. *Ann. Mo. Botanical Gard.* 62, 335–353. doi:10.2307/2395200

McKenna, M. C. (1983). Holarctic landmass rearrangement, cosmic events, and Cenozoic terrestrial organisms. *Ann. Mo. Botanical Gard.* 70, 459–489. doi:10.2307/2992083

Métais, G., Benammi, M., Chaimanee, Y., Jaeger, J.-J., Tun, T., Thein, T., et al. (2000). Discovery of new ruminant dental remains from the middle Eocene pondaung formation (Myanmar): Reassessment of the phylogenetic position of indomeryx. *Comptes Rendus de l'Académie des Sci. - Ser. IIA - Earth Planet. Sci.* 330, 805–811. doi:10.1016/s1251-8050(00)00184-1

Métais, G., Chaimanee, Y., Jaeger, J.-J., and Ducrocq, S. (2001). New remains of primitive ruminants from Thailand: Evidence of the early evolution of the Ruminantia in Asia. *Zool. Scr.* 30, 231–248. doi:10.1046/j.0300-3256.2001.00071.x

Métais, G., Coster, P. M., Kappelman, J. R., Licht, A., Ocakoğlu, F., Taylor, M. H., et al. (2018). Eocene metatherians from Anatolia illuminate the assembly of an island fauna during Deep Time. *PLoS ONE* 13, e0206181. doi:10.1371/journal.pone.0206181

Métais, G., Guo, J., and Beard, K. C. (2004). A new small dichobunid artiodactyl from Shanghuang (middle Eocene, eastern China): Implications for the early evolution of proto-selenodonts in Asia. *Bull. Carnegie Mus. Nat. Hist.* 36, 177–197. doi:10.2992/0145-9058(2004)36[177:ansdaf]2.0.co;2

Métais, G. (2006). New basal selenodont artiodactyls from the Pondaung Formation (late middle Eocene, Myanmar) and the phylogenetic relationships of early ruminants. *Ann. Carnegie Mus.* 75, 51–67. doi:10.2992/0097-4463(2006)75[51:nbsaft]2.0.co;2

Métais, G., Qi, T., Gu, J. W., and Beard, K. C. (2005). A new bunoselenodont artiodactyl from the Middle Eocene of China and the early record of selenodont artiodactyls in Asia. *J. Vertebrate Paleontology* 25, 994–997. doi:10.1671/0272-4634(2005)025[0994:anbaft]2.0.co;2

Métais, G., Qi, T., Guo, J. W., and Beard, K. C. (2008). Middle-eocene artiodactyls from Shanghuang (Jiangsu province, coastal China) and the diversity of basal dichobunoids in Asia. *Naturwissenschaften* 95, 1121–1135. doi:10.1007/s00114-008-0428-2

Métais, G., Soe, A. N., Marivaux, L., and Beard, K. C. (2007). Artiodactyls from the pondaung formation (Myanmar): New data and reevaluation of the south Asian faunal province during the middle Eocene. *Naturwissenschaften* 94, 759–768. doi:10.1007/s00114-007-0256-9

Métais, G., and Vislobokova, I. A. (2007). "Basal ruminants," in *The evolution of artiodactyls*. Editors D. R. Prothero and S. E. Foss (Baltimore: The Johns Hopkins University Press), 189–212.

Missiaen, P., and Gingerich, P. D. (2014). "New basal Perissodactyla (mammalia) from the lower Eocene ghazij formation of Pakistan," in *Contributions from the Museum of Paleontology* (Ann Arbor, Michigan: The University of Michigan), 32, 139–160.

Norris, C. A. (1999). The cranium of *Bunomeryx* (artiodactyla: Homacodontidae) from the upper Eocene uinta deposits of Utah and its implications for tylopod systematics. *J. Vertebrate Paleontology* 19, 742–751. doi:10.1080/02724634.1999.10011186

Orliac, M. J., and Ducrocq, S. (2012). Eocene raoellids (mammalia, cetartiodactyla) outside the Indian subcontinent: Palaeogeographical implications. *Geol. Mag.* 149, 80–92. doi:10.1017/s0016756811000586

Palcu, D. V., and Krijgsman, W. (2022). The dire straits of paratethys: Gateways to the anoxic giant of Eurasia. *Geol. Soc. Lond. Spec. Publ.* 523. in press. doi:10.1144/sp523-2021-73

Peterson, O. A. (1919). Report upon the material discovered in the upper Eocene of the uinta basin by earl douglas in the years 1908-1909, and by O. A. Peterson in 1912. *Ann. Carnegie Mus.* 12, 40–168. doi:10.5962/p.330969

Pickford, M., and Morales, J. (2003). New Listriodontinae (Mammalia, Suidae) from Europe and a review of listriodont evolution, biostratigraphy and biogeography. *Geodiversitas* 25, 347–404.

Rose, K. D. (1996). On the origin of the order artiodactyla. *Proc. Natl. Acad. Sci. U. S. A.* 93, 1705–1709. doi:10.1073/pnas.93.4.1705

Russell, D. E., and Zhai, R. J. (1987). The palaeogene of Asia: Mammals and stratigraphy. *Mémoires Du. Muséum Natl. d'Histoire Nat. Ser. C* 52, 1–488.

Schaeffer, B. (1947). Notes on the origin and function of the artiodactyl tarsus. *Am. Mus. Novitates* 1356, 1–24.

Simpson, G. G. (1945). The principles of classification and a classification of mammals. *Bull. Am. Mus. Nat. Hist.* 85, 1–350.

Sinclair, W. J. (1914). A revision of the bunodont artiodactyla of the middle and lower Eocene of North America. *Bull. Am. Mus. Nat. Hist.* 33, 267–295.

Singh Rana, R., Waqas, M., Orliac, M., Folie, A., and Smith, T. (2021). A new basal raoellid artiodactyl (mammalia) from the middle Eocene subathu group of rajouri district, Jammu and Kashmir, northwest himalaya, India. *Geobios* 66–67, 193–206. doi:10.1016/j.geobios.2020.12.003

Speijer, R. P., Pälike, H., Hollis, C. J., Hooker, J. J., and Ogg, J. G. (2020). "The Paleogene period," in *Geologic time scale 2020*. Editors F. M. Gradstein, J. G. Ogg, M. D. Schmitz, and G. M. Ogg (Amsterdam, Netherlands: Elsevier), 1087–1140.

Stehlin, H. G. (1910). Die Säugetiere des schweizerischen Eocaens, Sechster Teil: *Catodontherium–Dacrytherium–Leptotheridium–Anoplotherium–Diplobune–Xiphodon–Pseudamphimeryx–Amphimeryx–Dichodon–Haplomeryx–Tapirulus–Gelocus*–Nachträge–Artiodactyla incertae sedis–Schlussbetrachtungen über die Artiodactylen–Nachträge zu den Perissodactylen. *Abh. Schweiz. Palaeontologischen Ges.* 36, 838–1164.

Stehlin, H. G. (1906). Die Säugetiere des schweizerischen Eocaens, Vierter Teil: *Dichobune–Mouillacitherium–Meniscodon–Oxacron*. *Abh. Schweiz. Palaeontologischen Ges.* 33, 596–690.

Stucky, R. K. (1998). "Eocene bunodont and bunoselenodont Artiodactyla ("dichobunids")," in *Evolution of tertiary mammals of North America*. Editors C. M. Janis, K. M. Scott, and L. L. Jacobs (Cambridge: Cambridge University Press), 358–374.

Sudre, J., and Erfurt, J. (1996). Les artiodactyles du gisement yprésien terminal de Premontre (Aisne, France). *Palaeovertebrata* 25, 391–414.

Sudre, J. (1978). "Les Artiodactyles de l'Eocene moyen et superieur d'Europe occidentale (systematique et evolution)," in *Memoires et Travaux de l'institut de Montpellier de l'Ecole Pratique Des Hautes Etudes* (Montpellier: Ecole Pratique des Hautes Etudes, Institut de Montepellier), 7, 1–229.

Sudre, J. (1972). Révision des artiodactyles de l'Éocene moyen de Lissieu (Rhône). *Paleovertebrata* 5, 111–156.

Sudre, J., Russell, D. E., Louis, P., and Savage, D. E. (1983). Les artiodactyles de l'Eocene inferieur d'Europe (seconde partie). *Bull. Du. Mus. Natl. d'Histoire Nat.* 5, 339–365.

Theodor, J. M., Erfurt, J., and Métais, G. (2007). "The earliest artiodactyls: Diacodexeidae, Dichobunidae, Homacodontidae, leptochoeridae, and Raoellidae," in *The evolution of artiodactyls*. Editors D. R. Prothero and S. E. Foss (Baltimore: John Hopkins University Press), 32–58.

Theodor, J. M., Rose, K. D., and Erfurt, J. (2005). "Artiodactyla," in *The rise of placental mammals: Origins and relationships of the major extant clades*. Editors K. D. Rose and J. D. Archibald (Baltimore: Johns Hopkins University Press), 215–233.

Thewissen, J. G. M., Cooper, L. N., Clementz, M. T., Bajpai, S., and Tiwari, B. N. (2007). Whales originated from aquatic artiodactyls in the Eocene epoch of India. *Nature* 450, 1190–1194. doi:10.1038/nature06343

Thewissen, J. G. M., Gingerich, P. D., and Russell, D. E. (1987). "Artiodactyla and Perissodactyla (mammalia) from the early-middle Eocene kuldana formation of kohat (Pakistan)," in *Contributions from the Museum of Paleontology* (Ann Arbor, Michigan: The University of Michigan), 27, 247–274.

Thewissen, J. G. M., Nanda, A. C., and Bajpai, S. (2020). "*Indohyus*, endemic radiation of raoellid artiodactyls in the Eocene of India and Pakistan," in *Biological consequences of plate tectonics: New perspectives on post-gondwana break-up–A tribute to ashok sahni*. Editors G. V. R. Prasad and R. Patnaik (Cham: Springer International Publishing), 337–346.

Tissier, J., Becker, D., Codrea, V., Costeur, L., Fărcaş, C., Solomon, A., et al. (2018). New data on amynodontidae (mammalia, Perissodactyla) from eastern Europe: Phylogenetic and palaeobiogeographic implications around the eocene-oligocene transition. *PLoS ONE* 13, e0193774. doi:10.1371/journal.pone.0193774

Tsubamoto, T., Egi, N., Takai, M., Thaung, H., and Zin Maung Maung, T. (2013). A new genus and species of bunodont artiodactyl from the Eocene Pondaung Formation, Myanmar. *Paleontological Res.* 17, 297–311. doi:10.2517/1342-8144-17.4.297

Tsubamoto, T., Tun, S. T., Egi, N., Takai, M., Shigehara, N., Soe, A., et al. (2003). Reevaluation of some ungulate mammals from the Eocene pondaung formation, Myanmar. *Paleontological Res.* 7, 219–243. doi:10.2517/prpsj.7.219

Van der Made, J. G., and Han, D. (1994). Suoidea from the upper Miocene hominoid locality of Lufeng, Yunnan province, China. *Proc. Koninklijke Nederl. Akademie van Wetenschappen* 97, 27–82.

Van der Made, J. (1996). Listriodontinae (Suidae, Mammalia), their evolution, systematics and distribution in time and space. *Contributions Tert. Quat. Geol.* 33, 3–254.

Van der Made, J. (1997). Systematics and stratigraphy of the genera taucanamo and Schizochoerus and a classification of the palaeochoeridae (suoidea, mammalia). *Proc. Koninklijke Nederl. Akademie van Wetenschappen* 100, 127–139.

Viret, J. (1961). "Artiodactyla," in *Traité de Paléontologie*. Editor J. Piveteau (Paris: Masson et Cie), 887–1084.

Vislobokova, I. A. (2004b). A new representative of the family Raoellidae (suiformes) from the middle Eocene of khaichin-ula 2, Mongolia. *Paleontological J.* 38, 220–226.

Vislobokova, I. A. (1998). A new representative of the Hypertraguloidea (Tragulina, Ruminantia) from the Khoer-Dzan locality in Mongolia, with remarks on the relationships of the Hypertragulidae. *Am. Mus. Novitates* 3225, 1–24.

Vislobokova, I. A. (2002). *Archaeomeryx* (archaeomerycidae, Ruminantia): Morphology, ecology, and role in the evolution of the artiodactyla. *Paleontological J.* 36, S429–S522.

Vislobokova, I. A. (2004a). Artiodactyls from the middle Eocene of khaichin-ula II, Mongolia. *Paleontological J.* 38, 90–96.

Vislobokova, I. A. (2008). The oldest representative of Entelodontoidea (Artiodactyla, Suiformes) from the Middle Eocene of Khaichin Ula II, Mongolia, and some evolutionary features of this superfamily. *Paleontological J.* 42, 643–654. doi:10.1134/S0031030108060105

Wang, B. Y., and Qiu, Z. X. (2002). A new species of Entelodontidae (artiodactyla, mammalia) from late Eocene of Nei Mongol, China. *Vertebr. Palasiat.* 40, 194–202.

Wang, B. Y., Qiu, Z. X., Zhang, Q. Z., Wu, L. J., and Ning, P. J. (2009). Large mammals found from Houldjin formation near erenhot, nei mongol, China. *Vertebr. Palasiat.* 47, 85–110.

Wang, Y. Q., Li, Q., Bai, B., Jin, X., Mao, F. Y., and Meng, J. (2019). Paleogene integrative stratigraphy and timescale of China. *Sci. China Earth Sci.* 62, 287–309. doi:10.1007/s11430-018-9305-y

Wang, Y. Q., Meng, J., and Jin, X. (2012). Comments on Paleogene localities and stratigraphy in the Erlian Basin, nei mongol, China. *Vertebr. Palasiat.* 50, 181–203.

West, R. M. (1984). Paleontology and geology of the bridger formation, southern green river basin, souwester Wyoming, Part 7: Survey of bridgeran artiodactyla, including description of a skull and partial skeleton of *Antiacodon pygmaeus*. *Contributions Biol. Geol. Milwaukee Public Mus.* 56, 1–47.

Woodburne, M. O. (2004). "Global events and the North American mammalian biochronology," in *Late cretaceous and cenozoic mammals of North America*. Editor M. O. Woodburne (New York: Columbia University Press), 315–344.

Zhang, Y., Liu, Z., Fu, S., Jiang, S., Yao, N., and Wang, X. (2019). New understandings of the basement characteristics and evolution process of Erlian Basin. *Oil Geophys. Prospect.* 54, 404–416.

frontiers | Frontiers in Earth Science

TYPE Original Research
PUBLISHED 30 June 2023
DOI 10.3389/feart.2023.1171452

OPEN ACCESS

EDITED BY
Olev Vinn,
University of Tartu, Estonia

REVIEWED BY
Teuntje Hollaar,
University of Exeter, United Kingdom
Abraham Dabengwa,
University of the Witwatersrand, South Africa

*CORRESPONDENCE
Yuan-Qing Wang,
wangyuanqing@ivpp.ac.cn
Xiaoqiang Li,
lixiaoqiang@ivpp.ac.cn

†These authors have contributed equally to this work

RECEIVED 22 February 2023
ACCEPTED 21 June 2023
PUBLISHED 30 June 2023

CITATION
Zhou X, Wang J, Li Q, Bai B, Mao F, Li X and Wang Y-Q (2023), Late Paleocene to early Oligocene fire ecology of the south Mongolian highland.
Front. Earth Sci. 11:1171452.
doi: 10.3389/feart.2023.1171452

Late Paleocene to early Oligocene fire ecology of the south Mongolian highland

Xinying Zhou[1,2†], Jian Wang[1,3†], Qian Li[1], Bin Bai[1], Fangyuan Mao[1], Xiaoqiang Li[1,2*] and Yuan-Qing Wang[1,2*]

[1]Key Laboratory of Vertebrate Evolution and Human Origins of Chinese Academy of Sciences, Institute of Vertebrate Paleontology and Paleoanthropology, Beijing, China, [2]College of Earth and Planetary Sciences, University of Chinese Academy of Sciences, Beijing, China, [3]Department of Archaeology and Anthropology, University of Chinese Academy of Sciences, Beijing, China

Changes in fire ecology during warm and cold periods in the geological past are important because of their effects on terrestrial ecosystems and the global carbon cycle. We examined the charcoal concentrations of the Erden Obo section in Inner Mongolia to reconstruct the evolution of wildfire and their relationship to the regional vegetation from the Late Paleocene through Early Oligocene. Our data show that fire frequency were relatively high from the end of the Paleocene to the beginning of the Eocene, in accord with other paleofire records worldwide. However, low fire frequency occurred during the Early Eocene Climate Optimum (EECO), coincident with the change in the regional vegetation from shrubland to forest due to the strengthening of the regional rainfall, and we suggest that the humid climate may have been responsible for this decrease. High frequency fire occurred after the Middle Eocene, near-synchronously with the transition of the regional vegetation from forest to steppe. The high-frequency fire was most likely triggered by regional drought during the aridification process after the Middle Eocene. We propose that these temporal changes in the fire ecology were consistent within the northern temperate zone from the Late Paleocene through Early Oligocene, and we suggest that studies of global wildfires need to be evaluated within the context of paleovegetation zones and ecosystem evolution.

KEYWORDS

fire ecology, Eocene, Mongolia highland, vegetation, Erden Obo, Erlian basin

1 Introduction

During the Eocene, ~56–33.9 million years ago (Ma), the global climate system experienced a series of major adjustments, including the Paleocene–Eocene Thermal Maximum (PETM), the Early Eocene Climate Optimum (EECO), the Middle Eocene Climate Optimum (MECO), and the Eocene-Oligocene transition (EOT) events, which comprised the warmest intervals within the entire Cenozoic (Zachos et al., 2001; Barnet et al., 2019). Studies of the changes in terrestrial ecosystems, the global carbon cycle, and the global climate during the warming and cooling events of the Eocene have contributed to an improved understanding of the interactions among the climate system and the carbon cycle on a global scale (McInerney and Wing, 2011; Sun et al., 2014; Barnet et al., 2019).

Fire is a key mechanism for facilitating rapid exchanges among terrestrial carbon pools and the atmospheric and oceanic carbon pools (Bond and Keeley, 2005; Lasslop et al., 2019), and it has long been an important component of Earth's terrestrial

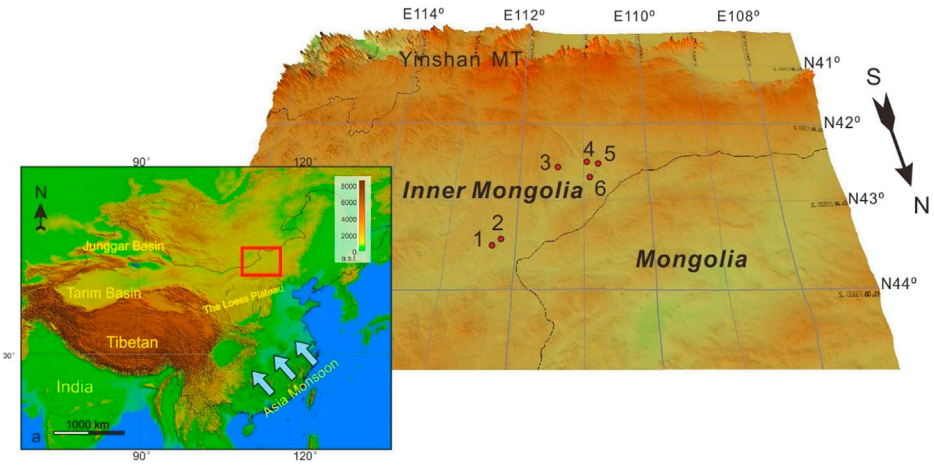

FIGURE 1
The study area, sedimentary section, and other sites mentioned in this study. 1. Arshanto; 2. Irdin Manha; 3. Erden Obo (this study); 4. Ulan Gochu; 5. Ula Usu; 6. Wulanhuxiu (modified from Wang et al., 2012; Bai et al., 2018).

ecosystems, affecting vegetation distributions, carbon cycling, and the global climate (Bond and Keeley, 2005; Reichstein et al., 2013; Lasslop et al., 2019). The ecological history of fire can provide important clues for understanding anomalous climate events from the Paleocene through Oligocene (Higgins and Schrag, 2004; Fung et al., 2019). The "wildfire hypothesis" proposed by Kurtz et al. (2003) suggests that widespread fire and peatland burning occurred globally at the Paleocene-Eocene transition, resulting in the release of huge quantities of light carbon during a brief interval (~0.17 Ma) and causing prominent negative $\delta^{13}C$ peak within benthic foraminifera in the global deep ocean. That ultimately triggered the Paleocene–Eocene Thermal Maximum (PETM) (Kurtz et al., 2003; Finkelstein et al., 2006). Although the "wildfire hypothesis" has been recently questioned, the role of terrestrial ecosystem changes and fire in explaining ocean carbon isotope records and global climate anomalies during the Paleocene remains important (McInerney and Wing, 2011; Fung et al., 2019). The key question is whether the terrestrial carbon pool could have released such a large amount of carbon in such a short interval, and we still lack extensive geological evidence to assess the extent and magnitude of the paleofires (Moore and Kurtz, 2008; McInerney and Wing, 2011).

The Mongolian Plateau is located on the edge of the current Asian summer monsoon system, and it is a key area for studying mammalian evolution and radiation (Meng et al., 1994; Wang et al., 2010). The Paleogene biostratigraphy of this region, based on fossil mammals, is by far the best documented within Asia (Bai et al., 2018; Li et al., 2018). Here, we present charcoal records from the Erden Obo section of the Erlian Basin in Inner Mongolia, which we use to reconstruct regional fire history and explore the fire dynamics from the Late Paleocene through Early Oligocene. Our results contribute to an improved understanding of the linkages among climate, vegetation and fire, with implications for predicting the rate and magnitude of future global warming.

2 Regional setting and research materials

The Erlian Basin, which today is part of the central and northern parts of Inner Mongolia Autonomous Region, is located on the edge of the East Asian monsoon and on the boundary between the North China and Siberian Plate. The basin is one of the large onshore sedimentary basins of East Asia and is ~1,000 km long from east to west and 20–220 km wide from north to south, with the total area of 101,000 km^2, bounded by the Songliao Basin to the east, the Hailar-Tamsag Basin and the East Gobi Basin to the north, and the Yingen-Ejinaqi Basin to the west (Meng et al., 2003). Meteorological records indicate modern annual precipitation is 139 mm, with the annual mean temperature varying between −2°C and 11°C, and 4.5°C on average. Recorded summer high temperatures can reach 41°C and winter temperatures are as low as −40°C.

The Erden Obo section in the central Erlian Basin is one of the most important Paleogene mammal fossil sites in the Mongolian highland (Figure 1). The Erden Obo [reported in Osborn (1929) as Urtyn Obo] section was first reported by Osborn (1929), based on Granger's (1928) sketch. Osborn (1929) divided the section into eight units from bottom to top (Figure 2): "Basal Red," "Basal White," "Lower Red," "Lower White" (19.8 m), "Middle Red" (21.3 m), "Middle White or Gray" (9.1 m), "Upper Red" (29.0 m), and "Upper White" (7.6 m) (Granger, 1928). The "red layer" is composed mainly of brick-red mudstone with muddy siltstone and silty mudstone, while the "white layer" consists mainly of fine or medium sand, coarse sandstone, and conglomerates. The sedimentary environment of these strata is flood plain, shallow lake and river sediment interbed.

In this study, we collected sediment samples from the Erden Obo section, following Granger's (1928) simple stratigraphic division; however, we remeasured the section with a level and the base was extended downwards. Our new measurements show that the thickness of the Erden Obo section from top to bottom is ~189 m, including 0–11.7 m for the upper white, 11.7–50.2 m for

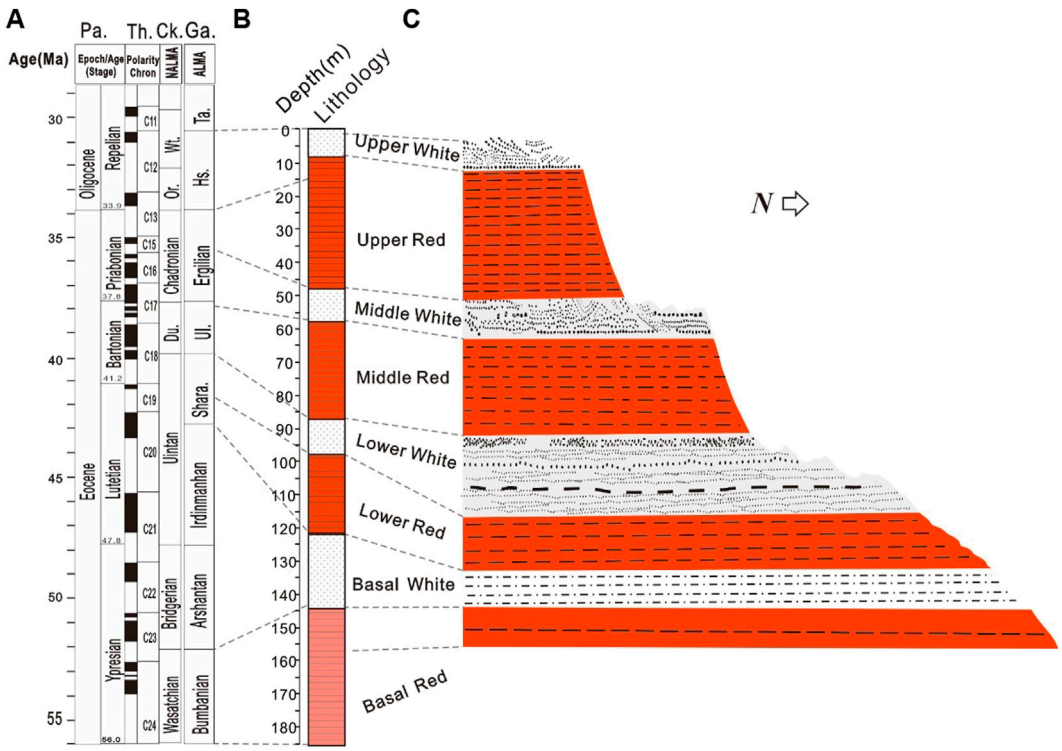

FIGURE 2
Biochronology based on large mammal fossils of the Erden Obo section (according to Bai et al., 2018). **(A)** Standard paleomagnetic stratigraphy, North American land mammal ages (NALMA), and Asian land mammal ages (ALMA). **(B)** Lithology of the Erden Obo section. **(C)** Field sketch of the Erden Obo section (Granger, 1928).

the upper red, 50.2–58.5 m for the middle white layer, 58.5–89.2 m for the middle red layer, 89.2–99.4 m for the lower white, 99.4–122.7 m for the lower red, 122.7–146 m for the bottom white, and 146–189 m for the basal red. Samples were collected from the bottom of the section downward at an average interval of 1.2 m. Around 1 kg of sediment was collected for each sample and the samples were taken from all eight deposition units.

3 Stratigraphy and chronology

The stratigraphic range of the Erlian Basin is nearly continuous from the Late Paleocene through Early Oligocene, and almost all the Eocene ALMAs except Bumbanian and Ergilian are based on the corresponding faunas of the basin. Various large and small mammalian fossils have been reported from different units at Erden Obo and they have contributed to the refinement of biostratigraphic correlations with other localities in the Erlian Basin (Jiang, 1983; Qi, 1990). The age determination of the Erden Obo section in this study is based mainly on biostratigraphic correlations (Figure 2A).

In the biostratigraphic correlations made in the 1930s, the "Basal Red" was regarded as the same stage as the Arshanto Formation, suggesting that the basal age was ~50 Ma (Osborn, 1929). Wang et al. (2012) suggested that the "Basal Red" should be the Nomogen Formation and the "Upper White" should be the upper Naogangdai Formation, while the correlation of the other layers at Erden Obo remains unclear (Wang et al., 2012). The magnetostratigraphic results for the Nohe Timbur and Huhe Boerhe sections show that the Nomogen Formation was mainly deposited from the Late Paleocene through earliest Eocene, with the age range of ~59.2–54.8 Ma. The Ashantou Formation spans the Early and Middle Eocene, with the age range of ~54.1–48.2 Ma. The age of the Ildinmanha Formation is Middle Eocene, constrained to ~48–47 Ma (Sun et al., 2009). Bai et al. (2018) comprehensively analyzed the temporal and spatial distribution of Paleogene perissodactyl species in the Erlian Basin based on published specimens and accordingly revised the most complete sedimentary section at Erden Obo, with the age range from Late Paleocene through Early Oligocene (Figures 2B, C).

Previous studies of the biostratigraphy and magnetostratigraphy (unpublished data) indicate that the depositional history of the Erden Obo section commenced at the end of the Paleocene and spans the early middle and late Eocene through Early Oligocene with the approximate age range of 55–30 Ma. Considering multiple factors, the chronostratigraphic framework referenced in this study is the same as that established by Bai et al. (2018) and Li et al. (2018).

4 Charcoal analysis

Charcoal is a direct product of the incomplete combustion of plant bodies by fire, and the concentration and frequency of charcoal

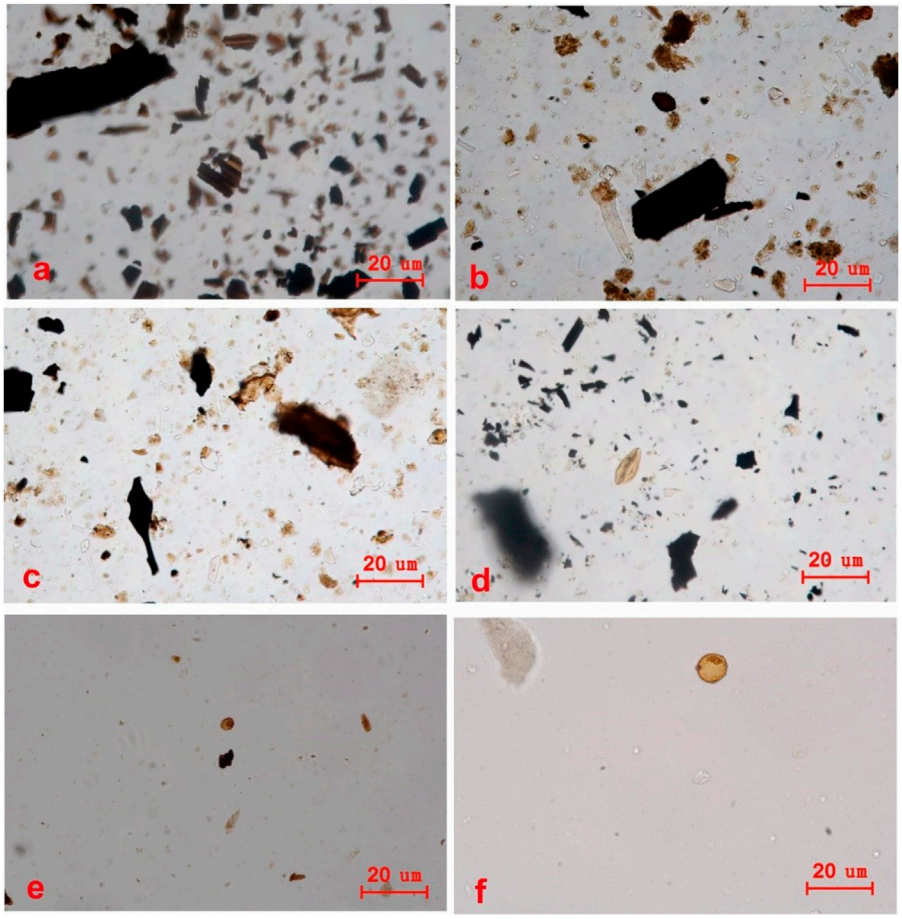

FIGURE 3
Microscope photographs of various concentrations of charcoal particles in pollen slides from the Erden Obo section. **(A,B)** High concentration sample (No. NN065, 99.4 m). **(C,D)** Moderate concentration sample (No. NN154, 10.2 m). **(E,F)** Low concentration sample (No. NN036, 146.7 m).

in the sediment indicate the intensity and frequency of paleo fire (Higuera et al., 2007). Fire history reconstruction inferred from sedimentary charcoal records is based on measuring screened charcoal area, estimating fragment volume, or counting fragment (Leys, B., et al., 2013). The reconstruction based on charcoal area is more explicit and stable than the reconstruction based on debris count (Leys, B., et al., 2013). Area-based reconstruction rather than particle counting methods should be used when debris is likely to affect debris abundance (Leys, B., et al., 2013; Higuera et al., 2007.

The microscopic charcoal particles encountered on pollen slides in this study were quantified with the point count method (Clark, 1982). Differences in charcoal size and size-class distribution are mainly caused by different preparation techniques (Tinner and Hu, 2003). This method provides a probability-based estimate of the Charcoal Area Concentration (CAC) of sediment samples, enabling the rapid quantification of the area rather than the total number of charcoal particles on a pollen slide, and the area and number concentrations of charcoal particles are highly correlated in standard pollen slides (Tinner and Hu, 2003). Hence it is not biased by the fragmentation of charcoal particles that occurs during pollen extraction or by sediment diagenesis (Clark, 1982). A total of 83 samples were collected between 0–190 m for microcharcoal analysis. For each sample, ~150 g of sediment was processed using standard palynological preparation procedures. The extraction procedures are as follows: sample was used for pollen analysis and pretreatment consisted of the following stages: 1) Addition of hydrochloric acid to remove carbonates; 2) flotation with 2.0 second-class heavy liquid flotation (with ZnCl2 and KI-ZnI2); 3) addition of a 1:9 solution of concentrated sulfuric acid and acetic anhydride; 4) suspension in glycerol and mounting on microscope slides.

One tablet containing a known number of *Lycopodium* spores (27,560) was added to estimate microcharcoal concentrations. Microscopic charcoal was point-counted during palynological identification, and each sample was examined at ×400 magnification for 500 fields of view (FOV) on pollen slides. The charcoal area concentration was calculated as:

$$Y = \frac{C}{M} \times \frac{L}{l} \times \frac{S}{G} \ (cm^2/g)$$

where Y is the charcoal area concentration (cm^2/g), C is the number of points covered by the counted charcoal, M is the total number of points in the 500 FOVs (5500 in this study), L is the number of *Lycopodium* spores (=27,560), l is the number of *Lycopodium* spores

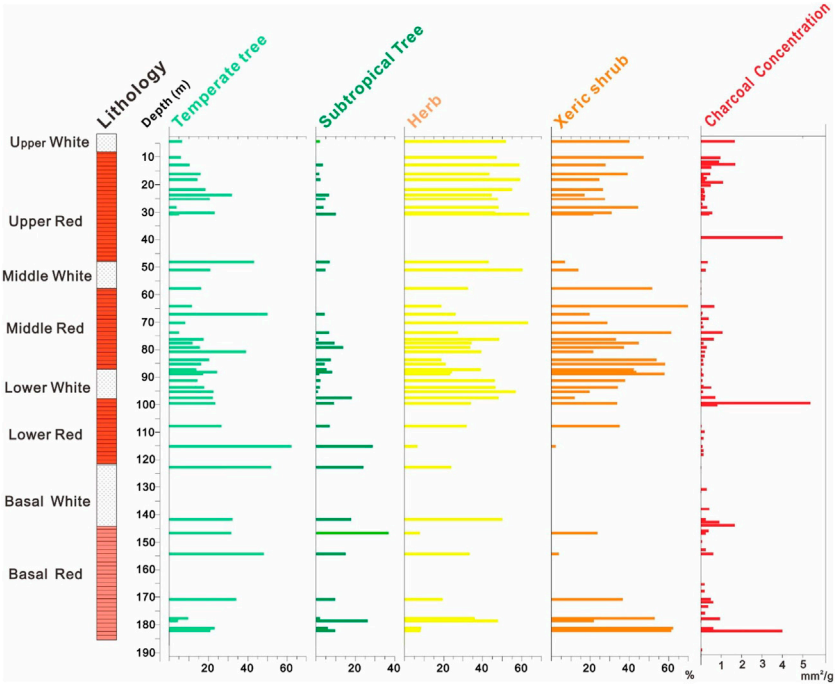

FIGURE 4
Depth profiles of microcharcoal concentrations and the percentages of selected pollen taxa within the Erden Obo section.

counted, S is the area of 500 FOVs (≈4.54 × 10^2 mm^2), and G is the weight of each sample (150 g).

5 Results

Examples of different microcharcoal concentrations in the sediments of Erden Obo are shown in Figure 3. The microcharcoal concentrations and pollen data were used to assess the dynamics of the regional vegetation and fire activity (Li et al., 2005; Miao et al., 2022). Charcoal particles were observed in 78 out of 83 samples, but the CAC values were low on average and they fluctuated substantially. The overall mean CAC is 0.493 mm^2/g and 39 samples had values <0.2 mm^2/g. Only 23 samples were above the mean value of 0.493 mm^2/g, and 8 samples had values >1 mm^2/g. Peak values were 4.008 mm^2/g at 182.2 m, 4.015 mm^2/g at 39.2 m, and 5.382 mm^2/g at 99.4 m, which is around ten times the overall mean value.

Overall, the CAC records show a high-low-high temporal pattern. First peak value of 4.01 mm^2/g occurs at the base of the profile (182.2 m), and the mean value (174–180 m) is also relatively high. In contrast, the mean value (0.326 mm^2/g) in the middle and lower middle parts of the section (105–174 m) is lower overall, and no charcoal particles were observed in the samples from the depths of 107.7, 122.7, and 131.7 m. However, the CAC increases abruptly above 100 m and reaches the maximum value (5.38 mm^2/g), while the CAC increases significantly above 40 m and reaches a third peak.

The charcoal area concentrations correlate quite well with the pollen stratigraphy (Figure 4). From the pollen data, the tree taxa occupied a large proportion in the early Eocene, but decreased significantly after about 42 Ma. At the same time, the types of herbaceous and xerophytic shrub increased dramatically. And there were several notable fluctuations. Stratigraphic levels with high charcoal concentrations are generally associated with lower tree pollen concentrations, especially subtropical taxa, and the microcharcoal concentrations are better correlated with higher proportions of xerophytic shrubs and herbaceous taxa. Additionally, considering that both high and low microcharcoal concentrations occur in both the white sandstone and red mudstone layers, there appears to be no relationship between the sedimentary facies and microcharcoal concentrations.

6 Discussion

Based on mammal fossils unearthed in Erden Obo section, the fauna of North America and the regional Palaeogene biostratigraphy, the age of Erden Aobao section has been determined to be from late Paleocene to Early Oligocene, including the early, middle and late Eocene strata, spanning about 56–30 Ma (Bai et al., 2018; Li et al., 2018). The stratigraphic-chronological correlation lines in Figures 2, 5 are shown, it is more certain that the “Basal Red” and Bumbanian Formation are at the same time, the date is late Paleocene-early Eocene, roughly 56–52 Ma; “Basal White” corresponds to Arshantan Formation (Early Eocene) and Irdinmanhan Formation (Middle Eocene), roughly 52–43 Ma; “Lower Red” corresponds to the lower part of Sharamulun Formation (Shara.) roughly 43–41 Ma; “Lower White” is equivalent to the upper of Sharamulun Formation, roughly 41–40 Ma; “Middle red” corresponds to Ulangechu (Ul.),

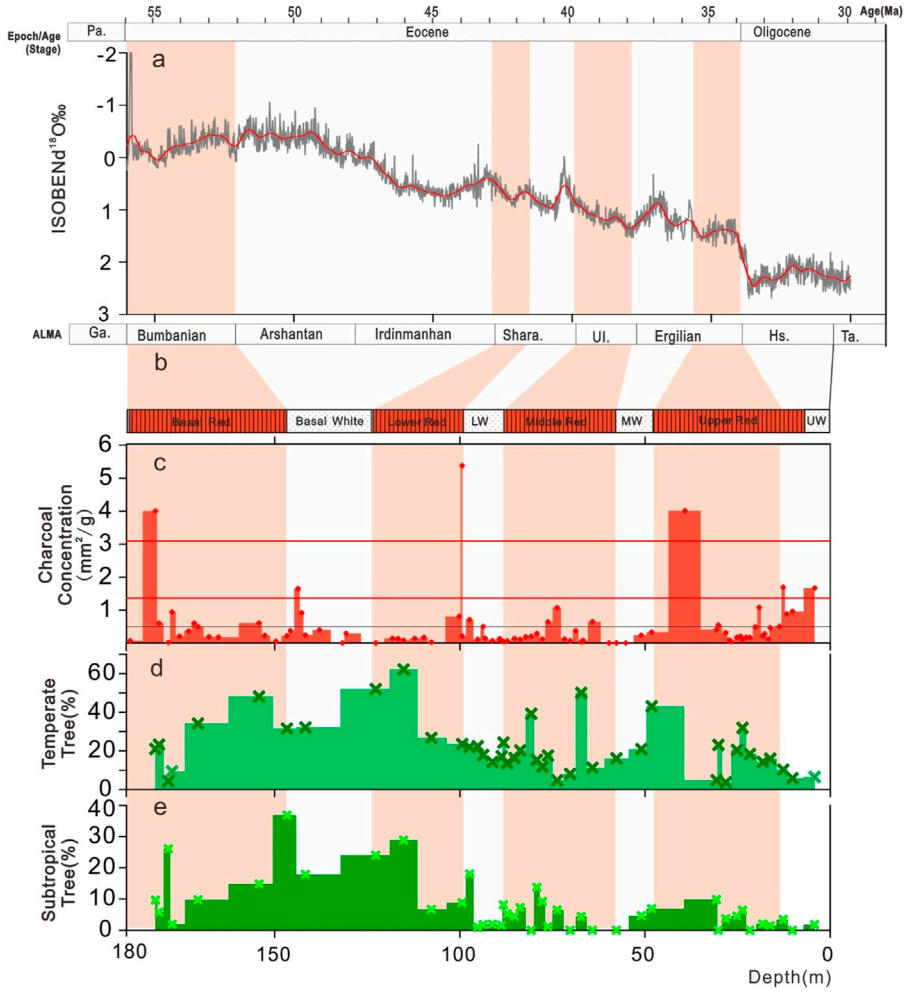

FIGURE 5
Comparison of fire evolution mechanisms and global changes on the Mongolian Plateau. **(A)** Global temperature as indicated by the benthic foraminiferal $\delta^{18}O$ record (Westerhold et al., 2020). **(B)** Correlation of the ALMA and the mammalian chronostratigraphy of the Erden Obo section. **(C)** CAC of the Erden Obo section. **(D,E)** Percentages of temperate and subtropical trees of the Erden Obo section. The pink shading represents geological ages corresponding to the lithostratigraphy of the Erden Obo section, based on the comparison of the ALMA.

roughly 40–38 Ma; "Middle White" is equivalent to the lower of the Erglian formation, roughly 38–36 Ma; The lower part of "Upper Red" corresponds to the upper part of the Erglian formation, roughly 36–34 Ma; The upper part of "Upper Red" and "Upper White" belong to the Oligocene, about 34–30 Ma.

Although the age of the Erden Obo section spans 56–30 Ma, the PETM event (~55.8 Ma) may not have been resolved using our data as it lasted only 0.17 Myr (Röhl et al., 2007), and the CAC data from Erden Obo are of insufficient resolution (~0.25 Myr) to capture it. Additionally, although the Erden Aobao section includes the most complete strata in Erlian Basin from the end of Paleocene to the early Oligocene, a regional sedimentary discontinuity and stratigraphic deficiencies may exist in the area. Nevertheless, the CAC data provide an overview of the Paleogene fire history on the south Mongolian Plateau, including the EECO, MECO, and EOT.

Our CAC record suggests that fires were infrequent in Erlian basin during the Late Paleocene through Early Oligocene, at least compared with Quaternary fire records from the surrounding area. Nearby Quarternary loess sediments had an average CAC of ~1–3 mm^2/g in Quaternary loess sediments adjacent to our study area (Li et al., 2009), and a CAC range of 0.03–57.77 mm^2/g in the Holocene sediments of Northeast China, with the average of 7.12 mm^2/g (Li et al., 2005). CAC values were as high as 100 mm^2/g during the late Holocene, as the result of anthropogenic factors (Li et al., 2007). In contrast, the mean CAC at Erden Obo is only 0.493 mm^2/g, with around half of the data values <0.2 mm^2/g. This indicates that fire activity on the Mongolian Plateau from the end of the Paleocene to the beginning of the Oligocene, including the entire Eocene, was relatively low compared to the Quaternary in northern China.

The modern global distribution of natural fires shows that high-frequency fires occur mainly in areas with strong seasonality, such as in seasonal rainforest in typical monsoon zones (Southeast Asia, South China) and shrub-steppe (Eastern Europe, eastern Inner Mongolia steppe) (Bond and Keeley, 2005; Reichstein et al., 2013; Hantson et al., 2015). Enhanced interannual climate variability,

i.e., extremely wet years followed by exceptionally dry years, promotes favorable fire conditions because of the annual accumulation of sufficient amounts of fuel-producing vegetation (e.g., grass) (Margolis and Balmat, 2009). Prolonged dry periods lead to widespread fires, which spread rapidly during the long dry season. In addition, fires may be less frequent during prolonged droughts if there is insufficient combustible biomass, while the vegetation composition and fire-prone plant taxa are also important factors in determining the fire propensity (Flannigan et al., 2009).

The temporal variations of our paleofire data may be related to the seasonal precipitation distribution and vegetation characteristics (Figure 5). High-latitude Sea surface temperatures (SST) increased by 10°C due to the high global temperatures in the Eocene (Zachos et al., 2001; Pearson et al., 2009). Tree taxa in tropical and subtropical areas, such as *Cycads*, *Pinus*, *Podocarpus*, *Rhus*, and Moraceae were widely distributed in the modern temperate regions of the Northern Hemisphere, suggesting a lower winter-summer temperature difference in northern temperate regions at that time (McInerney and Wing, 2011; Eberle and Greenwood, 2012; Lauretano et al., 2015). On the other hand, in terms of precipitation, the modern monsoon had not formed because the Tibetan Plateau did not yet exist, and water vapor from the Indian Ocean could not penetrate deeply into the Asian interior (Zhang et al., 2012). However, this effect during the EECO appears to have been offset by the increased precipitation in this region due to water vapor exchanges over land and sea driven by high temperatures (Quan et al., 2012; Licht et al., 2014). The precipitation in this region includes two components: sourced from the western Pacific and Indian Ocean in summer, and from the westerly belt in winter (Li et al., 2023). Therefore, the difference between dry and wet conditions in winter and summer was not significant, and as a result, the fire frequency throughout the Eocene was less frequent and intense than in modern monsoon rainforest and shrubland.

In terms of evolutionary trends, a significant three-stage (strong-weak-strong) temporal pattern is evident in Figures 4, 5. The microcharcoal concentration was the lowest in the Early Eocene (53–42 Ma, depth range 146–105 m), and no microcharcoal was visible in many layers. By contrast, CAC was much higher in the basal and upper parts of sections, indicating relatively intense fire activity during the Paleocene–Eocene transition and Early Eocene (depth interval 189–146 m, ~55–53 Ma) and the Late Eocene–Early Oligocene (depth interval 40–0 m, ~36–32 Ma). The degree of variation in charcoal concentrations of Erden Obo section is typical in studies of paleofire activity. Previous studies have shown that large wildfires typically burn hundreds of times as much woodland as ordinary fires (Artés et a., 2019), and that orders of magnitude differences in the amount of charcoal deposited on the ground can sometimes even be observed with the naked eye in the field.

Despite the relatively limited global data on Paleocene fires, it appears that the Late Paleocene–Early Eocene transition had a higher fire frequency than the EECO. Charcoal and palynological data from the Cobham lignite bed in southern England suggest that fire was sporadic in the Late Paleocene (Collinson et al., 2009), and that Eocene vegetation was characterized by a decrease in ferns, an increase in wetland plants, and a decrease in fire occurrence. Robson et al. (2015) studied 11 lignite seams within the Schöningen coal deposits in Germany and concluded that charcoal percentages during the Early Eocene did not indicate an increase in fire activity during the EECO.

Additionally, the record of particulate organic matter from IODP Site 302 suggests that fire activity was more active in the Paleocene than in the Early Eocene on land around the Arctic Ocean (Denis et al., 2017). These findings imply that the frequency and intensity of fire decreased from the Paleocene to the EECO, at least in the northern temperate zone (modern) during the Eocene, even though the EECO was the warmest period of the entire Cenozoic. High temperatures and seasonal drought have traditionally been considered to trigger fires (Flannigan et al., 2009). However, high heat exchange at the Earth's surface facilitated water exchange between the atmosphere, ocean, and land during the Early Eocene (Bowen et al., 2004; Licht et al., 2014), which resulted in the Earth acting more like a "steamer" than a "pan" (i.e., hot and humid rather than hot and dry) during the EECO. In short, the warm and humid global environment at this time led to a decrease in regional fire.

The proportion of temperate and subtropical trees in Erden Obo section was the highest during the EECO, indicating a relatively closed wet and warm forest ecosystem, which is in sharp contrast to the present-day desert-steppe with annual rainfall <150 mm (Wang et al., 2022). The increase in forest during the EECO occurred not only on the Mongolian Plateau but also on a global scale (Greenwood and Wing, 1995; Bowen et al., 2004; Eberle and Greenwood, 2012). At the same time, the Green River Formation of Utah and Colorado in North America was deposited within a set of large, unusually productive lakes (West et al., 2020), and subtropical palms and ginkgo trees expanded to Antarctica during the EECO. These observations reflect the fact that, at least during the EECO, global extreme heat caused warm and humid atmospheric circulation that promote the global expansion of tropic and subtropical forest, including inland Asia. After that, with the decrease of global temperature aroude 43 Ma, the proportion of trees in Erden Aobao section also decreased significantly. We can see the correlation between climate—vegetation and fire in our study area from the correlation between charcoal and pollen data.

The CAC data from the Erden Obo section recorded at least three major fire intervals during the Eocene. These events may be related to seasonal drought caused by abrupt global climate cooling during the Eocene, as the pollen evidence shows that these intervals are correlative with a decrease in tree pollen and an increase in herbaceous and xerophytic shrub pollen. Overall, regional fire activity was closely related to the evolution of the regional vegetation ecosystem. For example, several researchers have proposed that angiosperms triggered a new fire regime in the Cretaceous, which promoted the spread of angiosperms (Bond and Scott, 2010).

The fire intensity in the study region began to increase after around the Middle Eocene (depth 100 m, ~42 Ma), while the proportion of trees began to decrease and herbs and xerophytes increased significantly. Subsequently, during the Late Eocene (depth 45 m, ~37 Ma), the frequency and intensity of fires increased, accompanied by the maximum proportion of herbaceous vegetation. This process suggests that global temperatures decreased in the Middle and Late Eocene to Oligocene, and the

increased seasonal drought in temperate regions led to increased fire activity (Liu et al., 2009; Abels et al., 2011; Sun et al., 2014). We suggest that this dynamic change contributed to the evolution of steppe ecosystems and eventually to the formation of the northern steppe during the Oligocene.

In general, our CAC data from the Erden Aobao section indicate that wildfire activity in the Mongolian Plateau is associated with global temperature changes in a negative feedback mechanism from the end of the Paleocene to the beginning of the Oligocene, which is consistent with previous records in Europe and North America. The terrestrial vegetation system was closely related to fire activity. During the early Eocene warm period, the region's sub-tropical and temperate mixed woodland developed, and the regional climate became humid and the frequency of fire decreased. However, when the global temperature decreased in the middle and late Eocene, the regional grasslands/shrubs expanded, and fire activity began to increase. This means that when global temperatures are lower, more light carbon is released from terrestrial carbon pools through fire activity and deposited into oceans and lakes.

7 Conclusion

The CAC and palynological data for the Erden Obo section provide a history of the evolution of the fire ecology on the south Mongolian Plateau from the Late Paleocene through Early Oligocene. The overall low mean CAC values indicate that the Eocene fire activity on the Mongolian Plateau was less frequent and intense than within modern monsoon rainforest and shrubland. Fire activity was stronger during the Paleocene–Eocene and Late Eocene–Early Oligocene transition (depth interval 40–0 m) than during the EECO. Global high-temperature systems led to a wetter northern temperate zone during the EECO and regional fire activity was suppressed. Global temperatures decreased during the Middle and Late Eocene–Oligocene, increasing the occurrence of seasonal drought in temperate regions and leading to increased fire activity. All these factors together contributed to the evolution of the northern temperate grassland ecosystem in the Oligocene.

Data availability statement

The raw data supporting the conclusion of this article will be made available by the authors, without undue reservation.

Author contributions

Y-QW, XL and XZ designed the study. All authors participated in the fieldwork. FM performed the sample collection. JW and XZ conducted the experiments and data analysis. XZ and JW wrote the first draft. XL, Y-QW, BB and QL reviewed the final manuscript. All authors contributed to the paper and approved the submitted version.

Funding

This work is supported by the National Key Research and Development Program of China (22022YFF0801102), the CAS Project for Young Scientists in Basic Research (YSBR-019), the Strategic Priority Research Program of Chinese Academy of Sciences (XDB26000000), the National Natural Science Foundation of China (NSFC 41888101), and the Youth Innovation Promotion Association of the Chinese Academy of Sciences (2022071).

Acknowledgments

We would like to thank Dr. Yanxin Gong and Rancheng Xu for discussions on biostratigraphic comparisons in the Erlian Basin. Sincere thanks to Junnan Xu, Huihai Wang and Zhongshen Wang for pollen experiments. We are grateful to Prof. Jan Bloemendal for considerably improving the English language. The authors gratefully acknowledge the Handling Editor OV and two reviewers for their professional review comments.

Conflict of interest

The authors declare that the research was conducted in the absence of any commercial or financial relationships that could be construed as a potential conflict of interest.

Publisher's note

References

Abels, H. A., Dupont-Nivet, G., Xiao, G., Bosboom, R., and Krijgsman, W. (2011). Step-wise change of asian interior climate preceding the eocene–oligocene transition (EOT). *Palaeogeogr. Palaeoclimatol. Palaeoecol.* 299, 399–412. doi:10.1016/j.palaeo.2010.11.028

Artés, T., Oom, D., de RigoDurrant, D. T., Maianti, P., Libertà, G., San-Miguel-Ayanz, J., et al. (2019). A global wildfire dataset for the analysis of fire regimes and fire behaviour. *Sci. Data* 6, 296. doi:10.1038/s41597-019-0312-2

Bai, B., Wang, Y.-Q., Li, Q., Wang, H.-B., Mao, F.-Y., Gong, Y.-X., et al. (2018). Biostratigraphy and diversity of Paleogene perissodactyls from the Erlian Basin of inner Mongolia, China. *Am. Mus. Novitates* 3914, 1–60. doi:10.1206/3914.1

Barnet, J. S. K., Littler, K., Westerhold, T., Kroon, D., Leng, M. J., Bailey, I., et al. (2019). A high-fidelity benthic stable isotope record of late cretaceous–early Eocene climate change and carbon-cycling. *Paleoceanogr. Paleoclimatology* 34, 672–691. doi:10.1029/2019pa003556

Bond, W. J., and Keeley, J. E. (2005). Fire as a global 'herbivore': The ecology and evolution of flammable ecosystems. *Trends Ecol. Evol.* 20, 387–394. doi:10.1016/j.tree.2005.04.025

Bond, W. J., and Scott, A. C. (2010). Fire and the spread of flowering plants in the Cretaceous. *New Phytol.* 188, 1137–1150. doi:10.1111/j.1469-8137.2010.03418.x

Bowen, G. J., Beerling, D. J., Koch, P. L., Zachos, J. C., and Quattlebaum, T. (2004). A humid climate state during the Palaeocene/Eocene thermal maximum. *Nature* 432, 495–499. doi:10.1038/nature03115

Clark, R. L. (1982). Point count estimation of charcoal in pollen preparations and thin sections of sediments. *Pollen Spores* 24, 523–535.

Collinson, M. E., Steart, D. C., Harrington, G. J., Hooker, J. J., Scott, A. C., Allen, L. O., et al. (2009). Palynological evidence of vegetation dynamics in response to palaeoenvironmental change across the onset of the paleocene-eocene thermal maximum at Cobham, southern England. *Grana* 48, 38–66. doi:10.1080/00173130802707980

Denis, E. H., Pedentchouk, N., Schouten, S., Pagani, M., and Freeman, K. H. (2017). Fire and ecosystem change in the arctic across the paleocene–eocene thermal maximum. *Earth Planet. Sci. Lett.* 467, 149–156. doi:10.1016/j.epsl.2017.03.021

Eberle, J. J., and Greenwood, D. R. (2012). Life at the top of the greenhouse Eocene world—a review of the Eocene flora and vertebrate fauna from Canada's high arctic. *GSA Bull.* 124, 3–23. doi:10.1130/b30571.1

Finkelstein, D. B., Pratt, L. M., and Brassell, S. C. (2006). Can biomass burning produce a globally significant carbon-isotope excursion in the sedimentary record? *Earth Planet. Sci. Lett.* 250, 501–510. doi:10.1016/j.epsl.2006.08.010

Flannigan, M. D., Krawchuk, M. A., De Groot, W. J., Wotton, B. M., and Gowman, L. M. (2009). Implications of changing climate for global wildland fire. *Int. J. wildland fire* 18, 483–507. doi:10.1071/wf08187

Fung, M., Schaller, M., Hoff, C., Katz, M., and Wright, J. (2019). Widespread and intense wildfires at the Paleocene-Eocene boundary. *Geochem. Perspect. Lett.* 10, 1–6. doi:10.7185/geochemlet.1906

Granger, W. (1928). "Records of fossils collected in Mongolia. Central asiatic expeditions," in *Field books of the third asiatic expedition RBC51-E* (New York, NY, United States: American Museum of Natural History Library), 1–77.

Greenwood, D. R., and Wing, S. L. (1995). Eocene continental climates and latitudinal temperature gradients. *Geology* 23, 1044–1048. doi:10.1130/0091-7613(1995)023<1044:eccalt>2.3.co;2

Hantson, S., Pueyo, S., and Chuvieco, E. (2015). Global fire size distribution is driven by human impact and climate. *Glob. Ecol. Biogeogr.* 24, 77–86. doi:10.1111/geb.12246

Higgins, J. A., and Schrag, D. P. (2004). *Model simulations of the global carbon and sulfur cycles: Implications for the paleocene-eocene thermal maximum*. Washington, D.C., United States: American Geophysical Union.

Higuera, P. E., Peters, M. E., Brubaker, L. B., and Gavin, D. G. (2007). Understanding the origin and analysis of sediment-charcoal records with a simulation model. *Quat. Sci. Rev.* 26, 1790–1809. doi:10.1016/j.quascirev.2007.03.010

Jiang, H. X. (1983). Division of the Paleogene in the Erlian Basin of inner Mongolia. *Geol. Inn. Mogolia* 55, 18–36.

Kurtz, A. C., Kump, L. R., Arthur, M. A., Zachos, J. C., and Paytan, A. (2003). Early Cenozoic decoupling of the global carbon and sulfur cycles. *Paleoceanography* 18. doi:10.1029/2003pa000908

Lasslop, G., Coppola, A. I., Voulgarakis, A., Yue, C., and Veraverbeke, S. (2019). Influence of fire on the carbon cycle and climate. *Curr. Clim. Change Rep.* 5, 112–123. doi:10.1007/s40641-019-00128-9

Lauretano, V., Littler, K., Polling, M., Zachos, J. C., and Lourens, L. J. (2015). Frequency, magnitude and character of hyperthermal events at the onset of the Early Eocene Climatic Optimum. *Clim. Past* 11, 1313–1324. doi:10.5194/cp-11-1313-2015

Leys, B., Carcaillet, C., Dezileau, L., Ali, A. A., and Bradshaw, R. H. W. (2013). A comparison of charcoal measurements for reconstruction of Mediterranean paleo-fire frequency in the mountains of Corsica. *Quat. Res.* 79, 337–349. doi:10.1016/j.yqres.2013.01.003

Li, H., Yang, X., Scuderi, L. A., Hu, F., Liang, P., Jiang, Q., et al. (2023). East Gobi megalake systems reveal East Asian Monsoon dynamics over the last interglacial-glacial cycle. *Nat. Commun.* 14, 2103. doi:10.1038/s41467-023-37859-1

Li, Q., Mao, F.-Y., and Wang, Y.-Q. (2018). First record of Eocene fossil rodent assemblages from the lower part of the erden Obo section, Erlian Basin (nei mongol, China) and its biochronological implications. *Palaeobiodiversity Palaeoenvironments* 98, 259–276. doi:10.1007/s12549-017-0303-2

Li, X., Shang, X., Dodson, J., and Zhou, X. (2009). Holocene agriculture in the Guanzhong Basin in NW China indicated by pollen and charcoal evidence. *Holocene* 19, 1213–1220. doi:10.1177/0959683609345083

Li, X., Zhao, H., Yan, M., and Wang, S. (2005). Fire variations and relationship among fire and vegetation and climate during Holocene at sanjiang Plain,Northeast China. *Sci. Geogr. Sin.* 25, 177–182. doi:10.13249/j.cnki.sgs,2005.02.177

Li, X., Zhou, X., Zhou, J., Dodson, J., Zhang, H., and Shang, X. (2007). The earliest archaeobiological evidence of the broadening agriculture in China recorded at Xishanping site in Gansu Province. *Sci. China Ser. D Earth Sci.* 50, 1707–1714. doi:10.1007/s11430-007-0066-0

Licht, A., Van Cappelle, M., Abels, H. A., Ladant, J. B., Trabucho-Alexandre, J., France-Lanord, C., et al. (2014). Asian monsoons in a late Eocene greenhouse world. *Nature* 513, 501–506. doi:10.1038/nature13704

Liu, Z., Pagani, M., Zinniker, D., Deconto, R., Huber, M., Brinkhuis, H., et al. (2009). Global cooling during the eocene-oligocene climate transition. *Science* 323, 1187–1190. doi:10.1126/science.1166368

Margolis, E. Q., and Balmat, J. (2009). Fire history and fire–climate relationships along a fire regime gradient in the Santa Fe Municipal Watershed, NM, USA. *For. Ecol. Manag.* 258, 2416–2430. doi:10.1016/j.foreco.2009.08.019

Mcinerney, F. A., and Wing, S. L. (2011). The paleocene-eocene thermal maximum: A perturbation of carbon cycle, climate, and biosphere with implications for the future. *Annu. Rev. Earth Planet. Sci.* 39, 489–516. doi:10.1146/annurev-earth-040610-133431

Meng, J., Wyss, A. R., Dawson, M. R., and Zhai, R. (1994). Primitive fossil rodent from Inner Mongolia and its implications for mammalian phylogeny. *Nature* 370, 134–136. doi:10.1038/370134a0

Meng, Q., Hu, J., Jin, J., Zhang, Y., and Xu, D. (2003). Tectonics of the late Mesozoic wide extensional basin system in the China-Mongolia border region: Wide extensional basin system. *Basin Res.* 15, 397–415. doi:10.1046/j.1365-2117.2003.00209.x

Miao, Y., Nie, J., Hu, X., Wan, Z., Zhao, B., Zhao, Y., et al. (2022). Wildfire history and savanna expansion across southern Africa since the late Miocene. *Palaeogeogr. Palaeoclimatol. Palaeoecol.* 603, 111189. doi:10.1016/j.palaeo.2022.111189

Moore, E. A., and Kurtz, A. C. (2008). Black carbon in paleocene–eocene boundary sediments: A test of biomass combustion as the PETM trigger. *Palaeogeogr. Palaeoclimatol. Palaeoecol.* 267, 147–152. doi:10.1016/j.palaeo.2008.06.010

Osborn, H. F. (1929). Embolotherium, gen. Nov., of the ulan gochu, Mongolia. *Am. Mus. Novitates* 353, 1–20.

Pearson, P. N., Foster, G. L., and Wade, B. S. (2009). Atmospheric carbon dioxide through the Eocene–Oligocene climate transition. *Nature* 461, 1110–1113. doi:10.1038/nature08447

Qi, T. (1990). A Paleogene section at erden Obo, nei mongol and on the discovery of pastoralodon lacustris (pantodonta, mammalia) in that area. *Vertebr. Palasiat.* 28, 25–33. doi:10.19615/j.cnki.1000-3118.1990.01.003

Quan, C., Liu, Y.-S., and Utescher, T. (2012). Eocene monsoon prevalence over China: A paleobotanical perspective. *Palaeogeogr. Palaeoclimatol. Palaeoecol.* 365-366, 302–311. doi:10.1016/j.palaeo.2012.09.035

Reichstein, M., Bahn, M., Ciais, P., Frank, D., Mahecha, M. D., Seneviratne, S. I., et al. (2013). Climate extremes and the carbon cycle. *Nature* 500, 287–295. doi:10.1038/nature12350

Robson, B. E., Collinson, M. E., Riegel, W., Wilde, V., Scott, A. C., and Pancost, R. D. (2015). Early Paleogene wildfires in peat-forming environments at Schöningen, Germany. *Palaeogeogr. Palaeoclimatol. Palaeoecol.* 437, 53–62. doi:10.1016/j.palaeo.2015.07.016

Röhl, U., Westerhold, T., Bralower, T. J., and Zachos, J. C. (2007). On the duration of the Paleocene-Eocene thermal maximum (PETM). *Geochem. Geophys. Geosystems* 8. doi:10.1029/2007gc001784

Sun, B., Yue, L. P., Wang, Y. Q., Meng, J., Wang, J. Q., and Xu, Y. (2009). Magnetostratigraphy of the early Paleogene in the Erlian Basin. *J. Stratigr.* 33, 62–68.

Sun, J., Ni, X., Bi, S., Wu, W., Ye, J., Meng, J., et al. (2014). Synchronous turnover of flora, fauna and climate at the eocene–oligocene boundary in Asia. *Sci. Rep.* 4, 7463. doi:10.1038/srep07463

Tinner, W., and Hu, F. S. (2003). Size parameters, size-class distribution and area-number relationship of microscopic charcoal: Relevance for fire reconstruction. *Holocene* 13, 499–505. doi:10.1191/0959683603hl615rp

Wang, S., Li, R., Wu, Y., and Zhao, S. (2022). Effects of multi-temporal scale drought on vegetation dynamics in Inner Mongolia from 1982 to 2015, China. *Ecol. Indic.* 136, 108666. doi:10.1016/j.ecolind.2022.108666

Wang, Y., Meng, J., Beard, C. K., Li, Q., Ni, X., Gebo, D. L., et al. (2010). Early Paleogene stratigraphic sequences, mammalian evolution and its response to environmental changes in Erlian Basin, Inner Mongolia, China. *Sci. China Earth Sci.* 53, 1918–1926. doi:10.1007/s11430-010-4095-8

Wang, Y. Q., Meng, J., Jin, X., and Palasiatica, V. (2012). Comments on Paleogene localities and stratigraphy in the Erlian Basin, nei mongol, China. *Vertebr. Palasiat.* 50, 181–203. http://www.vertpala.ac.cn/EN/Y2012/V50/I3/181.

West, C. K., Greenwood, D. R., Reichgelt, T., Lowe, A. J., Vachon, J. M., and Basinger, J. F. (2020). Paleobotanical proxies for early Eocene climates and ecosystems in northern North America from middle to high latitudes. *Clim. Past.* 16, 1387–1410. doi:10.5194/cp-16-1387-2020

Zachos, J., Pagani, M., Sloan, L., Thomas, E., and Billups, K. (2001). Trends, rhythms, and aberrations in global climate 65 Ma to present. *Science* 292, 686–693. doi:10.1126/science.1059412

Zhang, Z., Flatøy, F., Wang, H., Bethke, I., Bentsen, M., and Guo, Z. (2012). Early Eocene Asian climate dominated by desert and steppe with limited monsoons. *J. Asian Earth Sci.* 44, 24–35. doi:10.1016/j.jseaes.2011.05.013

frontiers | Frontiers in Earth Science

TYPE Opinion
PUBLISHED 10 July 2023
DOI 10.3389/feart.2023.1203667

OPEN ACCESS

EDITED BY
Patrick G. Hatcher,
Old Dominion University, United States

REVIEWED BY
Mieczysław Wolsan,
Polish Academy of Sciences, Poland

*CORRESPONDENCE
Jesus A. Rivas,
rivas@nmhu.edu

RECEIVED 11 April 2023
ACCEPTED 27 June 2023
PUBLISHED 10 July 2023

CITATION
Rivas JA (2023), The missing river.
Front. Earth Sci. 11:1203667.
doi: 10.3389/feart.2023.1203667

The missing river

Jesus A. Rivas*

New Mexico Highlands University, Las Vegas, NM, United States

KEYWORDS

paleo-ecology, paleo-amazon, large rivers, marine incursion, marine derived lineages, pebas system, wetlands, *Eunectes*

Introduction

South America is the most diverse landmass in the world with highest diversity of species of multiple taxa of any other continent (Haffer, 2008; Rull, 2008; Pimm et al., 2014; Claramunt and Cracraft, 2015). South America's landscape has been very dynamic since the Cenozoic with abundant changes of major rivers, and developments of mega wetlands occupying substantial extensions of the existing continental areas (Albert et al., 2018). The flooding dynamic in the continent since the Andes started to raise, likely is responsible in large part for the high diversity of the continent (Ribas et al., 2007; Ribas et al.,2012; Rivas, 2020). The paleo-dynamics of South America landscape has been an area of interest in many very good recent studies reconstructing it. Unfortunately, on the interest of providing strong evidence-based reconstruction, some studies have proposed scenarios that fail to consider some of the basic laws of physics. In this contribution I review the literature of geological events and points out how some very good work that have been done recently adolesces consideration of some of the basic laws of physics, and often provides scenarios or explanation that are not the most parsimonious, or the most likely.

The lack of a river

When the South America separated from Gondwana it drained to the west by a major river located very much where the current Amazon is but running into the pacific (Lundberg et al., 1998). This river drained the same area that is now drained by the Amazon and Orinoco rivers. Currently these rivers, have a combined mean discharge of 246,600 (m^3/s^{-1}) (Latrubesse, 2015). Since this was a warmer period than the current one with no icecaps (Zachos et al., 2001) it is reasonable to assume that there was a lot more water circulating in the planet so this river would have been a true colossus. As South America moved west it collided with the Nazca plate initiating the rise of the Andes that ended up blocking the west drainage of the river some 30 mya (Lundberg et al., 1998). Blocking the flow of this mighty river with a 7,000 km mountain range would have produced the general flooding of the western part of the continent.

Early reconstructions of South America, showed the hypothetical location of this river and the consequences of the rise of the Andes (Lundberg et al., 1998). However, more recent reconstruction, while more advanced in data sources, fail to include this river (Hoorn et al., 2010b; Hoorn et al., 2022). This is quite an omission because the data shows that the continent was covered by rain forest throughout the Cenozoic (Colinvaux et al., 2000; Colinvaux and De Oliveira, 2002; Bush and Oliveira, 2006). A continent the size of South America receiving anywhere the amount of precipitation needed to sustain a rainforest (2,500–4,000 mm/year) (Holdridge, 1967) had to be drained by a very large river. Assuming that it did not have a river, defies the law of conservation of matter, or first law of thermodynamic since matter and energy are two sides of the same coin.

It is likely that the failure to include this large river has to do with the lack of an alluvial fan in the Pacific shore of South America. A river of this size would have produced a substantial alluvial fan in the ocean where it emptied its waters. Today the alluvial fan in the amazon stretches for 1200 KM from the shore (Pirmez et al., 1997; Mertes and Dunne, 2007). It stands to reason that this river would have had a comparable alluvial fan. What these argument fails to consider is that the Nazca plate, moves toward South America, at a speed of 68 mm/year (Norabuena et al., 1998) So, in the last 30 my, since the river stopped flowing, Nazca has moved 2040 km under South America which would have destroyed any alluvia fan that river had deposited. So the lack of the alluvial fan does not constitute evidence that there was not a river.

A mysterious mega-wetland

The failure to consider there that the Andes blocked a very large river has created controversies that could have been avoided from the beginning. One of the big questions about Pebas System was the source of its waters. It has been proposed that the weight of the Andes deformed the craton producing a depression below sea level that flooded the continent (Hoorn et al., 2010a). However, all the studies of the Pebas system describe it as a long-lived lacustrine or fluvial system of predominantly freshwater lakes and swamps that might have had episodic spots that had, at a maximum, short lived oligohaline patches (Wesselingh et al., 2002). Studies of stable isotopes (O/C and Sr) of ostracods and foraminifera provided compelling evidence that the water of the Pebas system was indeed fresh water (Wesselingh et al., 2002; Wesselingh et al., 2006; Vonhof et al., 2003), which mild salinity could derive from underwater aquifers (Gross and Piller, 2020). This explanation was dismissed in a later paper arguing the amount of water of Pebas was too large and it required a very large underwater aquifer to provide such amount of water. But no alternative explanation was provided other than the debunked possibility of ocean water (da Silva-Caminha et al., 2020).

What is missing in this debate is that fact that in South America's Cenozoic water, freshwater in particular, was not in short supply. Realizing that there was a mighty river that was dammed solves the problem in compliance with all the sedimentological and fossil evidence. The point that is missing in the debate is the realization that that Pebas was not a mysterious system that developed out of nowhere but just a big swamp created by a big dam (Rivas, 2020).

Discussion

Marine incursions in South America has been a dominant topic of discussion in the paleo-history of the continent; since as early as Darwin's observation of marine sea shells in the top of the Andes (Darwin, 1845). Data suggest that there were regular, but short lived, marine incursions constrained by forest and continental ecosystems (Uba et al., 2009). Despite numerous studies reporting marine incursions, there is considerable debate in how and where these marine incursions took place (Wesselingh et al., 2002; Wesselingh et al., 2006; Vonhof et al., 2003), or if they even took place at all (Díaz de Gamero, 1996; Vonhof et al., 2003; Gross et al., 2016; Gross and Piller, 2020; Rivas, 2020).

Part of the problem with these elusive marine incursions is that there has never been any evidence of a marine incursion *per se*. All that has been reported is *marine conditions*, based on presence of Marine Derived Lineages. If we go back to the basic scientific principle of parsimony, we would seek the simplest explanation for the data at hand. Marine incursions are often not the most parsimonious explanation or the one that better explains the data.

For starters, a true marine incursion would have brought a full assorment of marine organism, including stenohaline organism. However the data only shows the presence of Eurohaline organism such as Mangrove, ostracodes, other mollusks, foraminiferams, and Eurohaline fishes among others (Wesselingh et al., 2002; Wesselingh et al., 2006; Hoorn, 2006; Lundberg et al., 2010). All of these need only a very small level of salinity and are quite capable of dispersion through fresh water corridors connecting the Amazon with the Caribean (Gross and Piller, 2020).

An alternative, and simpler, explanation is that the water of the Big Dam could become oligohaline and back by local or regional weather changes (Furquim et al., 2010; Sepulchre et al., 2010; Rivas, 2020). If the contribution of rain from the Andes was very strong, it would bring eutrophic waters (Hoorn et al., 2022) that would have become oligo haline very quickly (Furquim et al., 2010). The development of marine conditions from freshwater bodies is far more parsimonious to explain the recurring mild marine conditions than continent wide flooding events such as marine incursion. In fact, the presence of haline environments today in Mato Grosso do Sul (Brazil), thousands of kilometers from the ocean shore (Furquim et al., 2010), provides irrefutable evidence that haline conditions are possible without marine influence.

Furthermore, one has to wonder if marine incursions were even possible. Díaz de Gamero (1996) provided compelling evidence that marine incursions from the Caribbean were not possible because of the flow of the big river which would have prevented the ocean from coming into the continent. Vonhof et al. (2003) points out this very phenomenon in Lake Maracaibo, Venezuela, pointing out that the southern part of the lake is fresh water despite having a direct connection to the ocean because the volume of its tributaries provide hydrostatic pressure to meet the ocean's. This would have been true with the waters of the Paleo-Orinoco/Amazon. The water already present in the continent would have prevented the ocean from coming in (Díaz de Gamero, 1996; Archer, 2005; Rivas, 2020).

Taking into consideration the continent was drained by a large river that was dammed by the Andes is important because of its consequences on the biodiversity of the continent. The flooding of the continent would have been a very slow process. Not only because it was lead by a geological process, such as the rise of the Andes, but also because of the flat and width of the basin. Every cm of depth that the river lost would have resulted in an imperceptible increase of the water level in its flood plains as its water spread over its wide basin. The very slow flooding perhaps did not produce a layer the sedimentological record we can recognize as a smoking gun of a flood but it would have produced a biological finger print on the diversity of species. The long time that took this change to occur would have given opportunity for natural selection to produce aquatic lineages adapted to the developing new conditions.

Looking at reptiles, we see the appearance of *Chelus*, an aquatic turtle specializing in small forest creeks around 70 mya (Wang et al., 2012). Also around 60 mya South American side-necked turtles (Podocnemidoidae) diversified into new lineages (Ferreira et al., 2018). At this time too, 60 mya, Alligatorids split into two lineages (Roberto et al., 2020), a larger one, Caiman that prefers rivers and lagoons, and *Paleosuchus* spp that is a smaller forest specialist living in small creeks inside the forest (Villamarín et al., 2021). Approximately 58 mya *Titanoboa* an aquatic lineages of snakes, split from terrestrial lineages (Head, 2009) and between 50–40 mya *Eunectes*, a group of aquatic snakes, diversifies from its terrestrial ancestors (Rivas et al. in prep). Also 40–35 mya Teidae a group of terrestrial lizards, diversifies producing two aquatic linages, *Crocodilurus* and *Dracaena* (Giugliano et al., 2007). Approximately, 40 mya, the caiman lineage had another split giving raise to the larger genus, *Melanosuchus*, which occupies large water bodies (Roberto et al., 2020). Last, approximately 49 mya we see the appearance of a strictly arboreal lineage of boids, *Corallus* (Colston et al., 2013). Specialization to living on the trees could be an evolutionary response of a flooded understory that was unavailable. While I have mentions only reptiles, we would have similar trend if we looked at Amphibians (Feng et al., 2017). Taken together, this scenario speaks of a generalized increase of habitat for aquatic lineages throughout the continent and supports the notion that the continent was flooding very slowly, consistent with the geological damming of a big river.

Ignoring that the continent had to have a big river, that was dammed by the Andes has created a lot of confusion and debate about the source of water of Pebas and perpetuated the believe in marine incursions, despite of abundant evidence to the contrary. Understanding that the discharge of the big river would have made marine incursions impossible help to put within context biogeographic processes in the continent. Applying basic principles of conservation of matter and seeking the most parsimonious explanations to the data would put most of these debates to rest.

Author contributions

The author confirms being the sole contributor of this work and has approved it for publication.

Acknowledgments

I thank P. Roa-Morales for seeding my mind with questions about South America paleohistory. I thank NMHU ORSP for publication funding.

Conflict of interest

The author declares that the research was conducted in the absence of any commercial or financial relationships that could be construed as a potential conflict of interest.

Publisher's note

References

Albert, J. S., Val, P., and Hoorn, C. (2018). The changing course of the amazon river in the neogene: Center stage for neotropical diversification. *Neotrop. Ichthyol.* 16, 1–24. doi:10.1590/1982-0224-20180033

Archer, A. W. (2005). Review of Amazonian depositional systems. *Fluv. Syst. VII* 35, 17–39. doi:10.1002/9781444304350.ch2

Bush, M. B., and Oliveira, P. E. De (2006). The rise and fall of the refugial hypothesis of amazonian speciation: A paleo-ecological perspective. *Biota Neotrop* 6, 2. doi:10.1590/S1676-06032006000100002

Claramunt, S., and Cracraft, J. (2015). A new time tree reveals Earth history's imprint on the evolution of modern birds. *Sci. Adv.* 1, e1501005–e1501013. doi:10.1126/sciadv.1501005

Colinvaux, P. A., and De Oliveira, P. E. (2002). Amazon plant diversity and climate through the Cenozoic. *Palaeogeogr. Palaeoclimatol. Palaeoecol.* 166, 51–63. doi:10.1016/s0031-0182(00)00201-7

Colinvaux, P. A., Oliveira, P. E., and Bush, M. B. (2000). Amazonian and neotropical plant communities on glacial time-scales: The failure of the aridity and refuge hypotheses. *Quat. Sci. Rev.* 19, 141–169. doi:10.1016/s0277-3791(99)00059-1

Colston, T. J., Grazziotin, F. G., Shepard, D. B., Vitt, L. J., Colli, G. R., Henderson, R. W., et al. (2013). Molecular systematics and historical biogeography of tree boas (Corallus spp). *Mol. Phylogenet. Evol.* 66, 953–959. doi:10.1016/j.ympev.2012.11.027

da Silva-Caminha, S. A. F., D'Apolito, C., Jaramillo, C., Espinosa, B. S., and Rueda, M. (2020). Palynostratigraphy of the ramon and solimões formations in the acre basin, Brazil. *J. South Am. Earth Sci.* 103, 102720. doi:10.1016/J.JSAMES.2020.102720

Darwin, C. (1845). *Journal of Researches into the natural History and Geology of the countries visited During the voyage Round the World of H.M.S. "Beagle" Under the Command of captain fitz roy*. London: Cambridge University Press. Available at: www.hn.psu.eduq/jimspdf.htm%5Cnwww.hn.psu.edu/faculty/jmanis/darwin.htm.

Díaz de Gamero, M. (1996). The changing course of the Orinoco river during the neogene: A review. *Palaeogeogr. Palaeoclimatol. Palaeoecol.* 123, 385–402. doi:10.1016/0031-0182(96)00115-0

Feng, Y. J., Blackburn, D. C., Liang, D., Hillis, D. M., Wake, D. B., Cannatella, D. C., et al. (2017). Phylogenomics reveals rapid, simultaneous diversification of three major clades of Gondwanan frogs at the Cretaceous–Paleogene boundary. *Proc. Natl. Acad. Sci.* 114, E5864–E5870. doi:10.1073/pnas.1704632114

Ferreira, G. S., Bronzati, M., Langer, M. C., and Sterli, J. (2018). Phylogeny, biogeography and diversification patterns of side-necked turtles (Testudines: Pleurodira). *R. Soc. Open Sci.* 5, 171773. doi:10.1098/rsos.171773

Furquim, S. A. C., Graham, R. C., Neto, J. P. Q., and Vidal-Torrado, P. (2010). Soil mineral Genesis and distribution in a saline lake landscape of the Pantanal Wetland, Brazil. *Geoderma* 154, 518–528. doi:10.1016/j.geoderma.2009.03.014

Giugliano, L. G., Collevatti, R. G., and Colli, G. R. (2007). Molecular dating and phylogenetic relationships among Teiidae (Squamata) inferred by molecular and morphological data. *Mol. Phylogenet. Evol.* 45, 168–179. doi:10.1016/j.ympev.2007.05.017

Gross, M., Ines, M., Ramos, F., and Piller, W. E. (2016). A minute ostracod \(Crustacea: Cytheromatidae\) from the miocene solimões formation \(Western amazonia, Brazil\): Evidence for marine incursions? *J. Syst. Palaeontol.* 14, 581–602. doi:10.1080/14772019.2015.1078850

Gross, M., and Piller, W. E. (2020). Saline waters in miocene western amazonia – an alternative view. *Front. Earth Sci.* 8, 1–15. doi:10.3389/feart.2020.00116

Haffer, J. (2008). Hypotheses to explain the origin of species in Amazonia. *Braz. J. Biogeogr.* 68, 917–947. doi:10.1590/s1519-69842008000500003

Head, J. J., Bloch, J. I., Hastings, A. K., Bourque, J. R., Cadena, E. A., Herrera, F. A., et al. (2009). Giant boid snake from the Palaeocene neotropics reveals hotter past equatorial temperatures. *Nature* 457, 715–717. doi:10.1038/nature07671

Holdridge, L. R. (1967). *Life zones ecology*. San Jose: Tropical Science Center.

Hoorn, C., Boschman, L. M., Kukla, T., Sciumbata, M., and Val, P. (2022). The Miocene wetland of Western Amazonia and its role in Neotropical biogeography. *Bot. J. Linn. Soc.* 199, 25–35. doi:10.1093/botlinnean/boab098

Hoorn, C. (2006). Mangrove forests and marine incursions in neogene amazonia (lower apaporis river, Colombia). *Palaios* 21, 197–209. doi:10.2110/palo.2005.p05-131

Hoorn, C., Wesselingh, F., Hovikoski, J., and Guerrero, J. (2010a). "Development of the amazonian mega-wetland (miocence; Brazil, Colombia, Peru, Bolivia)," in *Amazonia: Landscape and species evolution*. Editors C. Hoorn and F. Wesselingh (Oxford: Wiley-Blackwell), 123–142.

Hoorn, C., Wesselingh, F. P., Steege, H. ter, Bermudez, M. A., Mora, A., Sevink, J., et al. (2010b). Amazonia through time: Andean uplift, climate change, landscape evolution, and biodiversity. *Sci. (80-.)* 330, 927–931. doi:10.1126/science.1194585

Latrubesse, E. M. (2015). Large rivers, megafans and other quaternary avulsive fluvial systems: A potential "who's who" in the geological record. *Earth-Science Rev.* 146, 1–30. doi:10.1016/j.earscirev.2015.03.004

Lundberg, J. G., Marshall, L. G., Guerrero, J., Horton, B., Malabarba, M. C. S. L., and Wesselingh, F. (1998). "The stage for neotropical fish diversification: A history of tropical South American rivers," in *Phylogeny and classification of neotropical fishes*. Editors L. R. Malabarba, R. E. Reis, R. P. Vari, Z. M. S. Lucena, and C. A. S. Lucena (Porto Alegre: Edipucrs), 13–48.

Lundberg, J. G., SabajPérez, M. H. W. M. D., and Aguilera, O. A. (2010). "The Amazonian neogene fish fauna," in *Amazonia: Landscape and species evolution: A look into the past* (Wiley), 281–301.

Mertes, L. A. K., and Dunne, T. (2007). "Effects of tectonism, climate change, and sea-level change on the form and behaviour of the modern amazon river and its floodplain," in *Large rivers: Geomorphology and management*. Editor A. Gupta (Chichester: John Wiley & Sons, Ltd), 115–144. doi:10.1002/9780470723722.ch8

Norabuena, E., Leffler-Griffin, L., Mao, A., Dixon, T., Stein, S., Sacks, I. S., et al. (1998). Space geodetic observations of Nazca-South America convergence across the central Andes. *Sci. (80-* 279, 358–362. doi:10.1126/science.279.5349.358

Pimm, S. L., Jenkins, C. N., Abell, R., Brooks, T. M., Gittleman, J. L., Joppa, L. N., et al. (2014). The biodiversity of species and their rates of extinction, distribution, and protection. *Science* 80, 1246752. doi:10.1126/science.1246752

Pirmez, C., Flood, R. D., Baptiste, J., Yin, H., and Manley, P. L. (1997). Clay content, porosity and velocity of Amazon Fan sediments determined from ODP Leg 155 cores and wireline logs. *Geophys. Res. Lett.* 24, 317–320. doi:10.1029/96GL03469

Ribas, C. C., Aleixo, A., Nogueira, A. C. R. R., Miyaki, C. Y., and Cracraft, J. (2012). A palaeobiogeographic model for biotic diversification within Amazonia over the past three million years. *Proc. R. Soc. B Biol. Sci.* 279, 681–689. doi:10.1098/rspb.2011.1120

Ribas, C. C., Moyle, R. G., Miyaki, C. Y., and Cracraft, J. (2007). The assembly of montane biotas: Linking andean tectonics and climatic oscillations to independent regimes of diversification in pionus parrots. *Proc. R. Soc. B Biol. Sci.* 274, 2399–2408. doi:10.1098/rspb.2007.0613

Rivas, J. A. (2020). Climate changes and speciation pulses in a nearly flooded continent: Tackling the riddle of South America ' s high diversity. *Ecotrópicos* 32, 1–21. doi:10.53157/ecotropicos.32E0014

Roberto, I. J., Bittencourt, P. S., Muniz, F. L., Hernández-Rangel, S. M., Nóbrega, Y. C., Ávila, R. W., et al. (2020). Unexpected but unsurprising lineage diversity within the most widespread Neotropical crocodilian genus Caiman (Crocodylia, Alligatoridae). *Syst. Biodivers.* 18, 377–395. doi:10.1080/14772000.2020.1769222

Rull, V. (2008). Speciation timing and neotropical biodiversity: The Tertiary-Quaternary debate in the light of molecular phylogenetic evidence. *Mol. Ecol.* 17, 2722–2729. doi:10.1111/j.1365-294X.2008.03789.x

Sepulchre, P., Sloan, L. C., and Fluteau, F. (2010). "Modelling the response of Amazonian climate to the uplift of the Andean mountain range," in *Amazonia: Landscape and species evolution*. Editors C. Hoorn and F. Wesselingh (Oxford: Wiley-Blackwell), 211–222.

Uba, C. E., Hasler, C. A., Buatois, L. A., Schmitt, A. K., and Plessen, B. (2009). Isotopic, paleontologic, and ichnologic evidence for late Miocene pulses of marine incursions in the central Andes. *Geology* 37, 827–830. doi:10.1130/G30014A.1

Villamarín, F., Escobedo-Galván, A. H., Siroski, P., and Magnusson, W. E. (2021). "Geographic distribution, habitat, reproduction, and conservation status of crocodilians in the americas," in *Conservation genetics of new world crocodilians*. Editors R. B. Zucoloto, P. S. Amavet, L. M. Verdade, and I. P. Farias (Cham: Springer).

Vonhof, H. B., Wesselingh, F. P., Kaandorp, R. J. G., Davies, G. R., van Hinte, J. E., Guerrero, J., et al. (2003). Paleogeography of Miocene Western Amazonia: Isotopic composition of molluscan shells constrains the influence of marine incursions. *Bull. Geol. Soc. Am.* 115, 983–993. doi:10.1130/B25058.1

Wang, L., Zhou, X., Nie, L., Xia, X., Liu, L., Jiang, Y., et al. (2012). The complete mitochondrial genome sequences of Chelodina rugosa and Chelus fimbriata (pleurodira: Chelidae): Implications of a common absence of initiation sites (OL) in pleurodiran turtles. *Mol. Biol. Rep.* 39, 2097–2107. doi:10.1007/s11033-011-0957-1

Wesselingh, F. P., Kaandorp, R. J. G., Vonhof, H. B., Räsänen, M. E., Renema, W., Gingras, M., et al. (2006). The nature of aquatic landscapes in the miocene of Western amazonia: An integrated palaeontological and geochemical approach. *Scr. Geol.* 133, 363–393.

Wesselingh, F. P., Rasanen, M., Irion, G., Vonhof, H., Kaandorp, R., Renema, W., et al. (2002). Lake Pebas: Palaeoecological complex reconstruction in Western amazonia. *Cainozoic Res.* 1, 35–81.

Zachos, J., Pagani, H., Sloan, L., Thomas, E., and Billups, K. (2001). Trends, rhythms, and aberrations in global climate 65 Ma to present. *Science* 292, 686–693. doi:10.1126/science.1059412

Frontiers in Earth Science

Investigates the processes operating within the major spheres of our planet

Advances our understanding across the earth sciences, providing a theoretical background for better use of our planet's resources and equipping us to face major environmental challenges.

Discover the latest Research Topics

See more →

Frontiers

Avenue du Tribunal-Fédéral 34
1005 Lausanne, Switzerland
frontiersin.org

Contact us

+41 (0)21 510 17 00
frontiersin.org/about/contact